This is to certify that the
dissertation entitled

Design and Performance Tradeoffs of High-Gain Observers
with Applications
to the Control of Smart Material Actuated Systems

presented by

Jeffrey H. Ahrens

has been accepted towards fulfillment
of the requirements for the

Ph.D. degree in Electrical and Computer Engineering

Hassan Khalil
Major Professor's Signature

12/4/2006
Date

MSU is an Affirmative Action/Equal Opportunity Institution

DATE DUE	DATE DUE	DATE DUE
	OCT 0 5 2003	
	0823 11	

Design and Performance Tradeoffs of High-Gain Observers with Applications to the Control of Smart Material Actuated Systems

By

Jeffrey H. Ahrens

A DISSERTATION

Submitted to
Michigan State University
in partial fulfillment of the requirements
for the degree of

DOCTOR OF PHILOSOPHY

Department of Electrical and Computer Engineering

2006

ABSTRACT

Design and Performance Tradeoffs of High-Gain Observers with Applications to the Control of Smart Material Actuated Systems

By

Jeffrey H. Ahrens

The study of high-gain observers has typically involved properties that are asymptotically recovered as the gain is pushed higher. In any practical implementation of high-gain observers one will ultimately encounter performance tradeoffs associated with the choice of gain. These include tradeoffs between fast reconstruction of the system states, better rejection of modeling uncertainty, and closed-loop stability versus amplification of measurement noise, large transient response amplitude, and computational cost in the discrete-time case. We propose several high-gain observer designs and examine their effectiveness at dealing with these tradeoffs.

We examine the tradeoff between closed-loop stability and large observer transient response by considering a time-varying high-gain observer that is of the form of an extended Kalman filter (EKF). We highlight an important feature of the Riccati equation with respect to the observer transient and show closed-loop asymptotic stability for a particular class of nonlinear systems under EKF feedback. We compare the performance of the time-varying extended Kalman filter against a fixed-gain high-gain observer in terms of closed-loop stability and transient response.

To balance the tradeoff between state reconstruction speed during the observer transient with amplification of measurement noise at steady-state we propose a high-gain

observer that switches between two gain values. This scheme is able to quickly recover the system states during large estimation error and reduce the effect of measurement noise in a neighborhood of the origin of the estimation error. We argue boundedness of the trajectories of the closed-loop system.

Since closed-loop stability for sampled-data systems using high-gain observers follows for sufficiently small sampling periods, there is a tradeoff between elevated sampling rates and closed-loop performance. We consider a multirate sampled-data output feedback control design in order to relax the tradeoff between computational cost and closed-loop stability. This scheme employs control update rates that are fixed by a state feedback design with a sufficiently fast measurement sampling rate. We prove practical stabilization for the closed-loop system under multirate output feedback. We also argue stability with respect to a set in the presence of bounded disturbances.

For smart material actuated systems, the existence of significant hysteresis nonlinearity inherent in smart materials along with difficulties in measuring system states points to output feedback control designs employing hysteresis compensation. We apply our multirate output feedback scheme to a shape memory alloy actuated rotary joint by combining the observer with a hysteresis inversion controller. The rotary joint is modeled as a hysteresis operator of Preisach type combined with a dynamic system. Experimental results of the proposed scheme are reported.

This dissertation attempts to address certain criticisms of high-gain observers and thus may be of interest to both control theoreticians and practicing engineers.

To my family

ACKNOWLEDGMENTS

It's been said that a wise teacher teaches by example. I'm indebted to my advisor Dr. Hassan Khalil for being a patient and wise teacher. Many thanks are due to my co-advisor Dr. Xiaobo Tan for all the help, discussions, and use of the laboratory. I would like to thank Dr. Percy Pierre and Dr. Barbara O'Kelly for supporting my study at MSU. My colleagues at MSU especially: Sridhar, Leonid, Shahin, Eduardo, Uche, Zheng, Yang, Memon, and Shahid. To my father, Don, for teaching me the value of education and personal responsibility. To my mother, Martha, who's outlook on life has instilled in me confidence, optimism, and perseverance. And to my wife, Amy, for the boundless love, constant support, and infinite patience that have made all this possible.

TABLE OF CONTENTS

LIST OF TABLES

LIST OF FIGURES

CHAPTER 1

Introduction

Most nonlinear control design tools assume state feedback (i.e., measurement of all state variables) to achieve a desired goal. In many applications full state measurement is either impractical or not possible. In such cases, it is necessary to use alternate methods to obtain the system state information. One method is the use of observers to estimate the system states from the output measurements. For linear time-invariant systems

$$\begin{aligned} \dot{x} &= Ax + Bu \\ y &= Cx \end{aligned}$$

a state observer takes the form

$$\dot{\hat{x}} = A\hat{x} + Bu + H(y - C\hat{x})$$

This observer, referred to as a Luenberger observer, reproduces the right hand side of the system dynamics and is driven by the output error through the observer gain H. With the pair (A, C) detectable, H can be chosen to guarantee global convergence of the estimates $\hat{x}$ to the system states x. For a general class of nonlinear systems

$$\dot{x} = f(x, u)$$

$$y = h(x)$$

designing an observer to provide convergence outside a small neighborhood of the origin of the estimation error has proved to be challenging. To achieve nonlocal convergence, nonlinear observer designs typically exploit the special structure of a certain class of nonlinear systems. One such nonlinear observer is the high-gain observer. High-gain observers are applicable to a class of nonlinear systems that have the form

$$\dot{z} = \psi(x, z) \tag{1.1}$$

$$\dot{x} = Ax + B\phi(x, z, u) \tag{1.2}$$

$$y = Cx \tag{1.3}$$

$$\zeta = \Theta(x, z) \tag{1.4}$$

where u is the control input, $x \in \mathbb{R}^r$ and $z \in \mathbb{R}^\ell$ constitute the state vector, and y and ζ are the measured variables. The $r \times r$ matrix A, the $r \times 1$ matrix B, and the $1 \times r$ matrix C are given by

$$A = \begin{bmatrix} 0 & 1 & \cdots & \cdots & 0 \\ 0 & 0 & 1 & \cdots & 0 \\ \vdots & & & & \vdots \\ 0 & \cdots & \cdots & 0 & 1 \\ 0 & 0 & \cdots & \cdots & 0 \end{bmatrix}, B = \begin{bmatrix} 0 \\ 0 \\ \vdots \\ 0 \\ 1 \end{bmatrix} \tag{1.5}$$

$$C = \begin{bmatrix} 1 & 0 & \cdots & \cdots 0 \end{bmatrix} \tag{1.6}$$

One source for the model (1.1)-(1.4) is the normal form of input-output linearizable systems, as discussed in [36]. In addition to the normal form, this class of systems also arises in mechanical and electromechanical systems where the position is measured, but its derivatives, the velocity and acceleration, are not measured. In [26], Esfandiari and Khalil introduced a robust output feedback technique based on the use of high-gain ob-

servers. Output feedback is achieved by first considering a globally bounded partial state feedback controller given by

$$u = \gamma(x, \zeta)$$

that is designed to meet the performance objectives. Then, the state x is replaced by the estimate $\hat{x}$ that is generated by the high-gain observer

$$\dot{\hat{x}} = A\hat{x} + B\phi_0(\hat{x}, \zeta, u) + H(y - C\hat{x}) \tag{1.7}$$

where ϕ_0 is a known nominal model of ϕ and the observer gain H is designed as

$$H = \left[\frac{\alpha_1}{\varepsilon}, \frac{\alpha_2}{\varepsilon^2}, \ldots\ldots, \frac{\alpha_r}{\varepsilon^r}\right]^T \tag{1.8}$$

The α_i's are chosen such that the roots of

$$s^r + \alpha_1 s^{r-1} + \cdots + \alpha_{r-1} s + \alpha_r \tag{1.9}$$

have negative real parts. The output feedback controller is given by

$$u = \gamma(\hat{x}, \zeta)$$

Some of the key features of the high-gain observer can be seen by rescaling the estimation error according to

$$\xi_i = \frac{(x_i - \hat{x}_i)}{\varepsilon^{i-1}}$$

With this rescaling we can arrive at the following equation for the estimation error

$$\varepsilon\dot{\xi} = A_0\xi + \varepsilon B[\phi(x, z, \gamma(\hat{x}, \zeta)) - \phi_0(\hat{x}, \zeta, \gamma(\hat{x}, \zeta))] \tag{1.10}$$

where A_0 is a Hurwitz matrix. This equation shows that the effect of the modeling uncertainty $(\phi - \phi_0)$ is reduced with smaller ε. Also, this equation shows that the observer error evolves in a time scale t/ε, which is faster then the time scale of the plant. One attribute of the high-gain observer is what is known as the peaking phenomenon. Due to the gain structure (1.8), the observer will exhibit a transient response of the form

$$\frac{1}{\varepsilon} exp(-at/\varepsilon)$$

Notice that while this term will rapidly decay, the amplitude will be quite large. Thus, the transient response approaches an impulsive-like behavior as ε is pushed smaller. Peaking in the estimates can lead to large control magnitude which in turn can lead to instability if not properly handled. One way to do this is to globally bound the control by saturating it outside a compact region of interest. This will limit the control magnitude so that the plant does not experience the effects of peaking. Although globally bounding the control can prevent peaking from driving the system unstable, its effects will still be present in the control signal. Peaking can cause the control to swing quickly between its minimum and maximum values. This type of control behavior can lead to excessive power consumption or mechanical wear. Therefore, it is still desirable to avoid peaking in favor of a more well behaved control signal.

As we alluded to above, the closed-loop system under high-gain observer feedback will contain fast and slow time scales. This two-time scale nature of the closed-loop system allows it to be studied using singular perturbation analysis. The idea of combining a globally bounded state feedback control with a sufficiently fast high-gain observer was used by Atassi and Khalil [7] to prove a separation principle for the class of systems under consideration. They showed that by choosing ε sufficiently small, one can guarantee stability of the closed-loop system. In addition, they showed that as $\varepsilon \rightarrow 0$ the performance under output feedback using high-gain observers approaches the performance under state feedback.

In this thesis we will consider continuous-time as well as sampled-data systems. In sampled-data systems the actual process is continuous-time while the controller is implemented in discrete-time by digital computers. In [19], Dabroom and Khalil considered discrete-time implementation of the high-gain observer. Various discretization methods were studied to determine the most suitable algorithm and best choice of observer parameters. Furthermore, in [20], Dabroom and Khalil showed that an output feedback controller based on the discrete-time high-gain observer stabilizes the origin of the closed-loop system for sufficiently small sampling period T. In addition, it was shown that the performance under sampled-data output feedback asymptotically approaches the performance under continuous-time state feedback as $T \to 0$. In discrete-time, the sampling period of the observer is chosen proportional to the gain parameter ε. That is, $T = \alpha\varepsilon$ for some positive constant α. Thus, for the discrete-time high-gain observer, more accurate estimation of the system states is achieved by faster sampling of the output.

1.0.1 High-Gain Observer Performance Tradeoffs

The tradeoffs that concern us here are the ones that come with the choice of the gain parameter ε. Choosing smaller values of ε yields the following benefits: faster reconstruction of the system states, better rejection of modeling uncertainty, and recovery of the performance under state feedback. This comes at the expense of amplification of measurement noise, larger peaking amplitude, and more computational cost in the discrete-time case. On the other hand, with larger ε, one can expect reduced susceptibility to measurement noise, smaller peaking amplitude, and less computational demands in the discrete-time case. However, this comes with the price of slower state reconstruction and greater significance of the modeling error.

With this in mind, we consider the design and performance tradeoffs of closed-loop systems under output feedback using high-gain observers with application to the control of systems with smart material actuators. This will be done in four steps. First, we consider

a time-varying high-gain observer that is of the form of an extended Kalman filter (EKF). We will show that when applied to a class of nonlinear systems similar to (1.1)-(1.4), the closed-loop system under EKF feedback, when parameterized as a high-gain observer, is asymptotically stable. Further, we compare the performance of the extended Kalman filter with a fixed-gain high-gain observer to evaluate whether the added complexity of the EKF provides advantages in terms of closed-loop stability and the peaking phenomenon. Second, we highlight the tradeoff between state reconstruction and modeling uncertainty versus immunity to measurement noise and propose a switched-gain high-gain observer design to relax this tradeoff. Third, turning our attention to sampled-data systems, we consider a multirate sampled-data output feedback control design in order to relax the tradeoff between computational cost and closed-loop stability. Finally, we apply our multirate output feedback design to smart material actuated systems. We introduce each of these ideas here; additional background and discussion is given in the introduction to each chapter.

Extended Kalman Filters

The gain of the high-gain observer, as shown above, is designed by a pole placement approach. Atassi and Khalil [8] studied the high-gain observer for pole placement, algebraic Riccati equation, and Lyapunov equation-based algorithms. They were able to show that each of these three gain design methods, along with a globally bounded control, satisfies the separation result of [7]. Another observer for nonlinear systems is the extended Kalman filter [27]. The extended Kalman filter has been widely used in the areas of control and signal processing as a state estimator for nonlinear stochastic systems. The EKF is based on linearization about the current state estimate and on the covariance of the input and measurement noise, which are typically treated as stochastic processes. The

filter gain, $P(t)C^TR^{-1}$, is obtained from the solution to the Riccati equation

$$\dot{P} = A_1(\hat{x}(t))P + PA_1^T(\hat{x}(t)) + Q - PC^TR^{-1}CP \tag{1.11}$$

where Q and R are the input and output error covariance matrices, respectively. The matrix $A_1(\hat{x}(t))$ is obtained from the linearization of the nonlinear system about the current estimate. In the noise free case, the EKF can be parameterized to function as a deterministic observer for nonlinear systems. Furthermore, based on a particular choice of the covariance matrices, the EKF can be designed as a time-varying high-gain observer. We prove that under EKF feedback the origin of the closed-loop system is asymptotically stable and the estimation error converges exponentially. Further, we compare the benefits and limitations of observers with time-varying gain versus observers with fixed gain. This comparison will involve the value of ε that provides closed-loop stability and the susceptibility of the observer with respect to peaking.

Switched-Gain Observers

One common criticism of high-gain observers is their performance in the presence of measurement noise. We note that high observer gain tends to differentiate noise thereby degrading the performance of the closed-loop system. To deal with the tradeoff between state reconstruction speed and suppression of modeling uncertainty versus amplification of measurement noise we introduce a high-gain observer design where the gain matrix is switched between two values. We note that during the observer transient, it may be more desirable to use high-gain to quickly reconstruct the system states when the estimation error is large at the expense of increased impact of measurement noise. On the other hand, at steady-state, when the transient has died down, it is more desirable to use smaller gains to lessen the effect of noise. This is the basic idea behind the switched-gain observer. We use high-gain during the transient to quickly recover the state estimates, then once the estimation error has reached steady-state, we switch to a lower gain to reduce the effect

of measurement noise. We prove that under the switched-gain observer, all trajectories of the closed-loop system are bounded.

Multirate sampled-data output feedback control

Motivated by applications of control to smart material systems we seek to analyze the performance of a closed-loop system when multirate sampled-data output feedback is considered. For sampled-data state feedback the sampling period is dictated by the bandwidth of the closed-loop system. With discrete-time observers, a more accurate estimate of the system states can be obtained with faster sampling of the output. Here we consider a sampled-data system where the input and output are sampled at different rates. Using discrete-time high-gain observers, we note that the sampling frequency should be chosen proportional to the observer poles which are located at $O(1/\varepsilon)$. Therefore, the output sampling period decreases as ε decreases. We seek to balance the tradeoff between fast sampling rates, needed to guarantee stability under high-gain observer feedback, and the computational costs associated with elevated sampling rates. We start with a sampling rate that is chosen based on state feedback design. We show that stability of the closed-loop system can be achieved by using a sufficiently fast measurement sampling rate and a control update rate that is fixed by the same state feedback design. We prove practical stabilization of the origin of the closed-loop system under multirate output feedback. Further, in the presence of bounded disturbances in the closed-loop system we prove stabilization with respect to a set containing the origin. We show through simulation that the multirate scheme may be less susceptible to peaking than the single-rate scheme.

Smart Materials Actuators and Control

Finally, we will apply the multirate output feedback control design to the control of systems that employ smart materials as actuation devices. Smart materials exhibit significant hysteresis and we consider controller designs that employ hysteresis inversion algorithms

such as the one introduced by Tan and Baras in [63]. In general, these inversion algorithms are computationally demanding and controller designs based on them may place a constraint on the choice of sampling rate. We work with a model for smart material actuators that consists of a hysteresis operator in cascade with a linear dynamic system and use hysteresis inversion for feedforward compensation. In the presence of bounded hysteresis inversion error, we demonstrate the applicability of multirate output feedback control. Further, we present experimental results for the control of a shape memory alloy actuated robotic joint. This is done by applying a controller based on hysteresis inversion with a high-gain observer in the multirate scheme.

This thesis is divided into three parts. In the first part, we consider the extended Kalman filter as a time-varying high-gain observer and compare the EKF to a fixed-gain high-gain observer. This is covered in Chapter 2. In Chapter 3 we turn our attention to the effect of measurement noise and consider a switched-gain observer design. Chapters 4 and 5 consider multirate output feedback using high-gain observers and applications to the control of smart material actuated systems, respectively. Finally, Chapter 6 discusses the conclusions and future work.

CHAPTER 2

The Extended Kalman Filter as a Time-Varying High-Gain Observer

2.1 Introduction

In this chapter we examine a high-gain observer that has time-varying gain. This observer will be of the form of the well-known extended Kalman filter (EKF). Based on a parameterization of the EKF we provide stability results for closed-loop systems under EKF feedback. Further, through simulation, we study whether a time-varying high-gain observer is able to balance the tradeoff between closed-loop stability and large peaking transients in the observer. First, we provide some background on the extended Kalman filter.

Since the 1970's, the extended Kalman filter has seen successful application as a state estimator for nonlinear stochastic systems. See [27] and [62] for an introduction. In the noise free case, the EKF can be parameterized to function as an observer for deterministic nonlinear systems. In the 1990's, study of the stability and convergence properties was conducted. An early method for constructing deterministic observers as asymptotic limits of filters appeared in [9]. Additional work on the convergence properties of extended Kalman filters used as observers has been conducted in [11], [12], [21], [56], [57], [61].

Early convergence results were able to show that the EKF converges exponentially for general classes of systems, but these results were mostly local. Efforts to expand the domain of attraction appeared in [11] and [56]. In [56] a modification of the linearized system matrix was introduced to improve stability. In [11] a study of the influence of the disturbance covariance matrices Q and R on the convergence was conducted for the discrete-time case. The results of [11] show that choosing Q and R according to a linear matrix inequality can enlarge the domain of attraction. In [21] it was recognized that, for a particular parameterization of the covariance matrices, the EKF is a time-varying high-gain observer that asymptotically approaches a fixed-gain observer as the gain is pushed higher. Furthermore, it was shown that the EKF is a global exponential observer for a class of nonlinear systems transformable to the lower triangular form. This argument was based on a global Lipschitz property for the system nonlinearities.

To this point, analysis of the closed-loop system under EKF feedback has been limited. A separation result for a Kalman-like observer for a certain class of MIMO nonlinear systems was presented in [70]. This result made use of certain assumptions on the boundedness of the states of the system under control; these assumptions were consistent with the proposed application of feedback control of polymerization reactors. Global results were given under global Lipschitz conditions. Aside from very restrictive assumptions on the nonlinearities, exponential stability of the estimation error does not guarantee the behavior of the closed-loop system, even when the system under state feedback is exponentially stable [66]. Hence, it seems appropriate to study the behavior of the closed-loop system when an extended Kalman filter is used as an observer. Toward that end, we relax the global Lipschitz condition and consider a class of systems transformable to the special normal form with linear internal dynamics. Based on a parameterization of the Riccati equation, the closed-loop system under EKF feedback is placed in the standard singularly perturbed form. We note that by relaxing the global Lipschitz condition, difficulties may arise as a result of the peaking phenomenon. Peaking in the estimates can lead to

instability in the closed-loop system. This phenomenon is typically overcome by globally bounding the control outside a compact region of interest. In our situation, in addition to globally bounding the control, the time-varying matrices of the Riccati equation must be globally bounded in order to have a well defined solution. Previous convergence results relied on assuming that the solution to the Riccati matrix equation is bounded. In [9] and [61] observability conditions are given that ensure the boundedness of this solution. In this chapter we argue boundedness by using perturbation analysis. This is done by making use of standard results on time-invariant Riccati equations.

We begin in the next section by putting the EKF on a theoretical footing. We argue that the origin of the closed-loop system under EKF output feedback is asymptotically stable. In addition, we show that the observer error is semiglobally exponentially stable. In Section 2.3, we compare through simulation the use of the extended Kalman filter versus a fixed-gain high-gain observer. We study the performance of the EKF parameterized as a time-varying high-gain observer in terms of closed-loop stability and the peaking phenomenon.

2.2 Closed-Loop Stability Under EKF Feedback

Consider the system

$$\dot{z} = Fz + Gx_1 \tag{2.1}$$

$$\dot{x} = Ax + B\phi(z, x, u) \tag{2.2}$$

$$y = Cx \tag{2.3}$$

where $x \in \mathbb{R}^r$ and $z \in \mathbb{R}^\ell$ are the states, u is the input, and y is the output. The function ϕ is assumed to be continuously differentiable and satisfies $\phi(0,0,0) = 0$. The $\ell \times \ell$ matrix F is Hurwitz. The $r \times r$ matrix A, the $r \times 1$ matrix B, and the $1 \times r$ matrix C are the same as (1.5)-(1.6). The internal dynamics (2.1) are driven by the output $y = x_1$. Given

this structure, the system (2.1)-(2.2) is said to be in the special normal form [34]. Let $\chi = [z \;\; x]^T$ and rewrite (2.1)-(2.2) as

$$\dot{\chi} = f(\chi, u) \tag{2.4}$$

The extended Kalman filter for this system is given by

$$\dot{\hat{\chi}} = f(\hat{\chi}, u) + PC_e^T R^{-1}(y - C_e\hat{\chi}) \tag{2.5}$$

$$\dot{P} = A_e P + PA_e^T + Q - PC_e^T R^{-1} C_e P \tag{2.6}$$

where R, Q, and $P(0)$ are positive definite symmetric matrices and

$$C_e = [0_{1\times\ell} \;\; C] \tag{2.7}$$

The matrix A_e takes the form

$$A_e = \begin{bmatrix} A_{11} & A_{12} \\ A_{21} & A_{22} \end{bmatrix}$$

in which

$$A_{11} = F \;\; , \;\; A_{12} = [G \;\; 0 \;\; \cdots \;\; 0]_{\ell\times r}$$

$$A_{21} = B\frac{\partial\phi}{\partial z}(\hat{z}, \hat{x}, u) \;\; , \;\; A_{22} = A + A_0$$

where

$$A_0 = \begin{bmatrix} 0 & \cdots & \cdots & 0 \\ \vdots & & & \vdots \\ 0 & & & 0 \\ d\phi_1 & d\phi_2 & \cdots & d\phi_r \end{bmatrix}, \quad d\phi_i = \frac{\partial\phi}{\partial x_i}(\hat{z}, \hat{x}, u) \tag{2.8}$$

In the forthcoming equations, we will use A_{11} in place of F. We consider the state feedback controller

$$u = \gamma(z, x) \tag{2.9}$$

The closed-loop system under state feedback is given by

$$\dot{z} = A_{11}z + Gx_1 \tag{2.10}$$

$$\dot{x} = Ax + B\phi(z, x, \gamma(z, x)) \tag{2.11}$$

We state our assumptions.

Assumption 2.1

1. *The origin* $(x = 0, z = 0)$ *of (2.10)-(2.11) is globally asymptotically stable.*

2. *The function* γ *is locally Lipschitz in its arguments and globally bounded in* x*. Furthermore,* $\gamma(0, 0) = 0$.

In addition, we assume that the closed-loop system satisfies the following ISS property

Assumption 2.2 *The system*

$$\dot{z} = A_{11}z + Gx_1 \tag{2.12}$$

$$\dot{x} = Ax + B\phi(z, x, \gamma(z + v, x)) \tag{2.13}$$

with v *viewed as the input, is input-to-state stable (ISS).*

Assumption 2.3 *The functions*

$$\frac{\partial \phi}{\partial z}(\hat{z}, \hat{x}, u) \quad \textit{and} \quad \frac{\partial \phi}{\partial x_i}(\hat{z}, \hat{x}, u)$$

for $i = 1, \cdots, r$ *are globally bounded in* $\hat{z}$ *and* $\hat{x}$.[1]

Assumption 2.3 ensures that the matrices A_{21} and A_{22} of the Riccati equation are bounded. Globally bounding the control protects the plant from peaking. Bounding A_{21} and A_{22} protects the Riccati equation from peaking, ensuring a well defined solution. Due to the parameterization for Q (see below), peaking will appear only in the $\hat{x}$ estimates. However, for convenience we bound A_{21} and A_{22} in $\hat{z}$ as well. This simplifies the analysis by allowing the Riccati equation to be studied independently of the estimation equations. We parameterize Q in the following way

$$Q = \begin{bmatrix} Q_1 & Q_2 \\ Q_2^T & \frac{1}{\varepsilon^2} D^{-1} Q_3 D^{-1} \end{bmatrix} \tag{2.14}$$

where Q_1 and Q_3 are chosen to be positive definite symmetric, $D = diag[1, \varepsilon, \cdots, \varepsilon^{r-1}]$, and $\varepsilon > 0$. We take $R = 1$. The above parameterization produces a two-time scale behavior in the solution to the Riccati equation (2.6). We partition and scale P according to

$$P = \begin{bmatrix} P_1 & P_2 D^{-1} \\ D^{-1} P_2^T & \frac{1}{\varepsilon} D^{-1} P_3 D^{-1} \end{bmatrix} \tag{2.15}$$

where $P_1(0)$ and $P_3(0)$ are chosen to be positive definite and $P_2(0)$ is chosen so that P(0) is positive definite. Then, the observer can be written as

$$\dot{\hat{z}} = A_{11} \hat{z} + G \hat{x}_1 + P_2 D^{-1} C^T (y - C\hat{x}) \tag{2.16}$$

$$\dot{\hat{x}} = A\hat{x} + B\phi(\hat{z}, \hat{x}, u) + \frac{1}{\varepsilon} D^{-1} P_3 D^{-1} C^T (y - C\hat{x}) \tag{2.17}$$

The gain $\frac{1}{\varepsilon} D^{-1} P_3 D^{-1} C^T$ has the structure of a high-gain observer ([7], [21]). This was exploited in [21], using a parameterization similar to the above, to show global exponential

[1] *Global boundedness can always be achieved by saturating* $\hat{x}$ *and* $\hat{z}$ *outside a compact region of interest.*

stability of the extended Kalman filter. For the fast estimation error we use the standard rescaling

$$\xi_i = \frac{x_i - \hat{x}_i}{\varepsilon^{r-i}} \tag{2.18}$$

for $i = 1, \cdots, r$. Thus, $x - \hat{x} = D_2\xi$, where $D_2 = diag[\varepsilon^{r-1}, \varepsilon^{r-2}, \cdots, 1]$. Define the estimation error for the internal states by $\eta = z - \hat{z}$. The closed-loop system under output feedback can now be written in the standard singularly perturbed form

$$\begin{aligned}
\dot{z} &= A_{11}z + Gx_1 && (2.19)\\
\dot{x} &= Ax + B\phi(z, x, \gamma(z - \eta, x - D_2\xi)) && (2.20)\\
\dot{\eta} &= A_{11}\eta + \varepsilon^{r-1}(G - P_2C^T)\xi_1 && (2.21)\\
\varepsilon\dot{\xi} &= (A - P_3C^TC)\xi + \varepsilon B\delta(z, x, \eta, D_2\xi) && (2.22)\\
\dot{P}_1 &= A_{11}P_1 + P_1A_{11}^T + A_{12}P_2^T + P_2A_{12}^T + Q_1 - P_2C^TCP_2^T && (2.23)\\
\varepsilon\dot{P}_2 &= P_2(A + \varepsilon A_{0\varepsilon})^T - P_2C^TCP_3 + A_{12}P_3 + \varepsilon A_{11}P_2 \\
&\quad + \varepsilon P_1A_{21}^TD + \varepsilon Q_2D && (2.24)\\
\varepsilon\dot{P}_3 &= (A + \varepsilon A_{0\varepsilon})P_3 + P_3(A + \varepsilon A_{0\varepsilon})^T + Q_3 - P_3C^TCP_3 \\
&\quad + \varepsilon^2(P_2^TA_{21}^TD + DA_{21}P_2) && (2.25)
\end{aligned}$$

where $\delta = \phi(z, x, u) - \phi(\hat{z}, \hat{x}, u)$ and

$$A_{0\varepsilon} = \begin{bmatrix} 0 & \cdots & \cdots & 0 \\ \vdots & & & \vdots \\ 0 & & & 0 \\ \varepsilon^{r-1}d\phi_1 & \varepsilon^{r-2}d\phi_2 & \cdots & d\phi_r \end{bmatrix}$$

Note that $A_{12}D^{-1} = A_{12}$. Equations (2.19)-(2.21) and (2.23) characterize the "slow" dynamics and (2.22), (2.24), and (2.25) the "fast" ones. In the next two subsections we present stability results on the closed-loop system under EKF feedback (2.19)-(2.25).

2.2.1 Boundedness of the Riccati Equation

We begin by studying the Riccati equation (2.23)-(2.25) alone. To do so, we will treat A_{21} and A_{22} as bounded time-varying matrices and use perturbation theory to argue that the solutions of (2.23)-(2.25) are bounded. We have the following result.

Theorem 2.1 *Consider the closed-loop system (2.19)-(2.25) under output feedback. Let Assumptions 2.1-2.3 hold and let $\mathcal{M}$ and $\mathcal{N}$ be any compact subsets of $\mathbb{R}^{\ell+r+\ell}$ and $\mathbb{R}^r$ respectively. Then, for trajectories $(z, x, \eta) \times \hat{x}$ starting in $\mathcal{M} \times \mathcal{N}$ there exists ε_1^* such that, for all $0 < \varepsilon \leq \varepsilon_1^*$, $P(t)$ is bounded and $P_3(t)$ is positive definite for all $t \geq 0$, uniformly in ε.*

Proof: First, it can be checked that for all $(\hat{z}, \hat{x}) \in \mathbb{R}^{\ell+r}$ the pairs $(A_e(\hat{z}, \hat{x}), C_e)$ and $(A_e(\hat{z}, \hat{x}), \sqrt{Q})$ in (2.6) satisfy the notions of uniform detectability and uniform controllability given in [9], respectively. As a consequence, there exists a bounded solution $P(t)$ to (2.6) and also (2.23)-(2.25) through the rescaling (2.15). However, the bounds obtained have dependence on ε. For the analysis we need to show that the solution $P(t)$ of the rescaled Riccati equation (2.23)-(2.25) is bounded uniformly in ε. We begin by viewing the following equations as a nominal model ($\varepsilon = 0$ on the right hand side) of (2.23)-(2.25)

$$\dot{\bar{P}}_1 = A_{11}\bar{P}_1 + \bar{P}_1 A_{11}^T + A_{12}\bar{P}_2^T + \bar{P}_2 A_{12}^T + Q_1 - \bar{P}_2 C^T C \bar{P}_2^T \tag{2.26}$$

$$\varepsilon\dot{\bar{P}}_2 = \bar{P}_2(A - \bar{P}_3 C^T C)^T + A_{12}\bar{P}_3 \tag{2.27}$$

$$\varepsilon\dot{\bar{P}}_3 = A\bar{P}_3 + \bar{P}_3 A^T + Q_3 - \bar{P}_3 C^T C \bar{P}_3 \tag{2.28}$$

By standard results on Riccati equations [40], with Q_3 positive definite and (A, C) observable, (2.28) has a unique limiting solution $P_3^+ = P_3^{+T} > 0$ such that

$$A^+ \stackrel{def}{=} A - P_3^+ C^T C$$

is a Hurwitz matrix. Moreover, $\bar{P}_3(t)$ approaches P_3^+ exponentially fast [14], i.e.,

$$\|\bar{P}_3(t) - P_3^+\| \leq g_3 e^{-\sigma_3 t/\varepsilon} \tag{2.29}$$

for some positive constants g_3 and σ_3. For equation (2.27) it is easy to show that the limiting solution is given by

$$P_2^+ = -A_{12}P_3^+(A - P_3^+C^TC)^{-T} = A_{12} \tag{2.30}$$

where the second equality follows from $A_{12} = GC$, $CA^T = 0$, and $C(I - C^TC) = 0$. Rewrite (2.27) as

$$\varepsilon\dot{\bar{P}}_2 = \left(\bar{P}_2 - P_2^+\right)\left[A^+ - (\bar{P}_3 - P_3^+)C^TC\right]^T \tag{2.31}$$

By (2.29) and the fact that A^+ is a Hurwitz matrix we have that

$$\|\bar{P}_2(t) - P_2^+\| \leq g_2 e^{-\sigma_2 t/\varepsilon} \tag{2.32}$$

for some positive constants g_2 and σ_2. Since $\bar{P}_2(t)$ is bounded and A_{11} is Hurwitz, the solution to the Lyapunov equation (2.26) is bounded. Indeed we have

$$\|\bar{P}_1(t) - P_1^+\| \leq g_1 e^{-\sigma_1 t} \tag{2.33}$$

where P_1^+ is the limiting solution to (2.26) and g_1 and σ_1 are positive constants. Hence, each $\bar{P}_i$ is bounded uniformly in ε for all $t \geq 0$. We point out that equations (2.23)-(2.25) are ε perturbations of (2.26)-(2.28). We argue for the boundedness of $P(t)$ studying the error

$$\tilde{P} = P - \bar{P}$$

between the full system and the nominal system. Since, $\bar{P}(t)$ is bounded for all $t \geq 0$ we have that $\|\bar{P}(t)\| \leq \bar{N}$ for some positive constant $\bar{N}$. Consider the system

$$\begin{aligned}
\dot{\tilde{P}}_1 &= A_{11}\tilde{P}_1 + \tilde{P}_1 A_{11}^T + (A_{12} - \bar{P}_2 C^T C)\tilde{P}_2^T + \tilde{P}_2(A_{12} - \bar{P}_2 C^T C)^T \\
&\quad -\tilde{P}_2 C^T C \tilde{P}_2^T \qquad (2.34) \\
\varepsilon\dot{\tilde{P}}_2 &= \tilde{P}_2 A_2^T(t) + (A_{12} - \bar{P}_2 C^T C)\tilde{P}_3 - \tilde{P}_2 C^T C \tilde{P}_3 + \varepsilon Q_2 D \\
&\quad +\varepsilon A_{11}(\tilde{P}_2 + \bar{P}_2) + \varepsilon(\tilde{P}_1 + \bar{P}_1)A_{21}^T D + \varepsilon(\tilde{P}_2 + \bar{P}_2)A_{0\varepsilon}^T \qquad (2.35) \\
\varepsilon\dot{\tilde{P}}_3 &= A_2(t)\tilde{P}_3 + \tilde{P}_3 A_2^T(t) - \tilde{P}_3 C^T C \tilde{P}_3 + \varepsilon A_{0\varepsilon}(\tilde{P}_3 + \bar{P}_3) \\
&\quad +\varepsilon(\tilde{P}_3 + \bar{P}_3)A_{0\varepsilon}^T + \varepsilon^2(\tilde{P}_2 + \bar{P}_2)A_{21}^T D + \varepsilon^2 D A_{21}(\tilde{P}_2 + \bar{P}_2)^T \qquad (2.36)
\end{aligned}$$

where

$$A_2(t) = A^+ - (\bar{P}_3 - P_3^+)C^T C \qquad (2.37)$$

We use the *vec* operator to write (2.34)-(2.36) as a system of vector equations. This operator transforms a matrix to a vector by stacking the columns of the matrix from left to right starting with the first column on top. Let $\pi_i = vec(\tilde{P}_i)$, $\bar{\pi}_i = vec(\bar{P}_i)$, $\pi_{2T} = vec(\tilde{P}_2^T)$, $\bar{\pi}_{2T} = vec(\bar{P}_2^T)$, $q_2 = vec(Q_2)$, and $q_{2T} = vec(Q_2^T)$. Also, let

$$\pi_\varepsilon = \begin{bmatrix} \pi_2 \\ \pi_{2T} \\ \pi_3 \end{bmatrix}$$

Consider the following identity from Kronecker matrix algebra ([10], Ch. 7)

$$vec(ABC) = (C^T \otimes A)vec(B) \qquad (2.38)$$

Using this identify we can arrive at the following standard singularly perturbed vector equations

$$\dot{\pi}_1 = M_1\pi_1 + (M_2 + M_3(\pi_2))\,\pi_2 + M_4\pi_{2T} \tag{2.39}$$

$$\begin{aligned}\varepsilon\dot{\pi}_\varepsilon &= (N_1 + N_2(t) + N_3(\pi_\varepsilon))\,\pi_\varepsilon + \varepsilon\,(N_4\pi_\varepsilon + N_4\bar{\pi}_\varepsilon + N_5\pi_1 + N_5\bar{\pi}_1) \\ &\quad +\varepsilon N_q(q_2, q_{2T})\end{aligned} \tag{2.40}$$

where the matrices M_i and N_i are listed in Appendix A. By standard results on Kronecker products, we have that M_1 and N_1 are Hurwitz matrices and

$$\|M_3(\pi_2)\| \leq m_1\|\pi_2\| \quad , \quad \|N_3(\pi_\varepsilon)\| \leq n_1\|\pi_\varepsilon\| \tag{2.41}$$

for some positive constants m_1 and n_1. Furthermore, as discussed in Appendix A we have

$$\|N_2(t)\| \leq g_4 e^{-\sigma_4 t/\varepsilon} \tag{2.42}$$

for some positive constants g_4 and σ_4. Also, the matrices M_2, M_4, N_4, N_5, and $N_q(q_2, q_{2T})$ are bounded with bounds that are independent of ε. Consider (2.40) with $\varepsilon = 0$ on the right hand side

$$\varepsilon\dot{\pi}_\varepsilon = (N_1 + N_2(t) + N_3(\pi_\varepsilon))\,\pi_\varepsilon \tag{2.43}$$

It can be shown that the origin

$$\pi = \begin{bmatrix} \pi_1 \\ \pi_\varepsilon \end{bmatrix} = 0$$

of (2.39) and (2.43) is locally exponentially stable. Let S_1 and S_ε be the positive definite solutions to

$$S_1 M_1 + M_1^T S_1 = -I$$

and

$$S_\varepsilon N_1 + N_1^T S_\varepsilon = -I$$

Using $V = V_1(\pi_1) + V_2(\pi_\varepsilon)$ with

$$V_1 = \pi_1^T S_1 \pi_1 \quad and \quad V_2 = \pi_\varepsilon^T S_\varepsilon \pi_\varepsilon$$

it can be shown that there exist an ε_1 such that for all $0 < \varepsilon \leq \varepsilon_1$

$$\dot{V} \leq -c_2\|\pi\|^2 - \frac{c_3}{\varepsilon}\|\pi_\varepsilon\|^2 \tag{2.44}$$

in the set $\Omega_1 \stackrel{def}{=} \{\|\pi\| \leq c_1\}$ for some positive constants c_1, c_2, and c_3 independent of ε. Since (2.40) is an ε-perturbation of (2.43) we can use V as a Lyapunov function for (2.39)-(2.40) to arrive at

$$\dot{V} \leq -c_2\|\pi\|^2 - \left(\frac{c_3}{\varepsilon} - c_4\right)\|\pi_\varepsilon\|^2 + c_5\|\pi_\varepsilon\| + c_6\|\pi_\varepsilon\|\|\pi_1\| \tag{2.45}$$

where c_4, c_5, and c_6 are positive constants independent of ε. It is easy to show that there exist an ε_2 such that, for all $0 < \varepsilon \leq \varepsilon_2$ and all $\{\|\pi_\varepsilon\| \geq \varepsilon c_7\}$, $\dot{V} \leq 0$ where c_7 is independent of ε. Hence, we have that for ε sufficiently small the set

$$\Omega_\rho \stackrel{def}{=} \{\|\pi\| \leq \varepsilon\rho\}$$

is positively invariant and $\Omega_\rho \subset \Omega_1$, where ρ is some positive constant independent of ε. Since $\tilde{P}(0) = 0$, the solution starts in Ω_ρ. Also, since $\|\tilde{P}\| \leq c_8\|\pi\|$ for some $c_8 > 0$, it follows that

$$\|P\| \leq \|\bar{P}\| + \|\tilde{P}\| \leq \bar{N} + \varepsilon\rho c_8 \quad , \quad \forall \ t \geq 0$$

Therefore, $P(t)$ is bounded.

To show that $P_3(t)$ is positive definite for all $t \geq 0$ we can rewrite (2.25) in the following way

$$\varepsilon \dot{P}_3 = A_3(t)P_3 + P_3 A_3(t)^T + P_3 C^T C P_3 + Q_3 + \varepsilon \Psi_3(P_2, P_3, t, \varepsilon) \quad (2.46)$$

where

$$A_3(t) = A^+ - (\bar{P}_3 - P_3^+)C^T C - \tilde{P}_3 C^T C$$

and

$$\Psi_3 = \varepsilon D A_{21} P_2 + \varepsilon P_2^T A_{21}^T D + A_{0\varepsilon} P_3 + P_3 A_{0\varepsilon}^T$$

We note that $A_3(t)$ is bounded by some constant L for all $t \geq 0$. It can be shown that the corresponding state transition matrix satisfies

$$\|\Phi_3(t, \tau; \varepsilon)x\| \geq \|x\| e^{-2L(t-\tau)/\varepsilon} \quad (2.47)$$

Let

$$Q_P(t) = Q_3 + P_3 C^T C P_3 + \varepsilon \Psi_3(P_2, P_3, t, \varepsilon) \quad (2.48)$$

From the boundedness of Ψ_3, there exists ε_3 such that

$$0 < \kappa_1 I \leq Q_P(t) \leq \kappa_2 I$$

for all $0 < \varepsilon \leq \varepsilon_3$ where κ_1 and κ_2 are positive constants independent of ε. Also, since $P_3(0)$ is chosen to be positive definite we have

$$P_3(0) \geq \rho I > 0$$

for some positive constant ρ. Using the relation

$$x^T P_3(t)x = x^T \Phi_3(t,0;\varepsilon)P_3(0)\Phi_3^T(t,0;\varepsilon)x + \frac{1}{\varepsilon}\int_0^t x^T \Phi_3(t,\tau;\varepsilon)Q_P(\tau)\Phi_3^T(t,\tau;\varepsilon)x d\tau$$

along with (2.47) we can arrive at

$$x^T P_3(t)x \geq \left[\rho e^{-2Lt/\varepsilon} + \frac{\kappa_1}{2L}\left(1 - e^{-2Lt/\varepsilon}\right)\right]\|x\|^2 \tag{2.49}$$

Thus, there exist a positive constant c_9 independent of ε such that

$$x^T P_3(t)x \geq c_9\|x\|^2 \tag{2.50}$$

Therefore, $P_3(t)$ is positive definite for all $t \geq 0$. Taking $\varepsilon_1^* \leq \min\{\varepsilon_1, \varepsilon_2, \varepsilon_3\}$ completes the proof. $\lhd$

2.2.2 Closed-Loop System Stability

We are ready to state our results on the stability of the closed-loop system under EKF feedback.

Theorem 2.2 *Consider the closed-loop system (2.19)-(2.25) under output feedback. Let Assumptions 2.1-2.3 hold and let $\mathcal{M}$ and $\mathcal{N}$ be any compact subsets of $\mathbb{R}^{\ell+r+\ell}$ and $\mathbb{R}^r$, respectively. Then, for trajectories $(z, x, \eta) \times \hat{x}$ starting in $\mathcal{M} \times \mathcal{N}$ there exists ε_2^* such that, for all $0 < \varepsilon \leq \varepsilon_2^*$, the following holds:*

- *the origin $(z = \eta = 0, x = \xi = 0)$ of the closed-loop system is asymptotically stable and $\mathcal{M} \times \mathcal{N}$ is a subset of its region of attraction.*
- *The origin of the estimation error equations (2.21)-(2.22) is exponentially stable.*

Proof: In Theorem 2.1 it is shown that there exits ε_1^* such that, for all $0 < \varepsilon \leq \varepsilon_1^*$, $P(t)$ is bounded and $P_3(t)$ is positive definite for all $t \geq 0$. In particular

$$\beta_1 I \leq P_3(t) \leq \beta_2 I \tag{2.51}$$

where β_1 and β_2 are positive constants independent of ε. It can be seen that

$$S_3 = P_3^{-1}$$

satisfies

$$\begin{aligned} \varepsilon \dot{S}_3 &= -(A + \varepsilon A_{0\varepsilon})^T S_3 - S_3(A + \varepsilon A_{0\varepsilon}) + C^T C - S_3 Q_3 S_3 \\ &\quad -\varepsilon^2 S_3(DA_{21}P_2 + P_2^T A_{21}^T D)S_3 \end{aligned} \tag{2.52}$$

By the argument above S_3 will have a bounded, positive definite, symmetric solution for all $t \geq 0$. Hence,

$$\beta_3 I \leq S_3(t) \leq \beta_4 I \tag{2.53}$$

where β_3 and β_4 are positive constants independent of ε.

Boundedness and Ultimate Boundedness

Following analysis similar to [7] we argue that the trajectories (χ, η, ξ) are bounded and satisfy $\|(\chi(t), \eta(t))\| + \|\xi(t)\| \leq \mu$ for any $\mu > 0$ after some finite time $T^*(\mu)$. Denote the right hand side of (2.19)-(2.21) as

$$\dot{\chi} = f(\chi, \eta, D_2\xi) \tag{2.54}$$

$$\dot{\eta} = A_{11}\eta + \varepsilon^{r-1}(G - P_2 C^T)\xi_1 \tag{2.55}$$

With $\xi = 0$ we have from Assumptions 2.1 and 2.2 that (2.54)-(2.55) has a globally asymptotically stable equilibrium at the origin. Thus, there exists a positive definite radially unbounded function $V_1(\chi, \eta)$ and a positive definite function $U(\chi, \eta)$ such that

$$\frac{\partial V_1}{\partial \chi} f(\chi, \eta, 0) + \frac{\partial V_1}{\partial \eta} A_{11} \eta \leq -U(\chi, \eta) \tag{2.56}$$

for all χ and η. Let $\mathcal{M}$ be any compact subset of $\mathbb{R}^{\ell+r+\ell}$. Choose a positive constant c such that $c > max_{(\chi,\eta)\in\mathcal{M}} V_1(\chi, \eta)$. Then $\mathcal{M}$ is in the interior of the set $\Omega_c = \{V_1(\chi, \eta) \leq c\} \subset \mathbb{R}^{\ell+r+\ell}$. Let $\Lambda = \Omega_c \times \{W \leq \rho\varepsilon^2\}$. Due to the global boundedness of f and δ in $\hat{x}$, for all $(\chi, \eta) \in \Omega_c$ and $\xi \in \mathbb{R}^r$, we have

$$\|f(\chi, \eta, \xi)\| \leq k_1 \quad , \quad \|\delta(z, x, \eta, D_2\xi)\| \leq k_2 \tag{2.57}$$

where k_1 and k_2 are positive constants independent of ε. Furthermore, for any $0 < \tilde{\varepsilon} < 1$, there is L_1, independent of ε, such that for all $(\chi, \eta, \xi) \in \Lambda$ and every $0 < \tilde{\varepsilon} \leq \varepsilon$ we have,

$$\|f(\chi, \eta, \xi) - f(\chi, \eta, 0)\| \leq L_1 \|\xi\| \tag{2.58}$$

Letting $W(\xi) = \xi^T S_3 \xi$ and using (2.52) it can be shown that

$$\begin{aligned} \dot{W} \leq & -\frac{1}{\varepsilon}\xi^T \Big[C^T C + S_3 Q_3 S_3 + \varepsilon^2 S_3 (D A_{21} P_2 + P_2^T A_{21}^T D) S_3 + \varepsilon A_{0\varepsilon}^T S_3 \\ & + \varepsilon S_3 A_{0\varepsilon}\Big]\xi + \delta^T B^T S_3 \xi + \xi^T S_3 B \delta \end{aligned} \tag{2.59}$$

Due to the boundedness of P_2 from Theorem 2.1 and the global boundedness of $A_{0\varepsilon}$ and A_{21} in $\hat{x}$ and $\hat{z}$ we have

$$\|A_{0\varepsilon}\| \leq k_3 \quad , \quad \|D A_{21} P_2\| \leq k_4$$

for some positive constants k_3 and k_4. Thus, (2.59) simplifies to

$$\dot{W} \leq -\frac{1}{\varepsilon}(\beta_3^2\|Q_3\| - 2\varepsilon\beta_4 k_3 - 2\varepsilon^2\beta_4^2 k_4)\|\xi\|^2 + 2\beta_4\|\delta\|\|\xi\|$$

Therefore, with ε_4 chosen such that $2\varepsilon_4\beta_4 k_3 + 2\varepsilon_4^2\beta_4^2 k_4 \leq \frac{1}{2}\beta_3^2\|Q_3\|$, we have

$$\dot{V}_1 \leq -U(\chi,\eta) + L_1 L_2\|\xi\| + \varepsilon^{r-1}L_2\|G - P_2C^T\||\xi_1| \leq -U(\chi,\eta) + \varepsilon k_5 + \varepsilon^r k_6 \quad (2.60)$$

$$\dot{W} \leq -\frac{k_7}{2\varepsilon}\|\xi\|^2 + 2\beta_4\|\delta\|\|\xi\| \leq -\frac{k_7}{4\varepsilon}\|\xi\|^2 + 2\beta_4 k_2\|\xi\| \quad (2.61)$$

for all $0 < \varepsilon \leq \varepsilon_4$, and all $(\chi,\eta,\xi) \in \Omega_c \times \{W(\xi) \leq \rho\varepsilon^2\}$, where k_5, k_6, and k_7 are given by

$$k_5 = L_1 L_2\sqrt{\frac{\rho}{\beta_3}}$$

$$k_6 = L_2\tilde{k}\sqrt{\frac{\rho}{\beta_3}}$$

and $k_7 = \beta_3^2\|Q_3\|$ with $\rho = 64k_2^2\beta_4^3/k_7^2$ and L_2 an upper bound on $[\partial V_1/\partial\chi \ , \ \partial V_1/\partial\eta]$ in Ω_c. Also, from the boundedness of P_2

$$\|G - P_2C^T\| \leq \tilde{k} \quad (2.62)$$

for some positive constant $\tilde{k}$. Taking $\varepsilon_5 k_5 + \varepsilon_5^r k_6 \leq v$, where $v = \min_{(\chi,\eta)\in\partial\Omega_c} U(\chi,\eta)$, we have that, for every $0 < \varepsilon \leq \varepsilon_5$, $\dot{V}_1 \leq 0$ for all $(\chi,\eta,\xi) \in \{V_1(\chi,\eta) = c\} \times \{W(\xi) \leq \rho\varepsilon^2\}$ and $\dot{W} \leq 0$ for all $(\chi,\eta,\xi) \in \Omega_c \times \{W(\xi) = \rho\varepsilon^2\}$. Therefore, Λ is positively invariant.

For $(\chi(0),\eta(0),\hat{x}(0)) \in \mathcal{M} \times \mathcal{N}$, the initial rescaled error $\xi(0)$ satisfies $\|\xi(0)\| \leq k_s/\varepsilon^{r-1}$ for some nonnegative constant k_s dependent on $\mathcal{M}$ and $\mathcal{N}$. Since $(\chi(0),\eta(0))$ is in the interior of Ω_c, we have that

$$\|(\chi(t),\eta(t)) - (\chi(0),\eta(0))\| \leq k_1 t \quad (2.63)$$

while $(\chi(t), \eta(t)) \in \Omega_C$. Therefore, there is a finite time T_0 such that $(\chi(t), \eta(t)) \in \Omega_C$ for all $t \in [0, T_0]$. During this time interval

$$\dot{W} \leq -\frac{k_7}{4\varepsilon}\|\xi\|^2 \quad , \quad for \;\; W(\xi) \geq \rho\varepsilon^2$$

Therefore, it can be shown that

$$W(\xi(t)) \leq \frac{\beta_4 k_s^2}{\varepsilon^{2(r-1)}} exp\left(-\frac{k_7}{4\varepsilon\beta_4}t\right) \tag{2.64}$$

Choose ε_6 small enough that

$$T(\varepsilon) \stackrel{def}{=} \frac{4\varepsilon\beta_4}{k_7} ln\left(\frac{\beta_4 k_s^2}{\rho\varepsilon^{2r}}\right) \leq \frac{1}{2}T_0$$

Such an ε exists since $T(\varepsilon) \to 0$ as $\varepsilon \to 0$. Therefore, $W(\xi(t)) \leq \rho\varepsilon^2$ for every $0 < \varepsilon \leq \varepsilon_6$. Choosing $\varepsilon_1' = \min\{\varepsilon_1^*, \tilde{\varepsilon}, \varepsilon_4, \varepsilon_5, \varepsilon_6\}$ guarantees that, for every $0 < \varepsilon \leq \varepsilon_1'$, the trajectory $(\chi(t), \eta(t), \xi(t))$ enters Λ during the time interval $[0, T(\varepsilon)]$ and remains there for all $t \geq T(\varepsilon)$. Thus, the trajectory is bounded for all $t \geq T(\varepsilon)$. Also, for $t \in [0, T(\varepsilon)]$, the trajectory is bounded by equations (2.63) and (2.64).

To show ultimate boundedness, we begin by noting that inside Λ the trajectory ξ is $O(\varepsilon)$. Thus, we can find a $\varepsilon_7 = \varepsilon_7(\mu) \leq \varepsilon_1'$ such that, for every $0 < \varepsilon \leq \varepsilon_7$, we have

$$\|\xi(t)\| \leq \mu/2 \tag{2.65}$$

for all $t \geq T(\varepsilon_7)$. For all $(\chi, \eta, \xi) \in \Lambda$ we have that $\dot{V}_1 \leq -U(\chi, \eta) + \varepsilon k_5 + \varepsilon^r k_6$. Thus, for $(\chi, \eta) \notin \{U(\chi, \eta) \leq 2k_5\varepsilon + 2\varepsilon^r k_6 \stackrel{def}{=} \nu(\varepsilon)\}$

$$\dot{V}_1 \leq -\frac{1}{2}U(\chi, \eta) \tag{2.66}$$

Since $U(\chi,\eta)$ is positive definite and continuous, the set $\{U(\chi,\eta) \leq \nu(\varepsilon)\}$ is compact for sufficiently small ε. Let $c_0(\varepsilon) = \max_{U(\chi,\eta)\leq\nu(\varepsilon)} V_1(\chi,\eta)$; $c_0(\varepsilon)$ is nondecreasing and $\lim_{\varepsilon\to 0} c_0(\varepsilon) = 0$. Consider the compact set $\{V(\chi,\eta) \leq c_0(\varepsilon)\}$. We have $\{U(\chi,\eta) \leq \nu(\varepsilon)\} \subset \{V_1(\chi,\eta) \leq c_0(\varepsilon)\}$. Choose $\varepsilon_8 = \varepsilon_8(\mu) \leq \varepsilon_1'$ small enough such that, for all $\varepsilon \leq \varepsilon_8$, the set $\{U(\chi,\eta) \leq \nu(\varepsilon)\}$ is compact, the set $\{V_1(\chi,\eta) \leq c_0(\varepsilon)\}$ is in the interior of Ω_c, and

$$\{V_1(\chi,\eta) \leq c_0(\varepsilon)\} \subset \{\|(\chi,\eta)\| \leq \mu/2\} \tag{2.67}$$

Then, for all $(\chi,\eta) \in \Omega_c$, but $(\chi,\eta) \notin \{V_1(\chi,\eta) \leq c_0(\varepsilon)\}$, we have an inequality similar to (2.66). Therefore, the set $\{V_1(\chi,\eta) \leq c_0(\varepsilon)\} \times \{W(\xi) \leq \rho\varepsilon^2\}$ is positively invariant and every trajectory in $\Omega_c \times \{W(\xi) \leq \rho\varepsilon^2\}$ reaches $\{V_1(\chi,\eta) \leq c_0(\varepsilon)\} \times \{W(\xi) \leq \rho\varepsilon^2\}$ in finite time. Thus,

$$\|(\chi(t),\eta(t))\| \leq \mu/2 \tag{2.68}$$

for all $t \geq \tilde{T}$ for a finite time $\tilde{T} = \tilde{T}(\mu)$. Taking $\varepsilon_2' = \varepsilon_2'(\mu) = \min\{\varepsilon_7, \varepsilon_8\}$ it can be shown that

$$\|(\chi,\eta)\| + \|\xi\| \leq \mu$$

for all $t \geq T^*$ where $T^* = \max\{T(\varepsilon_7), \tilde{T}\}$.

Exponential Stability of the Estimation Error

From the ultimate boundedness of $(z,x,\hat{z},\hat{x})$ we can work locally to argue asymptotic stability of the closed-loop system. We have that $\|\delta(z,x,\eta,D_2\xi)\| \leq L_3\|\eta\| + L_4\|\xi\|$ for all $(\chi,\eta) \in B(0,\mu) \times \{\|\xi\| \leq \mu\}$ where μ is the ultimate bound from above and L_3 and L_4 are positive constants. Let

$$V_2 = \eta^T P_L \eta + \xi^T S_3 \xi \tag{2.69}$$

be a Lyapunov function candidate for the estimation error, where the positive definite matrix P_L satisfies $P_L A_{11} + A_{11}^T P_L = -I$. Using (2.55), the first inequality of (2.61), and (2.62) it can be shown that

$$\dot{V}_2 \leq -[\|\eta\| \quad \|\xi\|] \begin{bmatrix} 1 & -\varepsilon^{r-1}\tilde{k}\|P_L\| - \beta_4 L_3 \\ -\varepsilon^{r-1}\tilde{k}\|P_L\| - \beta_4 L_3 & \frac{k_7}{2\varepsilon} - 2\beta_4 L_4 \end{bmatrix} \begin{bmatrix} \|\eta\| \\ \|\xi\| \end{bmatrix}$$

It is easy to show that there exist ε_9 such that for all $0 < \varepsilon \leq \varepsilon_9$, the matrix above is positive definite. Thus, for all $(\chi(0), \eta(0), \xi(0))$ starting in $\mathcal{M} \times \mathcal{N}$ the estimation error, (η, ξ), converges exponentially.

Asymptotic Stability

Let $\zeta = [\eta \quad \xi]^T$. Asymptotic stability of the closed-loop system follows from the composite Lyapunov function

$$V(\chi, \eta, \xi) = \theta V_1(\chi, \eta) + (V_2(\zeta))^{1/2} \tag{2.70}$$

with $\theta > 0$. From the first inequality of (2.60) we have

$$\dot{V} \leq -\theta U(\chi, \eta) + \theta k_8 \|\zeta\| - k_9 \|\zeta\| \tag{2.71}$$

for $k_8 = L_1 L_2 + \varepsilon^{r-1} L_2 \tilde{k}$ and a positive constant k_9. Taking $\theta \leq k_9/2k_8$ yields asymptotic stability. Finally, choosing $\varepsilon_2^* = \min\{\varepsilon_2', \varepsilon_9\}$ completes the proof. $\triangleleft$

2.3 Comparison

In this section we use numerical examples to further study the EKF and compare the EKF that has a time-varying gain with a HGO that uses a fixed-gain. This is done by dividing

the section into three subsections. First, we examine the choice of control saturation or estimate saturation to globally bound the control in EKF feedback. We then examine the possible closed-loop stability advantages of using time-varying gains versus fixed gains. Finally, we present some results on the choice of initial condition of the Riccati equation to suppress peaking at the initial time instants.

2.3.1 Control Versus Estimate Saturation in the EKF

The stability results for locally Lipschitz nonlinear systems in Section 2.2 came at the expense of sacrificing global results for semiglobal ones. An essential factor in this sacrifice is the effect of peaking on the closed-loop system. In high-gain observers, peaking is caused by the special structure of the observer gain

$$H^T = \begin{bmatrix} \frac{\alpha_1}{\varepsilon} & \frac{\alpha_2}{\varepsilon^2} & \cdots & \frac{\alpha_r}{\varepsilon^r} \end{bmatrix} \tag{2.72}$$

For high-gain observers, peaking can be overcome by globally bounding the control outside a compact region of interest [26]. This can be done by using a saturation function on the controller. For the case of the extended Kalman filter, globally bounding the control alone is not enough. Peaking in the estimates may induce numerical difficulties in the solution to the Riccati differential equation (RDE) as the following example shows. Consider the system

$$\dot{x}_1 = x_2, \quad \dot{x}_2 = x_3, \quad \dot{x}_3 = x_3^a + u \tag{2.73}$$

and the feedback linearizing controller

$$u = -x_3^a - x_1 - 3x_2 - 3x_3 \tag{2.74}$$

where a will be chosen later on. By saturating the control outside a compact region of interest the effect of peaking can be overcome and the closed-loop system under (fixed-

gain) high-gain observer feedback can recover the response under state feedback as $\varepsilon \rightarrow 0$.

Let $a = 3$. Using the extended Kalman filter parameterized as in the previous section we have that the matrix $A + \varepsilon A_{0\varepsilon}$ in (2.25) is

$$A + \varepsilon A_{0\varepsilon} = \begin{bmatrix} 0 & 1 & 0 \\ 0 & 0 & 1 \\ 0 & 0 & 3\varepsilon\hat{x}_3^2 \end{bmatrix} \tag{2.75}$$

During any occurrence of peaking, the estimate $\hat{x}_3$ will become $O(1/\varepsilon^2)$. Therefore, from (2.75) with saturation only on the control, the RDE will contain unbounded terms as $\varepsilon \rightarrow 0$. This system was simulated for $\varepsilon = 0.01$ with $x_1(0) = 0.9$, $x_2(0) = x_3(0) = 0$, $\hat{x}_1(0) = \hat{x}_2(0) = \hat{x}_3(0) = 0$, $P(0) =$ Identity, $Q_3 = diag[3, 3, 1]$, and with the control saturated outside (-20,20). Denote the EKF gain by

$$H(t) = \frac{1}{\varepsilon} D^{-1} P_3(t) D^{-1} = \begin{bmatrix} h_1(t) \\ h_2(t) \\ h_3(t) \end{bmatrix}$$

Figure 2.1 illustrates the response of the system under control saturation. The peaking in $\hat{x}_3$ induces a very large gain (from the solution to the RDE) and this gain in turn exacerbates the peaking in the estimate. Figure 2.1 shows that the saturation of the control prevents the system states from deviating too much from their initial values, but the estimate $\hat{x}_3$ and the gain $h_3(t)$ have become prohibitively large. These difficulties are overcome by saturating the each estimate outside a compact region of interest. This will globally bound the control and the time-varying terms in the RDE. This approach is shown in Figure 2.2 where we have saturated $\hat{x}_1$, $\hat{x}_2$, and $\hat{x}_3$ outside (-2,2). Figure 2.2 shows that the estimate $\hat{x}_3$ saturates then quickly converges. Also, we see that the control remains bounded, the gain h_3 converges quickly to its steady-state value, and the output x_1 gracefully approaches the origin.

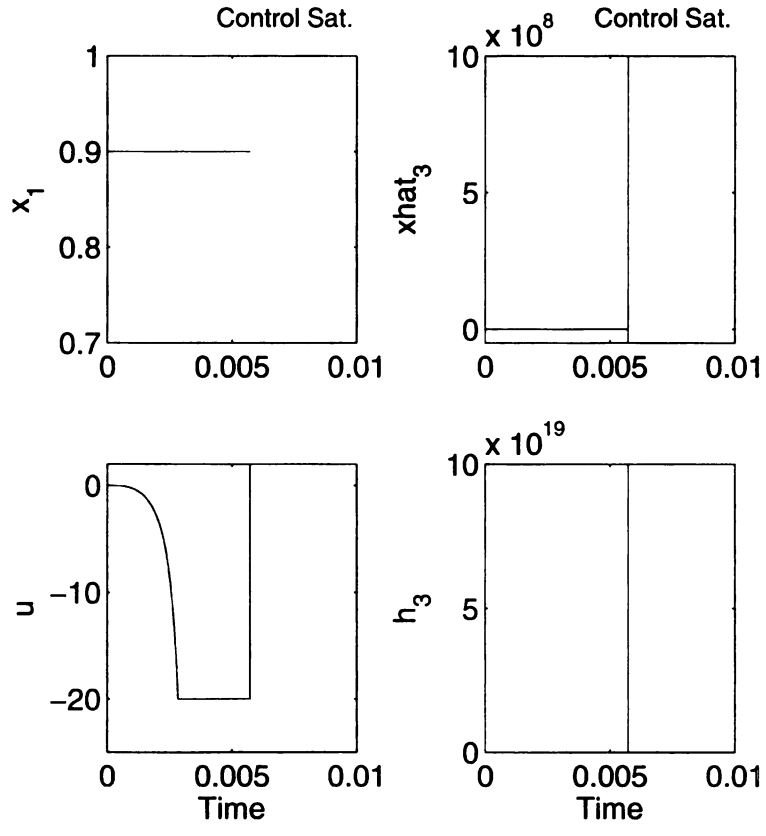

Figure 2.1. Simulation results showing the output x_1, the estimate $\hat{x}_3$, the control u, and the gain $h_3(t)$ for EKF feedback under control saturation only.

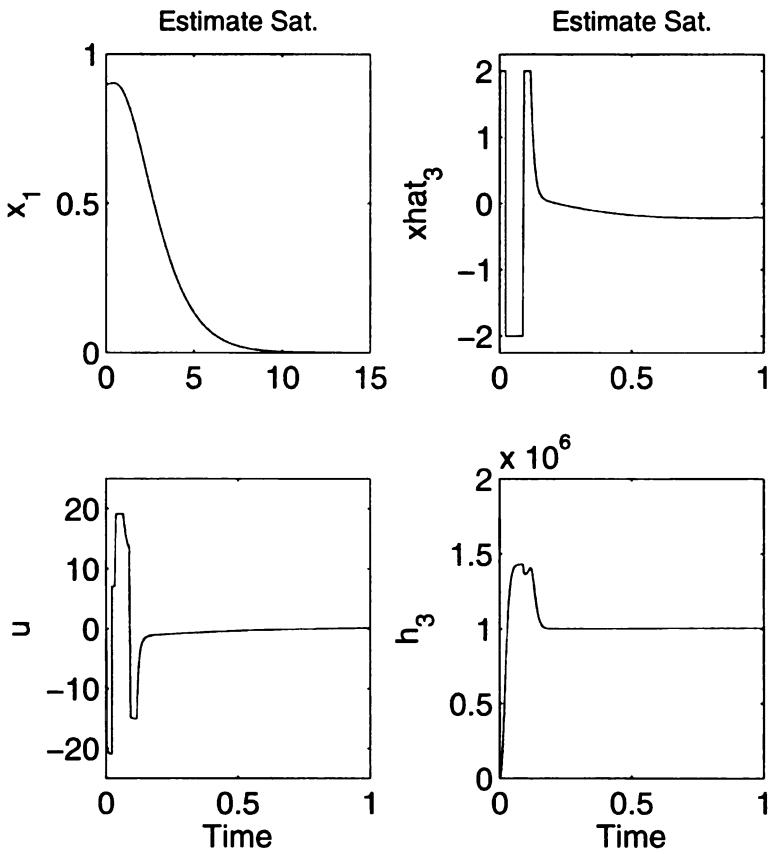

Figure 2.2. Simulation results showing the output x_1, the estimate $\hat{x}_3$, the control u, and the gain $h_3(t)$ for EKF feedback under estimate saturation.

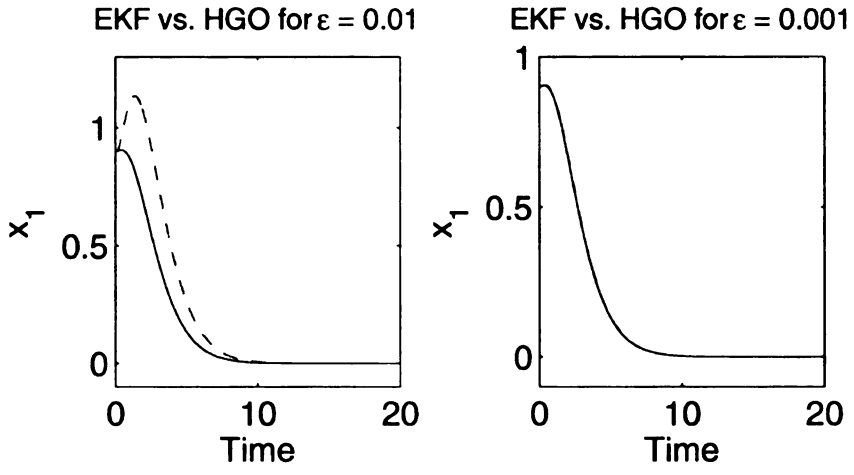

Figure 2.3. Simulation results showing the output x_1, for the EKF (solid) and HGO (dashed) for $\varepsilon = 0.01$ (left) and the EKF and HGO for $\varepsilon = 0.001$ (right).

2.3.2 EKF Versus a Fixed-Gain HGO

Like the HGO, the EKF achieves faster and more accurate reconstruction of the state x as $\varepsilon \rightarrow 0$. It can be shown from analysis similar to the above that the response for the EKF approaches the response for the HGO as $\varepsilon \rightarrow 0$. Here we illustrate this through a numerical example. We use a HGO with the following fixed-value for the gain matrix

$$H^T = \begin{bmatrix} 3/\varepsilon & 3/\varepsilon^2 & 1/\varepsilon^3 \end{bmatrix} \tag{2.76}$$

Figure 2.3 (left) plots the output $y = x_1$ of the closed-loop system for the EKF (solid) and the HGO (dashed) for $x_1(0) = 0.9$ and $\varepsilon = 0.01$ with all other parameters as above. Figure 2.3 (right) shows that the two responses have converged for $\varepsilon = 0.001$.

Considering the foregoing observation we note that for relatively "large" values of ε, the time-varying terms in the Riccati equation will have more influence over the closed-loop response. The question of whether the added complexity of the time-varying gain gives an advantage over a time-invariant gain is examined next. We consider the system

(2.73) for two cases. First, let $a = 3$. Through simulation of the system under state feedback control for initial conditions in the set $\{|x_i| \leq 5\}$, we selected a saturation level of 6 for each estimate. We chose

$$P(0) = \frac{1}{\varepsilon} D^{-1} P_3(0) D^{-1} = \begin{bmatrix} 3/\varepsilon & 3/\varepsilon^2 & 1/\varepsilon^3 \\ 3/\varepsilon^2 & 8/\varepsilon^3 & 3/\varepsilon^4 \\ 1/\varepsilon^3 & 3/\varepsilon^4 & 3/\varepsilon^5 \end{bmatrix} \tag{2.77}$$

which corresponds to the steady-state solution of the Riccati equation. The time-varying terms will cause the solution to deviate from this value. For the HGO we use the same gain matrix H as above, which is the steady-state value of the EKF gain. This system was simulated for $\varepsilon = 0.01$, $x_1(0) = 4.9$. Figure 2.4 shows the response of the output x_1 and the control signal u for the closed-loop system under EKF feedback (left) and the state x_3 and the control u for HGO feedback (right). The time-varying gain was able to stabilize the system where as the figure shows the state x_3 going unstable for the response under high-gain observer feedback. Figure 2.5 shows the response of the EKF gains for this example. The values of the fixed HGO gains are shown as dotted lines for reference. Here, the time-varying terms in the Riccati equation caused the gains to become large during the initial transient before settling close to the values of the HGO gains. This high-gain aided in stabilizing the closed-loop system. The response of the EKF estimates are shown in Figure 2.6. The estimates experience both positive and negative saturation, but quickly settle. We compare these observations with the second case where we now take $a = 2$ in (2.73) and (2.74). Simulating for $\varepsilon = 0.1$ we see that the fixed-gain high-gain observer was able to achieve stability and the time-varying observer went unstable as illustrated in Figure 2.7. This is a result of the sensitivity of the Riccati equation to the transient response of the estimates. Figure 2.8 illustrates this response. Here the estimates $\hat{x}_2$ and $\hat{x}_3$ experience prolonged negative saturation. Figure 2.9 shows the effect this has on the gain response. The gains actually decrease below the values

of the HGO gains for roughly 2.5 seconds. The estimates were unable to recover from saturation quickly enough to prevent the system states from blowing up. Again, these simulations were performed for "large" gains. We emphasize that both the EKF and the HGO can stabilize each system ($a = 2, 3$) by making ε small enough (e.g. $\varepsilon = 0.001$).

Due to linearization, we expect systems under EKF feedback to have an added degree of stability in a neighborhood of the origin of the estimation error $(x - \hat{x})$. To test this we reexamined the above simulation for $a = 2$ and 3 with $x_1(0) = 0.9$, $x_2(0) = x_2(0) = 0$, and $\hat{x}_1(0) = \hat{x}_2(0) = \hat{x}_3(0) = 0$. We ran the simulations for $\varepsilon \leq 1$ to determine the values of ε that made the EKF and HGO closed-loop feedback systems stable and unstable. For $a = 2$ we found that the closed-loop system under EKF feedback was stable for $\varepsilon \leq 1$. On the other hand, for HGO feedback the system was stable for $\varepsilon \leq 0.1$ and unstable for $\varepsilon = 0.2$. For $a = 3$ the EKF feedback system was stable for $\varepsilon \leq 0.01$ and unstable for $\varepsilon = 0.02$. With the HGO, stability was obtained for $\varepsilon \leq 0.001$ and instability resulted with $\varepsilon = 0.002$. These observations are summarized in Tables 2.1 and 2.2. Each of these tables show the values of ε for which the closed-loop system under EKF and HGO feedback are stable and unstable for both local $(x_1(0) - \hat{x}_1(0) = 0.9)$ and nonlocal $(x_1(0) - \hat{x}_1(0) = 4.9)$ estimation error. The tables show that, for these examples, the EKF does indeed have a local stability advantage. However, nonlocally the stability advantage depends upon the system under consideration ($a = 2$ or 3). As another example, we repeated these simulations for the following system

$$\dot{x}_1 = x_2, \quad \dot{x}_2 = x_3, \quad \dot{x}_3 = x_2^a + u \tag{2.78}$$

and the feedback linearizing controller

$$u = -x_2^a - x_1 - 3x_2 - 3x_3 \tag{2.79}$$

where we used $a = 2, 3$ and $P(0)$ and Q_3 were chosen as before. The results are given in

Local				Nonlocal		
	Stable	Unstable			Stable	Unstable
EKF	$\varepsilon \leq 1$	X		EKF	$\varepsilon \leq 0.05$	$\varepsilon = 0.1$
HGO	$\varepsilon \leq 0.15$	$\varepsilon = 0.2$		HGO	$\varepsilon \leq 0.12$	$\varepsilon = 0.15$

Table 2.1. Table showing the values of ε for which the closed-loop systems under EKF and HGO feedback are stable and unstable for system (2.73) with a=2 and a saturation level of 6. Shown are the values for the local results with $x_1(0) = 0.9$ (left) and the nonlocal results with $x_1(0) = 4.9$ (right).

Local				Nonlocal		
	Stable	Unstable			Stable	Unstable
EKF	$\varepsilon \leq 0.01$	$\varepsilon = 0.02$		EKF	$\varepsilon \leq 0.01$	$\varepsilon = 0.02$
HGO	$\varepsilon \leq 0.001$	$\varepsilon = 0.002$		HGO	$\varepsilon \leq 0.001$	$\varepsilon = 0.002$

Table 2.2. Table showing the values of ε for which the closed-loop systems under EKF and HGO feedback are stable and unstable for system (2.73) with a=3 and a saturation level of 6. Shown are the values for the local results with $x_1(0) = 0.9$ (left) and the nonlocal results with $x_1(0) = 4.9$ (right).

Tables 2.3 and 2.4, again for local and nonlocal estimation error. Again, we find that locally, the EKF has an added degree of stability. This added degree of stability for the EKF in a neighborhood of the origin of the estimation error was observed in other examples. However, from the nonlocal results in Tables 2.1-2.4, we see that nonlocally advantages to using a time-varying high-gain observer versus a fixed-gain high-gain observer appear to be at least system dependent.

2.3.3 Initialization of the Riccati Equation

In the previous subsection, the choice of the initial condition of the Riccati equation $P(0)$ was made to correspond to the fixed-gain values of the HGO. This was done in order to compare the effect of the time-varying terms in the EKF. Since the choice of $P(0)$ impacts

	Local				Nonlocal	
	Stable	Unstable			Stable	Unstable
EKF	$\varepsilon \leq 1$	X		EKF	$\varepsilon \leq 0.17$	$\varepsilon = 0.18$
HGO	$\varepsilon \leq 0.7$	$\varepsilon = 0.75$		HGO	$\varepsilon \leq 0.19$	$\varepsilon = 0.2$

Table 2.3. Table showing the values of ε for which the closed-loop systems under EKF and HGO feedback are stable and unstable for system (2.78) with a=2 and a saturation level of 10. Shown are the values for the local results with $x_1(0) = 0.9$ (left) and the nonlocal results with $x_1(0) = 4.9$ (right).

	Local				Nonlocal	
	Stable	Unstable			Stable	Unstable
EKF	$\varepsilon \leq 1$	X		EKF	$\varepsilon \leq 0.03$	$\varepsilon = 0.04$
HGO	$\varepsilon \leq 0.03$	$\varepsilon = 0.04$		HGO	$\varepsilon \leq 0.01$	$\varepsilon = 0.02$

Table 2.4. Table showing the values of ε for which the closed-loop systems under EKF and HGO feedback are stable and unstable for system (2.78) with a=3 and a saturation level of 10. Shown are the values for the local results with $x_1(0) = 0.9$ (left) and the nonlocal results with $x_1(0) = 4.9$ (right).

the transient response of the observer, it can also influence the stability of the closed-loop system. To see this, consider a simulation of (2.73)-(2.74) for $a = 2$, $x_1(0) = 4.9$, the saturation level equal to 6, and $\varepsilon = 0.1$. Under these conditions, and with $P(0)$ chosen as in (2.77), the closed-loop system under EKF feedback was unstable as shown in Figure 2.7. This time let $P(0) = I$, where I is the identity matrix. The plots on the left of Figure 2.10 show the response of the state x_1 and the control u. This figure shows that the closed-loop system is now stable. Now consider the same simulation, but this time with an impulsive-like disturbance of duration $0.01s$ and an amplitude of 300 that is experienced at the input of $\dot{x}_1$ at time $t = 20$. At steady-state the solution to the Riccati equation $P(t)$ will reach a value close to (2.77). Thus, any disturbance that has the effect of resetting the initial conditions of the system will induce a response similar to the case where $P(0)$ was given by (2.77). This can be seen in the plots on the right of Figure

2.10. Here we see that, after the disturbance at $t = 20$, the closed-loop system has once again become unstable. Thus the initial condition of the Riccati equation can improve stability of the closed-loop, but only for the initial transient. Afterwards, it is susceptible to steady-state disturbances.

Finally, we examine the effect of the initial condition of the Riccati equation on peaking in the EKF. Peaking occurs in high-gain observers, not necessarily because the gain is large, but because of the structure of the gain matrix. In Nonlinear Systems [36], it is remarked that peaking is "an intrinsic feature of any high-gain observer with $h_2 >> h_1 >> 1$." We consider once again the system (2.73) and control (2.74) for $a = 3$, $\varepsilon = 0.01$, $x_1(0) = 0.9$, $x_2(0) = x_3(0) = 0$, $\hat{x}_1(0) = \hat{x}_2(0) = \hat{x}_3(0) = 0$, $P(0) = I$, $Q_3 = diag[3, 3, 1]$, and with the estimates saturated outside $(-2, 2)$. Figure 2.11 shows that the estimates undergo peaking during the initial transient. Also shown are the gains h_1, h_2, and h_3. Here, the gains quickly approached values where $h_3 >> h_2 >> h_1 >> 1$. We can choose the initial condition of the Riccati equation to eliminate peaking during the initial transient. Consider the following initial condition for the Riccati equation

$$P(0) = \begin{bmatrix} 1 \times 10^6 & 1 & 1 \\ 1 & 1 & 0 \\ 1 & 0 & 1 \end{bmatrix}$$

With this choice we have that $h_1(0) >> h_2(0)$ and $h_1(0) >> h_3(0)$. Simulation with this initial condition was carried out and the result is shown in Figure 2.12. Comparison with Figure 2.11 shows that the peaking in the estimates has been suppressed. The figure also shows that the gain h_1 very quickly decreases toward its steady-state value. Initialization strategies to overcome peaking have been explored for observers with time-varying gains in [17], [33], and for sampled data output feedback control in [37]. However, as has been pointed out in [17] and [37], these designs may suffer from peaking through impulsive-like disturbances that occur after the initial transient. Therefore, the peaking phenomenon is

relevant irrespective of the initial gain choice.

2.4 Conclusions

Considering the tradeoff between closed-loop stability and peaking in a high-gain observer, we have considered the extended Kalman filter parameterized as a high-gain observer with time-varying gain. We have examined the closed-loop behavior of nonlinear systems in the special normal form under extended Kalman filter feedback. We have shown that the origin of the closed-loop system is asymptotically stable and the origin of the estimation error is exponentially stable. We have seen that in addition to globally bounding the control, the time-varying functions in the Riccati equation must be globally bounded for the Riccati equation to have a well defined solution. We have exploited the two-time scale nature of the partitioned Riccati equation to argue boundedness and positive definiteness of the solution. Through simulation we have compared the closed-loop performance of the time-varying EKF versus the time-invariant HGO. We have seen that the EKF with time-varying gain may provide closed-loop stability advantages over the fixed-gain observer. Globally this will depend on the particular system under consideration. However, the EKF appears to have an advantage locally. Furthermore, the Riccati equation can be initialized to eliminate peaking during the initial transients. Thus, for a particular system, a time-varying HGO may be able to achieve a better balance between closed-loop stability and suppression of peaking than a fixed-gain observer.

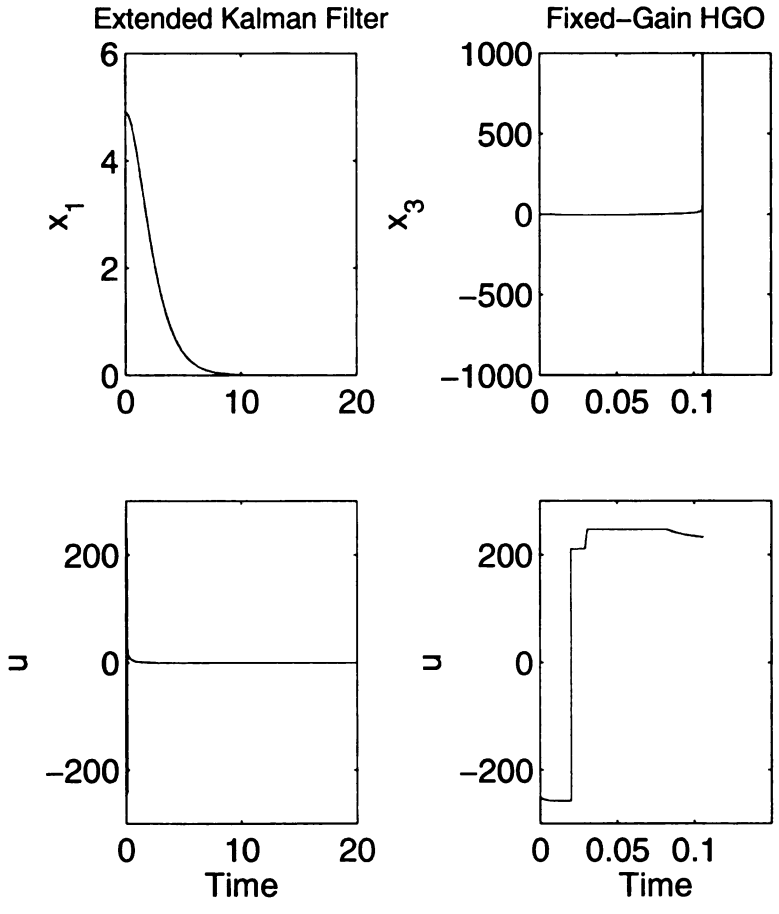

Figure 2.4. Simulation results showing the output x_1 and the control u for EKF feedback and the state x_3 and the control u for HGO feedback for $a = 3$.

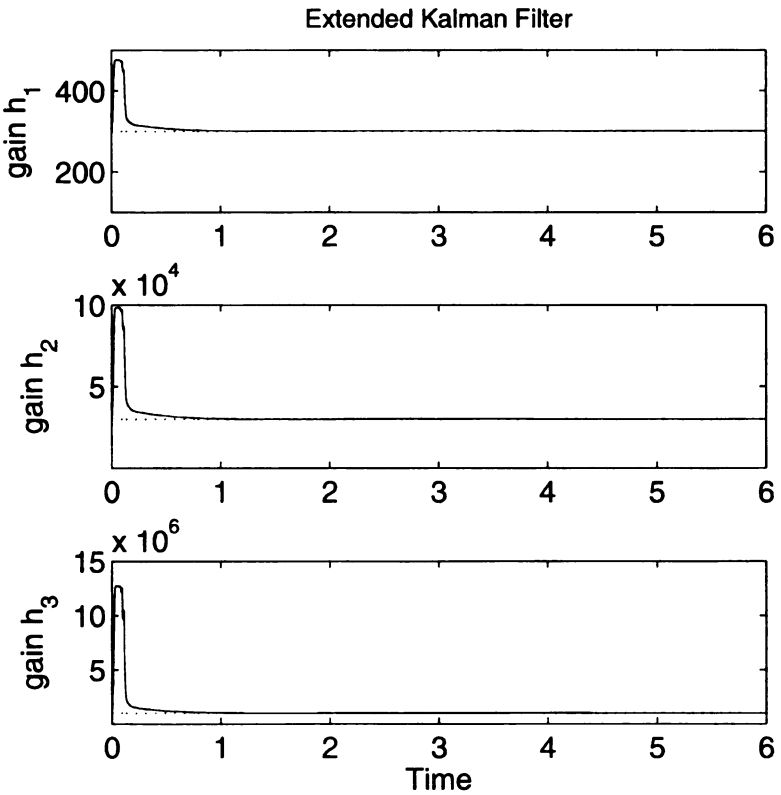

Figure 2.5. Simulation results showing the EKF observer gains h_1, h_2, and h_3 for $a = 3$.

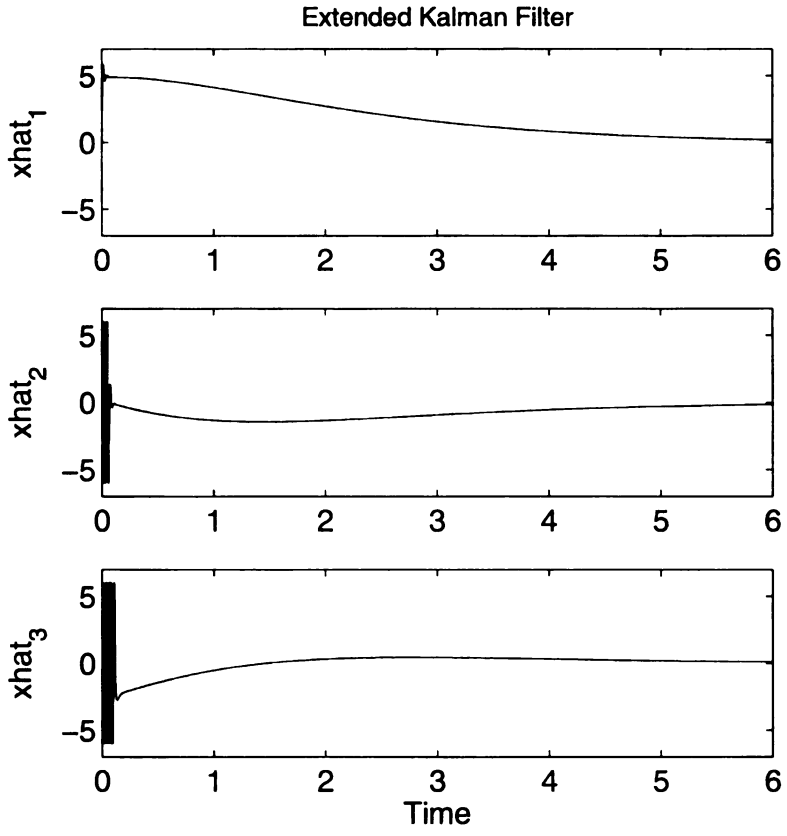

Figure 2.6. Simulation results showing the EKF observer estimates $\hat{x}_1$, $\hat{x}_2$, and $\hat{x}_3$ for $a = 3$.

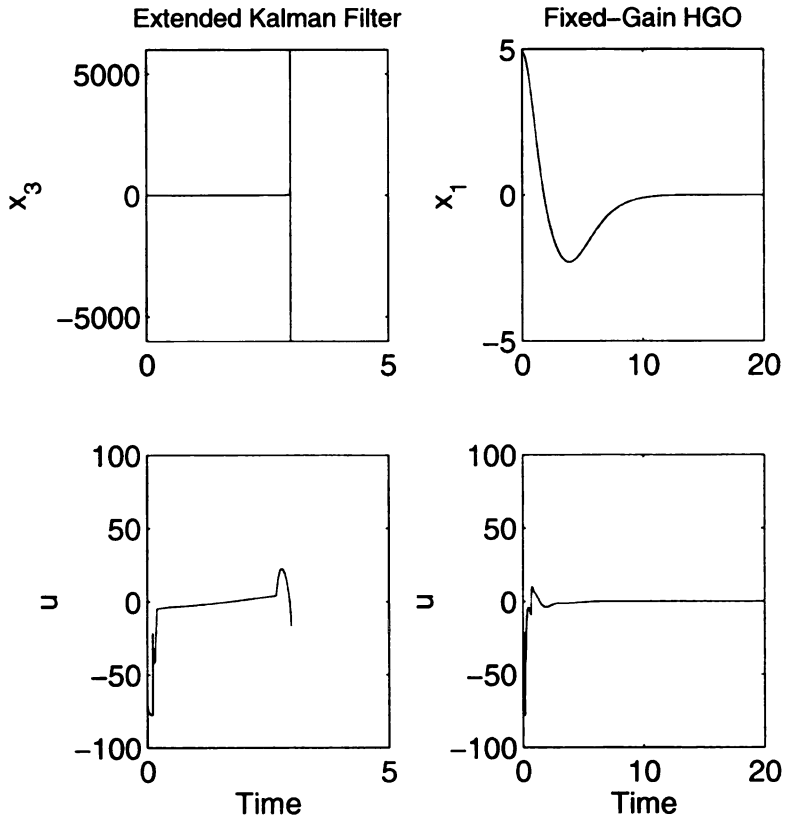

Figure 2.7. Simulation results showing the state x_3 and the control u for EKF feedback and the output x_1 and the control u for HGO feedback for $a = 2$

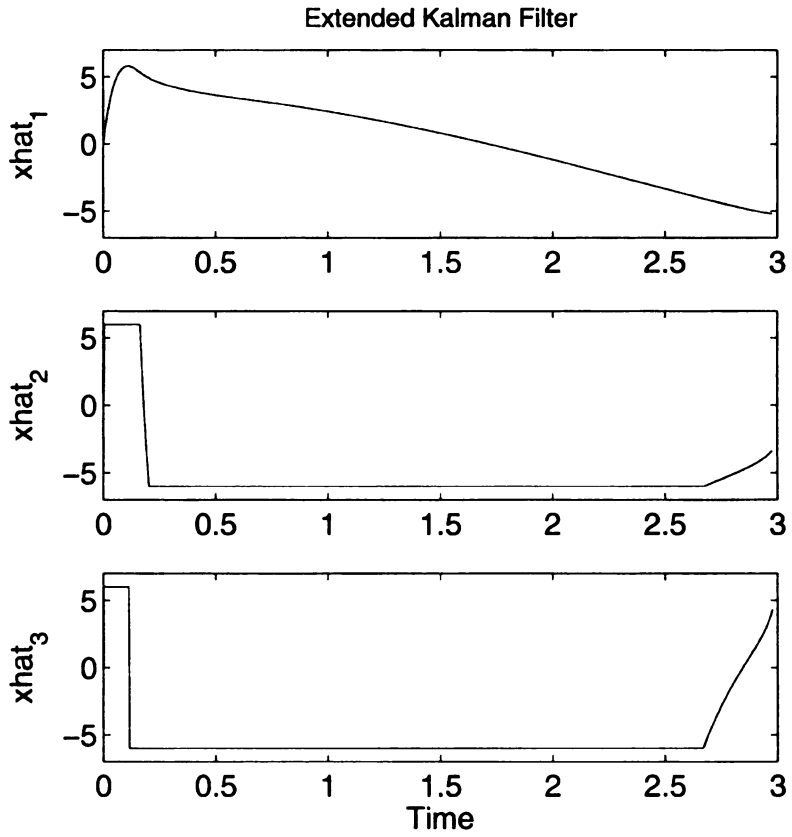

Figure 2.8. Simulation results showing the EKF observer estimates $\hat{x}_1$, $\hat{x}_2$, and $\hat{x}_3$ for $a = 2$.

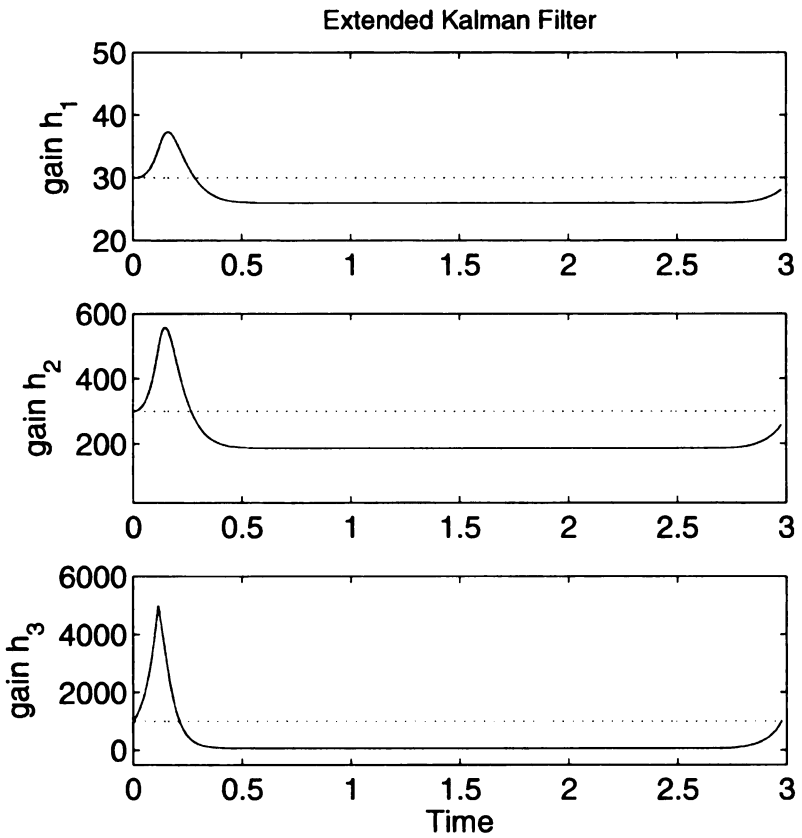

Figure 2.9. Simulation results showing the EKF observer gains h_1, h_2, and h_3 for $a = 2$.

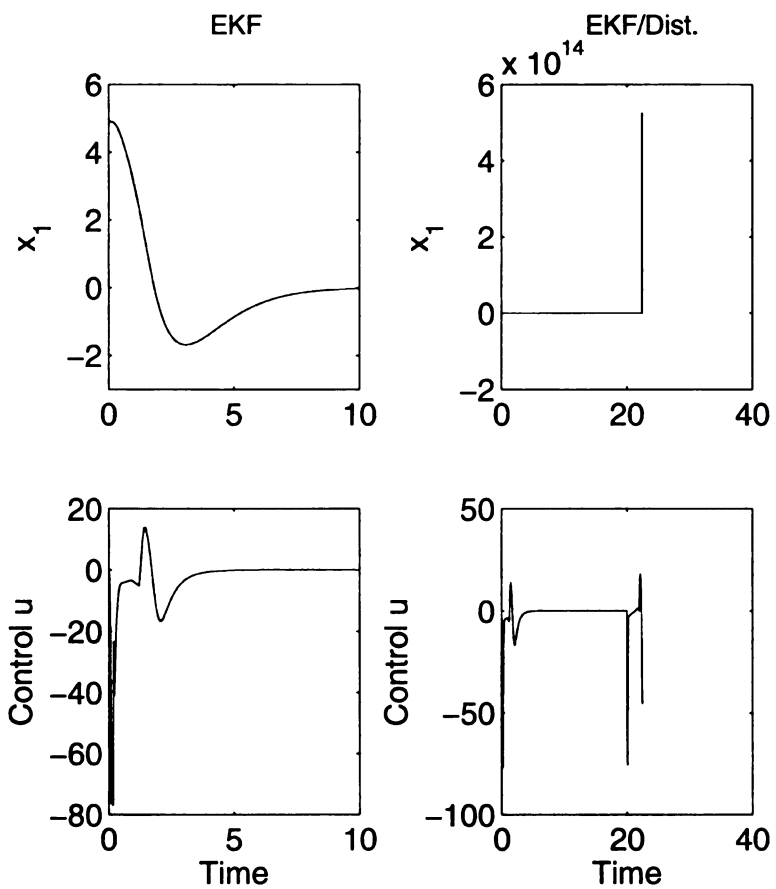

Figure 2.10. Simulation results showing the output x_1, and the control u for EKF feedback with $P(0) = I$. The plots on the left are stable, but the plots on the right become unstable due to an impulsive-like disturbance at $t = 20s$.

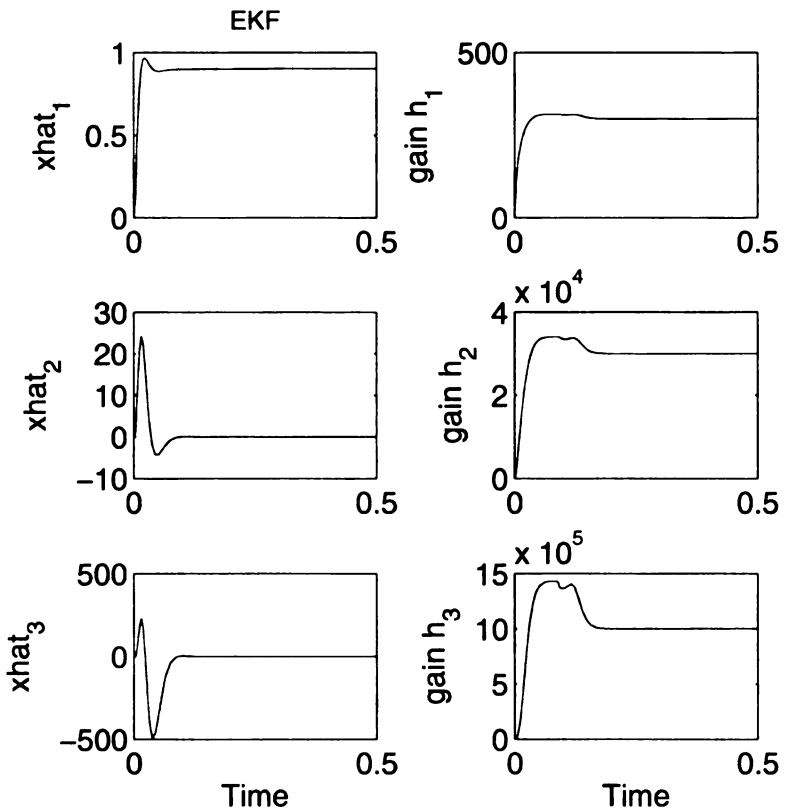

Figure 2.11. Simulation results illustrating peaking in the EKF observer estimates $\hat{x}_1$, $\hat{x}_2$, and $\hat{x}_3$ and the response of the observer gains h_1, h_2, and h_3.

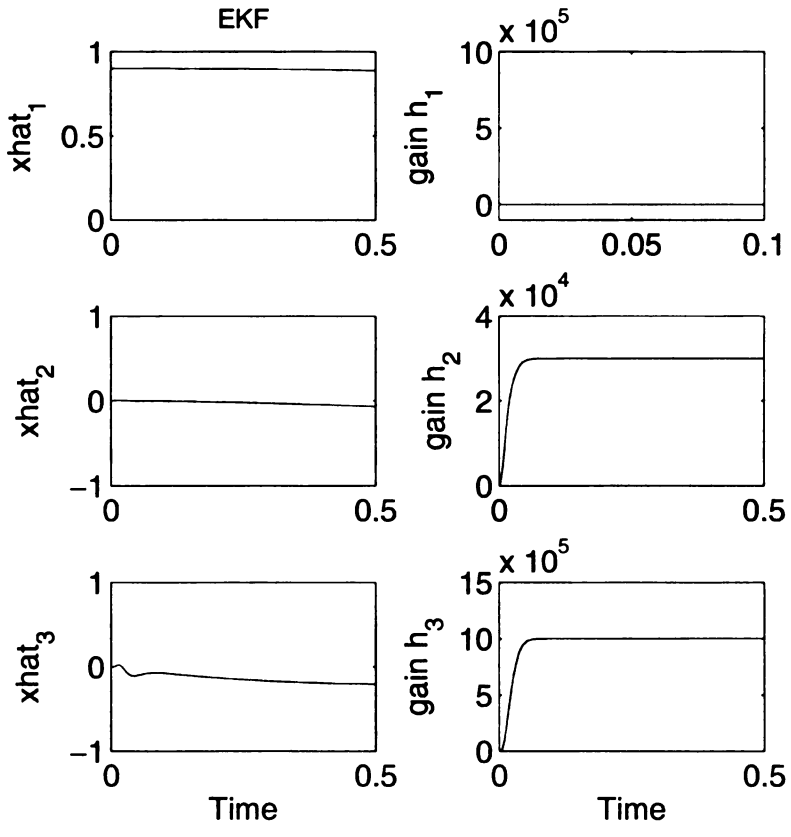

Figure 2.12. The response of the EKF observer estimates $\hat{x}_1$, $\hat{x}_2$, and $\hat{x}_3$ with Riccati initialization to suppress peaking. Also shown are the observer gains h_1, h_2, and h_3.

CHAPTER 3

Switched Gain High-Gain Observers

3.1 Introduction

It is well known from observer theory [40] that a tradeoff exists between the speed of state reconstruction and the immunity to measurement noise. The high-gain observer is known for having the ability to quickly reconstruct the system states and reject modeling disturbances [26]. In this chapter we examine the tradeoff between fast reconstruction of the states and rejection of modeling error versus the immunity to measurement noise for a high-gain observer. Based on this, we introduce a high-gain observer design where the gain matrix is switched between two values. The idea is to use high-gain during the transient to quickly recover the state estimates. Then once the estimation error has reached a steady-state threshold, we switch to a second gain to reduce the effect of measurement noise. A similar idea was explored in [46] for linear discrete-time filters. The authors combined two linear filters by switching gains based on the estimation error reaching a set containing the origin. A large gain is used outside this set to increase the filter bandwidth which reduces the estimation settling time. When operating inside the set, a lower gain is used to reduce bandwidth in order to accommodate the measurement noise. Switched-gain observers have also been considered in [25], where a high-gain observer was combined with a sliding term for estimation of nonlinear systems. The idea was to use

low-gain along with the sliding term to provide stability and avoid the large transients associated with high-gain. At a predetermined time, after the transient period, the gain is switched to a high value to provide better estimation and tracking. In this scheme, the effect of measurement noise was not considered.

The switched-gain scheme proposed in Section 3.3 uses high-gain during the transient period followed by a discontinuous switching. The switching event takes place when the estimation error $y - \hat{x}_1$ reaches a predetermined interval containing the origin. Due to the observer transient response the design contains a few special features. First, the observer eigenvalues are assigned to ensure that $y - \hat{x}_1$ decays monotonically towards the switching interval and reaches it in finite time. Second, a delay time is incorporated into the scheme that delays switching till after the observer transient response in order to prevent multiple gain switchings. Third, to avoid peaking after the switching event takes place, the ratio of the two gains may need to be restricted. Based on this, we study the closed-loop system under the switched-gain high-gain observer and argue that the trajectories of the closed-loop system are bounded.

Stability results for closed-loop systems under high-gain observer feedback in the presence of measurement disturbances can be found in [1] and [6]. For sampled-data high-gain observers the effects of measurement noise on the performance was studied in [19]. In [1] the limiting effect of increasing the gain of a high-gain observer on the trajectories of the closed-loop system in the presence of measurement noise was studied. A reference system based upon ideal differentiation of the measured output was introduced to compare the convergence properties of the high-gain observer. Also, in [6](Ch. 4) stability results for a class of nonlinear systems under HGO feedback in the presence measurement noise were provided. It was shown that, for sufficiently smooth disturbances, and given a state feedback controller that in the presence of the disturbance provides stability of the closed-loop system, the closed-loop system under HGO feedback can recover the performance of the state feedback system for sufficiently large observer gain. In [68], estimation error for

the HGO acting as a differentiator for noisy signals was studied. Also, guidelines for the choice of observer gain in the presence of measurement noise were provided.

In this chapter we also consider the high-gain observer acting as a differentiator for signals that may have large bandwidth in the presence of measurement noise. Again, the idea is to use high-gain when the signal of interest is quickly changing in order to achieve good estimation. Then, at steady-state a lower gain value is used to reduce the effect of measurement noise. In [67] Tilli and Montanari introduced a continuous switching scheme based on using a dead zone nonlinearity. Their estimator was designed to estimate *1st* and *2nd* derivatives of a measured signal corrupted by noise and exploit the variable bandwidth of this signal. In Section 3.5 we apply this nonlinear switching scheme to the high-gain observer and provide a numerical example to show its effectiveness.

3.2 Motivation

In this section, we motivate nonlinear switched-gain observers by discussing the tradeoff between state reconstruction and attenuation of measurement noise. We do so by studying the observer's estimation error. Consider the following nonlinear system

$$\dot{z} = \psi(x, z, u) \tag{3.1}$$

$$\dot{x} = Ax + B\phi(x, z, u) \tag{3.2}$$

$$y = Cx + v \tag{3.3}$$

$$\zeta = \Theta(x, z) \tag{3.4}$$

where u is the control input, $x \in \mathcal{X} \subseteq \mathbb{R}^r$ and $z \in \mathcal{Z} \subseteq \mathbb{R}^\ell$ are the states, and y and ζ are the measured variables. The measurement noise, $v(t)$, is a bounded measurable function. The functions ψ and ϕ are locally Lipschitz in their arguments over the domain of interest and satisfy $\psi(0,0,0) = \phi(0,0,0) = 0$. The $r \times r$ matrix A, the $r \times 1$ matrix B, and the $1 \times r$ matrix C are the same as (1.5)-(1.6).

The high-gain observer is designed for the system states (3.2) based on measurement of y. The tradeoff will concern reconstruction of the states x and rejection of noise v. For this reason, and for simplicity of presentation, we do not consider noise accompanying the measurement ζ. In addition, since it is the estimates of the derivatives of the output that are primarily affected by this tradeoff, we consider the above system where the relative degree r is greater than or equal to two. For $r = 1$, one may simply use the measured output. The observer for (3.2) has the form

$$\dot{\hat{x}} = A\hat{x} + B\phi_0(\hat{x}, \zeta, u) + H(y - C\hat{x}) \tag{3.5}$$

The gain is given by

$$H^T = \begin{bmatrix} \frac{\alpha_1}{\varepsilon} & \frac{\alpha_2}{\varepsilon^2} & \cdots & \frac{\alpha_r}{\varepsilon^r} \end{bmatrix} \tag{3.6}$$

where ε is a small positive parameter and the roots of

$$s^r + \alpha_1 s^{r-1} + \cdots + \alpha_{r-1} s + \alpha_r = 0 \tag{3.7}$$

have negative real parts.

Assumption 3.1 *The function ϕ_0 is locally Lipschitz in its arguments over the domain of interest, globally bounded in x, and satisfies $\phi_0(0, 0, 0) = 0$.*

We consider the partial state feedback controller

$$u = \gamma(x, \zeta) \tag{3.8}$$

The corresponding output feedback controller is given by

$$u = \gamma(\hat{x}, \zeta) \tag{3.9}$$

To examine the observation error $(x - \hat{x})$ we consider the following rescaling

$$\eta_i = \varepsilon^{i-1}(x_i - \hat{x}_i) \tag{3.10}$$

for $i = 1 \cdots r$. This rescaling differs from that of previous work on high-gain observers due to the presence of measurement noise. With this rescaling we have $D^{-1}(\varepsilon)\eta = x - \hat{x}$ where, $D(\varepsilon) = diag[1, \varepsilon, \cdots, \varepsilon^{r-1}]$. The closed-loop system under output feedback can be written in the following form

$$\dot{z} = \psi(x, z, \gamma(x - D^{-1}(\varepsilon)\eta, \zeta)) \tag{3.11}$$

$$\dot{x} = Ax + B\phi(x, z, \gamma(x - D^{-1}(\varepsilon)\eta, \zeta)) \tag{3.12}$$

$$\varepsilon\dot{\eta} = A_0\eta + \varepsilon^r B\delta(x, z, D^{-1}(\varepsilon)\eta) + B_2 v \tag{3.13}$$

where

$$\delta(x, z, D^{-1}(\varepsilon)\eta) = \phi(x, z, \gamma(\hat{x}, \zeta)) - \phi_0(\hat{x}, \zeta, \gamma(\hat{x}, \zeta))$$

and

$$A_0 = \begin{bmatrix} -\alpha_1 & 1 & \cdots & \cdots & 0 \\ -\alpha_2 & 0 & 1 & \cdots & 0 \\ \vdots & & & & \vdots \\ -\alpha_{r-1} & \cdots & \cdots & 0 & 1 \\ -\alpha_r & 0 & \cdots & \cdots & 0 \end{bmatrix}, B_2 = \begin{bmatrix} -\alpha_1 \\ -\alpha_2 \\ \vdots \\ -\alpha_r \end{bmatrix}$$

Setting $\eta = 0$ in (3.11)-(3.12) results in the noise-free, closed-loop system under state feedback

$$\dot{z} = \psi(x, z, \gamma(x, \zeta)) \tag{3.14}$$

$$\dot{x} = Ax + B\phi(x, z, \gamma(x, \zeta)) \tag{3.15}$$

We consider any state feedback control design that satisfies the following properties.

Assumption 3.2

1. *The origin* $(x = 0, z = 0)$ *of (3.14)-(3.15) is asymptotically stable and* $\mathcal{R}$ *is its region of attraction.*

2. *The function* γ *is locally Lipschitz in its arguments and globally bounded in* x*. Furthermore,* $\gamma(0,0) = 0$.

We operate under the following assumption on the measurement noise.

Assumption 3.3 *The measurement noise* $v(t)$ *is a measurable function that is bounded by a known upper bound; that is,*

$$|v(t)| \leq k_v \mu$$

To illustrate the tradeoff between state reconstruction and measurement noise immunity, we focus on Equation (3.13). Furthermore, these estimation error dynamics will be of primary concern in presenting and analyzing the switched gain observer design. With this in mind, let Ω_C be a compact subset of $\mathcal{R}$. Due to the global boundedness of $\delta(x, z, D^{-1}(\varepsilon)\eta)$ in $\hat{x}$, we have

$$\|\delta(x, z, D^{-1}(\varepsilon)\eta)\| \leq k_\delta$$

for all $(x, z) \in \Omega_C$ and some $k_\delta > 0$ independent of ε. For the time being we will operate under the assumption that $(x, z) \in \Omega_C$ and study the estimation error. Later we will study the behavior of the closed-loop system and show that if (x, z) starts in Ω_C then (x, z) will remain in Ω_C. Since A_0 is a Hurwitz matrix, we have $SA_0 + A_0^T S = -I$ for some positive definite symmetric matrix S. Take $W = \eta^T S \eta$ as a Lyapunov function candidate for the estimation error. It can be shown that

$$\dot{W} \leq -\frac{1}{\varepsilon}\|\eta\|^2 + 2\varepsilon^{r-1}\|\eta\|\|SB\|k_\delta + \frac{2}{\varepsilon}\|\eta\|\|SB_2\|k_v\mu \tag{3.16}$$

Furthermore, we have

$$\dot{W} \leq -\frac{1}{2\varepsilon\|S\|}W \tag{3.17}$$

for

$$W \geq 16\|S\| \left(\varepsilon^r \|SB\| k_\delta + \|SB_2\| k_v \mu\right)^2 \tag{3.18}$$

where $\|S\| = \lambda_{max}(S)$. Hence, the set

$$\{W(\eta(t)) \leq 16\|S\| \left(\varepsilon^r \|SB\| k_\delta + \|SB_2\| k_v \mu\right)^2\} \tag{3.19}$$

is positively invariant and η reaches this set in finite time $T(\varepsilon)$, where

$$\lim_{\varepsilon \to 0} T(\varepsilon) = 0$$

Inside this set η is bounded by

$$\|\eta\| \leq \varepsilon^r c_1 k_\delta + c_2 k_v \mu \tag{3.20}$$

where $c_1 = 4\|SB\|\sqrt{\frac{\|S\|}{\lambda_{min}(S)}}$ and $c_2 = 4\|SB_2\|\sqrt{\frac{\|S\|}{\lambda_{min}(S)}}$. Referring back to the rescaling (3.10) we have

$$\|x(t) - \hat{x}(t)\| \leq \|D^{-1}(\varepsilon)\| \|\eta\| \leq \varepsilon c_1 k_\delta + \frac{c_2}{\varepsilon^{r-1}} k_v \mu \tag{3.21}$$

as an ultimate bound for the estimation error. Consider the initial state $(x(t_0), \hat{x}(t_0))$. It can be shown that the initial error satisfies $\|\eta(t_0)\| \leq k_s$ for some $k_s \geq 0$ dependent on $\mathcal{M}$ and $\mathcal{N}$. From (3.17) and (3.18) we have

$$W(\eta(t)) \leq W(\eta(t_0)) exp\left(-\frac{\sigma_1 t}{\varepsilon}\right) \tag{3.22}$$

whenever (3.18) is satisfied, where $\sigma_1 = 1/(2\|S\|)$. Using (3.22) and the rescaling (3.10), it can be shown that, before reaching the bound (3.21), the error $(x(t) - \hat{x}(t))$ will be

bounded by

$$\|x(t) - \hat{x}(t)\| \leq \frac{\sigma_2}{\varepsilon^{r-1}} exp\left(-\frac{\sigma_1 t}{2\varepsilon}\right) \tag{3.23}$$

where $\sigma_2 = k_s\sqrt{\frac{\|S\|}{\lambda_{min}(S)}}$. The tradeoff between the speed of the reconstruction of the state and the rejection of the modeling error versus the immunity to measurement noise is clearly visible from equations (3.21) and (3.23). In the noise free case, the high-gain observer is designed to quickly reduce the state estimation error to a small value. However, the presence of measurement noise places a restriction on how large a gain we can choose. From equation (3.21) we see that for the estimation error to be $O(\varepsilon)$ or $O(1)$ the measurement noise magnitude must be $O(\varepsilon^r)$ or $O(\varepsilon^{r-1})$, respectively. This means that for $|v| \leq k_v\mu$, ε can be reduced to $O(\mu^{1/r})$ or $O(\mu^{1/(r-1)})$. We can see that attenuation of measurement noise requires larger values of ε (low gain). On the other hand, for fast estimation of the states and rejection of the modeling error we require smaller values of ε (higher gain).

3.3 Switched-gain observer

To relax the tradeoff discussed above, we propose a switched-gain observer. The switched-gain observer design is based on the output error $(y - \hat{x}_1)$ and a known upper bound on the measurement noise. The idea is to use a sufficiently large gain when the output error is large. This will provide fast reconstruction of the state estimates at the expense of increased measurement noise during the transient response. When the output error has reduced to a small value, we switch the gain to achieve a better balance between the input and measurement noise. The switching criteria is based upon the output error reaching a particular interval. Considering that estimates of the higher order derivatives will exhibit peaking we will have to exercise some care in determining when to switch. If we switch before the estimates of the higher order derivatives have recovered from peaking, it could have the effect of driving the output error outside the switching interval. We define the

switching interval as $\mathcal{I}_d = [-d, d]$ for some design parameter $d > 0$. We will discuss the choice of d later. We use the same observer design as before,

$$\dot{\hat{x}} = A\hat{x} + B\phi_0(\hat{x}, \zeta, u) + H(y - C\hat{x}) \tag{3.24}$$

but with the gain matrix, H, taken as

$$H^T = H_1^T = \begin{bmatrix} \frac{\alpha_1^1}{\varepsilon_1} & \frac{\alpha_2^1}{\varepsilon_1^2} & \cdots & \frac{\alpha_r^1}{\varepsilon_1^r} \end{bmatrix} \tag{3.25}$$

before switching and

$$H^T = H_2^T = \begin{bmatrix} \frac{\alpha_1^2}{\varepsilon_2} & \frac{\alpha_2^2}{\varepsilon_2^2} & \cdots & \frac{\alpha_r^2}{\varepsilon_2^r} \end{bmatrix} \tag{3.26}$$

after switching, where $0 < \varepsilon_1 < \varepsilon_2$. The constants α_i^j, $j = 1, 2$, and $i = 1, \cdots, r$, are chosen as in (3.7). The different sets of parameters, α_i^1's and α_i^2's allow for the flexibility of choosing the observer poles at different locations. In the analysis we will consider the closed-loop system under output feedback for two cases. For the case when the gain $H = H_2$ we use the same rescaling as above, $\eta_i = \varepsilon_2^{i-1}(x_i - \hat{x}_i)$. This will yield the same system of equations as (3.11)-(3.13) with ε replaced by ε_2. When the gain is given by H_1 we have, using the rescaling $\theta_i = \varepsilon_1^{i-1}(x_i - \hat{x}_i)$,

$$\dot{z} = \psi(x, z, \gamma(x - D^{-1}(\varepsilon_1)\theta, \zeta)) \tag{3.27}$$

$$\dot{x} = Ax + B\phi(x, z, \gamma(x - D^{-1}(\varepsilon_1)\theta, \zeta)) \tag{3.28}$$

$$\varepsilon_1\dot{\theta} = A_0\theta + \varepsilon_1^r B\delta(x, z, D^{-1}(\varepsilon_1)\theta) + B_2 v \tag{3.29}$$

We will focus on (3.27)-(3.29) for the moment. We would like switching of the gain to be based on detection of the output error entering the switching interval. As mentioned in the introduction, we need to include a delay between the time $(y - \hat{x}_1)$ enters the switching interval $\mathcal{I}_d$ and the time the gain is switched. A delay timer will be initiated

upon detection of $(y - \hat{x}_1)$ entering $\mathcal{I}_d$. However, the transient response of the observer may cause $(y - \hat{x}_1)$ to overshoot the switching interval. Our switching scheme will reset the delay timer whenever $(y - \hat{x}_1)$ exits the switching interval and restart the timer upon reentry of $(y - \hat{x}_1)$ into $\mathcal{I}_d$. Thus, overshoot of $\mathcal{I}_d$ may cause starting, resetting, and restarting of the delay timer. We can avoid this scenario and hasten the gain switching by designing the observer poles so that $(y - \hat{x}_1)$ does not overshoot $\mathcal{I}_d$. To see this, write the observer polynomial (3.7) as

$$(s^{r-1} + \beta_1 s^{r-2} + \cdots + \beta_{r-1} s + \beta_r)(s + \kappa) = 0 \tag{3.30}$$

where the first polynomial is Hurwitz with $O(1)$ roots and $\kappa \gg 1$. With this choice of polynomial roots, the system will exhibit two-time scale behavior. It will have a fast component that corresponds to the pole located at $-\kappa$ and $(r-1)$ slow components that correspond to the roots of

$$s^{r-1} + \beta_1 s^{r-2} + \cdots + \beta_{r-1} s + \beta_r = 0 \tag{3.31}$$

Considering this two-time scale choice of observer design, we can represent the estimation error in the singularly perturbed form. Toward that end, rewrite A_0 and B_2 in the following way:

$$A_0 = A_{01}\kappa + A_{02} \tag{3.32}$$

and

$$B_2 = B_{20}\kappa + B_{21} \tag{3.33}$$

where

$$A_{01} = \begin{bmatrix} -1 & 0 & \cdots & \cdots & 0 \\ -\beta_1 & 0 & 0 & \cdots & 0 \\ \vdots & & & & \vdots \\ -\beta_{r-2} & \cdots & \cdots & 0 & 0 \\ -\beta_{r-1} & 0 & \cdots & \cdots & 0 \end{bmatrix}, B_{20} = \begin{bmatrix} -1 \\ -\beta_1 \\ \vdots \\ -\beta_{r-2} \\ -\beta_{r-1} \end{bmatrix}$$

and

$$A_{02} = \begin{bmatrix} -\beta_1 & 1 & \cdots & \cdots & 0 \\ -\beta_2 & 0 & 1 & \cdots & 0 \\ \vdots & & & & \vdots \\ -\beta_{r-1} & \cdots & \cdots & 0 & 1 \\ 0 & 0 & \cdots & \cdots & 0 \end{bmatrix}, B_{21} = \begin{bmatrix} -\beta_1 \\ -\beta_2 \\ \vdots \\ -\beta_{r-1} \\ 0 \end{bmatrix}$$

To transform the system into the singularly perturbed form, we follow the procedure of [38]. First, notice that the direct sum of the range and null spaces of A_{01} span $\mathbb{R}^r$. Let the $r \times (r-1)$ matrix M and the $r \times 1$ matrix N be given by

$$M = \begin{bmatrix} 0 & 0 & \cdots & 0 \\ 1 & 0 & \cdots & 0 \\ 0 & 1 & \cdots & 0 \\ \vdots & \vdots & \ddots & \vdots \\ 0 & 0 & \cdots & 1 \end{bmatrix}, N = \begin{bmatrix} 1 \\ \beta_1 \\ \vdots \\ \beta_{r-1} \end{bmatrix}$$

The columns of M and N are the bases for the null-space and range-space of A_{01}, respectively. We define the inverse of a transformation matrix T as

$$T^{-1} = [M \;\; N]$$

With these matrices T is given by

$$T = \begin{bmatrix} P \\ Q \end{bmatrix}$$

where the $1 \times r$ matrix Q is

$$Q = [1 \;\; 0 \;\; \cdots \;\; 0]$$

and the $(r-1) \times r$ matrix P satisfies $PA_{01} = 0$; that is, the rows of P span the left null-space of A_{01}. Using the transformation matrix T, we consider the following change of variables

$$\begin{bmatrix} \xi \\ \theta_1 \end{bmatrix} = T\theta$$

According to [38] (Proposition 6.1) the change of coordinates $\xi = P\theta$ and $\theta_1 = Q\theta$ transforms the system (3.29) into

$$\varepsilon_1 \dot{\xi} = PA_{02}M\xi + PA_{02}N\theta_1 + \varepsilon_1^r PB\delta(x, z, x - \hat{x}) + PB_{21}v \tag{3.34}$$

$$\varepsilon_1 \dot{\theta_1} = QA_{02}M\xi + (\kappa QA_{01}N + QA_{02}N)\theta_1 - (\kappa + \beta_1)v \tag{3.35}$$

where we have used the relation $QA_{01}M = 0$. It is easy to show that $QA_{01}N = -1$, $QA_{02}M = Q$, and $A_{02}N = 0$. Therefore, we have

$$\varepsilon_1 \dot{\xi} = PA_{02}M\xi + \varepsilon_1^r PB\delta(x, z, x - \hat{x}) + PB_{21}v \tag{3.36}$$

$$\varepsilon_1 \dot{\theta_1} = \xi_1 - \kappa\theta_1 - (\kappa + \beta_1)v \tag{3.37}$$

Note that $\theta_1 = x_1 - \hat{x}_1$ and $PA_{02}M$ is a Hurwitz matrix. Using (3.36) and (3.37) it can be shown that, for an appropriate choice of d and κ, $(y - \hat{x}_1)$ will enter, and remain in, the switching interval. In fact, from (3.37) it can be shown that $(y - \hat{x}_1)$ will reach the switching interval during a time period $[t_0, t_0 + T_{12}\left(\frac{\varepsilon_1}{\kappa}\right)]$, where $T_{12}\left(\frac{\varepsilon_1}{\kappa}\right) \to 0$ as

$\frac{\varepsilon_1}{\kappa} \to 0$. We note that if the gain is switched before the transient response of the estimates of the higher order derivatives has settled it may cause the output error, $(y - \hat{x}_1)$, to leave the switching interval. This could result in repeated switching of the gain until the remaining trajectories recover from peaking. To avoid this scenario, once $(y - \hat{x}_1)$ enters the switching interval we delay switching by a time period T_d that depends upon the peaking period of the observer (3.29) to ensure that switching takes place after the trajectories of the estimation error θ have reached an invariant set.

3.3.1 Switching Scheme

Based on the above discussion, we use the following gain switching scheme for the observer (3.24):

1. Choose $H = H_1$ and reset the delay timer whenever $|y - \hat{x}_1| > d$.

2. Once $(y - \hat{x}_1)$ enters (or begins in) $[-d, d]$ start the delay timer; keep $H = H_1$.

3. After the delay time (of duration T_d) and while $(y - \hat{x}_1) \in [-d, d]$ switch to $H = H_2$.

From the foregoing development, we present the following analysis which illustrates the choice of the delay time duration T_d and switching interval $(\mathcal{I}_d)$ size d.

3.3.2 Switching Analysis

In order to examine the estimation error before switching, we begin by studying the slow and fast variables of the singularly perturbed system (3.36)-(3.37). Take $W_1(\xi, \theta_1) = W_{11}(\xi) + W_{12}(\theta_1) = \xi^T S_1 \xi + \frac{1}{2}\theta_1^2$ as a Lyapunov function candidate for (3.36)-(3.37), where the positive definite matrix S_1 satisfies $S_1(PA_{02}M) + (PA_{02}M)^T S_1 = -I$. Let $\|S_1\| = \lambda_{max}(S_1)$. Then

$$\dot{W}_1 \leq -\frac{1}{\varepsilon_1}\|\xi\|^2 + 2\|\xi\| \left[\varepsilon_1^{r-1}\|S_1 PB\|k_\delta + \frac{1}{\varepsilon_1}\|S_1 PB_{21}\|k_v\mu\right]$$

$$+\frac{1}{\varepsilon_1}|\theta_1||\xi_1| - \frac{\kappa}{\varepsilon_1}\theta_1^2 + \frac{(\kappa+\beta_1)}{\varepsilon_1}|\theta_1|k_v\mu$$

We have that $\dot{W}_1 \leq -\frac{1}{2\varepsilon_1}\|\xi\|^2 - \frac{\kappa}{2\varepsilon_1}\theta_1^2 \leq 0$ for

$$-\frac{\kappa}{4\varepsilon_1}\theta_1^2 - \frac{1}{4\varepsilon_1}\|\xi\|^2 + \frac{1}{\varepsilon_1}|\theta_1||\xi_1| \leq 0 \tag{3.38}$$

$$-\frac{1}{4\varepsilon_1}\|\xi\|^2 + 2\|\xi\|\left[\varepsilon_1^{r-1}\|S_1PB\|k_\delta + \frac{1}{\varepsilon_1}\|S_1PB_{21}\|k_v\mu\right] \leq 0 \tag{3.39}$$

$$-\frac{\kappa}{4\varepsilon_1}\theta_1^2 + \frac{(\kappa+\beta_1)}{\varepsilon_1}|\theta_1|k_v\mu \leq 0 \tag{3.40}$$

Inequality (3.38) is satisfied for $\kappa \geq 4$. Inequality (3.39) is satisfied for

$$\|\xi\| \geq 8\varepsilon_1^r\|S_1PB\|k_\delta + 8\|S_1PB_{21}\|k_v\mu \tag{3.41}$$

and inequality (3.40) is satisfied for

$$|\theta_1| \geq \frac{4(\kappa+\beta_1)}{\kappa}k_v\mu$$

Therefore, $\dot{W}_1 \leq 0$ for all

$$(\xi,\theta_1) \in \left\{ W_1(\xi,\theta_1) = 64\|S_1\|\left(k_\delta\|S_1PB\|\varepsilon_1^r + \|S_1PB_{21}\|k_v\mu\right)^2 + \frac{8(\kappa+\beta_1)^2}{\kappa^2}k_v^2\mu^2 \stackrel{def}{=} \varrho_1 \right\} \tag{3.42}$$

We have that the set $\Sigma_1 \stackrel{def}{=} \{W_1(\xi,\theta_1) \leq \varrho_1\}$ is positively invariant. Using the inequality

$$\lambda_{min}(S_1)\|\xi\|^2 + \frac{1}{2}\theta_1^2 \leq W_1(\xi,\theta_1)$$

we have, for (ξ,θ_1) in the set Σ_1,

$$\|\theta\| \leq \|M\|\|\xi\| + \|N\||\theta_1| \leq \|M\|\sqrt{\frac{\varrho_1}{\lambda_{min}(S_1)}} + \|N\|\sqrt{2\varrho_1} \tag{3.43}$$

From (3.42) it can be shown that θ is bounded by

$$\|\theta\| \leq c_4 k_\delta \varepsilon_1^r + c_5(\kappa) k_v \mu \tag{3.44}$$

where

$$c_4 = 8c_3\sqrt{\|S_1\|}\|S_1 PB\| \tag{3.45}$$

$$c_5(\kappa) = c_3\left(8\sqrt{\|S_1\|}\|S_1 PB_{21}\| + \frac{\sqrt{8}(\kappa+\beta_1)}{\kappa}\right) \tag{3.46}$$

and $c_3 = \dfrac{\|M\|}{\sqrt{\lambda_{min}(S_1)}} + \sqrt{2}\|N\|$. For $W_1(\xi,\theta_1) \geq \varrho_1$ we have

$$\dot{W}_1 \leq -\frac{1}{2\varepsilon_1\|S_1\|}W_{11} - \frac{\kappa}{\varepsilon_1}W_{12} \leq -\frac{\sigma_3}{\varepsilon_1}W_1 \tag{3.47}$$

where $\sigma_3 = \min\left\{\kappa, \dfrac{1}{2\|S_1\|}\right\}$. By the same argument used above, $\|\theta(t_0)\| \leq k_s$ for some $k_s \geq 0$, dependent on $\mathcal{M}$ and $\mathcal{N}$. Therefore, we have $\|\xi(t_0)\| \leq \|P\|k_s$, $|\theta_1(t_0)| \leq k_s$, and

$$W_1(\xi(t),\theta_1(t)) \leq \sigma_4 \ \ exp(-\sigma_3 t/\varepsilon_1) \tag{3.48}$$

where $\sigma_4 = (1/2 + \|S_1\|\|P\|^2)k_s^2$. In addition, we have that $(\xi(t),\theta_1(t))$ enters the set Σ_1 during the time interval $[t_0, t_0 + T_1(\varepsilon_1)]$ where

$$T_1(\varepsilon_1) = \frac{\varepsilon_1}{\sigma_3} ln\left(\frac{\sigma_4}{\varrho_1}\right) \tag{3.49}$$

We have from (3.43) and (3.48) that θ is bounded for all $t \geq t_0$ and ultimately bounded by (3.44).

Next we study the output error $(y - \hat{x}_1)$ by considering the Lyapunov function $W_{12} = \frac{1}{2}\theta_1^2$ for (3.37). Notice from equations (3.44) and (3.48) and the relation $\|\xi\| \leq \|P\|\|\theta\|$,

that ξ is bounded uniformly in ε_1 for all $\varepsilon_1 < 1$ and all $t \geq t_0$. Thus,

$$\|\xi\| \leq k_1$$

for some positive constant k_1 independent of ε_1. It is easy to show that $\dot{W}_{12} \leq -\frac{\kappa}{2\varepsilon_1}\theta_1^2 \leq 0$ for

$$|\theta_1| \geq \frac{2}{\kappa}\left(k_1 + (\kappa + \beta_1)k_v\mu\right) \tag{3.50}$$

Therefore, for all $\theta_1 \in \{W_{12}(\theta_1) = \frac{2}{\kappa^2}[k_1 + (\kappa+\beta_1)k_v\mu]^2 \stackrel{def}{=} \varrho_{12}\}$, $\dot{W}_{12} \leq -\frac{\kappa}{2\varepsilon_1}\theta_1^2 \leq 0$. We have that the set $\Sigma_{12} = \{W_{12}(\theta_1) \leq \varrho_{12}\}$ is positively invariant. Inside Σ_{12}, we have

$$|y - \hat{x}_1| \leq |\theta_1| + |v| \leq \frac{2}{\kappa}k_1 + \left(\frac{2(\kappa+\beta_1)}{\kappa} + 1\right)k_v\mu \stackrel{def}{=} \pi_1(\kappa) \tag{3.51}$$

Later we will choose κ sufficiently large so that $\pi_1(\kappa) < d$ and thus, $(y - \hat{x}_1)$ will be in the switching interval $\mathcal{I}_d$.

Next we compute the time at which $(y - \hat{x}_1)$ enters $\mathcal{I}_d$. We have for $W_{12}(\theta_1) \geq \varrho_{12}$

$$\dot{W}_{12} \leq -\frac{\kappa}{\varepsilon_1}W_{12} \tag{3.52}$$

Therefore,

$$W_{12}(\theta_1(t)) \leq W_{12}(t_0)exp(-\kappa t/\varepsilon_1) \tag{3.53}$$

Note that $|\theta_1(t_0)| \leq k_s$. Then

$$W_{12}(\theta_1(t)) \leq \frac{1}{2}k_s^2 exp(-\kappa t/\varepsilon_1) \tag{3.54}$$

In addition, we have that $W_{12}(\theta_1)$ enters the set Σ_{12} during the finite time interval $[t_0, t_0 + T_{12}(\frac{\varepsilon_1}{\kappa})]$ where

$$T_{12}\left(\frac{\varepsilon_1}{\kappa}\right) = \frac{\varepsilon_1}{\kappa}ln\left(\frac{k_s^2}{2\varrho_{12}}\right) \tag{3.55}$$

We note that for $\|\theta(t_0)\| \leq k_s$ and $|\theta_1(t_0)| \in \Sigma_{12}$, then $|y(t_0) - \hat{x}_1(t_0)| \leq \pi_1(\kappa)$ for all $t \geq t_0$. In other words, if d is chosen so that $\pi_1(\kappa) < d$, then for $(y(t_0) - \hat{x}_1(t_0))$ starting in the switching interval, it will remain in the switching interval for all $t \geq t_0$. Notice that for large enough κ, $T_{12}\left(\frac{\varepsilon_1}{\kappa}\right) < T_1(\varepsilon_1)$. This indicates that when $(y - \hat{x}_1)$ enters the switching interval, the estimates of the higher order derivatives, $\hat{x}$, may not have had enough time to recover from peaking to reach the invariant set Σ_1. If on the other hand, $T_{12}\left(\frac{\varepsilon_1}{\kappa}\right) \geq T_1(\varepsilon_1)$ then we can choose a delay time duration of 0. Therefore, we choose the switching delay timer duration (T_d) according to the following statement

$$\begin{cases} T_d > T_1 - T_{12}, & if \quad T_{12} < T_1 \\ T_d = 0, & if \quad T_{12} \geq T_1 \end{cases} \tag{3.56}$$

Thus, the delay timer begins when $(y - \hat{x}_1)$ enters $\mathcal{I}_d$ and lasts for duration T_d. After the time duration T_d, the gain is switched. Let T_s be the switching time. At the switching time, using (3.44), we have that the estimation error satisfies

$$|x_i - \hat{x}_i| \leq \frac{1}{\varepsilon_1^{i-1}}(c_4 k_\delta \varepsilon_1^r + c_5(\kappa) k_v \mu) \tag{3.57}$$

After switching we get

$$|\eta_i(T_s)| \leq \frac{\varepsilon_2^{i-1}}{\varepsilon_1^{i-1}}(c_4 k_\delta \varepsilon_1^r + c_5(\kappa) k_v \mu) \tag{3.58}$$

and

$$\|\eta(T_s)\| \leq c_4 k_\delta \varepsilon_2^{r-1} \varepsilon_1 + \frac{\varepsilon_2^{r-1}}{\varepsilon_1^{r-1}} c_5(\kappa) k_v \mu \tag{3.59}$$

Next we derive the ultimate bound on the estimation error η after switching. For the high-gain observer operating under the gain H_2 we have a result identical to the previous section (3.11)-(3.13) with $\varepsilon = \varepsilon_2$. Therefore, using $W_2 = \eta^T S_2 \eta$ as a Lyapunov function,

we have a positively invariant set Σ_2 given by

$$\Sigma_2 \stackrel{def}{=} \{W_2(\eta) \leq 16\|S_2\| \left(\varepsilon_2^r \|S_2 B\| k_\delta + \|S_2 B_2\| k_v \mu\right)^2 \stackrel{def}{=} \varrho_2\} \tag{3.60}$$

where the positive definite matrix S_2 satisfies $S_2 A_0 + A_0^T S_2 = -I$. Therefore, any η starting in Σ_2 will remain there and η will be ultimately bounded by

$$\|\eta\| \leq \varepsilon_2^r c_1 k_\delta + c_2 k_v \mu \tag{3.61}$$

where c_1 and c_2 are the same as (3.20) with $S = S_2$. It can be shown that, for all $W_2 \geq \varrho_2$,

$$W_2(\eta(t)) \leq \sigma_6 exp(-\sigma_5 t/\varepsilon_2) \tag{3.62}$$

where $\sigma_5 = 1/(2\|S_2\|)$ and $\sigma_6 = \|\eta(T_s)\|^2 \|S_2\|$. The trajectory η enters the invariant set Σ_2 during the time interval $[T_s, T_s + T_2(\varepsilon_2)]$, where $T_2(\varepsilon_2)$ is given by

$$T_2(\varepsilon_2) = \frac{\varepsilon_2}{\sigma_5} \ln\left(\frac{\sigma_6}{\varrho_2}\right) \tag{3.63}$$

From (3.61), we have that the output error is bounded by

$$|y - \hat{x}_1| \leq \|\eta\| + |v| \leq \varepsilon_2^r c_1 k_\delta + (1 + c_2) k_v \mu \stackrel{def}{=} \pi_2(\varepsilon_2, \mu) \tag{3.64}$$

We choose the size of the switching interval d such that $\pi_2(\varepsilon_2, \mu) < d$.

Referring back to (3.59) we see that if $\eta(T_s)$ is in the invariant set Σ_2, then $\eta(t)$ will remain in Σ_2 for all $t \geq T_s$. On the other hand, if $\eta(T_s)$ is outside Σ_2 then

$$\|\eta\| \geq 4\left(\varepsilon_2^r \|S_2 B\| k_\delta + \|S_2 B_2\| k_v \mu\right)$$

and

$$\dot{W}_2 \leq 0 \tag{3.65}$$

It follows that on the Lyapunov surface $W_2 = c$ where

$$c = \|S_2\| \left[c_4 k_\delta \varepsilon_2^{r-1} \varepsilon_1 + \frac{\varepsilon_2^{r-1}}{\varepsilon_1^{r-1}} c_5(\kappa) k_v \mu \right]^2$$

$\dot{W}_2 \leq 0$. Hence, the set $\{W_2(\eta) \leq c\}$ is positively invariant. Then we have

$$\|\eta(t)\| \leq c_6 \left[c_4 k_\delta \varepsilon_2^{r-1} \varepsilon_1 + \frac{\varepsilon_2^{r-1}}{\varepsilon_1^{r-1}} c_5(\kappa) k_v \mu \right] \tag{3.66}$$

for all $t \geq T_s$, where $c_6 = \frac{\|S_2\|}{\lambda_{min}(S_2)}$. From (3.66)

$$|y(t) - \hat{x}_1(t)| \leq c_6 \left[c_4 k_\delta \varepsilon_2^{r-1} \varepsilon_1 + \frac{\varepsilon_2^{r-1}}{\varepsilon_1^{r-1}} c_5(\kappa) k_v \mu \right] + k_v \mu \stackrel{def}{=} \pi_3(\kappa) \tag{3.67}$$

for all $t \geq T_s$. Let $\underline{\pi}_1 = \pi_1(\kappa)|_{\kappa \to \infty}$ and $\underline{\pi}_3 = \pi_3(\kappa)|_{\kappa \to \infty}$. Then

$$\underline{\pi}_1 = 3 k_v \mu$$

and, using (3.46),

$$\underline{\pi}_3 = c_6 \left[c_4 k_\delta \varepsilon_2^{r-1} \varepsilon_1 + c_3 \frac{\varepsilon_2^{r-1}}{\varepsilon_1^{r-1}} \left(8 \sqrt{\|S_1\| \|S_1 P B_{21}\|} + \sqrt{8} \right) k_v \mu \right] + k_v \mu$$

With ε_1, ε_2, k_v, and k_δ we choose $d > max\{\pi_2, \underline{\pi}_1, \underline{\pi}_3\}$. We can then choose κ large enough such that

$$\pi_1, \pi_3 < d$$

Finally, $\|\eta(t)\|$ will enter the set Σ_2 in finite time and be ultimately bounded by (3.61).

Choice of ε_1 and ε_2

Notice from Equation (3.67) that if $\varepsilon_1^{r-1} << \varepsilon_2^{r-1} k_v \mu$, then π_3 will be large. This may yield a large switching interval size compared to the ultimate bound π_2 in Equation (3.64). To relax this conservative switching interval size we can restrict the relationship between ε_1, ε_2, and μ. First, we choose ε_2 such that $\varepsilon_2^r \geq k_v \mu$. Then we take $0 < \varepsilon_1 < \varepsilon_2 < 1$ and $\varepsilon_1 = k_\varepsilon \varepsilon_2^2$ for some positive constant k_ε. With these choices π_3 will be $O(\varepsilon_2)$. The choice $\varepsilon_2 < 1$ is made in order to simplify the analysis and is reasonable in the presence of relatively small measurement noise magnitude. The theorem to follow guarantees that there exist ε^*, dependent on μ, such that, for all $(k_v \mu)^{1/r} \leq \varepsilon_2 \leq \varepsilon^*$, all closed-loop trajectories are bounded. Thus, if $(\varepsilon^*)^r \geq k_v \mu$ we can choose $(k_v \mu)^{1/r} \leq \varepsilon_2 \leq \varepsilon^*$ and ε_1, ε_2, and k_ε can be chosen to relax the state reconstruction speed and measurement noise tradeoff. With these observations in mind we state the following theorem.

Theorem 3.1 *Let Assumptions (3.1)-(3.3) hold and consider the plant (3.1)-(3.4), the output feedback controller (3.9), and the switched-gain observer (3.24) with the switching scheme as given in Section 3.3.1. Let $\mathcal{M}$ be any compact set in the interior of $\mathcal{R}$ and $\mathcal{N}$ be any compact subset of $\mathbb{R}^r$. Also, let $\varepsilon_2 \geq (k_v \mu)^{1/r}$ and $\varepsilon_1 = k_\varepsilon \varepsilon_2^2$ for positive constants k_v and k_ε. Then, there exist $\varepsilon^* > 0$ such that for every $(k_v \mu)^{1/r} \leq \varepsilon_2 \leq \varepsilon^*$,*

1. *the solutions $(z(t), x(t), \hat{x}(t))$ of the closed-loop system, starting in $\mathcal{M} \times \mathcal{N}$, are bounded for all $t \geq t_0$.*

2. *the estimation error η is ultimately bounded by (3.61).*

3. *the output error $(y - \hat{x}_1)$ enters the set $\mathcal{I}_d$ during a finite time interval $[t_0, t_0 + T_{12}]$ and remains there for all $t \geq T_{12}$ and for design parameters κ, d, and T_d chosen sufficiently large.*

Proof: We were able to show items (2) and (3) in the foregoing analysis provided that the

state (x, z) remained the compact set $\Omega_C \subset \mathcal{R}$. We argue here that if (x, z) starts in Ω_C then (x, z) will remain in Ω_C.

For simplicity let $\chi = [x \;\; z]^T$ and denote the right hand side of (3.1)-(3.2) as

$$f(\chi, u) = \begin{bmatrix} \psi(x, z, u) \\ Ax + B\phi(x, z, u) \end{bmatrix}$$

With this notation, the system equation under output feedback control (3.11)-(3.12) is given by

$$\dot{\chi} = f(\chi, \gamma(\hat{x}, \zeta))$$

and the closed-loop system under state feedback (3.14)-(3.15) is

$$\dot{\chi} = f(\chi, \gamma(x, \zeta)) \tag{3.68}$$

From Assumption 3.2, the origin of (3.68) is Asymptotically stable with region of attraction $\mathcal{R}$. By Theorem 4.17 of [36], there exists a smooth, positive definite function $V(\chi)$ and a continuous positive definite function $U(\chi)$, both defined for all $\chi \in \mathcal{R}$, such that

$$V(\chi) \to \infty \;\; as \;\; \chi \to \partial\mathcal{R}$$

$$\frac{\partial V}{\partial \chi} f(\chi, \gamma(x, \zeta)) \leq -U(\chi), \;\; \forall \chi \in \mathcal{R}$$

and for any $c > 0$, $\{V(\chi)\} \leq c\}$ is a compact subset of $\mathcal{R}$. Let $\mathcal{M}$ be any compact set in the interior of $\mathcal{R}$ and choose positive constants b and c such that $c > b > \max_{\chi \in \mathcal{M}} V(\chi)$. Then

$$\mathcal{S} \subset \Omega_b = \{V(\chi) \leq b\} \subset \Omega_c = \{V(\chi) \leq c\} \subset \mathcal{R}$$

Due to the global boundedness of f and δ in $\hat{x}$, for all $\chi \in \Omega_c$ and $\hat{x} \in \mathbb{R}^r$ we have

$$\|f(\chi, \gamma(\hat{x}, \zeta))\| \leq k_2, \quad \|\delta(x, z, x - \hat{x})\| \leq k_\delta$$

for some positive constants k_2 and k_δ independent of ε. Also, there exists an L_1, independent of ε such that

$$\|f(\chi, \gamma(\hat{x}, \zeta)) - f(\chi, \gamma(x, \zeta))\| \leq L_1 \|x - \hat{x}\|$$

Now, consider the set Σ_2 from (3.60). It was argued that this set is positively invariant provided that $(x, z) \in \Omega_c$. Since μ is $O(\varepsilon_2^r)$, η is $O(\varepsilon_2^r)$ inside Σ_2. Let L_2 be a upper bounded for $\|\partial V/\partial \chi\|$ over Ω_c. We have

$$\dot{V} \leq -U(\chi) + L_1 L_2 \|x - \hat{x}\| \leq -U(\chi) + \frac{L_1 L_2}{\varepsilon_2^{r-1}} \|\eta\| \leq -U(\chi) + c_7 \varepsilon_2$$

for all $(\chi, \eta) \in \Omega_c \times \Sigma_2$ and some positive constant c_7 independent of ε_2. Take $\varepsilon_3 = \vartheta / c_7$, where $\vartheta = \min_{\chi \in \partial \Omega_c} U(\chi)$. It can be shown that, for every $0 < \varepsilon_2 \leq \varepsilon_3$, we have $\dot{V}(\chi) \leq 0$ for all $(\chi, \eta) \in \{V(\chi) = c\} \times \Sigma_2$. Also, from the derivation of (3.60) we have that $\dot{W}_2 \leq 0$ for all $(\chi, \eta) \in \Omega_c \times \{W_2(\eta) = \varrho_2\}$. Therefore, the set $\Omega_c \times \Sigma_2$ is positively invariant.

Since $\chi(0) \in \mathcal{M}$, then $\chi(0)$ is in the interior of Ω_c. We have that

$$\|\chi(t) - \chi(0)\| \leq k_2 t \tag{3.69}$$

as long as $\chi(t) \in \Omega_c$. Therefore, there exists a finite time T^*, independent of ε_1 and ε_2, such that $\chi(t) \in \Omega_c$ for all $t \in [t_0, t_0 + T^*]$. We note from the above analysis that the estimation error η enters the set Σ_2 during the finite time period $[t_0, t_0 + T_1(\varepsilon_1) + T_2(\varepsilon_2)]$. Since $T_1(\varepsilon_1) \to 0$ as $\varepsilon_1 \to 0$ and $T_2(\varepsilon_2) \to 0$ as $\varepsilon_2 \to 0$, there exists ε_4 such that for all

$0 < \varepsilon_2 \leq \varepsilon_4$

$$t_0 + T_1(\varepsilon_1) + T_2(\varepsilon_2) \leq T^*$$

Hence, the trajectory (χ, η) enters the set $\Omega_c \times \Sigma_2$ during the finite time period $[t_0, t_0 + T_1(\varepsilon_1) + T_2(\varepsilon_2)]$ and remains there for all $t \geq t_0 + T_1(\varepsilon_1) + T_2(\varepsilon_2)$. Prior to entering this set, $\chi(t)$ is bounded by (3.69). Taking $\varepsilon^* = \min\{\varepsilon_3, \varepsilon_4\}$ and choosing $0 < \varepsilon_2 \leq \varepsilon^*$ guarantees that the closed-loop trajectories are bounded. $\lhd$

Several remarks are in order.

Remark 3.1 Modification of Theorem 3.1 to include the tracking problem at least requires the use of Lyapunov stability with respect to a set. For the tracking problem, the ultimate bound on the estimation error will depend on time-varying reference signals in addition to the noise and modeling error. If the reference signals are large they could have the effect of moving the output error outside the switching interval. This would cause repeated gain switching events every T_d seconds. One way to deal with this is to take the maximum values of the reference signals into consideration when choosing ε_1 and ε_2 and $\mathcal{I}_d$. These values can be chosen large enough that the reference signals do not cause repeated switching events. This approach is illustrated in the example of Section 3.4.

Remark 3.2 The parameter κ is chosen sufficiently large so that the output error $(y - \hat{x}_1)$ does not overshoot the switching interval during the transient period. Due to the switching scheme, this condition on the placement of the observer poles can be relaxed. Without this condition, as mentioned before, the output error may overshoot the switching interval, but the switching delay T_d along with the resetting of the switching delay when the output error leaves the switching interval would prevent repeated switching of the gain during this transient period. However, in this situation it may take longer for the switching event to occur than the case where κ is chosen to be large. The flexibility in choosing the location of the observer's poles allows for either design.

Remark 3.3 We note that at anytime an impulsive-like disturbance that has the effect

of resetting the initial conditions can cause the estimation error to leave the switching interval. When this occurs, from item 1 of the switching scheme above, the gain switches to the larger value in order to recover the estimates. This will be illustrated with a numerical example.

3.4 Gain Switching Example

We consider a field controlled DC motor [36] and design a controller based on feedback linearization so that the shaft angular velocity tracks the reference trajectory shown in Figure 3.3. The motor equations are given by

$$\dot{x}_1 = x_2 \tag{3.70}$$

$$\dot{x}_2 = \phi(x,u) \tag{3.71}$$

$$\dot{x}_3 = \psi(x,u) \tag{3.72}$$

$$y = x_1 + v \tag{3.73}$$

$$\theta_1 = x_3 \tag{3.74}$$

where x_1 is the rotor position, x_2 is the rotor angular velocity, x_3 is the armature current, and control u is the field current. The functions $\phi(x,u) = -0.1x_2 + 0.1x_3u$ and $\psi(x,u) = -2x_3 - 0.2x_2u + 200$. The estimates, $\hat{x}$, are saturated outside $[-100, 100]$. For the observer, we have $\phi_0(\hat{x},u) = -0.11x_2 + 0.1x_3u$, and we use the following gains

$$H_1^T = \begin{bmatrix} \frac{71}{\varepsilon_1} & \frac{70}{\varepsilon_1^2} \end{bmatrix} \tag{3.75}$$

$$H_2^T = \begin{bmatrix} \frac{2}{\varepsilon_2} & \frac{1}{\varepsilon_2^2} \end{bmatrix} \tag{3.76}$$

where $\varepsilon_1 = 0.0005$ and $\varepsilon_2 = 0.01$. The gain H_1 was chosen, using simulation, to ensure that the estimation error does not over shoot the switching zone. For the switching

threshold we use $d = 0.05$ and a delay time $T_d = 0.15s$. The initial conditions for the system and observer are $\hat{x}_1(0) = \pi$, $x_1(0) = x_2(0) = \hat{x}_2(0) = 0$. The measurement noise is generated by Simulink's "Uniform Random Number" block with magnitude limited within $[-0.0016, 0.0016]$ and sampling time set at 0.0008 seconds. This error magnitude is consistent with a 1000 c/r encoder. Figure 3.3 shows the velocity reference $\dot{r}$ (dotted) and the trajectory x_2 (solid) for the closed-loop system under the switched-gain observer. The two the plots are indistinguishable. The bottom figure plots the value of ε_i versus time illustrating the switching behavior. Figure 3.4 plots the tracking error, $e_1 = x_1 - r$, for the closed-loop system under the switched-gain observer ($\varepsilon = \varepsilon_i$, top), a fixed gain observer with $\varepsilon = \varepsilon_2 = 0.01$ (middle), and a fixed gain observer with $\varepsilon = \varepsilon_1 = 0.0005$ (bottom). Likewise, Figure 3.5 plots the tracking error, $e_2 = x_2 - \dot{r}$, for $\varepsilon = \varepsilon_i$ (top), $\varepsilon = \varepsilon_2$ (middle), and $\varepsilon = \varepsilon_1$ (bottom). These two plots show that the switched-gain observer has faster state reconstruction then the fixed-gain case with $\varepsilon = 0.01$. Figure 3.6 compares the steady-state error e_1 of the fixed-gain observer with $\varepsilon = 0.0005$ against the switched-gain observer and the observer under fixed-gain with $\varepsilon = 0.01$, respectively. This figure shows that the larger gain yields a better performance in the presence of a modeling error $\phi - \phi_0$. Figure 3.7 zooms in on the steady-state behavior of e_2 showing that more of the measurement noise is attenuated when the observer switches to the smaller gain. Table 3.1 compares the root mean square (R.M.S) values of the tracking errors for each of the three observer designs. The rows e_1 and e_2 list the R.M.S errors calculated over the entire simulation (0 to 10 seconds). To capture the steady-state behavior, we exclude the initial transient and calculate the R.M.S tracking errors from 3 seconds to 10 seconds. These values are listed in the rows $e_1(SS)$ and $e_2(SS)$. The switched-gain scheme shows better steady-state behavior in e_2. Figure 3.8 shows the behavior of the control signal u under each of the three cases. This plot shows the switched-gain observer recovers from peaking more quickly than the case with $\varepsilon = 0.01$, but with greater noise immunity at steady-state than the case where $\varepsilon = 0.0005$. Figure 3.9 shows the behavior

	Switched-gain	$\varepsilon = 0.01$	$\varepsilon = 0.0005$
e_1	0.0064	0.0741	0.0062
e_2	0.0761	0.6295	0.0626
e_1(SS)	0.0013	0.0013	9.37e-4
e_2(SS)	0.0026	0.0026	0.0108

Table 3.1. Comparison of R.M.S tracking errors $e_1 = x_1 - r$, $e_2 = x_2 - \dot{r}$, e_1 steady-state, and e_2 steady-state for the switched-gain scheme and two HGOs for $|v| \leq 0.0016$ and $\phi_0 \neq \phi$.

of the error $e_2 = x_2 - \dot{r}$ for the switched-gain observer (top) and a fixed-gain observer with $\varepsilon = \varepsilon_2$ (bottom) when an impulsive-like disturbance moves the estimation error $(x_1 - \hat{x}_1)$ outside $\mathcal{I}_d$. A measurement disturbance of magnitude 150 and duration 0.001 seconds is experienced at time 2.5 seconds. The observer switches to the larger gain and is able to recover more quickly than the case when $\varepsilon = 0.01$. To see the importance of the delay T_d, the behavior of the switched parameter ε is depicted in Figure 3.10 when the delay time T_d is set to zero. It can be seen that ε repeatedly switches between 0.01 and 0.0005. Figure 3.11 considers the stead-state tracking error e_1 simulated with larger noise $v \in [-0.016, 0.016]$. In this case the noise and modeling error tradeoff favors the smaller gain at steady-state. Table 3.2 compares the R.M.S values of the tracking errors e_1 and e_2 for each of the three cases. This table shows the advantage of the switched-gain observer in relaxing the noise and estimation tradeoff. We also simulated for the case when $\phi = \phi_0$ with the noise level bounded once again in $v \in [-0.0016, 0.0016]$. The error e_1 is shown in Figure 3.12 for this case. The steady-state tracking error e_1 is slightly improved at steady-state for the switched-gain and the fixed-gain observer with $\varepsilon = 0.01$. Table 3.3 compares the R.M.S values of the tracking errors e_1 and e_2 for each of the three cases. Again, the advantage of the switched-gain scheme is evident.

	Switched-gain	$\varepsilon = 0.01$	$\varepsilon = 0.0005$
e_1	0.0082	0.0741	0.0214
e_2	0.1070	0.6154	0.2046
e_1(SS)	0.0015	0.0015	0.0208
e_2(SS)	0.0248	0.0248	0.2107

Table 3.2. Comparison of R.M.S tracking errors $e_1 = x_1 - r$, $e_2 = x_2 - \dot{r}$, e_1 steady-state, and e_2 steady-state for the switched-gain scheme and two HGOs for $|v| \leq 0.016$ and $\phi_0 \neq \phi$.

	Switched-gain	$\varepsilon = 0.01$	$\varepsilon = 0.0005$
e_1	0.0063	0.0741	0.0037
e_2	0.0760	0.6294	0.0391
e_1(SS)	9.49e-5	9.49e-5	9.75e-5
e_2(SS)	0.0025	0.0025	0.0137

Table 3.3. Comparison of R.M.S tracking errors $e_1 = x_1 - r$, $e_2 = x_2 - \dot{r}$, e_1 steady-state, and e_2 steady-state for the switched-gain scheme and two HGOs for $|v| \leq 0.0016$ and $\phi_0 = \phi$.

3.5 Nonlinear Differentiation

Here we consider the high-gain observer used as a differentiator and employ a continuous nonlinear function to smoothly transition between two gain values. This nonlinear function is similar to the one used in [67] to deal with measurement noise. The differentiator takes the form of a linear high-gain observer

$$\dot{\hat{x}} = A\hat{x} + H(y - C\hat{x})$$

where the gain matrix H is the same as Equation (3.6). The observer estimates the derivatives of the measured signal $y(t) = \omega(t) + v(t)$, where $\omega(t)$ is the signal of interest that is corrupted by measurement noise $v(t)$. Let $\bar{\omega} = [\omega \ \dot{\omega} \ \cdots \ \omega^{(r-1)}]^T$, $\tilde{x}_i = x_i - \omega^{(i-1)}$,

and consider the rescaling $\eta_i = \varepsilon^{i-1}\tilde{x}_i$. This yields an estimation error equation similar to (3.13)

$$\varepsilon\dot{\eta} = A_0\eta + \varepsilon^r B\omega^{(r)} + B_2 v$$

Consider a second order differentiator ($r = 2$) and the following transfer functions

$$\tilde{x}_1 = \frac{\varepsilon^2}{\varepsilon^2 s^2 + \varepsilon\alpha_1 s + \alpha_2}\ddot{w} - \frac{\varepsilon\alpha_1 s + \alpha_2}{\varepsilon^2 s^2 + \varepsilon\alpha_1 s + \alpha_2} v \tag{3.77}$$

$$\tilde{x}_2 = \frac{\varepsilon^2 s + \varepsilon\alpha_1}{\varepsilon^2 s^2 + \varepsilon\alpha_1 s + \alpha_2}\ddot{w} - \frac{\alpha_2 s}{\varepsilon^2 s^2 + \varepsilon\alpha_1 s + \alpha_2} v \tag{3.78}$$

The tradeoff in choice of ε can clearly be seen. Accurate estimation is obtained through smaller values of ε, while rejection of measurement noise requires larger values of ε. Again, we will employ an observer scheme that transitions between two gain values in order to relax this tradeoff. For the discontinuous switching scheme of Section 3.3 we had to introduce a delay time in order to avoid multiple switchings as shown in Figure 3.10. This simplified the analysis by allowing only one switching event which can be viewed as a resetting of initial conditions. Rather than a discontinuous switch between two gains, we use a dead zone nonlinearity to smoothly transition between the gains. This is illustrated in the block diagram of Figure 3.1. The dead zone function output is zero for $y - \hat{x}_1$ within the dead zone $[-d, d]$, thus the gain is g_2. For $y - \hat{x}_1$ outside the dead zone, the gain is g_1 plus an offset value. This results in a continuous gain function as shown in Figure 3.2. Mathematically, the nonlinear gain function is given by

$$g^i(y - \hat{x}_1) = \begin{cases} g_2^i, & for \quad |y - \hat{x}_1| < d \\ g_1^i - d\left(g_1^i - g_2^i\right) sign(y - \hat{x}_1), & for \quad |y - \hat{x}_1| \geq d \end{cases} \tag{3.79}$$

for each power $i = 1 \cdots r - 1$. With

$$g_1 = \frac{1}{\varepsilon_1}, \quad g_2 = \frac{1}{\varepsilon_2}$$

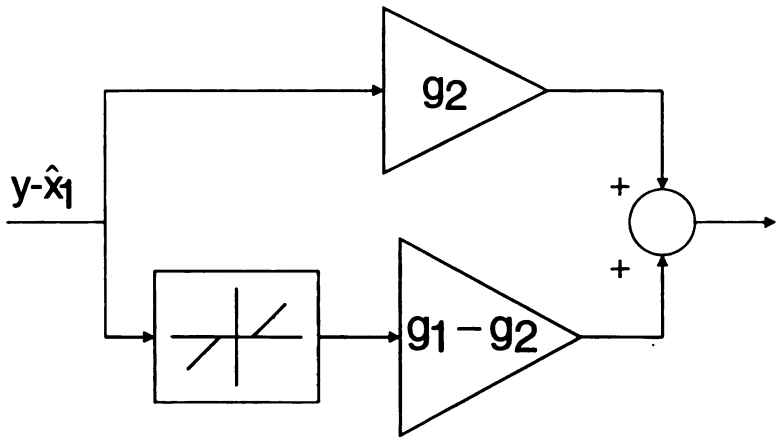

Figure 3.1. Diagram illustrating Dead Zone switching scheme.

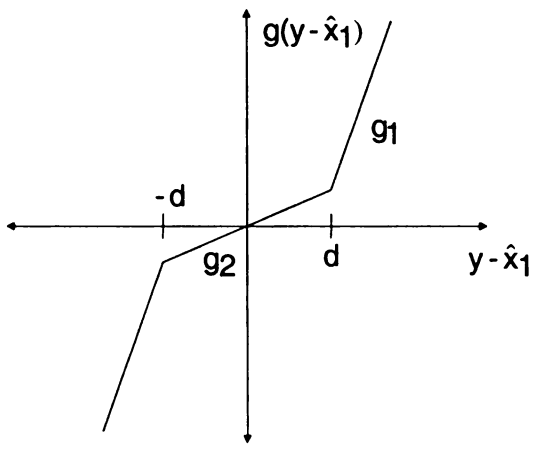

Figure 3.2. Plot of the nonlinear gain function.

the nonlinear high-gain observer is given by

$$\dot{\hat{x}} = A\hat{x} + G(y - \hat{x}_1)[y - \hat{x}_1] \tag{3.80}$$

where

$$G(y - \hat{x}_1) = \begin{bmatrix} \alpha_1 g(y - \hat{x}_1) \\ \alpha_2 g^2(y - \hat{x}_1) \\ \vdots \\ \alpha_{r-1} g^{r-1}(y - \hat{x}_1) \end{bmatrix}$$

Referring back to Equation (3.77), the idea behind the nonlinear observer can be described as follows. Let $|v| \leq k_v \mu$. Notice that when $\ddot{\omega}$ is zero, $|\tilde{x}_1| \leq K_1 k_v \mu$ for some positive constant K_1. Thus, by choosing the dead zone width to be $d \geq K_1 k_v \mu$ the nonlinear observer will use the smaller gain value during steady-state operation, when $\ddot{\omega}$ is zero or very small, thereby reducing the effect of noise. Now, suppose we are operating within the dead zone and $\varepsilon = \varepsilon_2$. Then we have that

$$|\tilde{x}_1| \leq K_2 \varepsilon_2 \ddot{w} + K_1 k_v \mu$$

for some positive constant K_2. If ω is quickly changing, $\ddot{\omega}$ is large and for a relatively large choice of ε_2, the product $\varepsilon_2 \ddot{w}$ may be large enough to move the estimation error $\tilde{x}_1$ outside the dead zone. Once outside the dead zone the nonlinear observer uses the larger gain to improve the estimation. During the fast transients, the output error may enter and leave the dead zone, but the continuous nonlinear function provides smooth switching between gains. The analysis behind the dead zone switching is complicated by the bias term. Using Lyapunov analysis, it is easy to show that the estimation error is bounded. However, starting outside the switching zone, it is difficult to show that the estimation error will reach the switching zone. This remains an open problem and we illustrate this scheme through a numerical example.

3.5.1 Deadzone Switching Example

We consider a signal $\omega(t)$ whose profile is shown in Figure 3.13 along with the first and second derivatives. We performed the simulation for three cases of a measurement noise that is a uniformly distributed function of time between [-3.14e-4, 3.14e-4]. Here we used Simulink's "Quantizer" block to generate the noise. The first case considers the nonlinear high-gain differentiator, Equation (3.80), for $g_1 = 1570$ and $g_2 = 188$. Then, for comparison, we simulated two linear high-gain observers; one with $g = 188$ and the other with $g = 1570$. Figure 3.14 shows the estimate $\hat{x}_3$ plotted against $\omega^{(2)}$ for the three cases. The figure shows that the dead zone scheme (top) was more effective in tracking the signal transients then the $g = 188$ linear observer and better at rejecting noise at steady-state than the $g = 1570$ linear observer. The relaxation of the tradeoff is emphasized in Figures 3.15 and 3.16. These Figures show the tracking error $\omega^{(2)} - \hat{x}_3$ for the three cases with Figure 3.16 zoomed in to capture the steady-state behavior. Notice the difference in the y axis scales. The improved performance with the dead zone scheme is clear. Also, we remark that the dead zone low noise estimator of [67] used first order filters and differentiators. Compared to [67], the high-gain observer scheme exhibits improved performance owing to the low pass filtering characteristic of the third order high-gain observer used in this example. This can be seen by comparing the dead zone HGO in Figures 3.15 and 3.16 with the low noise estimator in Figure 3.17.

3.6 Conclusions

We have derived relationships that exhibit the tradeoff between fast reconstruction of the states and rejection of modeling error versus the immunity to measurement noise for a high-gain observer. Based on this we have designed a switched-gain version of the high-gain observer in an attempt to relax the tradeoff between fast state reconstruction and rejection of measurement noise. To handle the peaking in the estimates we have included a

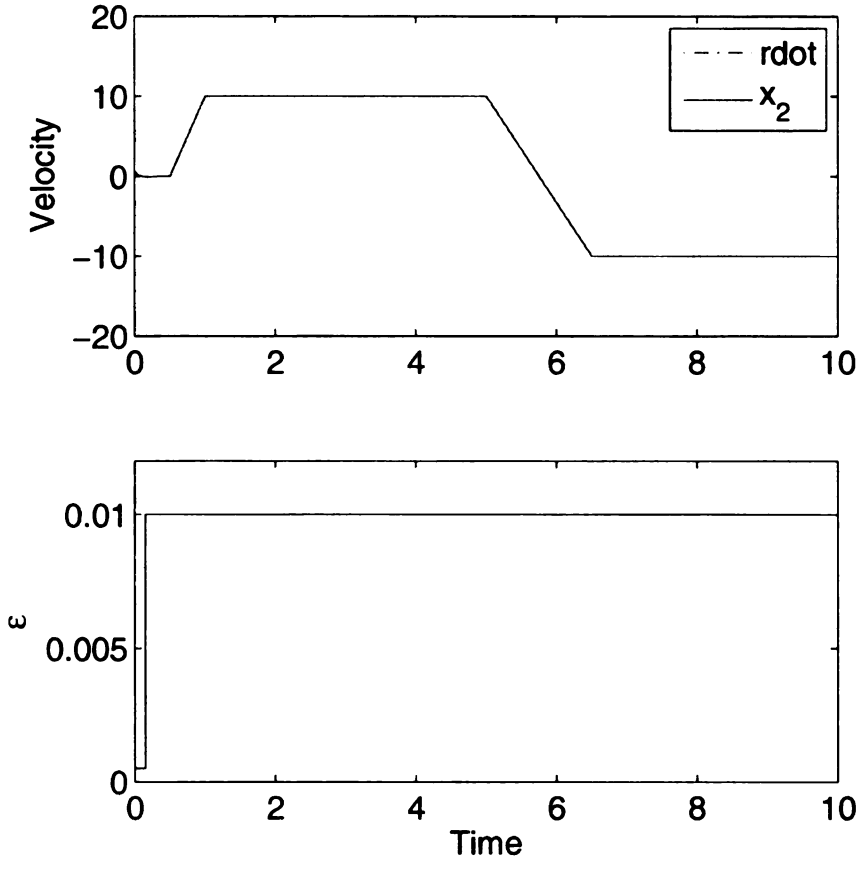

Figure 3.3. Top: The velocity reference trajectory ($\dot{r}$)(dotted) and x_2 under the switched observer (solid). Bottom: Switching behavior of the gain.

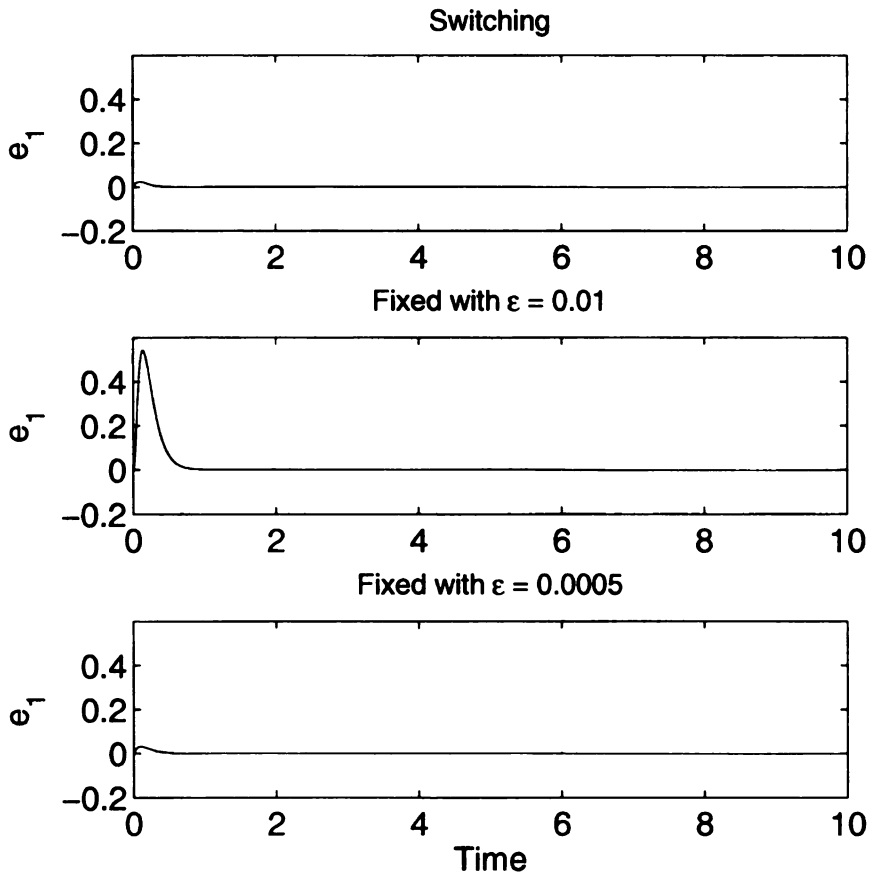

Figure 3.4. Position tracking error ($e_1 = x_1 - r$) for the switched-gain observer (top), the observer with $\varepsilon_2 = 0.01$ (middle), and the observer with $\varepsilon_1 = 5 \times 10^{-4}$ (bottom).

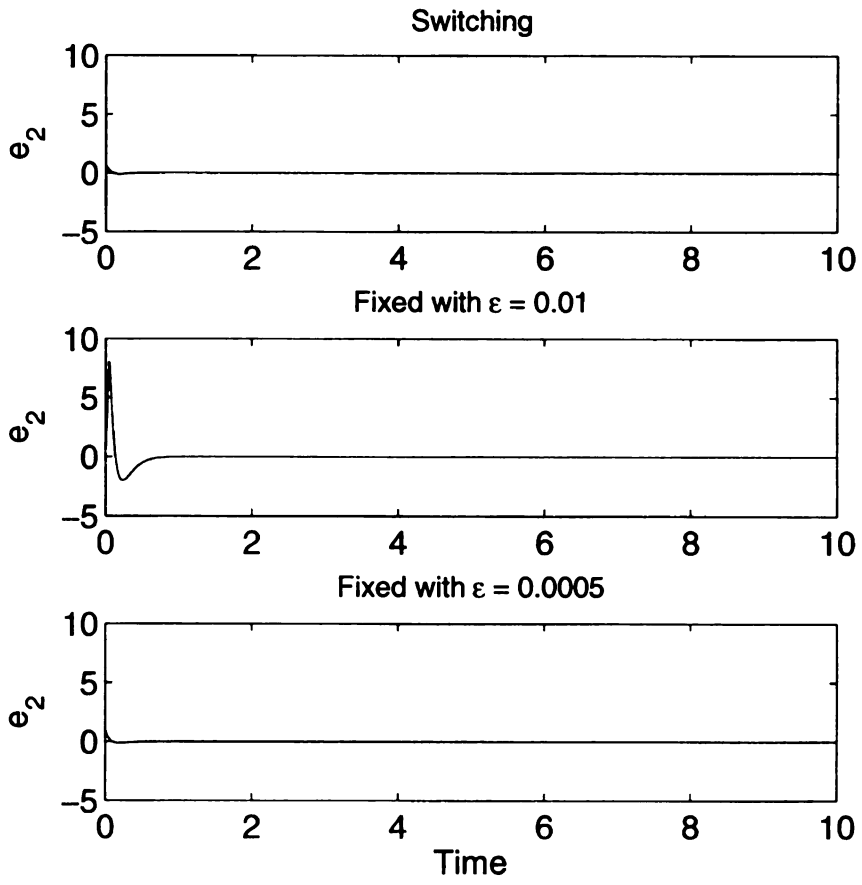

Figure 3.5. Tracking error ($e_2 = x_2 - \dot{r}$) for the switched-gain observer (top), the observer with $\varepsilon_2 = 0.01$ (middle), and the observer with $\varepsilon_1 = 5 \times 10^{-4}$ (bottom).

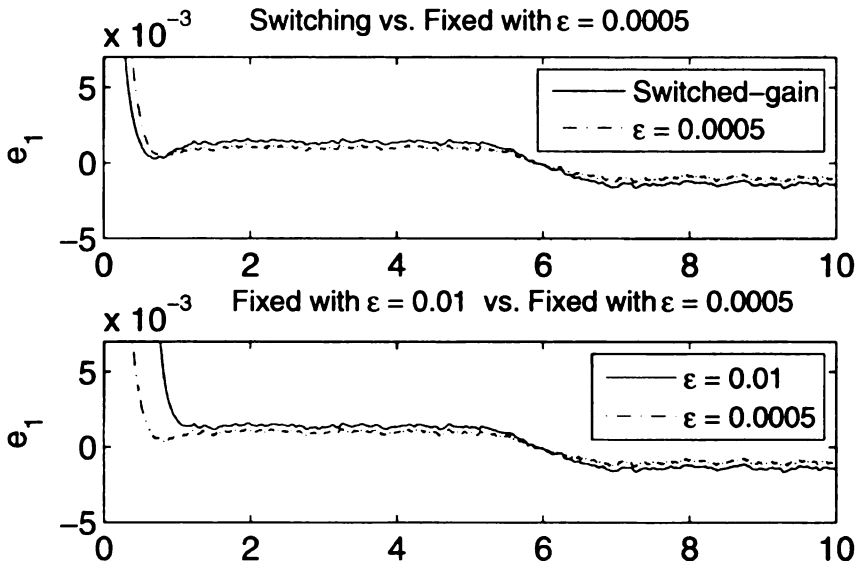

Figure 3.6. Steady-State tracking error ($e_1 = x_1 - r$) for the switched-gain observer plotted against the observer with $\varepsilon_1 = 5 \times 10^{-4}$ (top) and the observer with $\varepsilon_2 = 0.01$ plotted against the observer with $\varepsilon_1 = 5 \times 10^{-4}$ (bottom).

switching delay in our scheme. We've also considered a nonlinear high-gain differentiator with smooth switching based on dead zone nonlinearity. Numerical examples illustrate the effectiveness of each design.

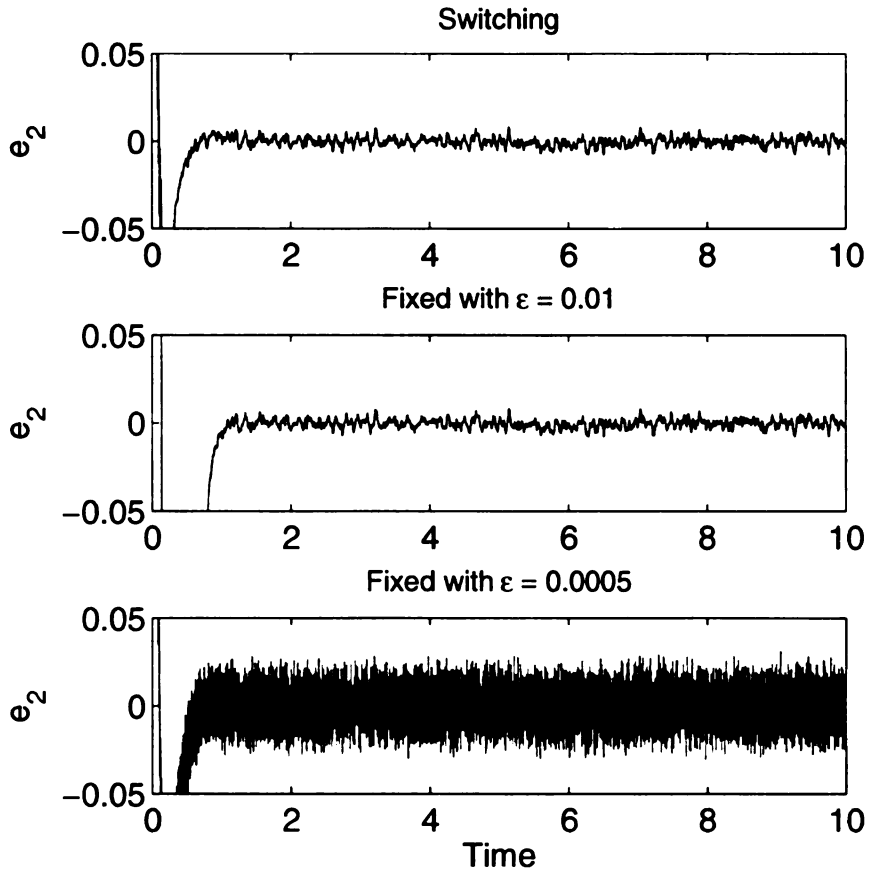

Figure 3.7. Steady-State tracking error ($e_2 = x_2 - \dot{r}$) for the switched-gain observer (top), the observer with $\varepsilon_2 = 0.01$ (middle), and the observer with $\varepsilon_1 = 5 \times 10^{-4}$ (bottom).

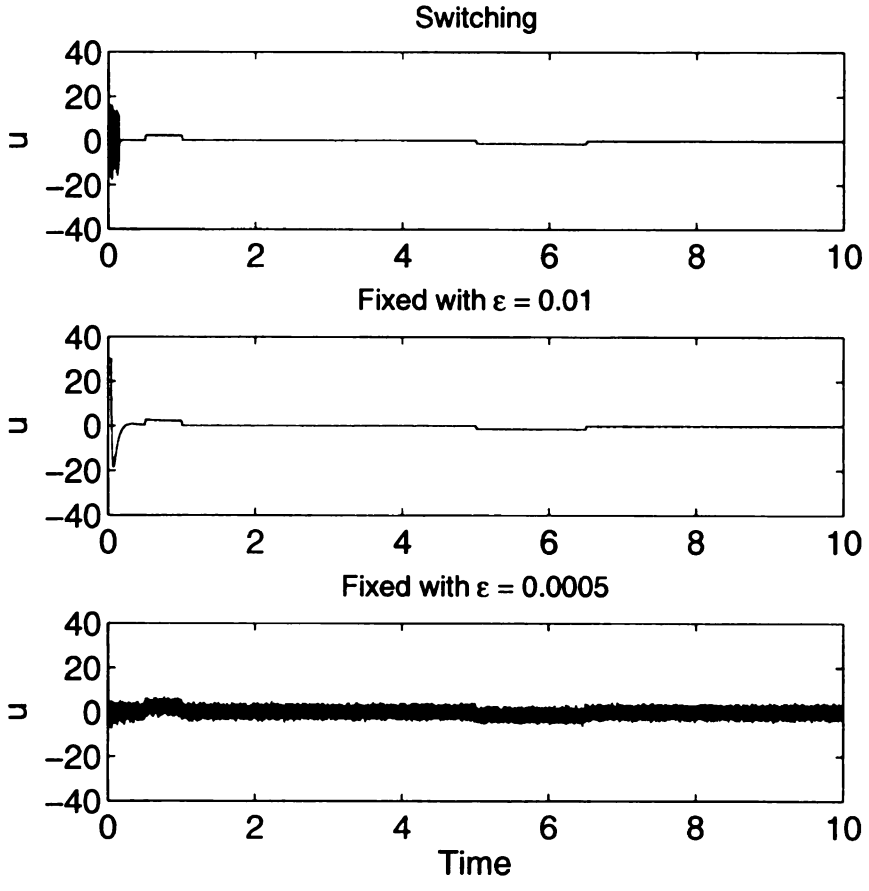

Figure 3.8. Behavior of the control for the three cases.

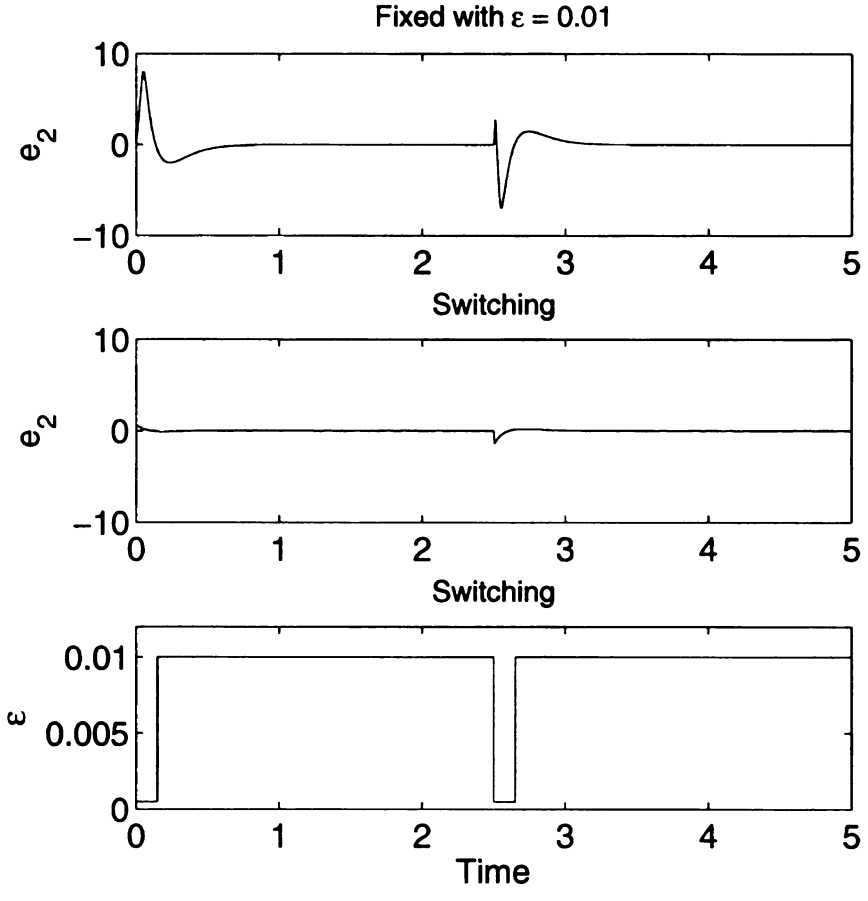

Figure 3.9. Tracking error ($e_2 = x_2 - \dot{r}$) for the observer with ε_2 (top) and the switched-gain observer (middle) for an impulsive-like disturbance at 2.5s. The bottom plot shows the switching behavior of the gain.

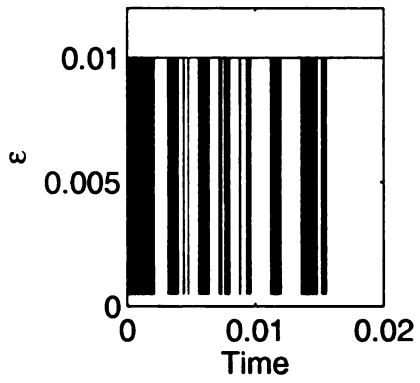

Figure 3.10. Switching behavior of the gain when $T_d = 0$.

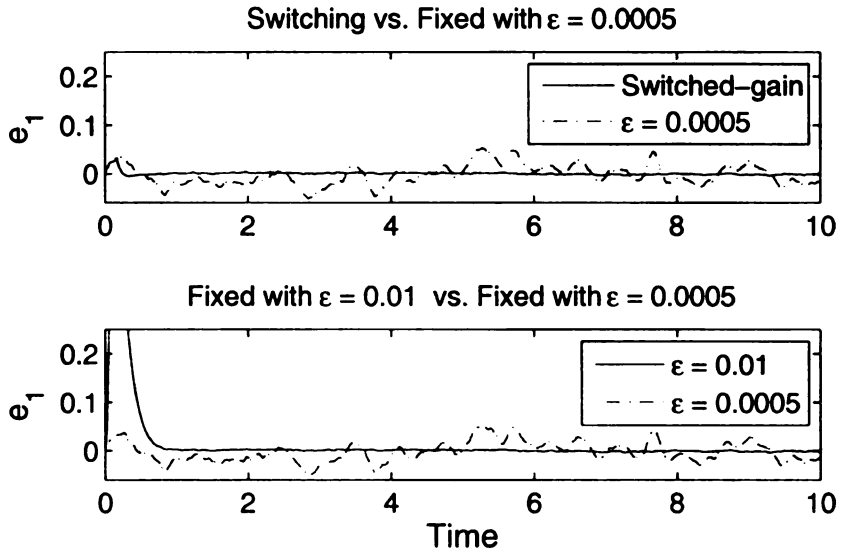

Figure 3.11. Steady-State tracking error ($e_1 = x_1 - r$) for the switched-gain observer plotted against the observer with $\varepsilon_1 = 5 \times 10^{-4}$ (top) and the observer with $\varepsilon_2 = 0.01$ plotted against the observer with $\varepsilon_1 = 5 \times 10^{-4}$ (bottom) with $|v| \leq 0.016$.

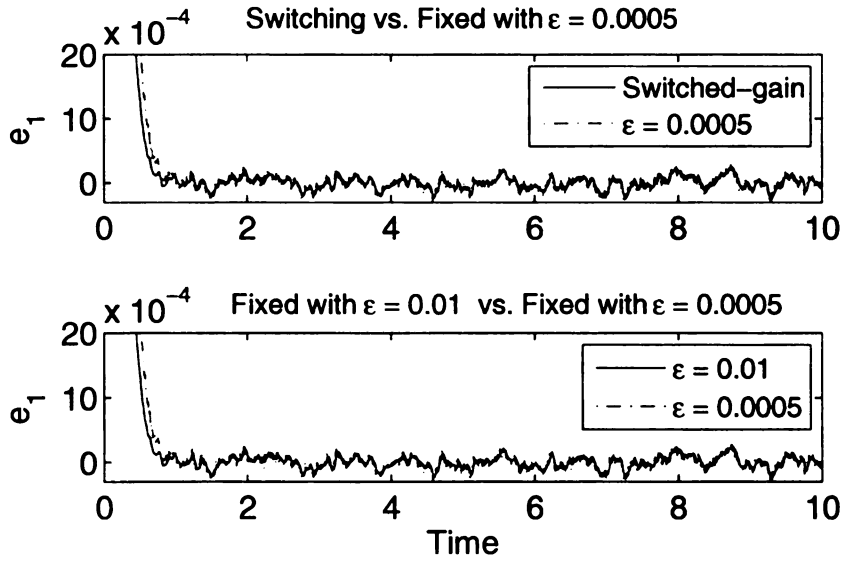

Figure 3.12. Steady-State tracking error ($e_1 = x_1 - r$) for the switched-gain observer plotted against the observer with $\varepsilon_1 = 5 \times 10^{-4}$ (top) and the observer with $\varepsilon_2 = 0.01$ plotted against the observer with $\varepsilon_1 = 5 \times 10^{-4}$ (bottom) with $|v| \leq 0.0016$ and $\phi_0 = \phi$.

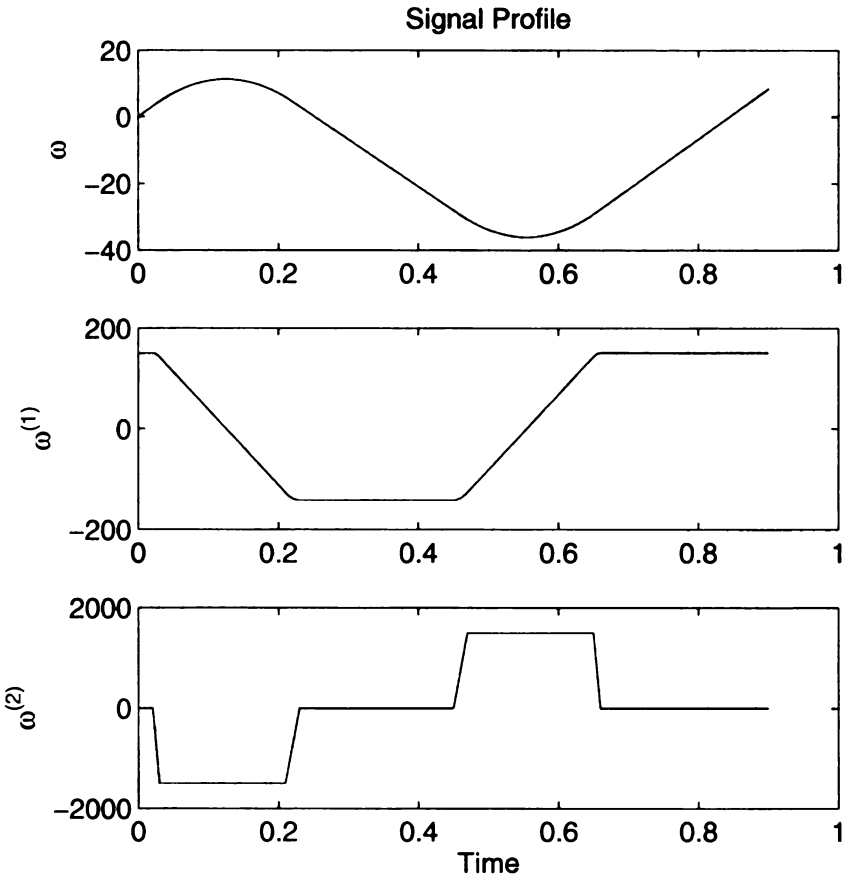

Figure 3.13. The signal $\omega(t)$ (top) and its first (middle) and second (bottom) derivatives.

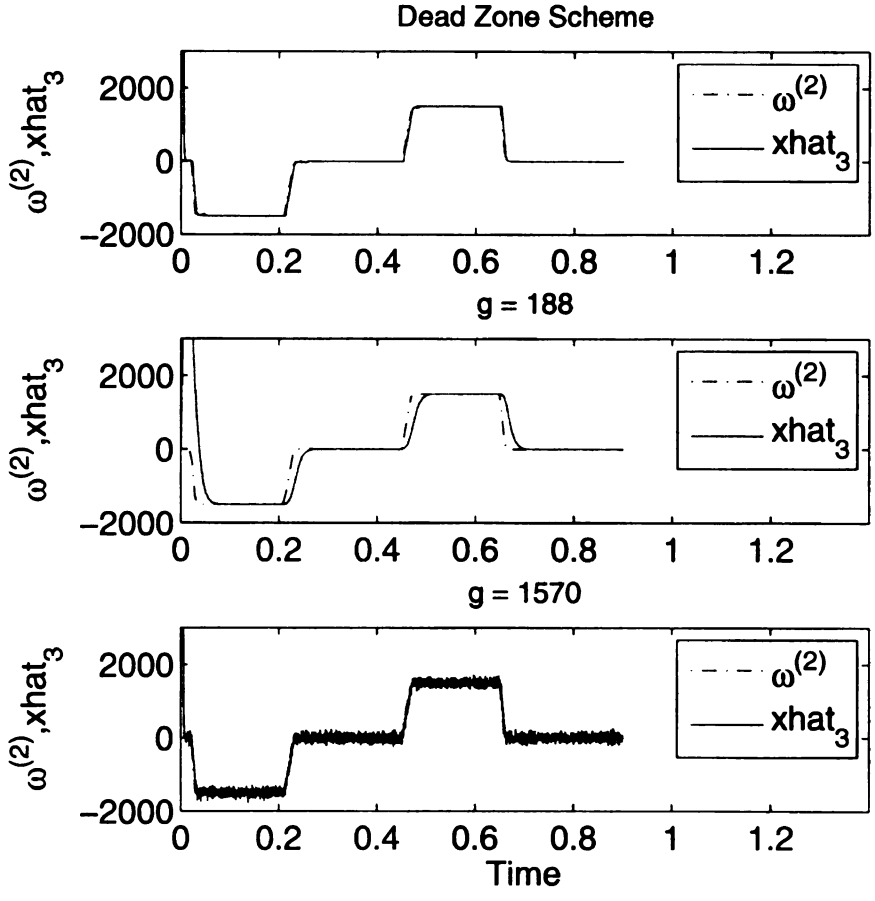

Figure 3.14. $\hat{x}_3$ versus $\omega^{(2)}$ for Dead Zone switching (top) Linear HGO with $g = 188$ (middle) and $g = 1570$ (bottom).

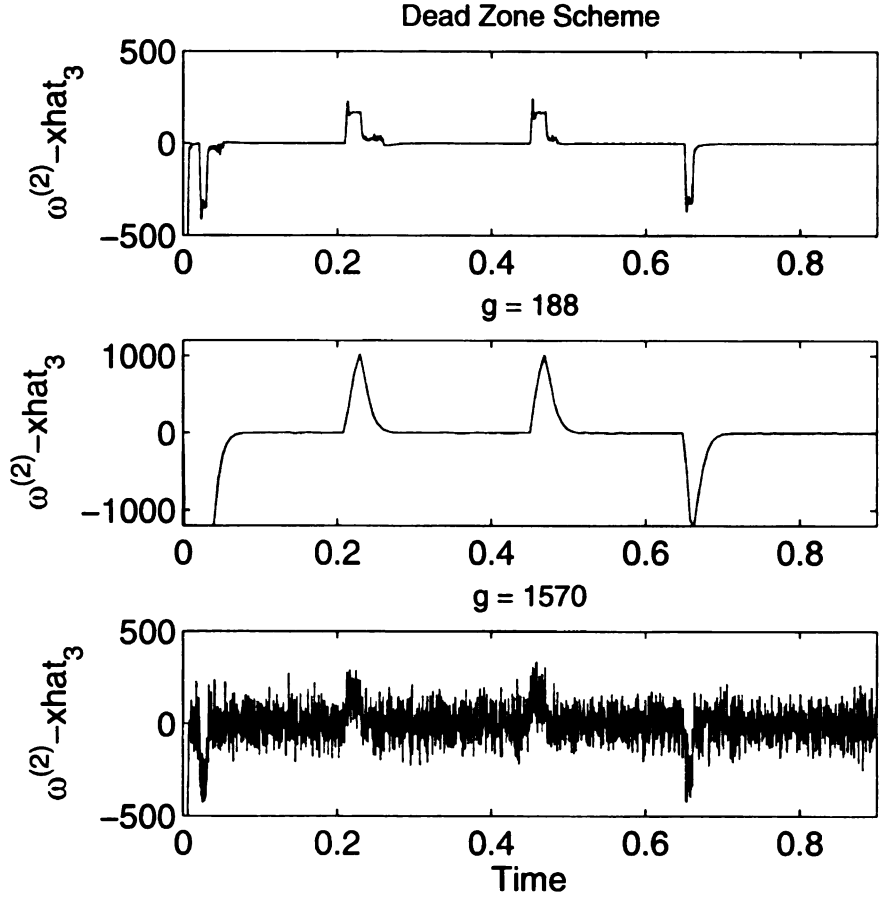

Figure 3.15. Tracking error $\omega^{(2)} - \hat{x}_3$ for Dead Zone switching (top) Linear HGO with $g = 188$ (middle) and $g = 1570$ (bottom).

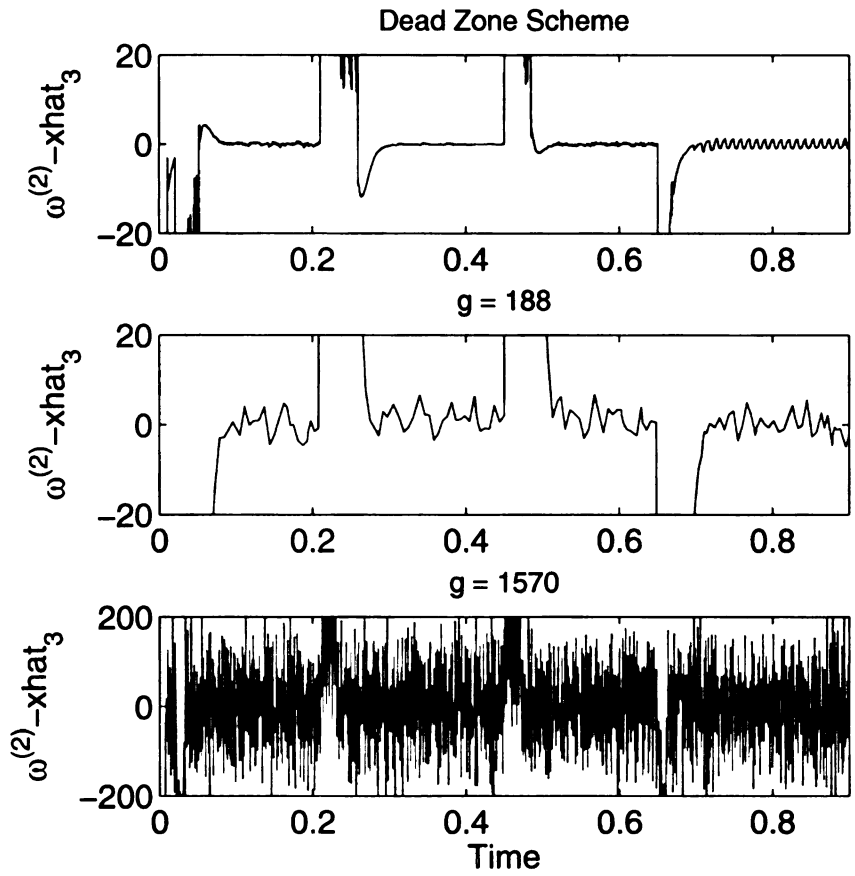

Figure 3.16. Zoomed in tracking error $\omega^{(2)} - \hat{x}_3$ for Dead Zone switching (top) Linear HGO with $g = 188$ (middle) and $g = 1570$ (bottom).

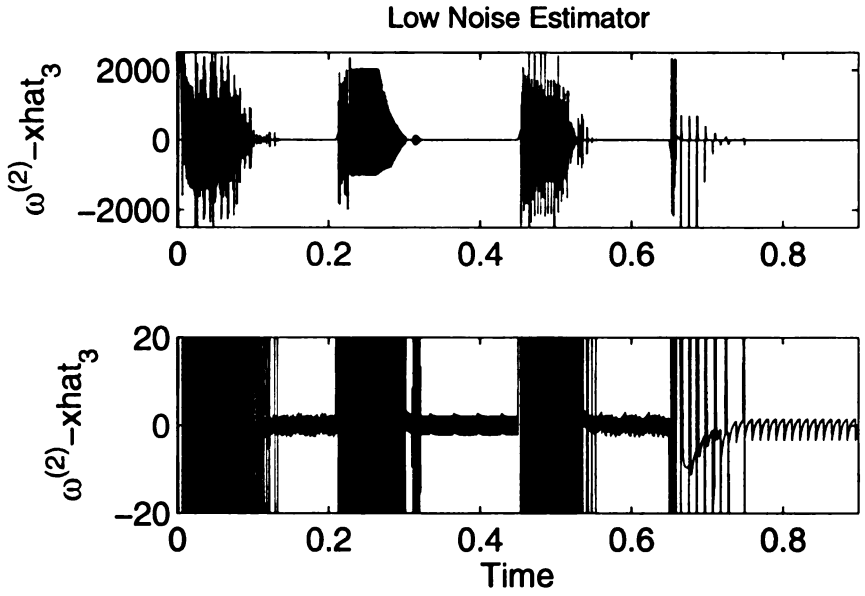

Figure 3.17. Tracking error $\omega^{(2)} - \hat{x}_3$ (top) and the zoomed in tracking error $\omega^{(2)} - \hat{x}_3$ (bottom) for the low noise estimator of [67].

CHAPTER 4

Multirate Sampled Data Output Feedback Using High Gain Observers

4.1 Introduction

The study of sampled-data systems has received significant attention due to the fact that modern control systems are almost always implemented digitally [4]. As discussed in [52], there are primarily three approaches for the design of digital controllers. First, is the design based on a continuous-time plant model followed by controller discretization and implementation through sample and hold methods. This approach is the most widely seen in the literature for nonlinear systems. See [5], [15], [18], [20], [30], [37], [41], [48], [53], [55], and [74]. Second, is design based on exact or approximate discrete-time plant models ignoring the intersampling behavior. This method is generally simpler for linear systems since an exact discrete-time model can be obtained, whereas for nonlinear systems this is typically not the case and approximate models must be used. See [44], [50], [51], [52], [54], and [60]. The third and least talked about approach in the literature is to design the controller based on a sampled-data model of the plant that takes into account the inter-sampling behavior. We briefly discuss the state of the art of sampled-data state feedback stabilization. In [18] it is shown that the sampled-data implementation of a controller

designed in continuous-time to globally stabilize the origin achieves semiglobal practical stabilization where the state can be brought arbitrarily close to the origin by choosing the sampling period T sufficiently small. In [53] and [74], given a continuous-time state feedback controller that exponentially stabilizes the origin, the sampled-data implementation can bring the state x to the origin as $t \to \infty$. This is shown both locally and globally, with the global results requiring the restrictive assumption of global exponential stability. Also, in [5] it is shown that convergence of the state to the origin can be achieved under sampled-data state feedback, but again for nonlocal results restrictive assumptions such as global exponential stability and globally Lipschitz functions are needed. In [54], multirate sampled-data stabilization in the presence of time delay was studied for the case when the control rate is made faster than the measurement rate. It is shown that the closed-loop multirate sampled-data system achieves asymptotic stabilization in the semiglobal practical sense.

Results on sampled-data output feedback and digital observer design can be found in [2], [20], [32], [37], [41], [49], and [59]. In [59], multirate design of a sliding-mode observer is considered, where the observer processing rate is higher than the control update rate. The observer processing rate is selected high enough to allow for accurate estimation. The control is operated at a lower rate to save on the computational expense. In [2], the authors study discrete-time observers designed for sampled-data nonlinear systems for two cases. In the first case the observer is designed for an approximate discrete-time plant and in the second one it is designed for a continuous-time plant then discretized. They study under what conditions, and how closely, the two designs achieve convergence to the exact discrete-time model. In [37], an observer is designed based on a discrete-time model and it is shown that the performance of a stabilizing continuous-time state feedback controller can be recovered by a sampled-data output feedback controller for sufficiently small sampling period. Two schemes for overcoming peaking during the initial transient are presented, one based on global boundedness of the control law and a second

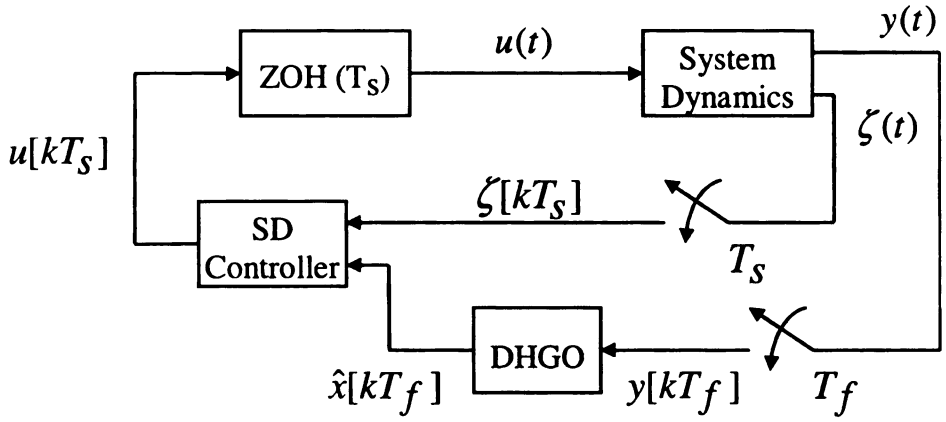

Figure 4.1. Block diagram illustrating the multirate output feedback control scheme.

based on maintaining the control at a fixed value during the observer transient period. The class of systems under consideration was the same as that of [20], where an output feedback controller is implemented by discretizing a controller designed under continuous-time state feedback and using a discrete-time high-gain observer to estimate the system states. It was shown that the output feedback controller stabilizes the origin of the closed-loop system for sufficiently small sampling period T. In addition, it was shown that the performance under sampled-data output feedback asymptotically approaches the performance under continuous-time state feedback as $T \to 0$. For the discrete-time high-gain observer, more accurate estimation of the system states is achieved by faster sampling of the output. Based on this observation , we seek to study the stability of a system under sampled-data output feedback using high-gain observers, where the control rate is fixed by the sampled-data state feedback design, while the output sampling rate is faster. This multirate sampled-data output feedback control scheme is illustrated in Figure 4.1 for the class of systems under consideration. We apply the control signal at the sample period T_S through a zero-order-hold where the control is held constant in between sampling points. The output y is sampled at a faster rate where we use the period $T_f < T_S$. The

measurement y is a driving term for the observer and it is the sampling rate of this output that we adjust to achieve more accurate estimation. The measurement ζ is used in the control and we sample it with the same period T_s. Consideration of multirate observers is motivated by asymptotic properties of high-gain observers and applications that may require computationally demanding controllers such has hysteresis inversion. The idea is that faster sampling of the output leads to faster and more accurate state estimation. On the other hand, slower control sampling allows time to process the control signal. This may be useful when the sampling rate of the control is chosen based on the performance of the closed-loop system under sampled-data state feedback. Throughout this chapter and the next we will refer to the sampled-data output feedback scheme that uses the same control and measurement sampling rates as the single-rate scheme. For single-rate output feedback using discrete-time high-gain observers, the sampling rate may have to be pushed higher than that of the sampled-data state feedback case in order to stabilize the closed-loop system. For the multirate case, stability can be achieved by making the output sampling sufficiently fast while maintaining the control sample rate that was designed under state feedback. This scheme may lead to a more computationally efficient controller. Different sampling rates for the control and the estimation has the additional benefit of isolating the control signal from the observer's initial transient. This can be done by initializing the control signal (i.e. keeping it fixed) until the observer has settled ([37], [4]). We will see that, due to the flexibility of the multirate scheme, initialization can be performed in as little as one sample period. This chapter is organized as follows. In Section 4.2 we develop the closed-loop system under multirate sampled-data output feedback. Section 4.3 provides the analytical results where we consider the stability of the closed-loop system under multirate output feedback control given a sampled-data state feedback controller that asymptotically stabilizes the origin. We show that the closed-loop system under multirate sampled-data output feedback achieves practical stabilization of the origin using the control sample rate of the state feedback design (T_s) and a sufficiently

large output measurement rate. In order to bring the trajectories of the closed-loop system to the origin under multirate output feedback, we need a stronger condition on the stability of the state feedback controller. We will show that the multirate scheme exponentially stabilizes the origin of the closed-loop system given an exponentially stabilizing state feedback controller. As we have seen, it is often the case that sampled-data state feedback control of nonlinear systems can only be shown to achieve practical stabilization of the origin. In addition, disturbances may also prevent asymptotic stabilization of the origin. In Section 4.4 we study the case where the sampled-data state feedback controller can only bring the trajectories of the closed-loop system to a set containing the origin. We use the notion of stability with respect to a compact set to show boundedness and ultimate boundedness of the closed-loop system under multirate output feedback. Also, with a view toward practical implementation of the multirate observer, we discuss the tracking problem and integral control. Finally, in Section 4.5 a numerical example seeks to highlight some of the stability properties of the multirate output feedback controller and its ability to handle peaking in the estimates.

4.2 Multirate Output Feedback Control

We consider the following class of systems

$$\dot{z} = \psi(x, z, u) \tag{4.1}$$

$$\dot{x} = Ax + B\phi(x, z, u) \tag{4.2}$$

$$y = Cx \tag{4.3}$$

$$\zeta = \Theta(x, z) \tag{4.4}$$

where $x \in \mathbb{R}^r$ and $z \in \mathbb{R}^\ell$ are the states, u is the input, y and ζ are the measured outputs. The functions ϕ, ψ, and Θ are locally Lipschitz in their arguments over the domain of interest and satisfy $\phi(0,0,0) = 0$, $\psi(0,0,0) = 0$, $\Theta(0,0) = 0$. The $r \times r$ matrix A, the

$r \times 1$ matrix B, and the $1 \times r$ matrix C are the same as (1.5)-(1.6). The multirate output feedback controller is implemented using the high-gain observer

$$\dot{\hat{x}} = A\hat{x} + B\phi_0(\hat{x}, \zeta, u) + H(y - C\hat{x}) \tag{4.5}$$

where the function ϕ_0 is locally Lipschitz in its arguments over the domain of interest, globally bounded in x, and satisfies $\phi_0(0,0,0) = 0$. The gain matrix is given by

$$H^T = \begin{bmatrix} \frac{\alpha_1}{\varepsilon} & \frac{\alpha_2}{\varepsilon^2} & \cdots & \frac{\alpha_r}{\varepsilon^r} \end{bmatrix} \tag{4.6}$$

where ε is a small positive parameter and the roots of

$$s^r + \alpha_1 s^{r-1} + \cdots + \alpha_{r-1} s + \alpha_r = 0 \tag{4.7}$$

have negative real parts. We consider the following partial state feedback controller

$$u = \gamma(x, \zeta) \tag{4.8}$$

where γ is locally Lipschitz in its arguments over the domain of interest and $\gamma(0,0) = 0$. Let $\chi = [z \;\; x]^T$ and rewrite (4.1)-(4.2) as

$$\dot{\chi} = F(\chi, u) \tag{4.9}$$

where

$$F(\chi, u) = \begin{bmatrix} \psi(x, z, u) \\ Ax + B\phi(x, z, u) \end{bmatrix}$$

Then, we can write the closed-loop system under continuous-time state feedback as

$$\dot{\chi} = F(\chi) \tag{4.10}$$

The solution of (4.9) over the sampling period $[kT_s, kT_s + T_s]$ is given by

$$\chi(t) = \chi(k) + (t - kT_s)F(\chi(k), u(k)) + \int_{kT_s}^{t} [F(\chi(\sigma), u(k)) - F(\chi(k)), u(k))]d\sigma \quad (4.11)$$

Since the function F is locally Lipschitz we can use the Gronwall-Bellman inequality to show that

$$\|\chi(t) - \chi(k)\| \leq \frac{1}{L_1}\left[e^{(t-kT_s)L_1} - 1\right] \|F(\chi(k), u(k))\| \quad (4.12)$$

for all $t \in [kT_s, kT_s + T_s]$ where L_1 is a Lipschitz constant of F with respect to χ over the domain of interest. We have

$$\chi(k+1) = \chi(k) + T_s F(\chi(k), u(k)) + T_s^2 \Phi(\chi(k), u(k), T_s) \quad (4.13)$$

where Φ is locally Lipschitz in (χ, u). This model and equation (4.12) describe the discrete-time plant dynamics and the intersampling behavior, respectively. The discretized high-gain observer is implemented by first scaling the observer states according to

$$q = D\hat{x} \quad (4.14)$$

where $D = diag[1, \varepsilon, \cdots, \varepsilon^{r-1}]$. This yields

$$\dot{q} = \frac{1}{\varepsilon}[A_o q + H_o y + \varepsilon^r B \phi_0(D^{-1}q, \zeta, u)] \quad (4.15)$$

where $A_o = \varepsilon D(A - HC)D^{-1} = A - H_o C$ and

$$H_o = \varepsilon DH = \begin{bmatrix} \alpha_1 \\ \alpha_2 \\ \vdots \\ \alpha_r \end{bmatrix}$$

This nonlinear observer is discretized using the forward difference method. For the dynamics under fast sampling we use the index n to indicate the sampling points that are equally spaced with period T_f. We obtain

$$q(n+1) = A_f q(n) + B_f y(n) + \varepsilon^{r-1} T_f B \phi_0(D^{-1} q(n), \zeta(k), u(k)) \quad (4.16)$$

$$\hat{x}(n) = C_f q(n) \quad (4.17)$$

We point out that u and ζ evolve in the slow sampling time k and are constant for all n where $nT_f \in [kT_S, kT_S + T_S)$. The matrices A_f, B_f, and C_f are given by

$$A_f = I + \frac{T_f}{\varepsilon} A_o, \quad B_f = \frac{T_f}{\varepsilon} H_o, \quad C_f = D^{-1}$$

As in [20] we take $\alpha = T_f/\varepsilon$ where α is a finite positive value and must be chosen such that the matrix A_f has all its eigenvalues inside the unit circle. This ratio indicates that the fast sampling frequency increases as the gain increases. The observer estimates are downsampled for use in the output feedback controller. Using the relation

$$h = \frac{T_S}{T_f} = \frac{T_S}{\varepsilon \alpha}$$

we employ the following notation to denote the value of the vector of estimates under the slow sampling period

$$\hat{x}_S(k) = \hat{x}(\lfloor hk \rfloor) \quad (4.18)$$

where $\lfloor w \rfloor$ indicates the greatest integer less than or equal to w. This gives the following output feedback controller

$$u(k) = \gamma(\hat{x}_S(k), \zeta(k)) \quad (4.19)$$

In the introduction chapter we have seen that this controller will need to be globally bounded outside a compact region of interest in order to overcome the peaking phe-

nomenon. As discussed in [37], peaking in the initial time instant can be overcome by setting the control to some arbitrary values and then using the observer estimates after they have recovered from peaking. We take a similar approach here by using the following control

$$\left.\begin{aligned} u(k) &= u_0(k), && for \quad 0 \le k < k_0 \\ u(k) &= \gamma(\hat{x}_S(k), \zeta(k)), && for \quad k \ge k_0 \end{aligned}\right\} \tag{4.20}$$

Because of the flexibility of the multirate scheme, we can choose the output sampling rate sufficiently fast so that the estimates recover from peaking during the period $[0, T_S]$. In this case we only have to set the control to some initial value $u(0) = u_0(0)$. Furthermore, the states of the plant $\chi(t)$ will not grow by more than $O(T_S)$ from its initial condition during this period. As we will discuss later on, the control still needs to be globally bounded to prevent any peaking that occurs after the initial time. Still, the control scheme (4.20) prevents controller saturation during the first time instants. In some situations, choosing the output sampling rate fast enough that the observer peaking passes during the interval $[0, T_S]$ may require T_f to be prohibitively small. Further, the sampling period T_f that guarantees certain closed-loop performance need not be as small. In the forthcoming analysis we will consider the choice of T_f that is sufficient to guarantee boundedness of the closed-loop system. Then, we will remark on the choice of T_f that avoids peaking.

In what follows, we will need to describe the plant dynamics in the fast sampling time n. So, consider the solution to equation (4.9) over the fast sampling period $[nT_f, nT_f + T_f]$

$$\chi(t) = \chi(n) + (t - nT_f)F(\chi(n), u(k)) + \int_{nT_f}^{t} [F(\chi(\sigma), u(k)) - F(\chi(n)), u(k))]d\sigma$$

where again the control $u(k)$ is constant for all $nT_f \in [kT_S, kT_S + T_S)$. Also, consider

$$\|\chi(t) - \chi(n)\| \le \frac{1}{L_1}\left[e^{(t-nT_f)L_1} - 1\right] \|F(\chi(n), u(k))\| \tag{4.21}$$

which describes the intersampling behavior under the fast sampling time n. Then by the

same argument used to arrive at (4.13), we get

$$\chi(n+1) = \chi(n) + T_f F(\chi(n), u(k)) + T_f^2 \Phi(\chi(n), u(k), T_f) \tag{4.22}$$

where Φ is locally Lipschitz in (χ, u). For the analysis we will also need a model that describes the observer error dynamics. This will require a discrete-time model of (4.2) under the fast sampling rate that makes use of its special structure and the properties of the matrices A, B, and C. In addition, deriving the observer-error equation requires rescaling of the estimation error. The details of these derivations are similar to [20] and are covered next. First, observe that

$$DB = \varepsilon^{r-1} B \ , \ CD = C \ , \ \varepsilon^i D A^i = A^i D \ , \ A^r = 0 \tag{4.23}$$

The solution to (4.2) can be written as

$$\begin{aligned} x(t) &= e^{A(t-nT_f)} x(n) + \int_{nT_f}^{t} e^{A(t-\tau)} B d\tau \phi(x(n), z(n), u(k)) \\ &\quad + \int_{nT_f}^{t} e^{A(t-\tau)} B \Delta(\tau) d\tau \end{aligned} \tag{4.24}$$

where $\Delta(\tau) = \phi(x(\tau), z(\tau), u(k)) - \phi(x(n), z(n), u(k))$. Using (4.23) we have

$$D e^{At} B = D \sum_{i=0}^{r-1} \frac{t^i}{i!} A^i B = \sum_{i=0}^{r-1} \frac{t^i}{\varepsilon^i i!} A^i D B = \varepsilon^{r-1} e^{At/\varepsilon} B \tag{4.25}$$

and thus

$$\begin{aligned} &\int_{nT_f}^{nT_f+T_f} e^{A(nT_f+T_f-\tau)} B \Delta(\tau) d\tau \\ &\qquad = \varepsilon^{r-1} D^{-1} \int_{nT_f}^{nT_f+T_f} e^{A(nT_f+T_f-\tau)/\varepsilon} B \Delta(\tau) d\tau \end{aligned} \tag{4.26}$$

We can show that the right-hand side term is $O(\varepsilon^2)$. This is seen from the Lipschitz property of ϕ

$$\|\phi(x(t), z(t), u(k)) - \phi(x(n), z(n), u(k))\| \leq L_\phi \|\chi(t) - \chi(n)\| \quad , \quad L_\phi > 0$$

together with equation (4.21). We arrive at the equation

$$\begin{aligned} x(n+1) &= e^{AT_f} x(n) + \int_0^{T_f} e^{At} dt B\phi(x(n), z(n), u(k)) \\ &\quad + \varepsilon^{r+1} D^{-1} R(\chi(n), u(k), \varepsilon) \end{aligned} \tag{4.27}$$

where R is locally Lipschitz in $(\chi(n), u(k))$ and uniformly bounded in ε for ε sufficiently small. We now consider the following estimation error rescaling

$$\xi(n) = \frac{1}{\varepsilon^{r-1}} \left[D(x(n) - \hat{x}(n)) - LDx(n) \right]$$

The matrix L is used to eliminate terms in the estimation error dynamics that appear with negative powers of ε as will be seen below. It satisfies

$$A_f L + (e^{A\alpha} - A_f - B_f C) - L e^{A\alpha} = 0 \tag{4.28}$$

Using the property $A^r = 0$, the solution to this equation can be found to be

$$L = \sum_{i=1}^{r} (I - A_f)^{-i} (e^{A\alpha} - A_f - B_f C)(I - e^{A\alpha})^{i-1}$$

Using (4.16),(4.17) and (4.27) we have

$$\begin{aligned} \xi(n+1) &= A_f \xi(n) + \frac{1}{\varepsilon^{r-1}} [A_f LD + De^{AT_f} - A_f D - B_f CD - LDe^{AT_f}] x(n) \\ &\quad + \frac{1}{\varepsilon^{r-1}} (I - L) D \int_0^{T_f} e^{At} dt B\phi - T_f B\phi_0 + \varepsilon^2 (I - L) R \end{aligned} \tag{4.29}$$

Again from (4.23) we have that

$$De^{AT_f} = D\sum_{i=0}^{r-1}\frac{T_f^i}{i!}A^i = \sum_{i=0}^{r-1}\frac{\alpha^i}{i!}A^iD = e^{A\alpha}D$$

with this identity, (4.25), and (4.28), equation (4.29) simplifies to

$$\begin{aligned}\xi(n+1) = A_f\xi(n) + \varepsilon(I-L)D\int_0^{\alpha} e^{As}dsB\phi(x(n),z(n),u(k)) \\ -\varepsilon[\alpha B\phi_0(\hat{x}(n),\zeta(k),u(k)) - \varepsilon(I-L)R(\chi(n),u(k),\varepsilon)]\end{aligned}$$

where $\hat{x}$ is given by

$$\hat{x}(n) = [I - D^{-1}LD]x(n) - \varepsilon^{r-1}D^{-1}\xi(n)$$

Clearly the term $\varepsilon^{r-1}D^{-1}$ is $O(1)$. Let $X = e^{A\alpha} - A_f - B_fC$. The term $D^{-1}LD$, which is given by

$$D^{-1}LD = \sum_{i=1}^{r}[D^{-1}(I-A_f)^{-1}D]^{i-1}[D^{-1}(I-A_f)^{-1}XD][D^{-1}(I-e^{A\alpha})D]^{i-1}$$

can be shown to be $O(\varepsilon)$. This is verified by making use of (4.23) to show that

$$XD = [e^{A\alpha} - A_f - B_fC]D = D[e^{AT_f} - I - T_fA]$$

From the series expansion of e^{AT_f}, it can be seen that XD is $O(\varepsilon^2)$. It is straightforward to show the following

$$\begin{aligned}&D^{-1}(I-A_f)^{-1}D = -\frac{1}{\alpha}D^{-1}A_0^{-1}D \\ &D^{-1}(I-A_f)^{-1}XD = -\frac{1}{\alpha}D^{-1}A_0^{-1}XD = -\frac{1}{\alpha}D^{-1}A_0^{-1}D[e^{AT_f} - I - T_fA] \\ &D^{-1}(I-e^{A\alpha})D = (I-e^{AT_f})\end{aligned}$$

Also, $D^{-1}A_0^{-1}D$ as seen from

$$D^{-1}A_0^{-1}D = \begin{bmatrix} 0 & 0 & \cdots & 0 & -\varepsilon^{r-1}/\alpha_r \\ 1/\varepsilon & 0 & \cdots & 0 & -\varepsilon^{r-2}\alpha_1/\alpha_r \\ 0 & 1/\varepsilon & 0 & \cdots & -\varepsilon^{r-3}\alpha_2/\alpha_r \\ \vdots & & & \vdots & \vdots \\ 0 & 0 & \cdots & 1/\varepsilon & -\alpha_{r-1}/\alpha_r \end{bmatrix}$$

is order of $O(1/\varepsilon)$. From the foregoing, $D^{-1}LD$ is $O(\varepsilon)$. Finally, we obtain the following relation for the estimation error dynamics.

$$\xi(n+1) = A_f\xi(n) + \varepsilon\mathcal{G}(\chi(n), \xi(n), \zeta(k), u(k), \varepsilon) \tag{4.30}$$

$$\hat{x}(n) = [I - \varepsilon N_2(\varepsilon)]x(n) + N_1(\varepsilon)\xi(n) \tag{4.31}$$

where A_f has all its eigenvalues inside the unit circle, $\mathcal{G}$ is locally Lipschitz in its arguments and uniformly bounded in ε, for ε sufficiently small, $\mathcal{G}$ and γ are globally bounded in $\hat{x}$, and the matrices N_1, N_2 are analytic functions of ε. Using (4.13) and the control (4.20) we can write the closed-loop system under multirate output feedback as

$$\chi(k+1) = \chi(k) + T_s\mathcal{F}(\chi(k), \xi_s(k), T_s, \varepsilon) \tag{4.32}$$

$$\xi(n+1) = A_f\xi(n) + \varepsilon\mathcal{G}(\chi(n), \xi(n), \zeta(k), u(k), \varepsilon) \tag{4.33}$$

$$\hat{x}_s(k) = [I - \varepsilon N_2(\varepsilon)]x(k) + N_1(\varepsilon)\xi_s(k) \tag{4.34}$$

where $\xi_s(k) = \xi(\lfloor hk \rfloor)$. Also, the function $\mathcal{F}$, locally Lipschitz with respect to χ and ξ_s, is given by

$$\mathcal{F}(\chi, \xi_s, T_s, \varepsilon) = F(\chi(k), u(k)) + T_s\Phi(\chi(k), u(k), T_s) \tag{4.35}$$

with $u(k)$ taken from (4.20) and (4.34).

4.3 Stabilization of the Origin

In this section we study the stability of the closed-loop system under multirate output feedback control. Based on the existence of a single-rate sampled-data state feedback controller that globally asymptotically stabilizes the origin of the closed-loop system we show that the multirate output feedback controller achieves ultimate boundedness of all closed-loop trajectories. We then study the stability of the closed-loop system when an exponentially stabilizing state feedback controller is considered. The closed-loop system under the single(slow)-rate sampled-data state feedback control

$$u(k) = \gamma(x(k), \zeta(k)) \tag{4.36}$$

is given by

$$\chi(k+1) = \chi(k) + T_s F(\chi(k), \gamma(x(k), \zeta(k))) + T_s^2 \Phi(\chi(k), \gamma(x(k), \zeta(k)), T_s)$$

Observe from (4.34) that by setting $\varepsilon = 0$ and $\xi = 0$ we have $\hat{x}_s(k) = x(k)$ and the control (4.20) is identical to (4.36). Therefore, from (4.35) we obtain the following reduced system

$$\chi(k+1) = \chi(k) + T_s \mathcal{F}(\chi(k), 0, T_s, 0) \tag{4.37}$$

which is the closed-loop system under sampled-data state feedback. We make the following assumption

Assumption 4.1

1. *The origin ($\chi = 0$) of (4.37) is globally asymptotically stable.*

2. *The function γ is locally Lipschitz in its arguments and globally bound in x.*

Global boundedness can be achieved by saturating the control outside a compact region of interest.

4.3.1 Boundedness and Ultimate Boundedness

We have the following result which shows boundedness and ultimate boundedness of the closed-loop system.

Theorem 4.1 *Consider equations (4.32)-(4.34) and the control (4.20). Let Assumption 4.1 hold and let $\mathcal{M}$ and $\mathcal{N}$ be any compact subsets of $\mathbb{R}^{\ell+r}$ and $\mathbb{R}^r$ respectively. Then, for trajectories $(z,x) \times \hat{x}$ starting in $\mathcal{M} \times \mathcal{N}$ the following holds*

- *There exists ε_1^* such that, for all $0 < \varepsilon \leq \varepsilon_1^*$, $\chi(t)$ is bounded for all $t \geq 0$ and $\xi(n)$ is bounded for all $n \geq 0$.*
- *Given any $\mu \geq 0$, there exists $\varepsilon_2^* > 0$, $t^* > 0$ and $n^* > 0$, such that for every $0 < \varepsilon \leq \varepsilon_2^*$, we have*

$$\|\xi(n)\| + \|\chi(t)\| \leq \mu \quad \forall \quad t \geq t^*, \quad \text{and} \quad n \geq n^* \tag{4.38}$$

Proof: First, consider the closed-loop system under sampled-data state feedback (4.37). From Assumption 4.1 and the discrete-time converse Lyapunov theorem of [35] there is a smooth Lyapunov function $V(\chi)$ that satisfies

$$\alpha_1(\|\chi\|) \leq V(\chi) \leq \alpha_2(\|\chi\|) \tag{4.39}$$

$$V(\chi(k) + T_s\mathcal{F}(\chi(k), 0, T_s, 0)) - V(\chi(k)) \leq -\alpha_3(\|\chi\|) \tag{4.40}$$

where α_1 and α_2 are class $\mathcal{K}_\infty$ functions and α_3 is a continuous positive definite function. We note that the Lyapunov function $V(\chi)$ will, in general, depend on the sampling period T_s, but since we are working with a fixed T_s we can proceed without difficulty. Let Ω_1 denote the compact set $\{V(\chi) \leq c_1\}$. We choose $c_1 > \max_{\chi \in \mathcal{M}} V(\chi)$ so that $\mathcal{M}$ is in the interior of Ω_1. We take $W(\xi) = \xi^T P \xi$ as the Lyapunov function for the observer error dynamics where P is positive definite and satisfies $A_f^T P A_f - P = -I$. Also, from

([58], Ch. 23, Th. 23.7) we have that $\|P\| > 1$. Consider the following sets

$$\Omega_2 = \{V(\chi) \leq c_2\}, \quad \Lambda = \Omega_2 \times \{W(\xi) \leq c_3\varepsilon^2\}$$

where $c_3 > 0$ and Ω_2 is a compact subset of $\mathbb{R}^{\ell+r}$ for any $c_2 > 0$. We take $c_2 > c_1$ so that $\mathcal{M} \subset \Omega_1 \subset \Omega_2$ and we show that for $\chi(0)$ starting in $\mathcal{M}$, $\chi(k)$ remains in Ω_2. Due to the boundedness of γ and $\mathcal{G}$ in $\hat{x}$ we have for all $(\chi, \xi) \in \Omega_1 \times \mathbb{R}^r$

$$\|\mathcal{F}(\chi, \xi_s, T_s, \varepsilon)\| \leq K_1, \quad \|\mathcal{G}(\chi, \xi, \zeta, u)\| \leq K_2$$

where K_1 and K_2 are positive constants independent of ε. From equations (4.20), (4.34), (4.36), and the Lipschitz property of $\mathcal{F}$ with respect to x

$$\|\mathcal{F}(\chi, 0, T_s, 0) - \mathcal{F}(\chi, \xi_s, T_s, \varepsilon)\| \leq \varepsilon K_3 \|\chi(k)\| + K_4 \|\xi_s(k)\|$$

for all $(\chi, \xi) \in \Lambda$ and for some positive constants K_3 and K_4 independent of ε. From the foregoing, it can be shown that in the set Λ

$$V(\chi(k+1)) = V(\chi(k) + T_s\mathcal{F}(\chi, \xi_s, T_s, \varepsilon)) \leq V(\chi(k)) - \alpha_3(\|\chi(k)\|) + \varepsilon T_s K_5 \quad (4.41)$$

for some positive constant K_5. We can choose ε small enough that $\chi(k) \in \{V(\chi(k)) \leq c_1\}$ cannot leave Ω_2 and thus Ω_2 is positively invariant. This can be seen from

$$V(\chi(k+1)) \leq c_1 + \varepsilon T_s K_5 < c_2$$

for $V(\chi(k)) \leq c_1$, $\varepsilon < \varepsilon_1 \stackrel{def}{=} (c_2 - c_1)/T_s K_5$. Likewise, for $c_1 \leq V(\chi(k)) \leq c_2$

$$V(\chi(k+1)) \leq c_2 - K_6 + \varepsilon T_s K_5 < c_2$$

for $\varepsilon < \varepsilon_2 \stackrel{def}{=} K_6/(K_5 T_s)$ where

$$K_6 = \min_{c_1 \le V(\chi(k)) \le c_2} \alpha_3(\|\chi\|)$$

For the observer error dynamics (4.33), we can arrive at

$$W(\xi(n+1)) \le \left(1 - \frac{1}{\|P\|}\right) W(\xi(n)) + \varepsilon K_7 \|\xi(n)\| + \varepsilon^2 K_8 \tag{4.42}$$

for some positive constants K_7 and K_8. For $\xi(n) \in \{W(\xi(n)) \le c_3\varepsilon^2\}$, we obtain

$$W(\xi(n+1)) \le \left(1 - \frac{1}{\|P\|}\right) c_3\varepsilon^2 + \varepsilon^2 K_7 \sqrt{\frac{c_3}{\lambda_{min}(P)}} + \varepsilon^2 K_8 \tag{4.43}$$

It can be seen that for c_3 large enough, $W(\xi(n+1)) \le c_3\varepsilon^2$. Therefore, Λ is positively invariant.

With the initial conditions $(\chi(0), \hat{x}(0)) \in \mathcal{M} \times \mathcal{N}$ we have that $\|\xi(0)\| \le l/\varepsilon^{r-1}$, where l depends on $\mathcal{M}$ and $\mathcal{N}$. Since $\mathcal{M}$ is in the interior of Ω_1, $\chi(0)$ is in Ω_1. We have that

$$\|\chi(k) - \chi(0)\| \le T_s K_1 k \tag{4.44}$$

as long as $\chi(k) \in \Omega_1$. Hence, $\chi(k)$ remains in Ω_1 for $k \le K_9/T_s$ for some positive constant K_9. With $\chi(k) \in \Omega_1$ and $\xi \notin \{W(\xi) \le c_3\varepsilon^2\}$, we can rewrite (4.42) as

$$W(\xi(n+1)) \le \left(1 - \frac{1}{2\|P\|}\right) W(\xi(n)) - \frac{1}{2\|P\|} W(\xi(n)) + \varepsilon K_7 \sqrt{\frac{W(\xi(n))}{\lambda_{min}(P)}} + \varepsilon^2 K_8 \tag{4.45}$$

Then for $W(\xi) \ge c_3\varepsilon^2$, we can choose c_3 large enough that

$$W(\xi(n+1)) \le \lambda W(\xi(n))$$

for $0 < \lambda = (1 - 1/(2\|P\|)) < 1$. Hence,

$$W(\xi(n)) \leq \lambda^n \|P\| \frac{l^2}{\varepsilon^{2r-2}} \tag{4.46}$$

And ξ enters $\{W(\xi) \leq c_3\varepsilon^2\}$ for

$$\lambda^n \|P\| \frac{l^2}{\varepsilon^{2r-2}} \leq \varepsilon^2 c_3$$

To show boundedness of trajectories, let

$$\bar{n}(\varepsilon) = \frac{ln\left(\frac{\|P\|l^2}{c_3\varepsilon^{2r}}\right)}{ln(1/\lambda)} \tag{4.47}$$

and note that $\xi \in \{W(\xi) \leq c_3\varepsilon^2\}$ for all $n \geq \bar{n}(\varepsilon)$. From (4.44), $\chi(k) \in \Omega_2$ for all $k \leq K_9/T_s$. We can select ε_3 such that for all $0 < \varepsilon \leq \varepsilon_3$, $T_f\bar{n}(\varepsilon) < T_s k \leq K_9$. This can be seen by using equation (4.47) to obtain

$$\varepsilon\alpha ln\left(\frac{\|P\|l^2}{c_3\varepsilon^{2r}}\right) < K_9 ln(1/\lambda)$$

where the left-hand side tends to zero as $\varepsilon \to 0$. Therefore, $\chi(k)$ enters Ω_2 during the time interval $[0, \lfloor\frac{K_9}{T_s}\rfloor]$ and is bounded by (4.44) prior to entering this set. The trajectory $\xi(n)$ enters the set $\{W(\xi) \leq c_3\varepsilon^2\}$ during the time period $[0, \lceil\bar{n}(\varepsilon)\rceil]$ (where the notation $\lceil\bar{n}\rceil$ denotes the largest integer greater than or equal to $\bar{n}$) and remains there for all $n \geq \bar{n}(\varepsilon)$. Furthermore, it is bounded by (4.46) prior to entering this set. From (4.12) and (4.20) it follows that all closed-loop trajectories are bounded by choosing $\varepsilon_1^* = min(\varepsilon_1, \varepsilon_2, \varepsilon_3)$.

Ultimate boundedness follows by an argument similar to [20]. Indeed since $\xi(n) \in \{W(\xi(n)) \leq c_3\varepsilon^2\}$, then given any $\mu > 0$ we can find ε_4 dependent on μ such that $\|\xi(n)\| \leq \frac{1}{2}\mu$ for all $n \geq \bar{n}(\varepsilon)$ and all $0 < \varepsilon \leq \varepsilon_4$. Now, consider the compact set

$\{\alpha_3(\|\chi(k)\|) \leq 2\varepsilon T_s K_5\}$ and let

$$\omega_1(\varepsilon) = \max_{\alpha_3(\|\chi\|) \leq 2\varepsilon T_s K_5} V(\chi)$$

and note that $\omega_1(\varepsilon) \to 0$ as $\varepsilon \to 0$. We have that the set $\{V(\chi) \leq \omega_1(\varepsilon)\}$ is compact and $\{\alpha_3(\|\chi\|) \leq 2\varepsilon T_s K_5\} \subset \{V(\chi) \leq \omega_1(\varepsilon)\}$. Rewrite equation (4.41) as

$$V(\chi(k+1)) \leq V(\chi(k)) - \frac{1}{2}\alpha_3(\|\chi(k)\|) - \left(\frac{1}{2}\alpha_3(\|\chi(k)\|) - \varepsilon T_s K_5\right)$$

Therefore, with $V(\chi(0)) \geq \omega_1(\varepsilon)$, we have that whenever $V(\chi(k)) \geq \omega_1(\varepsilon)$

$$V(\chi(k+1)) \leq V(\chi(0)) - \sum_{i=0}^{k} \frac{1}{2}\alpha_3(\|\chi(i)\|) \leq V(\chi(0)) - \varepsilon T_s K_5 (k+1)$$

Thus there exists a finite time k^* such that $\chi(k^*)$ enters the set $\{V(\chi) \leq \omega_1(\varepsilon)\}$. Now, consider the time $k \geq k^*$. For $\chi(k) \in \{V(\chi) \leq \omega_1(\varepsilon)\}$ and $\alpha_3(\|\chi(k)\|) > 2\varepsilon T_s K_5$ we obtain

$$V(\chi(k+1)) \leq \omega_1(\varepsilon) - \frac{1}{2}\alpha_3(\|\chi(k)\|) < \omega_1(\varepsilon)$$

Therefore, $\chi(k+1)$ remains in the set $\chi(k) \in \{V(\chi) \leq \omega_1(\varepsilon)\}$. On the other hand, for $\chi(k) \in \{V(\chi) \leq \omega_1(\varepsilon)\}$ and $\alpha_3(\|\chi(k)\|) \leq 2\varepsilon T_s K_5$ we have

$$V(\chi(k+1)) \leq \omega_1(\varepsilon) + \varepsilon T_s K_5 \stackrel{def}{=} \omega_2(\varepsilon)$$

Hence, $\chi(k+1)$ may leave $\{V(\chi) \leq \omega_1(\varepsilon)\}$ but remains in a set defined by $\{V(\chi) \leq \omega_2(\varepsilon)\}$ where $\omega_2(\varepsilon) \to 0$ as $\varepsilon \to 0$. Now, for $\chi(k)$ in the set $\{\omega_1(\varepsilon) < V(\chi) \leq \omega_2(\varepsilon)\}$, we have $\alpha_3(\|\chi(k)\|) > 2\varepsilon T_s K_5$. Therefore

$$V(\chi(k+1)) \leq V(\chi(k)) - \frac{1}{2}\alpha_3(\|\chi(k)\|) < \omega_2(\varepsilon)$$

Thus,

$$V(\chi(k+1)) \leq \omega_2(\varepsilon) \quad , \quad \forall k \geq k^*$$

In other words, for $\chi(k)$ belonging to the set $\{V(\chi) \leq \omega_1(\varepsilon)\}$ at time $k = k^*$, then $\chi(k)$ must be in the set $\{V(\chi) \leq \omega_2(\varepsilon)\}$ for all $k \geq k^* + 1$. From equation (4.39)

$$\|\chi(k)\| \leq \alpha_1^{-1}(\omega_2(\varepsilon))$$

for all $k \geq k^* + 1$. Using this, equation (4.12), and the control equation (4.20) together with (4.34) then we can find an ε_5 dependent on μ such that $\|\chi(t)\| \leq \frac{1}{2}\mu$ for all $0 < \varepsilon \leq \varepsilon_5$ and all $t \geq t^*$ for a finite time t^*. From the foregoing, we obtain (4.38) where $\varepsilon_2^* = \min(\varepsilon_4, \varepsilon_5)$. $\lhd$

Remark 4.1 *Using the control scheme (4.20) we can choose ε sufficiently small such that the estimation error ξ reduces to an $O(\varepsilon)$ during the time interval $[0, T_s]$, thereby isolating the controller from the observer transient. To do so we must select the fast sampling period, $T_f = \varepsilon\alpha$, such that*

$$T_f \lceil \bar{n}(\varepsilon) \rceil < T_s \tag{4.48}$$

From equation (4.47) there exists an ε^* such that (4.48) is satisfied for all $\varepsilon \leq \varepsilon^*$. Therefore, the trajectory $\xi(n)$ recovers from peaking during the interval $[0, \lceil \bar{n}(\varepsilon) \rceil]$ and remains bounded and $O(\varepsilon)$ thereafter. Furthermore, During $[0, T_s]$, the state of the plant $\chi(t)$ cannot grow by more than

$$\|\chi(t) - \chi(0)\| \leq K_{10} T_s \|F(\chi(0), u_0)\|$$

for some positive constant K_{10}.

Here we comment on the recovery of the performance of the multirate sampled-data closed-loop system under output feedback to the performance under state feedback; both continuous and sampled-data.

Remark 4.2 *In [20] it was shown that the single-rate sampled-data output feedback controller recovers the performance of the continuous-time state feedback controller as the sampling frequency and the observer gain become sufficiently large. For the multirate output feedback case, with a fixed* T_s

$$\|\chi_r(t) - \chi(t)\| \leq \delta(T_s)$$

for some continuous function $\delta(T_s)$ *and where* χ_r *is the solution of the closed-loop system under continuous-time state feedback. When comparing the multirate case to the sampled-data state feedback case, a similar result holds since the two controllers will be different over the first sampling period and thus the trajectories will differ by an order* $O(T_s)$.

4.3.2 Exponential Stability of the Origin

In the next theorem, given an exponentially stabilizing sampled-data state feedback controller, we show that the trajectories of the closed-loop system under the multirate scheme converge to the origin exponentially fast. We study the closed-loop system in the slow sample time k and show that the discrete-time trajectories converge exponentially. To do so, we will need a description of equation (4.30) in the slow sampling time k. For simplicity, we will consider the ratio of the sampling rates

$$h = \frac{T_s}{T_f}$$

to be a positive integer. Also, we will work locally, so consider a ball $B(0, \varrho_1)$ of radius $\varrho_1 > 0$ around the origin $(\chi, \xi) = (0, 0)$. The results of the previous theorem guarantee that for ε small enough, the trajectories will enter this set in finite time. Furthermore,

we will assume that the functions $F(\chi, u)$ and $\gamma(x, \zeta)$ are continuously differentiable in a neighborhood of the origin. We begin by studying (4.30) over one slow time period $[k, k+1]$. Consider the discrete-time state equation and the estimation error dynamics in the fast sampling time n

$$\chi(n+1) = \chi(n) + T_f F(\chi(n), u(k)) + T_f^2 \Phi(\chi(n), u(k), T_f) \tag{4.49}$$

$$\xi(n+1) = A_f \xi(n) + \varepsilon \mathcal{G}(\chi(n), \xi(n), \zeta(k), u(k), \varepsilon) \tag{4.50}$$

The accumulation of (4.50) over the interval $hk \leq n \leq h(k+1)$ is performed as follows, where for convenience we represent $\zeta(k)$ and $u(k)$ by the index k

$$\begin{aligned}
\xi(hk+1) &= A_f \xi(hk) + \varepsilon \mathcal{G}\left(\chi(hk), \xi(hk), k, \varepsilon\right) \\
\xi(hk+2) &= A_f^2 \xi(hk) + \varepsilon A_f \mathcal{G}(\chi(hk), \xi(hk), k, \varepsilon) \\
&\quad + \varepsilon \mathcal{G}(\chi(hk) + T_f F(\chi(hk), k) + T_f^2 \Phi(\chi(hk), k, T_f), A_f \xi(hk) + \varepsilon \mathcal{G}, k, \varepsilon) \\
\vdots &= \qquad\qquad \vdots \\
\xi(hk+h) &= A_f^h \xi(hk) + \varepsilon w(\chi(hk), \xi(hk), k, \varepsilon)
\end{aligned}$$

Note that h is $O(1/\varepsilon)$ and that the function w will contain a summation of h terms of order $O(\varepsilon)$ each. Thus, it is not clear that εw will remain $O(\varepsilon)$. To show this, we will use a change of variables. First, we note that (4.49)-(4.50) has a two-time scale behavior. For equation (4.50), we have the quasi-steady-state relation

$$\xi(n) = A_f \xi(n) + \varepsilon \mathcal{G}(\chi(n), \xi(n), \zeta(k), u(k), \varepsilon)$$

We seek a solution to the above equation in the form

$$\xi(n) = \varphi(\chi(n), \zeta(k), u(k), \varepsilon) \tag{4.51}$$

where φ is a continuously differentiable function of its arguments and $\varphi(0,0,0,0) = 0$. This equation describes an $(r+\ell)$-dimensional manifold in the $(2r+\ell)$-dimensional state space of (χ, ξ) and is called the slow manifold of (4.49) and (4.50). Evaluating (4.51) at $n+1$ and substituting the difference equations (4.49) and (4.50) results in the following manifold condition

$$\begin{aligned} 0 &= A_f \varphi(\chi(n), \zeta(k), u(k), \varepsilon) + \varepsilon \mathcal{G}\left(\chi(n), \varphi(\chi(n), \zeta(k), u(k), \varepsilon)\right), \zeta, u, \varepsilon) \\ &\quad -\varphi\left(\chi(n) + T_f F(\chi(n), u(k)) + T_f^2 \Phi(\chi(n), u(k), T_f), \zeta(k), u(k), \varepsilon\right) \end{aligned} \tag{4.52}$$

Setting $\varepsilon = 0$ we have

$$(I - A_f)\varphi(\chi(n), \zeta(k), u(k), 0) = 0 \tag{4.53}$$

Because $|\lambda(A_f)| < 1$, $(I - A_f)$ is nonsingular. Therefore, $\varphi(\chi, \zeta, u, 0) = 0$. Using the implicit function theorem ([72]) we have that $\varphi(\chi, \zeta, u, \varepsilon)$ satisfies (4.52) for ε sufficiently small. Furthermore, due to (4.53) this function is $O(\varepsilon)$. Consider now the change of variables

$$\eta(n) = \xi(n) - \varphi(\chi(n), \zeta(k), u(k), \varepsilon) \tag{4.54}$$

which along with (4.52) results in

$$\begin{aligned} \eta(n+1) &= A_f \eta(n) + \varepsilon[\mathcal{G}\left(\chi(n), \eta(n) + \varphi(\chi(n), \zeta(k), u(k), \varepsilon), \zeta(k), u(k), \varepsilon\right) \\ &\quad - \mathcal{G}\left(\chi(n), \varphi(\chi(n), \zeta(k), u(k), \varepsilon), \zeta(k), u(k), \varepsilon\right)] \end{aligned}$$

We rewrite the right hand side as

$$\eta(n+1) = A_f \eta(n) + \varepsilon \tilde{\mathcal{G}}\left(\chi(n), \eta(n), \zeta(k), u(k), \varepsilon\right) \tag{4.55}$$

where

$$\tilde{\mathcal{G}}\left(\chi(n), 0, \zeta(k), u(k), \varepsilon\right) = 0 \tag{4.56}$$

Therefore, $\eta = 0$ is an equilibrium point of the transformed system. The function $\tilde{\mathcal{G}}$ is continuously differentiable with convex domain $B(0, \varrho_1)$. From ([36], ex. 3.23, pg. 108) we have the following relation

$$\begin{aligned} \tilde{\mathcal{G}}\left(\chi(n), \eta(n), \zeta(k), u(k), \varepsilon\right) &= \int_0^1 \frac{\partial \tilde{\mathcal{G}}}{\partial \eta}(\chi, \sigma\eta, \zeta, u, \varepsilon) d\sigma \ \ \eta \\ &\stackrel{def}{=} \tilde{B}(\chi(n), \eta(n), \zeta(k), u(k), \varepsilon)\eta \end{aligned} \tag{4.57}$$

Due to the fact that χ and ξ are bounded and belong to the set $B(0, \varrho_1)$, we can treat the equation

$$\eta(n+1) = \left[A_f + \varepsilon \tilde{B}(\chi(n), \eta(n), \zeta(k), u(k), \varepsilon)\right] \eta(n) \tag{4.58}$$

as a time-varying linear system. Let

$$\tilde{A}(n) = A_f + \varepsilon \tilde{B}(\chi(n), \eta(n), \zeta(k), u(k), \varepsilon) \tag{4.59}$$

Since

$$|\lambda(A_f)| \leq \lambda_1 < 1 \tag{4.60}$$

for some positive constant λ_1, It follows from ([58], Th. 24.7) that, for ε sufficiently small, the state transition matrix, $\Phi_{\tilde{A}}(n, n_0)$, of (4.58) satisfies

$$\|\Phi_{\tilde{A}}(n, n_0)\| \leq \kappa_1 \lambda_2^{n-n_0} \tag{4.61}$$

where $0 < \lambda_2 < 1$ and κ_1 is a positive constant. In addition, it can be shown that there exist ε_1 such that the following properties are satisfied uniformly in ε for all $0 < \varepsilon \leq \varepsilon_1$

$$|\lambda(\tilde{A})| \leq c_1 \ \ , \ \ \|\tilde{A}\| \leq c_2 \ \ , \ \ \|\tilde{A}(n) - A_f\| \leq c_3 \varepsilon \tag{4.62}$$

where c_1, c_2, and c_3 are positive constants. Now let

$$\Upsilon(n, n_0) = \Phi_{\tilde{A}}(n, n_0) - A_f^{n-n_0} \tag{4.63}$$

It can be shown that (Appendix A) there exist positive constants ε_2, κ_2, and $0 < \lambda_3 < 1$ such that for all $0 < \varepsilon \leq \varepsilon_2$

$$\|\Upsilon(n, n_0)\| \leq \varepsilon \kappa_2 \lambda_3^{n-n_0} \tag{4.64}$$

From (4.58) we have

$$\eta(n) = \left[A_f^{n-n_0} + \Upsilon(n, n_0)\right] \eta(n_0)$$

The accumulation over the period $[hk \leq n \leq h(k+1)]$ is given by

$$\eta(hk+h) = \left[A_f^h + \Upsilon(hk+h, hk)\right] \eta(hk) \tag{4.65}$$

Since h is $O(1/\varepsilon)$ and $|\lambda(A_f)| < 1$ we have that

$$A_f^h = O(\varepsilon)$$

Using this and the fact that Υ is $O(\varepsilon)$, we rewrite (4.65) as

$$\eta(hk+h) = \varepsilon G(\eta(hk), \chi(hk), \zeta(k), u(k), \varepsilon)$$

where the function G is continuously differentiable. We now have an equation that describes the evolution of the estimation error in the slow sample time k. Consider the control (4.20) and equation (4.31)

$$u(k) = \gamma(\hat{x}(hk), \zeta(k)) \tag{4.66}$$

$$\hat{x}(hk) = [I - \varepsilon N_2] x(hk) + N_1 \xi(hk) \tag{4.67}$$

and substitute these expressions into (4.54)

$$\eta(hk) = \xi(hk) - \varphi(\chi(hk), \zeta(k), \gamma([I - \varepsilon N_2]x(hk) + N_1\xi(hk), \zeta(k)), \varepsilon)$$

Dropping the h notation, we redefine the right-hand side of the above equation as

$$\eta(k) = \xi(k) - \tilde{\varphi}(\chi(k), \xi(k), \varepsilon)$$

where $\tilde{\varphi}$ is continuously differentiable. By noting that $\tilde{\varphi} = 0$ for $\varepsilon = 0$, the implicit function theorem shows us that there is an open set $\mathcal{V}$ containing $(\eta, \xi, \varepsilon) = 0$ such that

$$\xi(k) = \vartheta(\eta(k), \chi(k), \varepsilon) \tag{4.68}$$

where the function ϑ is continuously differentiable in $\mathcal{V}$. From the ultimate boundedness of Theorem 4.1, we can choose ε small enough to guarantee that we are in $\mathcal{V}$. Now, using (4.66), (4.67), and (4.68), we write the closed-loop system in the slow sample time in terms of χ and η as

$$\chi(k+1) = \chi(k) + T_S\mathcal{F}(\chi(k), \vartheta(\eta(k), \chi(k), \varepsilon), T_S, \varepsilon) \tag{4.69}$$

$$\eta(k+1) = \varepsilon G(\eta(k), \chi(k), \zeta(k), \varepsilon) \tag{4.70}$$

We have the following result.

Theorem 4.2 *Assume that the origin ($\chi = 0$) of (4.37) is exponentially stable and the functions $F(\chi, u)$ and $\gamma(x, \zeta)$ are continuously differentiable in a neighborhood of the origin. Then there exists $\varepsilon_3^* > 0$ such that for all $0 < \varepsilon \leq \varepsilon_3^*$ the origin of (4.69)-(4.70) is exponentially stable. That is*

$$\|\eta(k)\| \leq c_1\lambda_4^k \quad , \quad \|\chi(k)\| \leq c_2\lambda_5^k \quad , \quad \forall k \geq k^* > 0$$

for some positive integer k^*, positive constants c_1 and c_2, $|\lambda_4| < 1$ and $|\lambda_5| < 1$. Furthermore, $\chi(t)$ decays to zero exponentially fast

$$\|\chi(t)\| \leq c_3 e^{-\lambda_6 t} \quad , \quad \forall t \geq 0$$

for some positive constants c_3 and λ_6.

Proof: Again, the results of Theorem 4.1 allow us to work locally. Setting $\eta = 0$ and $\varepsilon = 0$ in (4.69) results in the reduced system

$$\chi(k+1) = \chi(k) + T_s \mathcal{F}(\chi(k), 0, T_s, 0)$$

which is the closed-loop system under sampled-data state feedback. Linearizing about $\chi = 0$ we obtain

$$\chi(k+1) = A_{11}\chi(k)$$

where $|\lambda(A_{11})| < 1$ by hypothesis. Next, we linearize the full system (4.69)-(4.70) about $(\chi, \eta) = (0, 0)$ to obtain

$$\chi(k+1) = (A_{11} + \varepsilon A_{12})\chi(k) + A_{13}\eta(k) + T_s g_1(\chi, \eta, T_s, \varepsilon) \tag{4.71}$$

$$\eta(k+1) = \varepsilon A_{21}\chi(k) + \varepsilon A_{22}\eta(k) + \varepsilon g_2(\eta, \chi, \varepsilon) \tag{4.72}$$

where g_1 and g_2 are continuous functions. We have that for any $\gamma_1 > 0$ and $\gamma_2 > 0$ there exit $\varrho_2 > 0$ such that

$$\|g_1\|_2 < \gamma_1 \|(\chi, \eta)\|_2 \quad , \quad \|g_2\|_2 < \gamma_2 \|(\chi, \eta)\|_2$$

for all $\|(\chi, \eta)\|_2 < \varrho_2$. Since $\tilde{\varphi}$ is continuous, we can choose ϱ_1 so that $(\chi, \xi) \in B(0, \varrho_1)$ implies $\|(\chi, \eta)\|_2 < \varrho_2$ through the change of variables $\eta = \xi - \tilde{\varphi}$. We need to weaken the variable η in the linear part of equation (4.71). This is accomplished by choosing a

matrix M that satisfies

$$(A_{11} + \varepsilon A_{12})M + A_{13} - \varepsilon M A_{21} M - \varepsilon M A_{22} = 0$$

Now, consider the composite Lyapunov function

$$V(\chi(k), \eta(k)) = [\chi - M\eta]^T P_{11} [\chi - M\eta] + \theta \eta^T \eta$$

where the matrix P_{11} is positive definite and satisfies $A_{11}^T P_{11} A_{11} - P_{11} = -I$. It can be shown that there is θ sufficiently large and ε_3 sufficiently small such that the following relation holds uniformly in ε for all $0 < \varepsilon \leq \varepsilon_3$.

$$\delta_1 \|(\chi, \eta)\|^2 \leq V \leq \delta_2 \|(\chi, \eta)\|^2$$

where δ_1, δ_2 are positive constants. We have

$$\Delta V \leq -\mathcal{Y}^T \Pi \mathcal{Y}$$

where

$$\mathcal{Y} = \begin{bmatrix} \|\chi(k)\| \\ \|\eta(k)\| \end{bmatrix}, \Pi = \begin{bmatrix} \pi_1 & \pi_2 \\ \pi_2 & \pi_3 \end{bmatrix}$$

$$\pi_1 = 1 - \varepsilon\beta_1(\theta) - \beta_2\gamma_1 - \beta_3\gamma_1^2 - \varepsilon^2\beta_4\gamma_1\gamma_2 - \varepsilon\beta_5\gamma_2 - \varepsilon(\beta_6 + \varepsilon\beta_7(\theta))\gamma_2^2$$

$$\pi_2 = -\lambda_{max}(M) - \varepsilon\beta_8(\theta)$$

$$\pi_3 = (\theta + \lambda_{min}(M)) - \varepsilon\beta_9(\theta) - \beta_2\gamma_1 - \beta_3\gamma_1^2 - \varepsilon^2\beta_4\gamma_1\gamma_2 - \varepsilon\beta_5\gamma_2 - \varepsilon(\beta_6 + \varepsilon\beta_7(\theta))\gamma_2^2$$

for some positive constants β_i that, in general, depend on T_s. Also, as shown, β_i may depend on θ. Therefore, there exist γ_1, dependent on T_s but independent of ε, ε_4 dependent on θ, and θ sufficiently large such that for all $0 < \varepsilon \leq \varepsilon_4$ the matrix Π is positive

definite. Therefore, from the ultimate boundedness of χ and ξ

$$\|\mathcal{Y}(k)\| \leq C_1 \lambda^{(k-k^*)} \quad \forall \quad k \geq k^*$$

for some positive integer k^* and positive constants C_1 and $\lambda < 1$. Using (4.12), (4.20) and the fact that $\chi(t)$ is bounded for all $t \geq 0$, it can be shown that $\chi(t)$ is exponentially convergent for all $0 < \varepsilon \leq \varepsilon_3^* = min\{\varepsilon_1, \varepsilon_2, \varepsilon_3, \varepsilon_4\}$. $\lhd$

4.4 Stabilization with Respect to a Compact Set

In the previous section we dealt with the case where a sampled-data state feedback controller was designed to make the origin of the closed-loop system an asymptotically stable equilibrium point. Here we consider the case when the sampled-data state feedback controller, rather than stabilize the origin, brings the trajectory $\chi(k)$ to some forward invariant compact set. This situation my arise in the presence of a bounded disturbance where the sampled-data state feedback controller can only achieve stabilization of the trajectories to a set. Also, as mentioned in the introduction, in many cases sampled-data state feedback controllers can only be shown to practically stabilize the origin. The results provided in this section are motivated by applications to the control of smart material systems, where one may consider hysteresis inversion compensation. Such inversion compensation may be inexact and lead to bounded disturbances in the closed-loop system. We will also discuss extending the results of this section to the tracking problem and integral control, both of which can lead to controllers that are unable to asymptotically stabilize the origin of the closed-loop system.

4.4.1 Definitions and Problem Formulation

Consider the following general nonlinear discrete-time system

$$x(k+1) = f(x(k), d(k)) \tag{4.73}$$

where $k \in \mathbb{Z}_+$, $x(k) \in \mathbb{R}^n$, $d(k) \in \mathcal{D}$, with $\mathcal{D}$ a compact subset of $\mathbb{R}^d$, and where $f : \mathbb{R}^n \times \mathcal{D} \to \mathbb{R}^n$ is continuous. The function f is locally Lipschitz in x, uniformly in d if for each compact set Ω of $\mathbb{R}^n$ there is a constant L such that

$$\|f(x,d) - f(y,d)\| \leq L\|x - y\|$$

for all $x, y \in \Omega$ and $d \in \mathcal{D}$.

Let $\mathcal{M}_{\mathcal{D}}$ be the set of all functions from $\mathbb{Z}_+$ to $\mathcal{D}$ and let $x(k, k_0, x_0, d)$ denote the solution of (4.73) with initial state $x(k_0) = x_0$ and $d \in \mathcal{M}_{\mathcal{D}}$. The set $\mathcal{A}$ is forward invariant if for each $x_0 \in \mathcal{A}$, $x(k, k_0, x_0, d) \in \mathcal{A}$ for all $k \geq k_0$. Also, let $\mathcal{A}$ be a nonempty compact subset of $\mathbb{R}^n$. The distance of a trajectory $\vartheta \in \mathbb{R}^n$ to the set $\mathcal{A}$ is given by

$$|\vartheta|_{\mathcal{A}} = \inf_{\eta \in \mathcal{A}} \|\vartheta - \eta\|$$

We work with the notion of stability with respect to a set given in [35].

Definition 4.1 *The system (4.73) is Uniformly Globally Asymptotically Stable (UGAS) with respect to a compact invariant set $\mathcal{A}$ if the following two properties hold:*

1. *Uniform Stability: There exist a $\mathcal{K}_\infty$ function δ such that for any $\epsilon > 0$*

$$|x(k, k_0, x_0, d)|_{\mathcal{A}} \leq \epsilon \quad \forall k \geq k_0, \quad \forall k_0 \in \mathbb{Z}_+, \quad \forall d \in \mathcal{M}_{\mathcal{D}} \tag{4.74}$$

   whenever $|x_0|_{\mathcal{A}} \leq \delta(\epsilon)$.

2. *Uniform Global Attraction: For any $r, \epsilon > 0$, there exist some $T \in \mathbb{Z}_+$ such that for*

every $d \in \mathcal{M}_{\mathcal{D}}$ *and* $k_0 \in \mathbb{Z}_+$

$$|x(k, k_0, x_0, d)|_{\mathcal{A}} < \epsilon \quad \forall k \geq k_0 + T \tag{4.75}$$

whenever $|x_0|_{\mathcal{A}} \leq \delta(\epsilon)$.

To facilitate the forthcoming analysis, we derive the system equations once more in order to illustrate the dependence on the disturbance. So, consider again the system from above

$$\dot{z} = \psi(x, z, d, u) \tag{4.76}$$

$$\dot{x} = Ax + B\phi(x, z, d, u) \tag{4.77}$$

$$y = Cx \tag{4.78}$$

$$\zeta = \Theta(x, z) \tag{4.79}$$

where the right-hand side now depends on an unknown but bounded disturbance d. This disturbance take values in a known compact set $\mathcal{D}$. For the sampled data analysis, we make the following assumption.

Assumption 4.2 *The disturbance* d *is constant over the period* $[kT_S, kT_S + T_S)$

Remark 4.3 *In general, this assumption is restrictive, but as we will see in the next chapter it is valid when performing closed-loop, sampled-data, analysis of certain classes of systems with hysteresis nonlinearity at the input. In Subsection 4.4.3 we will discuss the extension of the results described here to the case of disturbances that vary continuously in* t.

With the right-hand side written as

$$F(\chi, d, u) = \begin{bmatrix} \psi(x, z, d, u) \\ Ax + B\phi(x, z, d, u) \end{bmatrix}$$

we can describe the discrete-time plant dynamics, as in (4.13), sampled at a rate of $1/T_S$ by

$$\chi(k+1) = \chi(k) + T_S F(\chi(k), d(k), u(k)) + T_S^2 \Phi(\chi(k), d(k), u(k), T_S) \tag{4.80}$$

We consider the partial state feedback controller (4.8) and the discrete-time equivalent

$$u(k) = \gamma(x(k), \zeta(k)) \tag{4.81}$$

This controller together with (4.80) satisfies the following assumptions.

Assumption 4.3

1. *The function γ is locally Lipschitz in x and ζ and globally bound in x.*
2. *The closed-loop system (4.80)-(4.81) is uniformly globally asymptotically stable with respect to the compact invariant set $\mathcal{A}$.*

The system (4.76)-(4.79) satisfies:

Assumption 4.4 *The functions ϕ, ψ, and Θ are locally Lipschitz in x, z, and u uniformly in d.*

As a consequence of this assumption, and by arguments used to arrive at (4.13), the function Φ is locally Lipschitz in χ and u uniformly in d. We use the same observer (4.16)-(4.17) and change of variables (4.31) as above to arrive at the observer error dynamics

$$\begin{aligned} \xi(n+1) &= A_f \xi(n) + \varepsilon \mathcal{G}(\chi(n), \xi(n), d(k), \zeta(k), u(k), \varepsilon) && (4.82) \\ \hat{x}(n) &= [I - \varepsilon N_2(\varepsilon)] x(n) + N_1(\varepsilon) \xi(n) && (4.83) \end{aligned}$$

Then, the closed-loop system under multirate control is given by

$$\begin{aligned} \chi(k+1) &= \chi(k) + T_S \mathcal{F}(\chi(k), \xi_S(k), d(k), T_S, \varepsilon) && (4.84) \\ \xi(n+1) &= A_f \xi(n) + \varepsilon \mathcal{G}(\chi(n), \xi(n), d(k), \zeta(k), u(k), \varepsilon) && (4.85) \end{aligned}$$

$$\hat{x}_S(k) \;=\; [I - \varepsilon N_2(\varepsilon)]x(k) + N_1(\varepsilon)\xi_S(k) \tag{4.86}$$

where the function $\mathcal{F}$ is locally Lipschitz in χ and ξ_S uniformly in d and is given by

$$\mathcal{F}(\chi, \xi_S, d, T_S, \varepsilon) = F(\chi(k), d(k), u(k)) + T_S\Phi(\chi(k), d(k), u(k), T_S)$$

with $u(k)$ taken from (4.20).

From assumption 4.3 we have that the discrete-time plant (4.80) under control (4.81) is uniformly globally asymptotically stable with respect to the compact invariant set $\mathcal{A}$. The discrete-time converse Lyapunov theorem (Theorem 1 of [35]) guarantees the existence of a smooth Lyapunov function $V(\chi)$ that satisfies

$$\alpha_1(|\chi|_{\mathcal{A}}) \leq V(\chi) \leq \alpha_2(|\chi|_{\mathcal{A}}) \tag{4.87}$$

$$\Delta V(\chi) = V(\chi(k+1)) - V(\chi(k)) \leq -\alpha_3(|\chi|_{\mathcal{A}}) \tag{4.88}$$

for all $\chi \in \mathbb{R}^{\ell+r}$ and $d \in \mathcal{D}$ where α_1 and α_2 are class $\mathcal{K}_\infty$ functions and α_3 is a continuous positive definite function.

4.4.2 Boundedness and Ultimate Boundedness

We have the following result

Theorem 4.3 *Consider (4.84)-(4.86) and the control (4.20). Let Assumptions 4.3-4.4 hold and let $\mathcal{M}$ and $\mathcal{N}$ be any compact subsets of $\mathbb{R}^{\ell+r}$ and $\mathbb{R}^r$, respectively. Then, for trajectories $(z, x) \times \hat{x}$ starting in $\mathcal{M} \times \mathcal{N}$ the following holds*

- *There exists ε_4^* such that, for all $0 < \varepsilon \leq \varepsilon_4^*$, $\chi(t)$ is bounded for all $t \geq 0$ and $\xi(n)$ is bounded for all $n \geq 0$.*
- *Given any $\mu \geq 0$, there exists $\varepsilon_5^* > 0$, $k^* > 0$ and $n^* > 0$, such that for every*

$0 < \varepsilon \leq \varepsilon_5^*$, *we have*

$$\|\xi(n)\| + |\chi(k)|_{\mathcal{A}} \leq \mu \quad \forall \quad k \geq k^*, \quad \textit{and} \quad n \geq n^* \tag{4.89}$$

Proof: Let Ω_1 denote the compact set $\{V(\chi) \leq c_1\}$ for any $c_1 > 0$. We take $W(\xi) = \xi^T P \xi$ as the Lyapunov function for the observer error dynamics where P is positive definite and satisfies $A_f^T P A_f - P = -I$ and $\|P\| > 1$. Let $c_2 > c_1$, $c_3 > 0$ and consider the following sets

$$\Omega_2 = \{V(\chi) \leq c_2\}, \quad \Lambda = \Omega_2 \times \{W(\xi) \leq c_3 \varepsilon^2\}$$

Due to the boundedness of γ and $\mathcal{G}$ in $\hat{x}$ we have for all $(\chi, \xi) \in \Omega \times \mathbb{R}^r$ and for all $d \in \mathcal{D}$

$$\|\mathcal{F}(\chi, \xi_s, d, T_s, \varepsilon)\| \leq K_1, \quad \|\mathcal{G}(\chi, \xi, d, \zeta, u)\| \leq K_2$$

where K_1 and K_2 are positive constants independent of ε. From equations (4.20), (4.81), (4.86), and since $\mathcal{F}$ is Lipschitz with respect to x uniformly in d

$$\|\mathcal{F}(\chi, 0, d, T_s, 0) - \mathcal{F}(\chi, \xi_s, d, T_s, \varepsilon)\| \leq \varepsilon K_3 \|\chi(k)\| + K_4 \|\xi_s(k)\|$$

for all $(\chi, \xi) \in \Omega \times \mathbb{R}^r$, all $d \in \mathcal{D}$, and for some positive constants K_3 and K_4 independent of ε. From the foregoing, it can be shown that in the set Λ

$$V(\chi(k+1)) = V(\chi(k) + T_s \mathcal{F}(\chi, \xi_s, d, T_s, \varepsilon)) \leq V(\chi(k)) - \alpha_3(|\chi|_{\mathcal{A}}) + \varepsilon T_s K_5 \tag{4.90}$$

and

$$W(\xi(n+1)) \leq \left(1 - \frac{1}{\|P\|}\right) W(\xi(n)) + \varepsilon K_6 \|\xi\| + \varepsilon^2 K_7 \tag{4.91}$$

for some positive constants K_5, K_6, and K_7. Repeating arguments as in Theorem 4.1 boundedness of the closed-loop trajectories follows for both cases of controller design discussed in the previous section.

Ultimate boundedness follows by showing that equation (4.90) satisfies

$$V(\chi(k+1)) \leq V(\chi(k)) - \frac{1}{2}\alpha_3(|\chi(k)|_{\mathcal{A}})$$

for $\alpha_3(|\chi(k)|_{\mathcal{A}}) \geq 2\varepsilon T_s K_4$. Let

$$\omega(\varepsilon) = 2\varepsilon T_s K_4 + \max_{\alpha_3(|\chi(k)|_{\mathcal{A}}) \leq 2\varepsilon T_s K_4} V(\chi(k))$$

As in Theorem 4.1, using (4.87) we can show that there is a $k^* > 0$ such that for all $k \geq k^*$

$$|\chi(k)|_{\mathcal{A}} \leq \alpha_1^{-1}(\omega(\varepsilon))$$

where $\omega(\varepsilon) \to 0$ as $\varepsilon \to 0$. We have that $\|\xi(n)\|$ enters the set $\{W(\xi(n)) \leq c_3\varepsilon^2\}$ in finite time. Using this fact, we can find an ε_5^* such that (4.89) is satisfied for all $\varepsilon \leq \varepsilon_5^*$. $\lhd$

Remark 4.4 *We remark on the intersampling behavior of the closed-loop system. Theorem 4.3 shows that $\chi(t)$ is bounded for all $t \geq 0$ and that $\chi(k)$ and $\xi(n)$ are bounded and ultimately bounded. Using equation (4.12), it can be seen that the continuous-time trajectories of the closed-loop system cannot grow by more than an order of T_s in between samples. That is*

$$\|\chi(t) - \chi(k)\| \leq O(T_s)$$

4.4.3 The Tracking Problem, Integral Control, and Disturbances

In anticipation of the simulation and experimental results of the next chapter, we consider the tracking problem and a controller that contains integral action. For the tracking problem, the closed-loop system will be driven by time-varying reference signals and stabilization of the origin may not be possible. Therefore, we will consider stabilization to a set containing the origin. To generalize the discussion of Subsection 4.4.1 we will

allow the system to depend on disturbances that vary continuously in t. We derive the closed-loop system under multirate sampled-data output feedback and discuss extending the results of the previous Subsection to the case considered here.

Consider the system (4.76)-(4.79). Ideally, we'd like the output y, in the absence of disturbances, to asymptotically track a reference signal $y_R(t)$. We consider reference signals that satisfy the following

1. $y_R(t)$ and its derivatives up to and including $y_R^{(r)}(t)$ are Lipschitz continuous functions of t and belong to the compact set $\mathcal{R}$.

2. The signals are available online.

Let $Y_R(t) = [y_R(t) \;\; \dot{y}_R(t) \;\; \cdots \;\; y_R^{(r-1)}(t)]^T$ and set $e = x - Y_R$. We can rewrite the system dynamics in the error coordinates

$$\dot{z} = \psi(e + Y_R(t), z, d(t), u) \tag{4.92}$$

$$\dot{e} = Ae + B\phi(e + Y_R(t), z, d(t), u) - y_R^{(r)}(t) \tag{4.93}$$

The right-hand side depends on an unknown but bounded disturbance $d(t)$. This disturbance take values in a known compact set $\mathcal{D} \subset \mathbb{R}^d$. We further assume that $d(t)$ is Lipschitz continuous in t. That is

$$\|d(t_1) - d(t_2)\| \leq L_d|t_1 - t_2|$$

for some positive constant L_d. To simplify the notation, let $\chi_e = [z \;\; e]^T$ and $\mathcal{Y}_R = [Y_R \;\; y_R^{(r)}]^T$. Also, define the right-hand side of (4.92)-(4.93) by the function $F(\chi_e(t), d(t), \mathcal{Y}_R(t), u)$. The solution to (4.92)-(4.93) over the period $[kT_s, kT_s + T_s]$ is given by

$$\chi_e(t) = \chi_e(k) + \int_{kT_s}^{t} F(\chi_e(\tau), d(\tau), \mathcal{Y}_R(\tau), u(k))d\tau$$

By adding and subtracting terms to the right-hand side and using the Lipschitz property of the function F we can arrive at

$$\begin{aligned}\|\chi_e(t) - \chi_e(k)\| \leq\ & (t - kT_s)\|F(\chi_e(k), d(k), \mathcal{Y}_R(k), u(k))\| \\ & + L_1 \int_{kT_s}^{t} \|\chi_e(\tau) - \chi_e(kT_s)\| d\tau + L_2 \int_{kT_s}^{t} \|d(\tau) - d(kT_s)\| d\tau \\ & + L_3 \int_{kT_s}^{t} \|\mathcal{Y}_R(\tau) - \mathcal{Y}_R(kT_s)\| d\tau\end{aligned}$$

where L_1, L_2, and L_3 are Lipschitz constants of F with respect χ_e, d, and $\mathcal{Y}_R$, respectively. From the Lipschitz property of $\mathcal{Y}_R$ and d this simplifies to

$$\begin{aligned}\|\chi_e(t) - \chi_e(k)\| \leq\ & (t - kT_s)\|F(\chi_e(k), d(k), \mathcal{Y}_R(k), u(k))\| + L_4(t - kT_s)^2 \\ & + L_1 \int_{kT_s}^{t} \|\chi_e(\tau) - \chi_e(kT_s)\| d\tau\end{aligned}$$

for some positive constant L_4. Applying Gronwall-Bellman to the above equation results in the following inequality

$$\begin{aligned}\|\chi_e(t) - \chi_e(k)\| \leq\ & \frac{1}{L_1}\left[e^{(t-kT_s)L_1} - 1\right] \|F(\chi_e(k), d(k), \mathcal{Y}_R(k), u(k))\| \\ & + \frac{2L_4}{L_1}\left[e^{(t-kT_s)L_1} - 1 - T_s\right]\end{aligned} \tag{4.94}$$

Using the notation $d[k] = \{d(t) : t \in [kT_s, kT_s + T_s]\}$ and $\mathcal{Y}_R[k] = \{\mathcal{Y}_R(t) : t \in [kT_s, kT_s + T_s]\}$ we can write the discrete-time dynamics in the following way

$$\chi_e(k+1) = \chi_e(k) + T_s F(\chi_e(k), d(k), \mathcal{Y}_R(k), u(k)) + T_s^2 \Phi(\chi_e(k), d[k], \mathcal{Y}_R[k], u(k), T_s) \tag{4.95}$$

We consider the sampled-data state feedback controller with integral action using the Forward Euler method

$$\sigma(k+1) = \sigma(k) + T_s(y(k) - y_R(k)) \tag{4.96}$$

$$u(k) = \gamma(\sigma(k), x(k), \zeta(k), \mathcal{Y}_R(k)) \tag{4.97}$$

To study the system using such a controller, we can augment the state equation (4.95) with (4.96)

$$\begin{bmatrix} \sigma(k+1) \\ \chi e(k+1) \end{bmatrix} = \begin{bmatrix} \sigma(k) \\ \chi e(k) \end{bmatrix} + T_s \begin{bmatrix} y(k) - y_R(k) \\ F(\chi e(k), d(k), \mathcal{Y}_R(k), u(k)) \end{bmatrix} + T_s^2 \begin{bmatrix} 0 \\ \Phi(\chi e(k), d[k], \mathcal{Y}_R[k], u(k), T_s) \end{bmatrix} \tag{4.98}$$

We operate under the assumption that the controller (4.97) achieves asymptotic stabilization of a compact set $\mathcal{A}$ containing the origin $(\sigma, \chi e) = 0$ of (4.98).

Assumption 4.5

1. *The function γ is locally Lipschitz in σ, x and ζ and globally bound in σ and x.*
2. *The closed-loop system (4.97)-(4.98) is uniformly globally asymptotically stable with respect to the compact invariant set $\mathcal{A}$.*

Assumption 4.6 *The functions ϕ, ψ, and Θ are locally Lipschitz in x, z, and u uniformly in d and $\mathcal{Y}_R$.*

As in the previous subsection, we need a converse Lyapunov result for the analysis. The proof of the converse Lyapunov Theorem given by Jiang and Wang [35] for UGAS nonlinear systems relies on the fact that the disturbance is discrete and takes on values in a compact set. Their work parallels the work of Lin, Sontag, and Wang [42] where a converse Lyapunov Theorem was presented for continuous-time systems with disturbances. It is expected that based on the results of these groups a converse Lyapunov Theorem can be proven for discrete-time systems affected by continuous-time disturbances that also takes values in a compact set. We don't pursue this extension here, however we proceed by making the following assumption

Assumption 4.7 *Let* $\chi_a = [\sigma \;\; \chi_e]^T$. *There exists a smooth Lyapunov function* $V(\chi_a)$ *that satisfies*

$$\alpha_1(|\chi_a|_{\mathcal{A}}) \leq V(\chi_a) \leq \alpha_2(|\chi_a|_{\mathcal{A}}) \tag{4.99}$$

$$\Delta V(\chi_a) = V(\chi_a(k+1)) - V(\chi_a(k)) \leq -\alpha_3(|\chi_a|_{\mathcal{A}}) \tag{4.100}$$

for all $\chi_a \in \mathbb{R}^{\ell+r+1}$, *all* $d \in \mathcal{D}$, *and all* $\mathcal{Y}_R \in \mathcal{R}$ *where* α_1 *and* α_2 *are class* $\mathcal{K}_\infty$ *functions and* α_3 *is a continuous positive definite function.*

Based on the foregoing, with the closed-loop system under multirate sampled-data output feedback using the observer (4.16)-(4.17) and the controller

$$u(k) = \gamma(\sigma(k), \hat{x}(k), \zeta(k), \mathcal{Y}_R(k)) \tag{4.101}$$

we have the following result, the proof of which is similar to that of Theorem 4.3.

Theorem 4.4 *Consider the state and control, equations (4.98) and (4.101), respectively, along with the multirate observer (4.16)-(4.17). Let Assumptions 4.5-4.7 hold and let* $\mathcal{M}$ *and* $\mathcal{N}$ *be any compact subsets of* $\mathbb{R}^{\ell+r}$ *and* $\mathbb{R}^r$ *respectively. Then, for trajectories* $(z, x) \times \hat{x}$ *starting in* $\mathcal{M} \times \mathcal{N}$ *the following holds*

- *There exists* ε_6^* *such that, for all* $0 < \varepsilon \leq \varepsilon_6^*$, $\chi_e(t)$ *is bounded for all* $t \geq 0$, $\sigma(k)$ *is bounded for all* $k \geq 0$, *and* $\xi(n)$ *is bounded for all* $n \geq 0$.

- *Given any* $\mu \geq 0$, *there exists* $\varepsilon_7^* > 0$, $k^* > 0$ *and* $n^* > 0$, *such that for every* $0 < \varepsilon \leq \varepsilon_7^*$, *we have*

$$\|\xi(n)\| + |\chi_e(k)|_{\mathcal{A}} \leq \mu \;\; \forall \;\; k \geq k^*, \;\; \textit{and} \;\; n \geq n^* \tag{4.102}$$

4.5 Example

Consider the system

$$\begin{aligned} \dot{x}_1 &= x_2 \\ \dot{x}_2 &= x_3 \\ \dot{x}_3 &= x_2^3 + u \\ y &= x_1 \end{aligned}$$

together with the state feedback linearizing control law implemented in discrete-time

$$u(k) = -x_2^3(k) - 3x_3(k) - 3x_2(k) - x_1(k)$$

We determine through simulation that a sampling period of $T = 0.2$ is sufficient to stabilize the origin of the closed-loop system. For initial conditions in the set $\{|x_i| \leq 1\}$ the control saturation level $\{|u| \leq 10\}$ was chosen based on simulation under sampled-data state feedback. Using the observer (4.16)-(4.17), the closed-loop system under sampled-data output feedback is simulated for $x_1(0) = 0.9$ and $x_2(0) = x_3(0) = \hat{x}_1(0) = \hat{x}_2(0) = \hat{x}_3(0) = 0$. With these initial conditions, the control $u(0) = u_0(0) = 0$. Figure 4.2 shows the response of the output and control for the single-rate output feedback case with $T_s = 0.2$ and $\varepsilon = 0.2$ and for the multirate output feedback case where $T_s = 0.2$, $T_f = 0.04$ and $\varepsilon = 0.04$. For comparison, the response under sampled-data state feedback with sampling period $T = 0.2$ is also given. The plots show that the multirate case, with the more accurate estimation, is able to stabilize the system. Also, it can be seen that the control under the multirate scheme avoids peaking. Figure 4.3 shows that the estimates recover from peaking and converge to the states during the period $[0, 0.2]$, thereby isolating the control from the observer transient. Clearly, the single-rate case was unable stabilize the system for this choice of sampling period, but we reiterate the point

made in the introduction that for sufficiently small sampling period the single-rate case will stabilize the closed-loop system. This is shown in the next simulation example where we examine the transient performance of the single-rate and multirate output feedback control schemes in the presence of disturbances and initial estimation error. The single-rate scheme is simulated for $T_S = 0.1$, $\varepsilon = 0.1$ and again for $T_S = 0.01$, $\varepsilon = 0.01$. For the multirate scheme we use $T_S = 0.1$, $T_f = 0.01$, and $\varepsilon = 0.01$. Figure 4.4 shows that both responses of the single-rate scheme undergo peaking from the initial estimation error and consequently, the control response saturates. Consistent with high-gain observer theory [20], the single-rate scheme with the faster sampling period recovers more quickly. The multirate scheme however avoids controller saturation. Three fast samples or 0.03 seconds were enough for the multirate estimates to recover from peaking. In all three cases, the control was held at a constant value $u = 0$ over the first input sampling period T_S. Figure 4.4 also shows similar behavior in the three cases when an impulsive-like disturbance of duration $0.001s$ and an amplitude of 300 is experienced at the input of $\dot{x}_1$ at time $t = 10$. For the multirate scheme the observer was able to recover from the disturbance before the next control step was initiated. This can be seen from Figure 4.5 where the estimates are plotted against the states. The top set of figures show the peaking in each estimate, and the bottom set focuses on the behavior around $t = 10s$. Here, the estimates can be seen to experience a transient between slow samples taken at $\{10, 10.1\}$. However, if the disturbance occurs toward the end of the current control step, the next control step may be computed before the estimates recover from peaking. This situation is illustrated in Figure 4.6 where the impulsive-like disturbance is felt at $t = 7.087$. The single-rate case is also plotted where $T_S = 0.01$. The single-rate case experiences negative followed by positive saturation during successive samples. The multirate case on the other hand experiences negative saturation during one sample and then settles. These results show that the multirate scheme compared to the single-rate scheme is less sensitive to the peaking phenomenon, but still requires a globally bounded control.

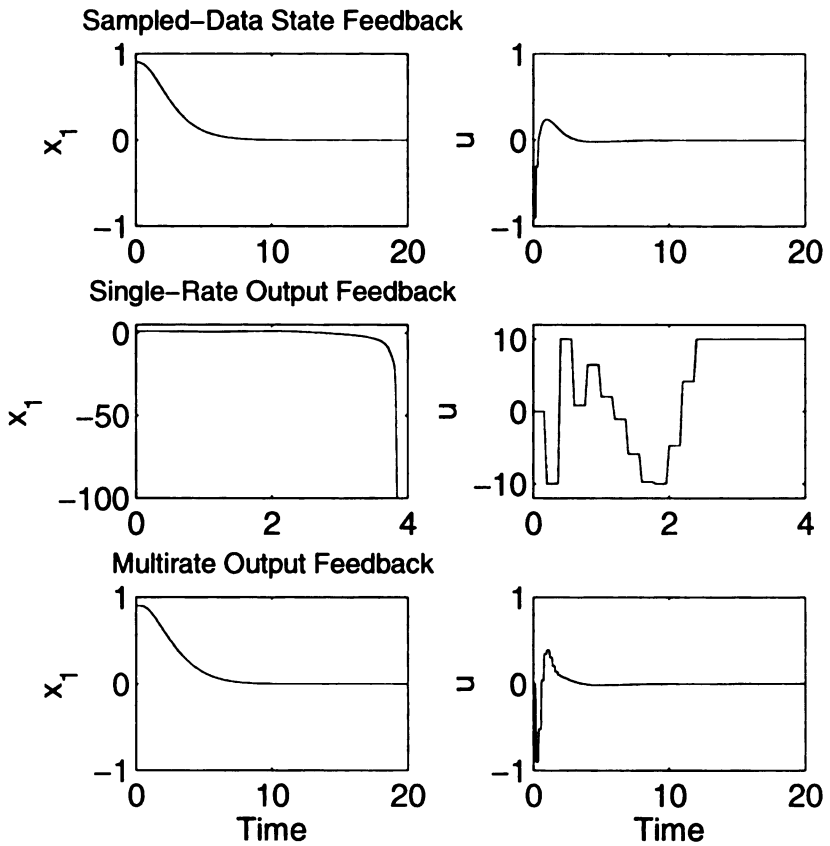

Figure 4.2. Simulation results showing the output x_1 and the control u for sampled-data state feedback (top) with $T = 0.2$, single-rate output feedback (middle) with $T_s = \varepsilon = 0.2$, and multirate output feedback (bottom) with $T_s = 0.2$ and $T_f = \varepsilon = 0.04$.

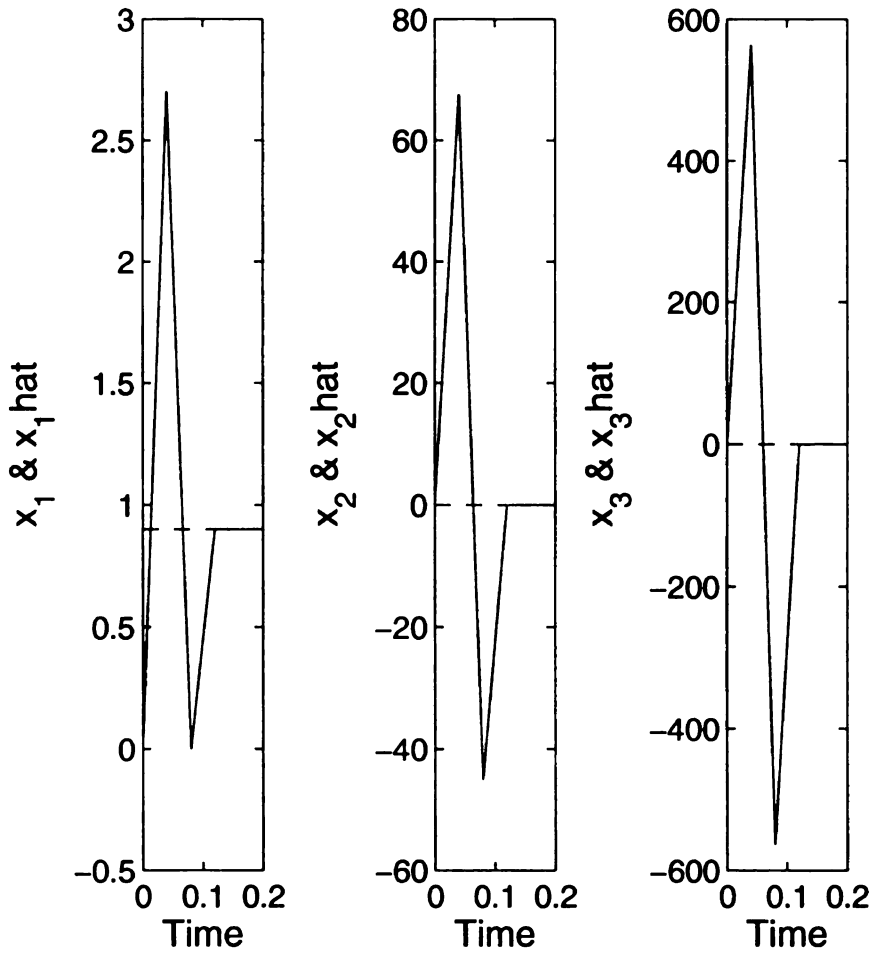

Figure 4.3. Simulation results showing the transient response of the multirate observer estimates (solid) versus the system states (dashed).

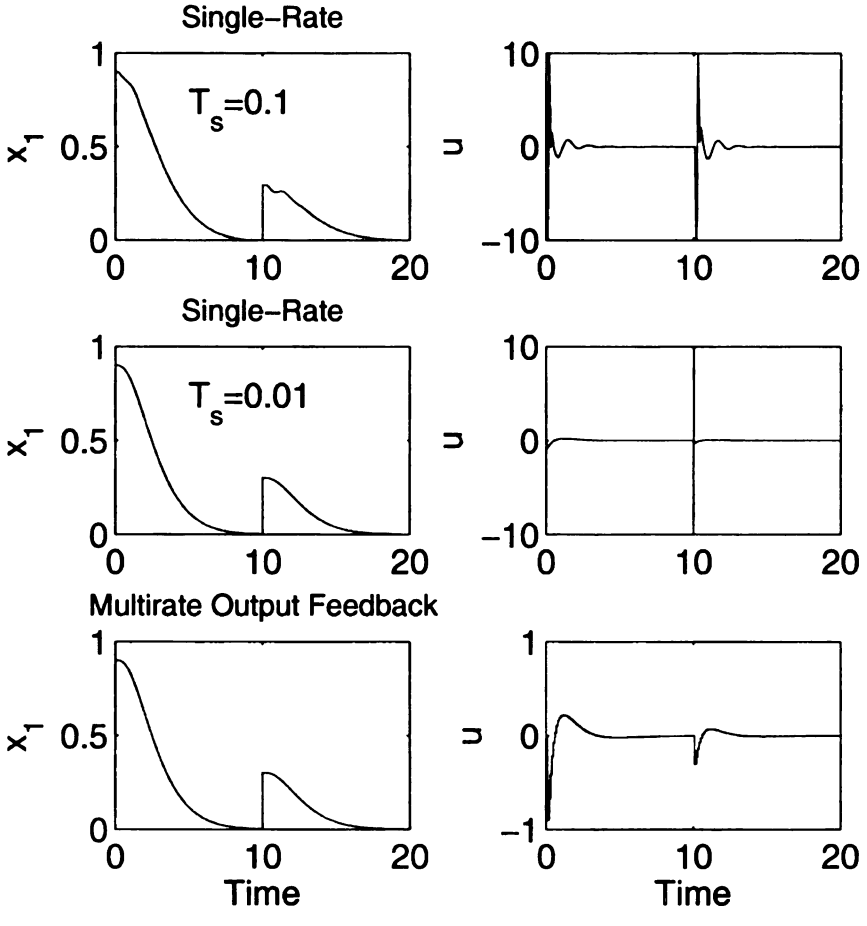

Figure 4.4. Simulation results for an impulsive-like disturbance at $t = 10$. Shown are the output x_1 and the control u for two cases of single-rate sampled-data output feedback, (1) $\varepsilon = 0.1$, $T_S = 0.1$ (2) $\varepsilon = 0.01$, $T_S = 0.01$, and multirate sampled-data output feedback, where $\varepsilon = 0.01$, $T_S = 0.1$, and $T_f = 0.01$.

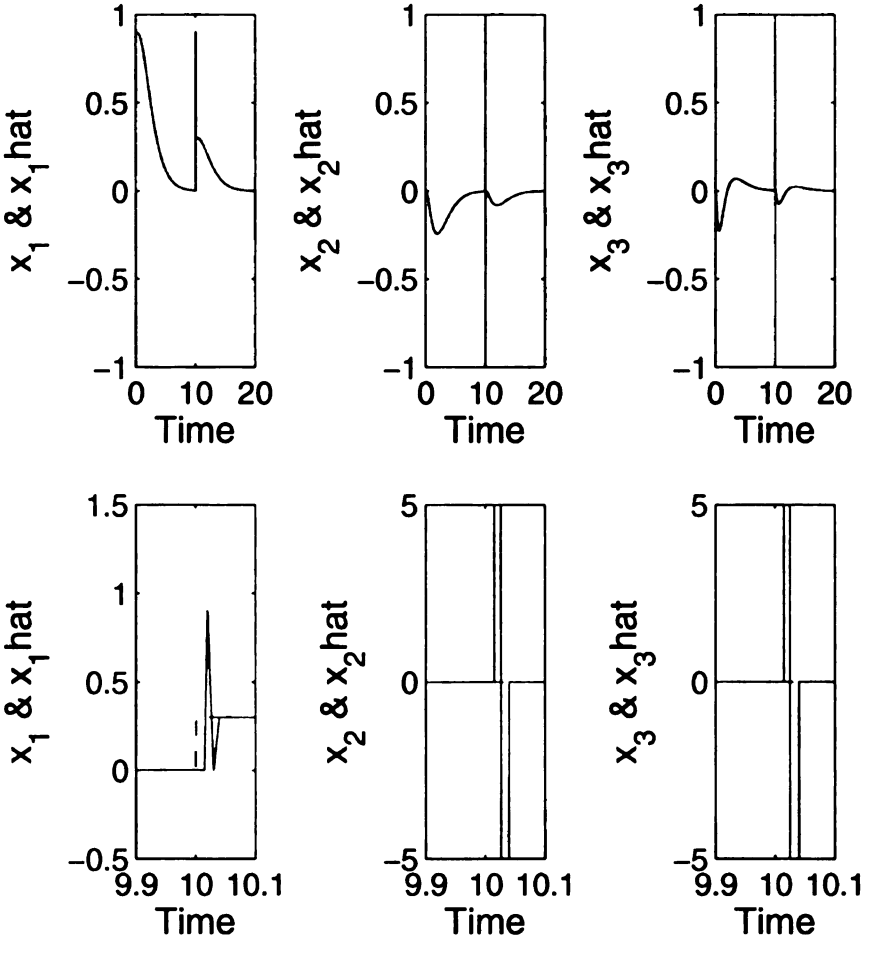

Figure 4.5. Simulation results for an impulsive-like disturbance at $t = 10$. Shown are the multirate observer estimates (solid) versus the system states (dashed) for the entire simulation run (top) and zoomed in on the transient response at $t = 10$ (bottom).

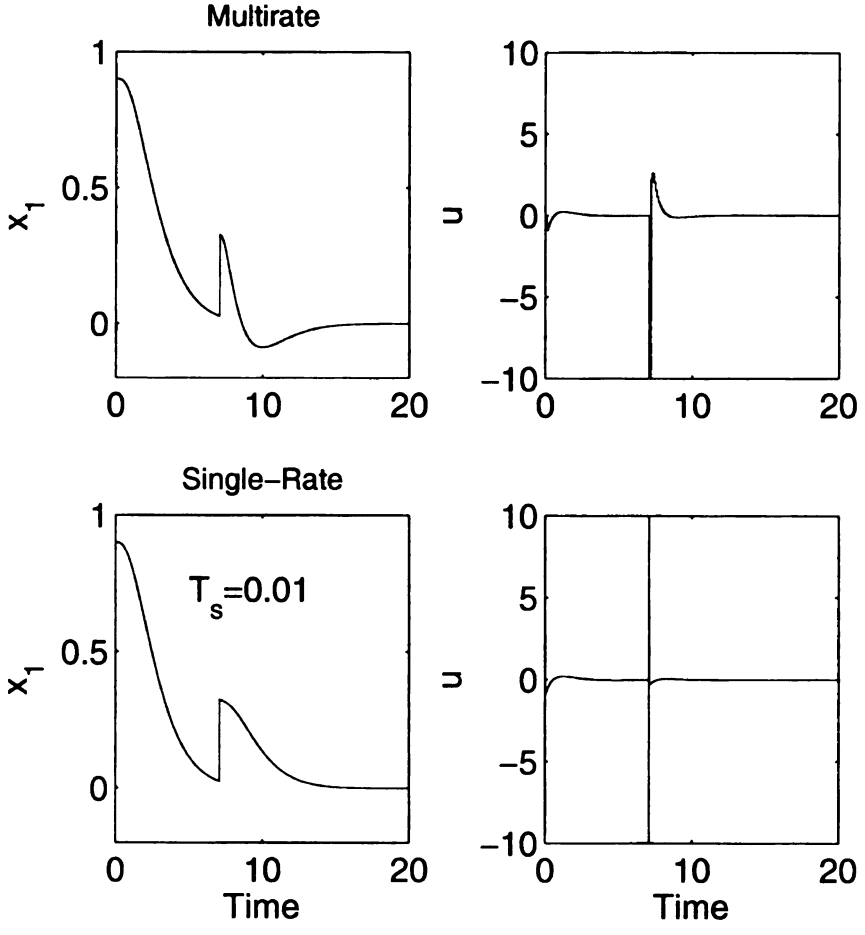

Figure 4.6. Simulation results for an impulsive-like disturbance at $t = 7.087$. Shown are the output x_1 and the control u for multirate sampled-data output feedback, where $\varepsilon = 0.01$, $T_S = 0.1$, and $T_f = 0.01$ (top), and single-rate sampled-data output feedback, where $\varepsilon = 0.01$, $T_S = 0.01$ (bottom).

4.6 Conclusions

We have studied multirate sampled-data output feedback control of a class of nonlinear systems using high-gain observers. Based upon a given asymptotically stabilizing state feedback controller and input sampling rate, we were able to show that the scheme practically stabilizes the origin of the closed-loop system. We also examined stabilization with respect to a compact positively invariant set. We have also seen that initialization of the controller can overcome the peaking phenomenon as in [37]. Initialization represents the state of the art of digital control. In [4], Astrom and Wittenmark mention that "it is important to set the controller state appropriately when the controller is switched on." This is done to prevent large switching transients. They go on stating that "for an algorithm with an explicit observer, the controller state may be initialized by keeping the control signal fixed for the time required for the observer to settle." As we have seen, both analytically and through numerical example, the multirate scheme can be designed such that controller initialization need only be preformed for one slow sample. In addition, the multirate scheme appears to be less sensitive than the single-rate scheme to impulsive-like disturbances that may occur at an unknown time.

CHAPTER 5

Application to Smart Material Actuated Systems

5.1 Introduction

In this Chapter we are motivated by applications to smart material actuated systems that may employ computationally demanding controllers such as hysteresis inversion algorithms [63]. Control difficulties are listed among the main drawbacks to the use of smart material actuators [24]. This is due to the nonlinear behavior of the material and difficulties in measuring the state variables. Smart materials such as piezoelectrics, shape memory alloys, magnetorheological and electrorheological fluids, and magnetostrictives represent an area of research that has recently received significant attention due to their broad application potential. Computer technology has motivated the recent interest in this area, as they allow for efficient control of these systems. Smart materials exhibit significant nonlinear behavior, not the least of which is the hysteresis that is inherent in these materials. Control techniques for systems with hysteresis have recently received renewed attention due to the possible application of smart materials in actuator designs [47]. Hysteretic nonlinearities can severely limit a system's operation resulting in undesirable inaccuracies, oscillations, and even instability of the closed-loop system [65]. Moreover,

tight control is needed when smart material actuators are used in applications such as micropositioning. For these applications it is necessary to compensate for the hysteresis.

We consider a class of nonlinear systems actuated by a smart material actuator. The model we use is shown in Figure 5.1, where the actuator portion appears in the dotted box. This actuator is comprised of a hysteresis operator, denoted by Γ, in cascade with linear dynamics. Smart material actuator models of this form are discussed in [16] and [69]. The fundamental approach [65] to dealing with hysteretic nonlinearities, and the one we use here, is to use an inversion control scheme as shown in Figure 5.3. Here the hysteresis is preceded by its right inverse, denoted by $\hat{\Gamma}^{-1}$, so that its effect is canceled. There are a number of methods available to characterize a hysteretic nonlinearity that result from physics-based and phenomenological models. Some of these models can be found in [13], [45], and [71]. These models come with varying levels of complexity and accuracy. Modeling the hysteretic behavior is complicated by the fact that the output depends not only on the instantaneous input, but also on the history of its operation. For a good control design, phenomenological models that characterize the hysteresis must be sufficiently accurate, applicable for controller design, and efficient enough for real-time application. In this work we will use the Preisach operator. The reason for this is that the Preisach operator provides a very general description of the hysteresis. And from [63] a computationally efficient discrete inversion algorithm is readily available. The analysis in this case will be complicated by the fact that, in general, the error resulting from inexact inversion or hysteresis modeling error will be nonvanishing. Hence, the closed-loop state feedback system may not have an asymptotically stable equilibrium point, but rather will have an ultimately bounded solution. Thus, we seek to apply the results of the previous chapter by studying multirate output feedback in the presence of hysteresis inversion error. We consider a bounded hysteresis inversion error e_i and a closed, invariant set $\mathcal{A}$ that contains the origin and whose size is determined by e_i. We start with the assumption that there exists a sampled-data state feedback controller that achieves stabilization with

respect to $\mathcal{A}$ in the presence of hysteresis inversion error. With such a controller, we show that the closed-loop trajectories under multirate output feedback will come arbitrarily close to the set $\mathcal{A}$.

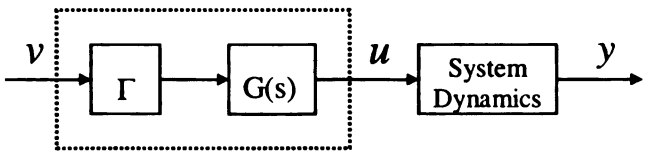

Figure 5.1. Model structure of a smart actuator and plant.

This chapter is organized as follows. In Section 5.2 we present the class of nonlinear systems under consideration. We also discuss the Preisach operator as a model for the smart material hysteresis. In Section 5.3 we derive the closed-loop sampled-data system by including the smart material actuator model and show that this model fits the development of Chapter 4. We also give a simulation example to illustrate the ideas. In Section 5.4 we present experimental results based on multirate output feedback control of a shape memory alloy actuated rotary joint. Finally, in Section 5.5 we draw our conclusions.

5.2 Model

5.2.1 Class of Systems

For the system dynamics in Figure 5.1 we consider again the following class of nonlinear systems

$$\dot{z} = \psi(x, z, u) \tag{5.1}$$

$$\dot{x} = Ax + B\phi(x, z, u) \tag{5.2}$$

$$y = Cx \tag{5.3}$$

$$\zeta = \Theta(x, z) \tag{5.4}$$

where $x \in \mathbb{R}^r$ and $z \in \mathbb{R}^\ell$ are the states, u is the input, y and ζ are the measured outputs. The functions ϕ, ψ, and Θ are locally Lipschitz in their arguments over the domain of interest and satisfy $\phi(0,0,0) = 0$, $\psi(0,0,0) = 0$, $\Theta(0,0) = 0$. The $r \times r$ matrix A, the $r \times 1$ matrix B, and the $1 \times r$ matrix C are of the same structure as (1.5)-(1.6).

5.2.2 Preisach Operator

The hysteresis is modeled using a Preisach operator, which we review here. Detailed discussion of hysteresis modeling including the Preisach operator can be found in the monographs [45] and [71]. The Preisach operator is comprised of delayed rely elements $\hat{\gamma}_{(b,a)}$ called hysterons. The switching thresholds of these elements are denoted by (b, a) as shown in Fig. 5.2. The output of the hysteron is described by $w(t) = \hat{\gamma}_{(b,a)}[v, \varsigma]$,

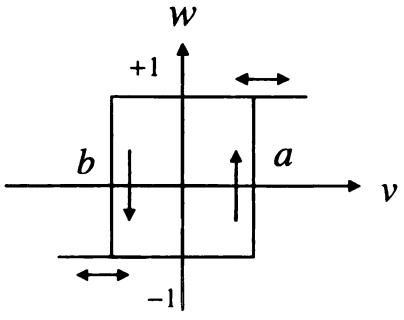

Figure 5.2. Delayed relay.

$\forall t \in [0, T]$, where v is a continuous function on $[0, T]$ and $\varsigma \in \{-1, 1\}$ is an initial

configuration. The Preisach operator can be described as a weighted superposition of all hysterons. Define the *Preisach plane* as $\mathcal{P}_0 \stackrel{def}{=} \{(b,a) \in \mathbb{R}^2 : b \leq a\}$. Each pair (b,a) is identified with the hysteron $\hat{\gamma}_{(b,a)}$. Let ς_0 be an initial configuration of all hysterons, $\varsigma_0 : \mathcal{P}_0 \to \{-1,1\}$. The output of the Preisach operator is given by

$$\Gamma[v,\varsigma_0](t) = \int_{\mathcal{P}_0} \hat{\gamma}_{(b,a)}[v,\varsigma_0](t)d\nu(b,a) \tag{5.5}$$

where ν is called the *Preisach measure.* If ν is nonsingular (see [45]), then (5.5) can be written as

$$\Gamma[v,\varsigma_0](t) = \int_{\mathcal{P}_0} \mu(b,a)\hat{\gamma}_{(b,a)}[v,\varsigma_0](t)dbda \tag{5.6}$$

where the weighting μ is called the *Preisach density.* It is assumed that $\mu \geq 0$ and $\mu(b,a) = 0$ if $b < b_0$ or $a > a_0$, where $a_0 = -b_0 = s_0$ for some positive constant s_0. Consider the finite triangular area $\mathcal{P} \stackrel{def}{=} \{(b,a) \in \mathcal{P}_0 | b \geq b_0, a \leq a_0\}$. At any time t, we can divide $\mathcal{P}$ into two regions, $\mathcal{P}_+$ and $\mathcal{P}_-$, where $\mathcal{P}_+$ ($\mathcal{P}_-$, resp.) consists of points (b,a) such that $\hat{\gamma}_{(b,a)}$ at time t is $+1$ (-1, resp.). The boundary between $\mathcal{P}_+$ and $\mathcal{P}_-$ is called the memory curve, which characterizes the memory of the Preisach operator. The set of all memory curves is denoted by Λ and λ_0 is called the initial memory curve. We make use of the following properties of the Preisach operator.

Theorem 5.1 *[71]. Let v be continuous on $[0,T]$ and $\lambda_0 \in \Lambda$.*

1. *(Rate Independence) If $\vartheta : [0,T] \to [0,T]$ is an increasing continuous function such that $\vartheta(0) = 0$ and $\vartheta(T) = T$, then $\Gamma[v(\vartheta(t)),\lambda_0] = \Gamma[v,\lambda_0](\vartheta(t))$, $\forall \lambda \in [0,T]$.*

2. *(Piecewise Monotonicity) If v is either nondecreasing or nonincreasing on some interval in $[0,T]$, then so is $\Gamma[v,\lambda_0]$.*

The hysteresis nonlinearity can be identified by discretizing the input range into L uniform intervals, which generates a discretization grid on the Preisach plane. The Preisach operator can then be approximated by assuming that inside each cell of the grid, the

Preisach density function is constant. This piecewise constant approximation to an unknown density function can be found by identifying the weighting masses for each cell, using a constrained least squares algorithm, and then distributing each mass uniformly over the corresponding cell [63], [64].

5.3 Output Feedback Control

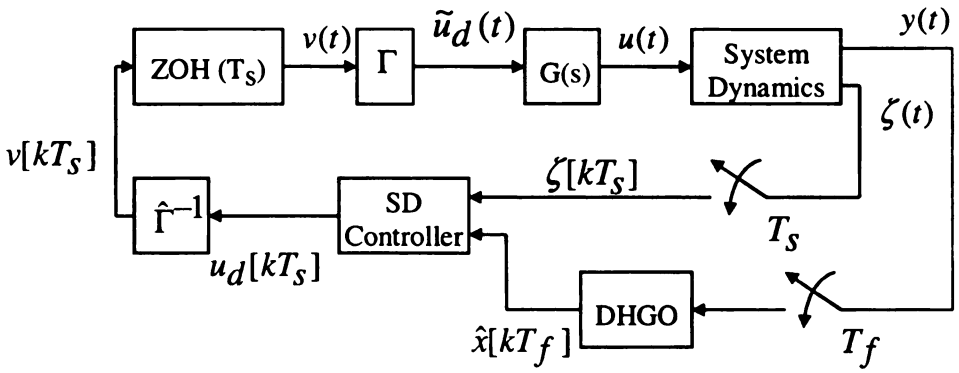

Figure 5.3. Diagram of the multirate control scheme with hysteresis inversion.

The idea behind the control scheme is shown in Figure 5.3. Hysteresis inversion is used to compensate for the hysteresis nonlinearity in the smart material actuator. This inversion is subject to modeling error and the sampled-data controller is designed to stabilize the system dynamics in the presence of this error. Here we sample the output ζ with sampling period T_S. We apply the control signal at the same rate through a zero-order-hold (ZOH) where the control is held constant in between sampling points. The output y is sampled at a faster rate where we use the period $T_f < T_S$. As discussed above, we consider a discretization of level L of the Preisach operator. Also, let the

Preisach density function μ be nonnegative and constant within each cell. Given an initial memory curve λ_0 and a desired value u_d, the inversion problem is to find a value v such that $u_d = \Gamma[v, \lambda_0]$. This is done by applying the algorithm that is given in [63] and reproduced in Appendix C. This is an iterative algorithm and it yields the exact solution in a finite number of iterations. The inversion error results from the error in identifying the weighting masses and in the level discretization, thus it can be quantified in these terms. To see this let

$$v = \hat{\Gamma}^{-1}[u_d, \lambda_0] \tag{5.7}$$

$$\tilde{u}_d = \Gamma[v, \lambda_0] \tag{5.8}$$

as shown in Figure 5.3. The inversion error is defined by

$$e_i \stackrel{def}{=} \tilde{u}_d - u_d \tag{5.9}$$

Given a bounded sequence u_d it can be shown (Appendix C) that the inversion error satisfies a bound of the form

$$\|e_i\|_\infty \leq C_s \delta_i + \frac{k_1}{L} \tag{5.10}$$

for some positive constant k_1, where δ_i is the error in identification of the weighting masses and C_s is the saturation of the hysteresis. Saturation is common in smart materials. For example, magnetostrictives exhibit magnetization saturation and shape memory alloys exhibit strain saturation. Equation (5.10) shows that the inversion error decreases with decreasing identification error and with ever-finer discretization grids (increasing the level L). Now, let

$$\dot{\sigma}_a = A_1 \sigma_a + B_1 \tilde{u}_d \tag{5.11}$$

$$y_a = C_1 \sigma_a \tag{5.12}$$

$$\tilde{u}_d = \Gamma[v, \lambda_0] \tag{5.13}$$

be a realization of the actuator dynamics $G(s)$, where $\sigma_a \in \mathbb{R}^a$. Using (5.7), (5.8), and (5.9), we can augment the system (5.1)-(5.4) with the actuator dynamics. We have

$$\dot{\sigma}_a = A_1\sigma_a + B_1 u_d + B_1 e_i \tag{5.14}$$

$$\dot{z} = \psi(x, z, C_1\sigma_a) \tag{5.15}$$

$$\dot{x} = Ax + B\phi(x, z, C_1\sigma_a) \tag{5.16}$$

$$y = Cx \tag{5.17}$$

$$\zeta = \Theta(x, z) \tag{5.18}$$

It is this equivalent system that the output feedback controller is tasked with stabilizing based on the measurements y and ζ. This is done by first designing a partial state feedback controller based on the state x and the measurement ζ. When designing the controller u_d it may be desirable to take into consideration any information about the additive inversion error e_i, such as a known upper bound. One may apply robust nonlinear control design tools such as those discussed in Chapter 14 of [36]. The next step in the design is to implement the same controller in sampled-data with the state x replaced by the estimate $\hat{x}$ that is calculated from the measurement y using a discrete-time high-gain observer. The partial state feedback controller is given by

$$u_d = \gamma(x, \zeta) \tag{5.19}$$

where γ is locally Lipschitz in its arguments over the domain of interest and $\gamma(0, 0) = 0$. We use the high-gain observer

$$\dot{\hat{x}} = A\hat{x} + B\phi_0(\hat{x}, \zeta, u_d) + H(y - C\hat{x}) \tag{5.20}$$

where the function ϕ_0 is locally Lipschitz in its arguments over the domain of interest, globally bounded in x, and satisfies $\phi_0(0,0,0) = 0$.

Now, let $\chi = [\sigma_a \quad z \quad x]^T$ and rewrite (5.14)-(5.16) as

$$\dot{\chi} = F(\chi, u_d + e_i) \tag{5.21}$$

where

$$F(\chi, u_d + e_i) = \begin{bmatrix} A_1\sigma_a + B_1(u_d + e_i) \\ \psi(x, z, C_1\sigma_a) \\ Ax + B\phi(x, z, C_1\sigma_a) \end{bmatrix}$$

The control v is applied to the system through a zero-order-hold, thus it is held constant in between sampling points. Due to the rate independence of the Preisach operator, $\tilde{u}_d$ will also be constant in between sampling points. We denote the signal at the kth sampling point by $\tilde{u}_d(k) = u_d(k) + e_i(k)$. The solution of (5.21) over the sampling period $[kT_s, kT_s + T_s]$ is given by

$$\begin{aligned} \chi(t) &= \chi(k) + (t - kT_s)F(\chi(k), u_d(k) + e_i(k)) \\ &\quad + \int_{kT_s}^{t} [F(\chi(\sigma), u_d(k) + e_i(k)) - F(\chi(k), u_d(k) + e_i(k))]d\sigma \end{aligned}$$

As was done in Section 4.2 of Chapter 4 we can arrive at the discrete-time system

$$\chi(k+1) = \chi(k) + T_sF(\chi(k), u_d(k) + e_i(k)) + T_s^2\Phi(\chi(k), u_d(k) + e_i(k), T_s) \tag{5.22}$$

where Φ is locally Lipschitz in $(\chi, u_d + e_i)$. We use the discrete-time high-gain observer (4.16)-(4.17) that is sampled with the fast sampling period T_f

$$\begin{aligned} q(n+1) &= A_f q(n) + B_f y(n) + \varepsilon^{r-1} T_f B\phi_0(D^{-1}q(n), \zeta(k), u_d(k)) && (5.23) \\ \hat{x}(n) &= C_f q(n) && (5.24) \end{aligned}$$

We point out that u and ζ evolve in the slow sampling time k and are constant for all n where $nT_f \in [kT_s, kT_s + T_s)$. The output feedback controller is given by

$$u_d(k) = \gamma(\hat{x}_s(k), \zeta(k)) \tag{5.25}$$

where $\hat{x}_s(k) = \hat{x}(\lfloor hk \rfloor)$ and $h = T_s/T_f$. Following the procedure of Section 4.2 , Chapter 4 we can arrive at the estimation error equation

$$\xi(n+1) = A_f \xi(n) + \varepsilon \mathcal{G}(\chi(n), \xi(n), e_i(k), \zeta(k), u_d(k), \varepsilon)$$

where $\mathcal{G}$ is locally Lipschitz in its arguments, uniformly bounded in ε, for ε sufficiently small, and globally bounded in $\hat{x}$. We arrive at the closed-loop system under multirate output feedback control

$$\chi(k+1) = \chi(k) + T_s \mathcal{F}(\chi(k), \xi_s(k), e_i(k), T_s, \varepsilon) \tag{5.26}$$

$$\xi(n+1) = A_f \xi(n) + \varepsilon \mathcal{G}(\chi(n), \xi(n), e_i(k), \zeta(k), u_d(k), \varepsilon) \tag{5.27}$$

$$\hat{x}_s(k) = [I - \varepsilon N_2(\varepsilon)] x(k) + N_1(\varepsilon) \xi_s(k) \tag{5.28}$$

where $\xi_s(k) = \xi(\lfloor hk \rfloor)$ and

$$\begin{aligned} \mathcal{F}(\chi, \xi_s, e_i, T_s, \varepsilon) = {} & F(\chi(k), u_d(k) + e_i(k)) \\ & + T_s \Phi(\chi(k), u_d(k) + e_i(k), T_s) \end{aligned} \tag{5.29}$$

is locally Lipschitz with respect to χ and ξ_s. The matrices N_1 and N_2 are defined as in Equation (4.31). Furthermore, we have that the inversion error $e_i(\cdot)$ takes values in a known compact set $\mathcal{D} \subset \mathbb{R}$. Let $\mathcal{M}_{\mathcal{D}}$ be the set of all functions from $\mathbb{Z}_+$ to $\mathcal{D}$ and Let $e_i \in \mathcal{M}_{\mathcal{D}}$. In the presence of the inversion error, the equations (5.26)-(5.28) fit the closed-loop system equations (4.84)-(4.86) that were developed in Section 4.4.1. Therefore, with

a single-rate sampled-data state feedback controller that renders a closed set containing the origin uniformly globally asymptotically stable we can apply Theorem 4.3 of Section 4.4.

Let $\mathcal{A}$ be a compact, invariant subset of $\mathbb{R}^{r+\ell+a}$ that contains the origin. The size of $\mathcal{A}$ depends on the size of the hysteresis inversion error e_i. Let $\mathcal{M}_{\mathcal{D}}$ be the set of all functions from $\mathbb{Z}_+$ to $\mathcal{D}$. Using (5.29) it can be shown that the closed-loop system under the single (slow)-rate sampled-data state feedback control

$$u_d(k) = \gamma(x(k), \zeta(k)) \tag{5.30}$$

is given by

$$\chi(k+1) = \chi(k) + T_s \mathcal{F}(\chi(k), 0, e_i(k), T_s, 0) \tag{5.31}$$

We have the following result.

Theorem 5.2 *Consider equations (5.26)-(5.28) and the control (5.25). Let* $e_i \in \mathcal{M}_{\mathcal{D}}$ *and suppose that*

1. *The origin* ($\chi = 0$) *of (5.31) is UGAS with respect to the compact set* $\mathcal{A}$*;*

2. *The function* γ *is locally Lipschitz in its arguments and globally bounded in* x*.*

Let $\mathcal{M}$ *and* $\mathcal{N}$ *be any compact subsets of* $\mathbb{R}^{\ell+r+a}$ *and* $\mathbb{R}^r$ *respectively. Then, for trajectories* $(\sigma_a, z, x) \times \hat{x}$ *starting in* $\mathcal{M} \times \mathcal{N}$ *the following holds*

- *There exists* ε_1^* *such that, for all* $0 < \varepsilon \leq \varepsilon_1^*$, $\chi(t)$ *is bounded for all* $t \geq 0$ *and* $\xi(n)$ *is bounded for all* $n \geq 0$.

- *Given any* $\nu \geq 0$, *there exists* $\varepsilon_2^* > 0$, $k^* > 0$ *and* $n^* > 0$, *such that for every* $0 < \varepsilon \leq \varepsilon_2^*$, *we have*

$$\|\xi(n)\| + |\chi(k)|_{\mathcal{A}} \leq \nu \quad \forall \quad k \geq k^*, \quad \textit{and} \quad n \geq n^*$$

5.3.1 Simulation example

In this section we illustrate the above analytical results by considering the following nonlinear system with hysteresis at the input

$$\begin{aligned} \dot{z} &= -z^3 + x_1 \\ \dot{x}_1 &= x_2 \ , \ \dot{x}_2 = x_3 \ , \ \dot{x}_3 = 3x_1^3 + z + \Gamma[v, \lambda_0] \\ y &= x_1 \\ \zeta &= z \end{aligned}$$

This system fits the class of systems under consideration and we use a controller based on state feedback design in cascade with a hysteresis inversion operator. The hysteresis nonlinearity is implemented using a Preisach operator with 10 levels. The weighting masses are uniformly distributed in each of the 55 cells. Figure 5.4 shows the major loop of the hysteresis. This hysteresis operator saturates for input values outside $[-71, 71]$

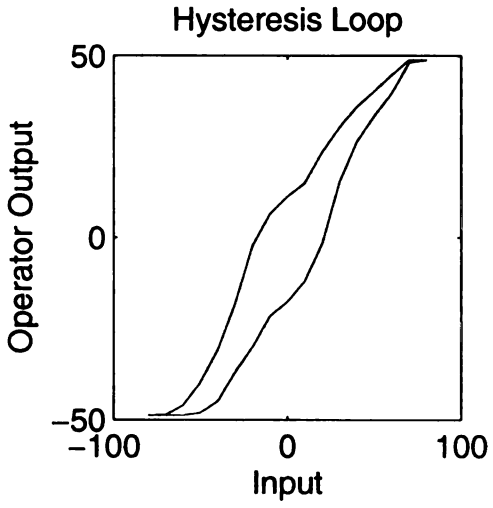

Figure 5.4. Hysteresis loop based on the Preisach operator used in the simulation example.

and has a maximum and minimum output value of ± 48.812. First, we consider the case where the hysteresis operator is exactly known and thus there is no inversion error. To compensate for the hysteresis, we use an inversion operator given by

$$v = \Gamma^{-1}[u_d, \lambda_0] \tag{5.32}$$

The state feedback controller is designed assuming that the hysteresis operator has been completely canceled and we use a sliding mode controller to stabilize the origin of the nonlinear system. This controller is given by

$$u_d = -\beta(x) sat\left(\frac{x_1 + 2x_2 + x_3}{0.1}\right) \tag{5.33}$$

where

$$\beta(x, z) = |z| + |x_2| + 2|x_3| + 3|x_1|^3 + 1 \tag{5.34}$$

It can be shown that, with the hysteresis completely canceled, this controller globally asymptotically stabilizes the origin of the closed-loop system. First, we consider a simulation based on sampled-data state feedback. We sample each output, y and ζ, with sampling period $T = 0.005$ seconds and simulate the continuous-time plant controlled by the discrete-time controller. The control signal is held constant between sampling points by using a zero-order-hold that also uses a sampling period of $T = 0.005$ seconds. Figure 5.5 shows that the sampled-data state feedback controller stabilizes the origin of closed-loop system. The plot of the hysteresis inversion error (bottom right) shows exact inversion has been achieved. To simulate the output feedback control we use the discrete-time high-gain observer (5.23)-(5.24) with

$$\phi_0 = 3\hat{x}_1^3 + \zeta + u_d$$

For the observer parameters we choose $\alpha_1 = \alpha_2 = 3$, $\alpha_3 = 1$. Also, we take $\alpha = 1$ so that $T_f = \varepsilon$. Using this observer the single-rate output feedback case is simulated, where we choose the control sampling period $T_s = 0.005$ and measurement sampling period $T_f = 0.005$. Figure 5.6 shows that the system is unstable at this sampling-rate. Using the multirate output feedback scheme we sample ζ with period $T_s = 0.005$ seconds and y with period $T_f = 0.001$ seconds. The control update rate is the same as the state feedback design $T_s = 0.005$. Under multirate output feedback, the closed-loop system is stable as shown in Figure 5.7. Now consider the case with inexact hysteresis inversion, where we use the approximate inversion operator

$$v = \hat{\Gamma}^{-1}[u_d, \lambda_0] \tag{5.35}$$

Furthermore, we assume that there is at most 20% error in identifying the weighting masses. Based on this assumption we have the following known bound for the inversion error

$$|e_i| \leq 9.7624$$

In the presence of this error, the control (5.33)-(5.34) can no longer guarantee stability of the closed-loop system. In order to deal with the hysteresis inversion error, we must modify the control design. We do so by adding 10 to the function $\beta(x, z)$ to dominate the inversion error. This function is now given by

$$\beta(x, z) = |z| + |x_2| + 2|x_3| + 3|x_1|^3 + 11 \tag{5.36}$$

and the controller will be robust with respect to the hysteresis inversion error. We simulate this system where the Preisach weighting masses are randomly perturbed by as much as 20%. The actual hysteresis inversion error satisfies

$$|e_i| \leq 6.61$$

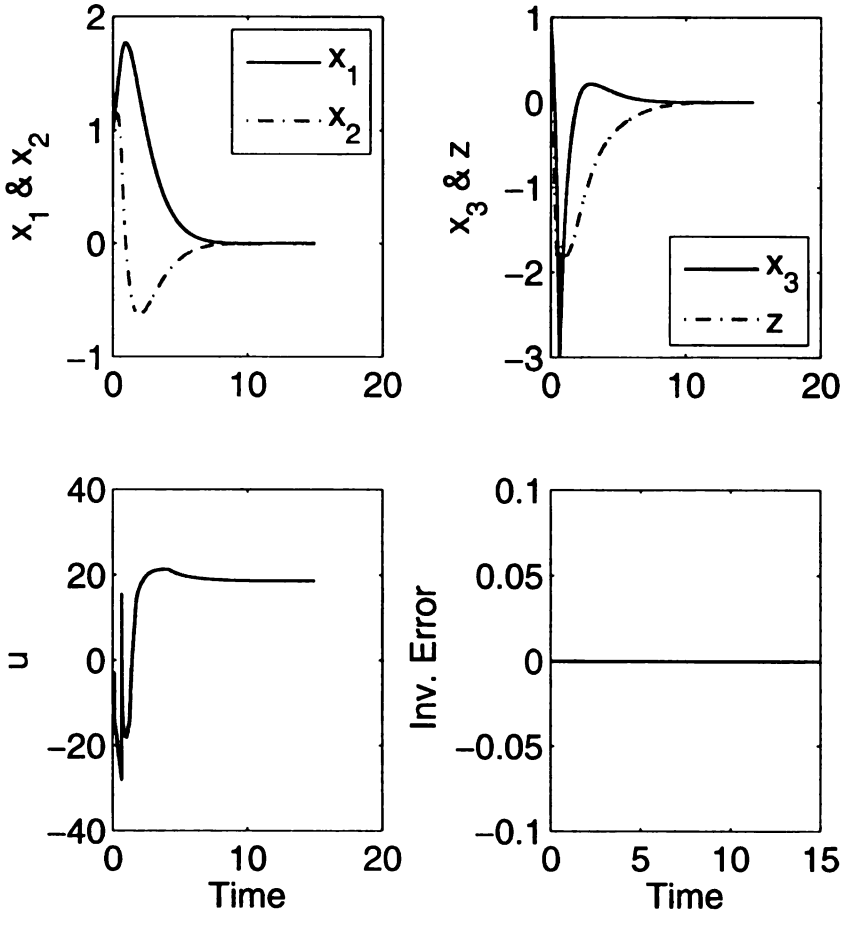

Figure 5.5. The state (top), the control (bottom left), and the inversion error (bottom right) for sampled-data state feedback with exact inversion and $T = 0.005$.

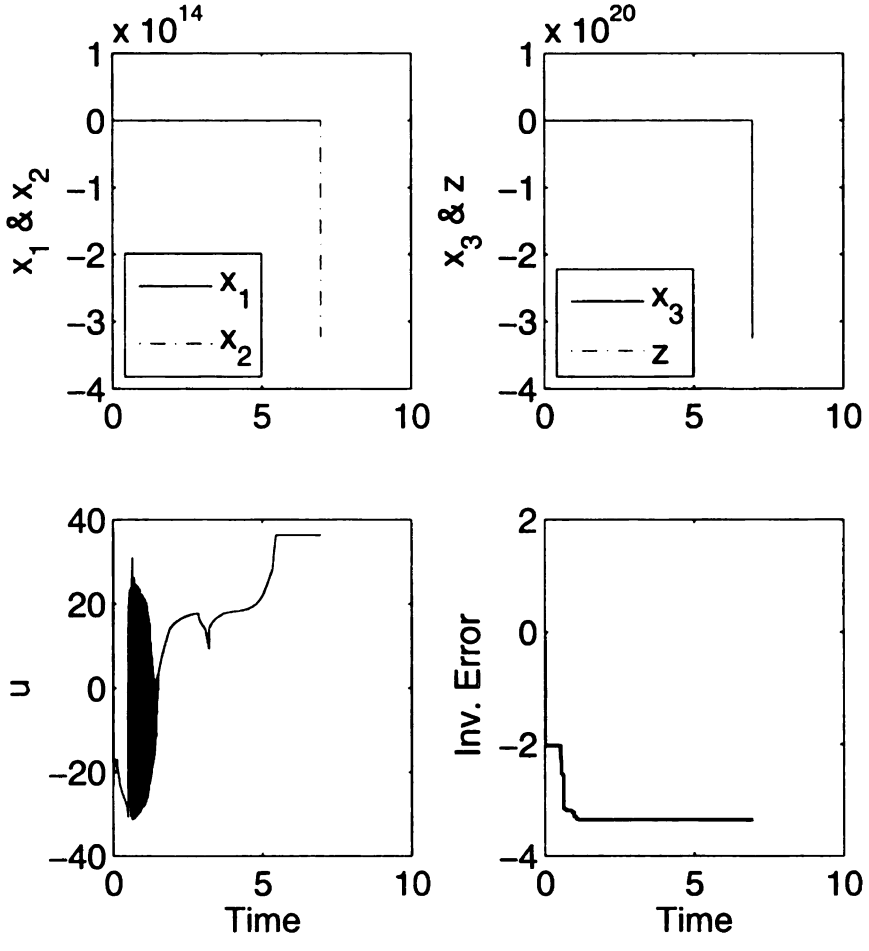

Figure 5.6. The state (top), the control (bottom left), and the inversion error (bottom right) for single-rate sampled-data output feedback with exact inversion and $T_S = 0.005$.

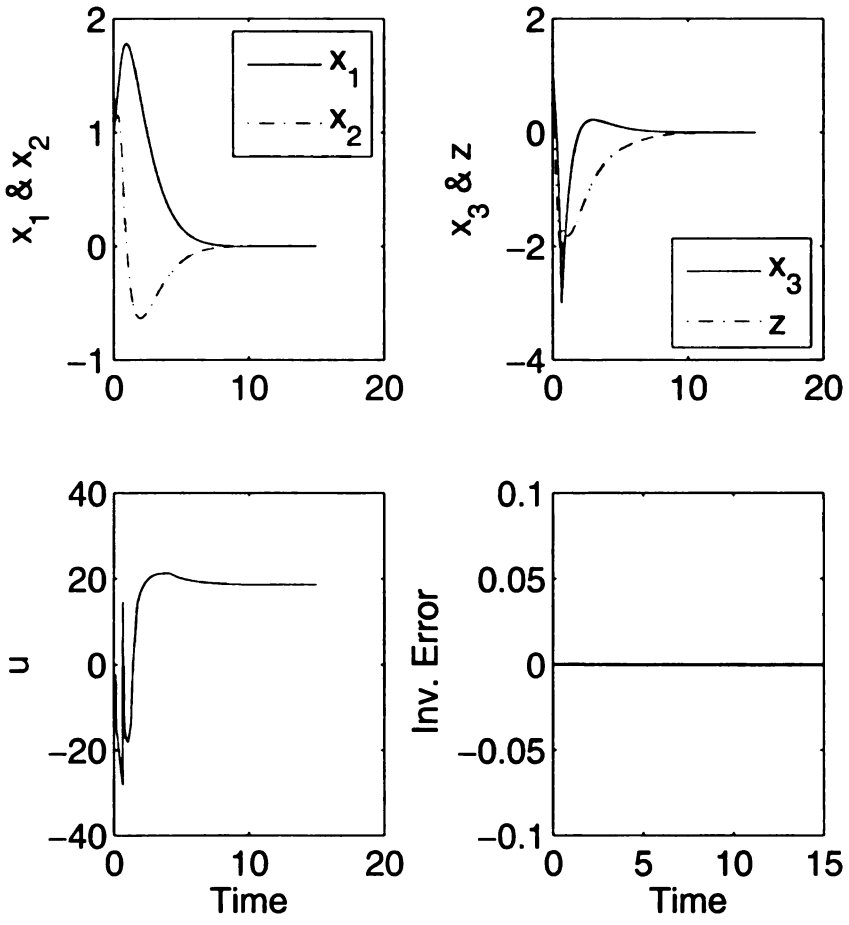

Figure 5.7. The state (top), the control (bottom left), and the inversion error (bottom right) for multirate sampled-data output feedback with exact inversion, $T_S = 0.005$, and $T_f = 0.001$.

Simulating the sampled-data state feedback control, with sampling period $T = 0.005$ seconds, we see from Figure 5.8 that the new controller is able to stabilize the origin of the closed-loop system in the presence of the inversion error. This error is visible in the bottom right plot. Now consider the single-rate output feedback case with $T_s = 0.005$. With the redesigned controller the closed-loop system is stable, but the control signal exhibits large oscillatory behavior as shown in Figure 5.9. In addition, a small oscillation can be seen in the transient response of the state z. In Figure 5.10 we can see that for the multirate output feedback case with $T_s = 0.005$ and $T_f = 0.001$ the response is stable and the control signal behaves well.

5.4 Experimental Results: Control of a Shape Memory Alloy Actuator

In this section, we apply multirate output feedback control to a shape memory alloy (SMA) actuated robotic joint. SMAs are metallic materials that exhibit coupling between thermal and mechanical energy domains. The *shape memory effect* (SME) results from a transition between two structural phases that is hysteretic in nature. For more detailed information on the SME consult [23]. The name shape memory results from the materials ability to "remember" an initial shape. For example, SMA wire can be stretched and upon heating the wire, it will contract back to its initial shape. Thus, this thermal/mechanical coupling has motivated the use of SMA as an actuator. Control of shape memory alloy actuated systems can be found in [3], [22], [24], and [31]. Also, control and modeling of hysteresis in SMA has been considered in [28], [29], [43], and [73]. Figure 5.11 shows a diagram of the rotary joint. This two-wire configuration is referred to as a *differential-type* actuator. The rotating joint consists of a 0.5 inch diameter shaft and two Nitinol wires 10.28 inches in length and 0.008 inches in diameter. These wires are stretched by 2% of their length. Alternate heating and cooling of the two wires provides clockwise (CW)

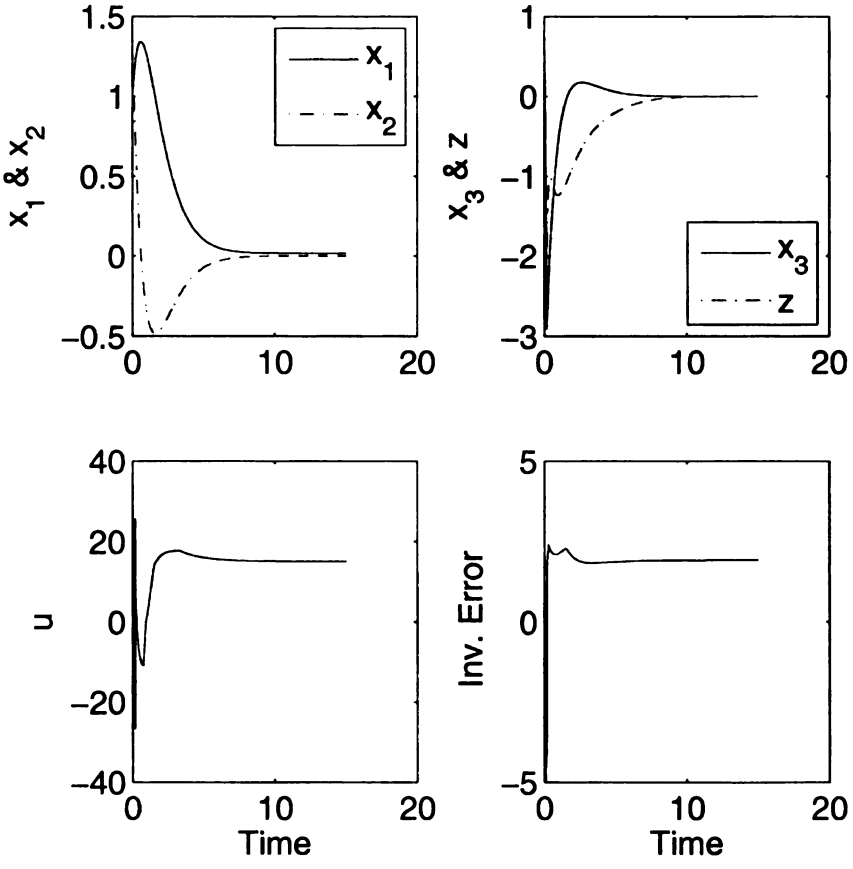

Figure 5.8. The state (top), the control (bottom left), and the inversion error (bottom right) for sampled-data state feedback with inversion error and $T = 0.005$.

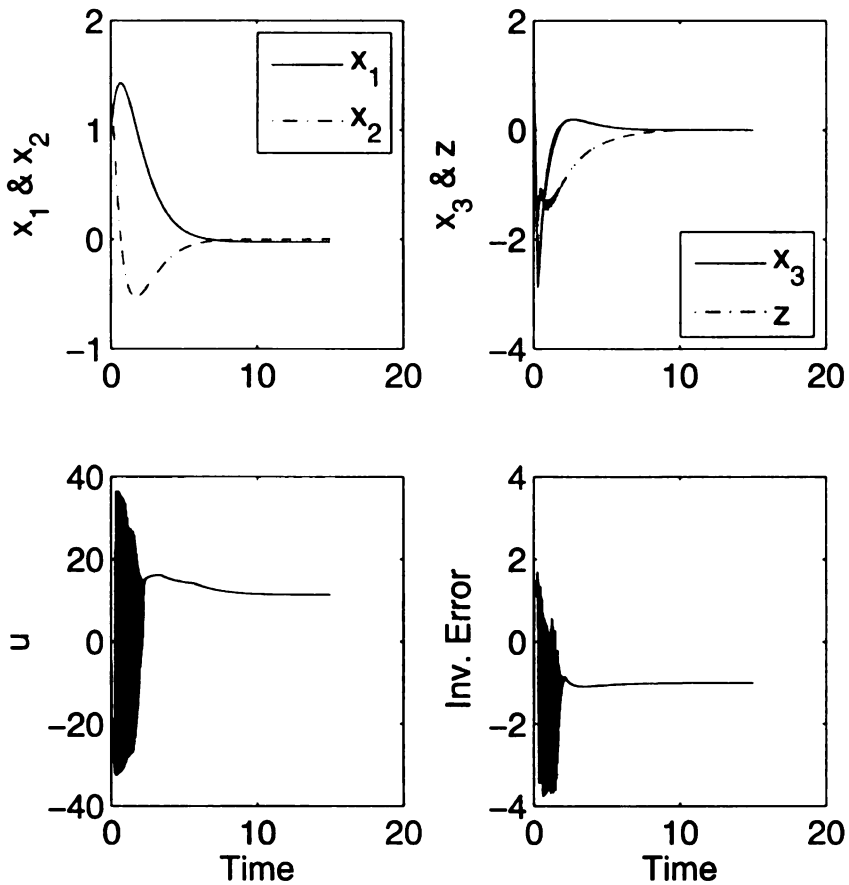

Figure 5.9. The state (top), the control (bottom left), and the inversion error (bottom right) for single-rate sampled-data output feedback with inversion error and $T_S = 0.005$.

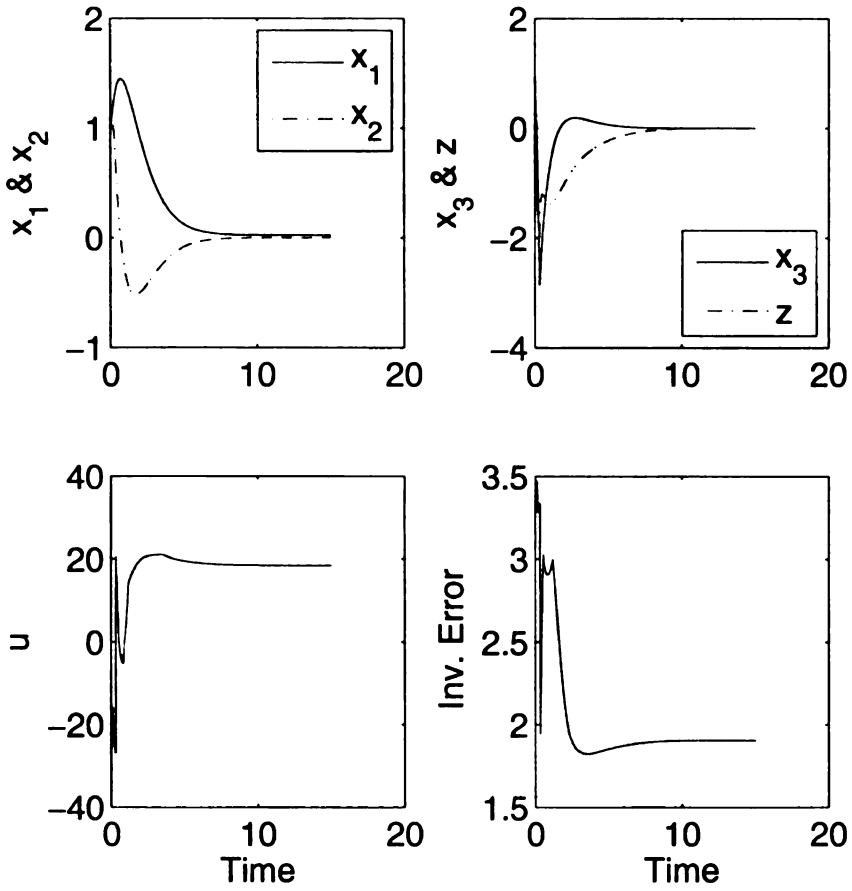

Figure 5.10. The state (top), the control (bottom left), and the inversion error (bottom right) for multirate sampled-data output feedback with inversion error, $T_s = 0.005$, and $T_f = 0.001$.

and counterclockwise (CCW) rotation. Bipolar current is supplied to the actuator where positive current gives CW rotation and negative current gives CCW rotation. With this configuration, the actuator can achieve up to 60 degrees rotation in each direction. Figure 5.12 shows a simplified diagram of the electrical setup. We use a PC with a Pentium IV processor running dSpace ControlDesk, a real-time control and data acquisition software package. The controller is programmed using Simulink and ControlDesk compiles and downloads the real-time application to a DSP board for monitoring and control. The bipolar input current is generated by a voltage controlled current (VCC) amplifier and a pair of diodes routes the current through the appropriate SMA wire; positive current through one wire and negative through the other. The joint rotation angle is obtained through an 8192 counts/rev incremental encoder. The DSP board reads the encoder measurement after A/D conversion.

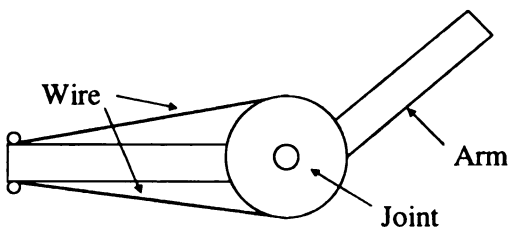

Figure 5.11. Robotic joint actuated by two SMA wires.

5.4.1 Actuator Model

We will use a model of the form shown in Figure 5.1 by identifying a Preisach operator and linear dynamics. For shape memory alloy, there are heat dynamics that relate the input current to wire temperature. The relationship between the wire temperature and

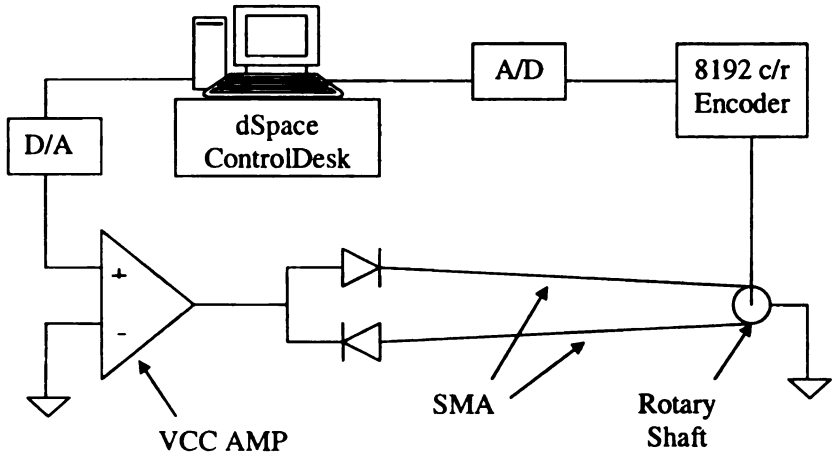

Figure 5.12. Electrical Diagram.

the resulting force of contraction is hysteretic. Thus, the temperature dynamics typically precede the hysteresis in a model of the material. We will approximate the temperature dynamics by using a static gain. We expect this approximation to be valid for relatively low frequency signals. We begin by deriving the temperature equation. The relationship between the temperature in the wire and the supplied current can be described by the following lumped heat transfer equation

$$\rho c V \frac{dT}{dt} = -hA(T - T_{amb}) + Ri^2 \tag{5.37}$$

where

ρ = wire density $[kg\ m^{-3}]$

c = wire specific heat $[J\ kg^{-1}\ {}^{\circ}C^{-1}]$

V = wire volume $[m^3]$

T = wire temperature $[^{\circ}C]$

t = time $[s]$

Diameter= 0.008 $in.$
Length= 10.28 $in.$
$R = 8.37\ \Omega$
$\rho = 6504.78\ kg\ m^{-3}$
$c = 837\ J\ kg^{-1}\ ^{\circ}C^{-1}$
$h = 68.97\ W\ m^{-2}\ ^{\circ}C^{-1}$

Table 5.1. SMA wire physical parameters, where ρ, c, h, and the diameter are specified by the manufacturer and the length and resistance R are measured.

h = heat transfer coefficient $[W\ m^{-2}\ ^{\circ}C^{-1}]$

A = wire surface area $[m^2]$

T_{amb} = ambient temperature $[^{\circ}C]$

R = wire resistance $[\Omega]$

i = current $[A]$

Let $\tilde{T} = T - T_{amb}$. We have the following transfer function that describes the heat dynamics of each SMA wire

$$\frac{\tilde{T}}{i^2} = \frac{b}{s+a} \stackrel{def}{=} G_{HT}(s) \tag{5.38}$$

where, by applying the values given in Table 5.1

$$a = -0.2494 \quad , \quad b = 181.5618$$

At dc, the relationship between current and temperature is given by

$$\tilde{T} = \frac{b}{a} i^2 \tag{5.39}$$

Next we capture the hysteresis in the actuator by identifying a Preisach operator that maps the static relationship between the temperature and the measured rotation angle. To do so, we first map the current to the rotation angle and then use (5.39) to obtain the temperature values. We limit the input current to values within the range $[-0.6A, 0.6A]$ and divide this range into 10 equally spaced intervals. The supplied current is shown in Figure 5.13 (top right). The current is held constant for a period of 45 seconds to allow the angle to settle to a steady-state value. The measured rotation angle is shown in Figure 5.13 (top left). The measured angle data fluctuates slightly after reaching steady-state for each 45 second period. To obtain a single angular value, the measurement is averaged over each 45 second period. Identification of the Preisach weights is conducted using a constrained least squares algorithm as discussed in [63] and [64]. We discretized the Preisach plane into 9 levels and used the input-output data to identify the 45 Preisach weighting masses. The identified hysteresis nonlinearity is illustrated in Figure 5.13 (bottom left). This operator maps the input current to the measured angle. Now consider

$$\tilde{T} = sign(i)\frac{b}{a}i^2 \tag{5.40}$$

Using this relationship we can construct a Preisach operator that maps the temperature $\tilde{T}$ to the measured angle. Since the current is bipolar, the *sign* function tells us which wire is being heated. Positive temperature values correspond to the heat of one wire and negative temperatures to the heat of the other. Based on the values for a and b, the temperature range is $[-262.078^{\circ}C, 262.078^{\circ}C]$. The temperature/angle map is shown in 5.13 (bottom right) and the identified Preisach weights are shown in Figure 5.14. A simulation of the operator is shown in Figure 5.15. The simulation data and the experimentally obtained data are indistinguishable, thus the Preisach operator captures the behavior of the identified hysteresis.

Next we used the identified parameters to construct a hysteresis inversion operator that maps rotation angle to temperature. In order to test the hysteresis inversion model

we conducted an open-loop inversion experiment. We supplied the following sequence of desired rotation angles to the inversion algorithm

$$\{-40, -30, -20 - 10, 0, 10, 20, 30, 40, 30, 20, 10, 0, -10, -20, -30, -40\}$$

Using the inversion algorithm and (5.40) a set of input current values were generated and these are shown in Figure 5.16 (top left). Each current value was held constant for a period of 45 seconds. The measured angle is shown in the top right plot. We averaged the measured angles over each 45 second period and obtained the values shown in Figure 5.16 (bottom left). These values are plotted against the desired angles for comparison. Figure 5.16 (bottom right) illustrates how close the hysteresis inversion comes to achieving linearity by plotting the averaged measured angles against the desired angles. A significant amount of the nonlinearity has been canceled.

To get a sense of the dynamic behavior of the SMA actuator, we conducted identification experiments for the linear dynamics. This was done by supplying the actuator with the sinusoidal current signal $i = 0.5sin(wt)$, where the frequency took the following values

$$w = \{0.02, 0.06, 0.2, 0.3, 0.4, 0.6, 0.8, 1.0, 1.2, 1.4, 1.6, 1.8, 2.0, 2.2\}$$

The resulting frequency response, normalized to obtain unity gain at dc, is plotted in Figure 5.17. We were able to obtain a reasonably good fit to the identified frequency response using the following second order system

$$TF_{fit} = \frac{0.5}{s^2 + 2.25 + 0.5} \tag{5.41}$$

as shown in Figure 5.17.

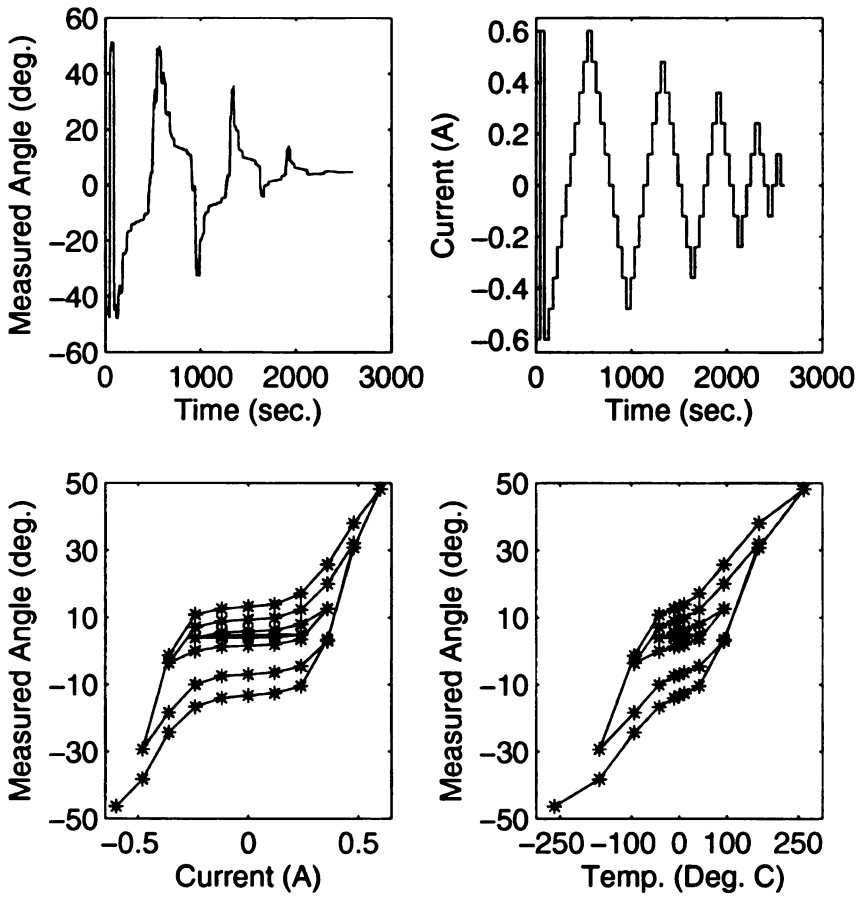

Figure 5.13. Plot showing the measured output, current input, and identified hysteresis nonlinearity.

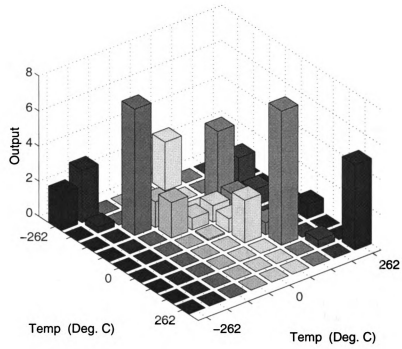

Figure 5.14. Identified Preisach weighting masses.

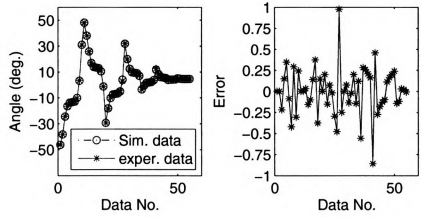

Figure 5.15. Simulation of the identified Preisach operator versus the measured data (left) and the error between the two (right).

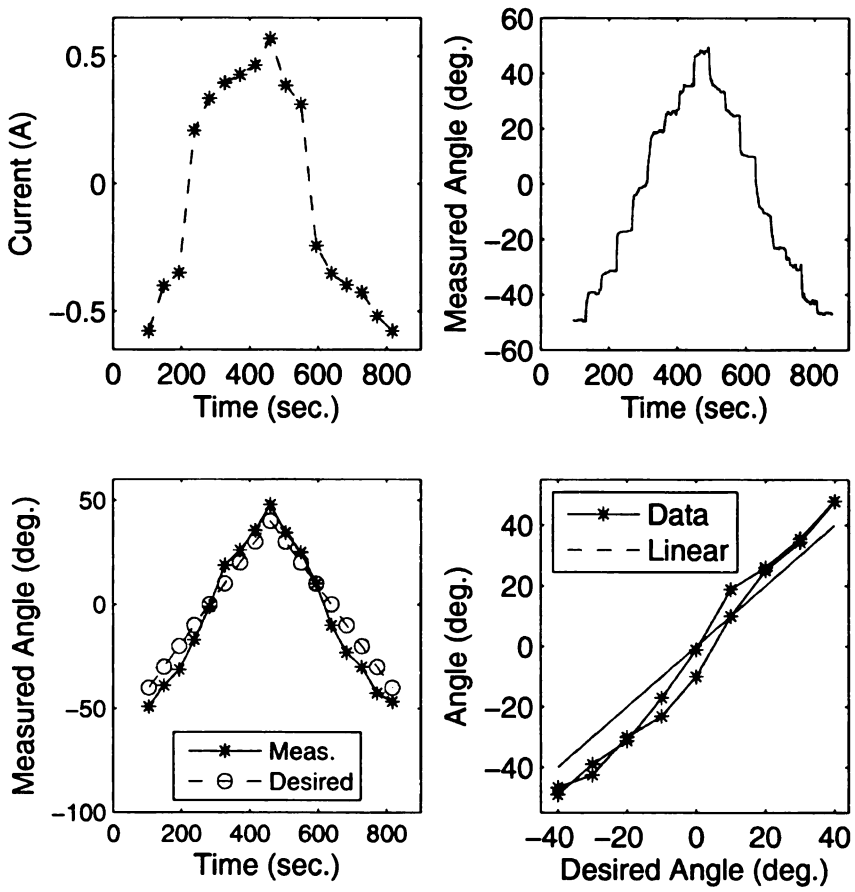

Figure 5.16. Plot showing the results of an open-loop hysteresis inversion experiment.

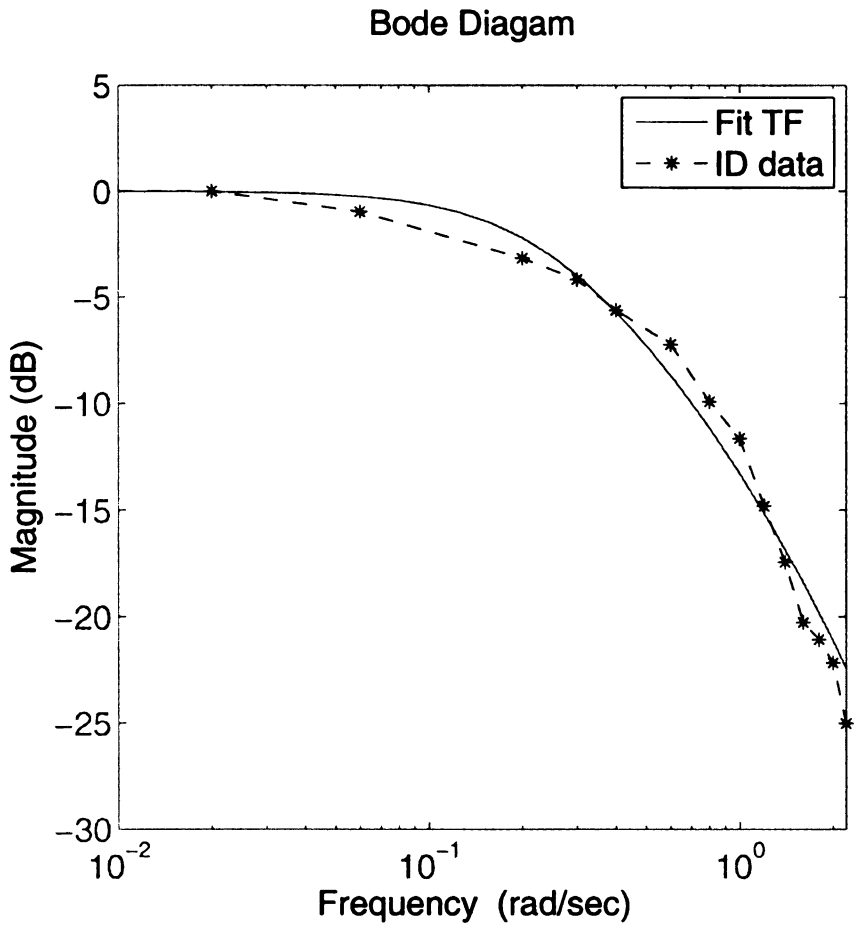

Figure 5.17. Experimentally obtained SMA actuator normalized frequency response (dashed) and the response of the transfer function (5.41) (solid).

To close the loop, we use PID as our sampled-data controller in cascade with the hysteresis inversion operator as in Figure 5.3. This controller takes the following form

$$\sigma(k+1) = \sigma(k) + T_s(\hat{x}_1(k) - r(k)) \tag{5.42}$$

$$u_d(k) = -k_i\sigma(k) - k_p(\hat{x}_1(k) - r(k)) - k_d(\hat{x}_2(k) - r_d(k)) \tag{5.43}$$

where T_s is the slow sample period, k_i, k_p, and k_d are positive constants, $\hat{x}_1$ is an estimate of the joint rotation angle θ and $\hat{x}_2$ an estimate for the angular velocity ω. Also, r and r_d are the angle and angular velocity reference trajectories, respectively. The current supplied to the actuator is given by

$$i = sign(v_i)\sqrt{|v_i|} \tag{5.44}$$

$$v_i = k_g\hat{\Gamma}^{-1}[u_d(k), \lambda_0] \tag{5.45}$$

where the gain k_g will be chosen proportional to $\frac{a}{b}$, which is the inverse of the dc gain of (5.38). This term provides an additional degree of freedom in the control design. The *sign* function provides bipolar current for CW and CCW rotation. To test the effectiveness of the hysteresis inversion, we will present results for PID control with and without the inversion. In both cases, the control current i is saturated outside $[-0.7A, 0.7A]$. To implement the output feedback controller we use a linear discrete-time high-gain observer, equations (5.23)-(5.24) with $\phi_0 = 0$. This observer estimates the rotation angle θ and angular velocity ω of the rotary joint and these estimates are used in the controller (5.42)-(5.43). It is discretized using the forward difference method and the observer parameters are taken to be $\alpha_1 = 2$ and $\alpha_2 = 1$. In every experiment we choose the relation between T_f and ε to be $T_f = 0.3\varepsilon$. In the forthcoming experiments we will compare the multirate (MR) output feedback control scheme with two single-rate (SR) schemes. One SR scheme will be used where the sampling period is chosen to be the same as the MR scheme's control sampling period. We will refer to this scheme as slow single-rate. Similarly, fast

single-rate will refer to the scheme that uses a sampling period the same as the MR scheme's fast measurement sampling period T_f.

5.4.2 Experimental Results on Regulation

We begin with a regulation experiment, where the controller attempts to rotate the joint to a desired angle θ_d and maintain it there. Thus, $r = \theta_d$ and $r_d = 0$ in (5.43). Figure 5.18 shows the results of an experiment with the target angle equal to -15 degrees. The plot compares the response of a single-rate controller (top) with a sampling period of $0.05s$ against the response of the multirate controller (middle) where the measurement period was $T_f = 0.005s$ and the control sampling period was $T_S = 0.05s$. Hysteresis inversion was used in the top two plots and the controller parameters were taken to be $k_i = 0.1$, $kp = 30$, $k_d = 4$, and $k_g = 0.028$. As can be clearly seen, the single-rate scheme was unable to stabilize the system under this large sampling period. The response exhibits an oscillation that can lead to early fatigue of the SMA, which results in a loss of the shape memory effect. On the other hand, the multirate controller, with the more accurate state estimation, was able to achieve stabilization. The bottom plot in Figure 5.18 shows the result of a MR regulation experiment without the hysteresis inversion. Here the PID gains were taken as $k_i = 0$, $kp = 5$, and $k_d = 0.1$. This controller yields good tracking performance with a much more well behaved control signal. In general, in the case of regulation to a fixed angle, the controller without hysteresis inversion outperformed the controller with the inversion. This is may be attributable to the sensitivity of the Preisach operator to the sensor noise. In all our experiments, computing power limited us to a maximum of 9 levels. Figure 5.19 compares the response of slow SR with $T_S = 0.001$, MR with $T_S = 0.001$ and $T_f = 0.0001$, and fast SR $T_S = 0.0001$ for a PID controller without inversion. Again, we used the gains $k_i = 0$, $kp = 5$, and $k_d = 0.1$. The steady-state error shows that each scheme achieves good regulation, where the target angle is now -20 degrees. Figure 5.20 plots the current signal for each scheme. The noise was considerably

amplified for the MR and the fast SR.

A series of experiments were conducted for decreasing values of the sampling periods T_S and T_f. Comparisons between the MR scheme and the fast and slow SR schemes were made. For the MR scheme, we fixed the slow sampling period T_S and ran experiments for several values of the fast sampling period $T_f < T_S$. We then chose the fast sampling period from this set that yielded the smallest root mean square (R.M.S) regulation error $(\theta - r)$. We repeated these experiments for several values of slow sampling period T_S. The resulting R.M.S errors of the MR scheme were compared to the R.M.S errors of the corresponding slow and fast SR schemes. The results of these experiments are shown in Figure 5.21. The plot on the top compares MR with slow SR under PID without inversion. The y axis represents the R.M.S error and the x axis represents the sampling period of the SR scheme which is the same as control sampling period of the MR scheme. The measurement sampling period of the MR observer is printed next to each data point. At $T_S = 0.01$ the SR scheme was not stable, but the MR scheme with $T_f = 0.005$ was stable. For $T_S \leq 0.005$ the SR scheme is stable and the MR scheme does slightly better in each case. The plot on the bottom compares MR with fast SR where, the x axis is the sampling period of the SR scheme which is the same as measurement sampling period of the MR observer. The control sampling period is printed next to each data point for the MR scheme. The R.M.S errors are close for each case as both schemes achieve good regulation. Note that the resolution of the encoder is 0.0439 degrees. In general, the R.M.S error tended to decrease slightly as the sampling period decreased. We point out that sensor noise tends to increase with faster output sampling. Thus, we expect faster output sampling to improve tracking performance only up to a point, after which the noise will begin to deteriorate the performance. This appears to be the case in Figure 5.21 where the performance for all three observers was close for a sampling period less than 0.005 seconds.

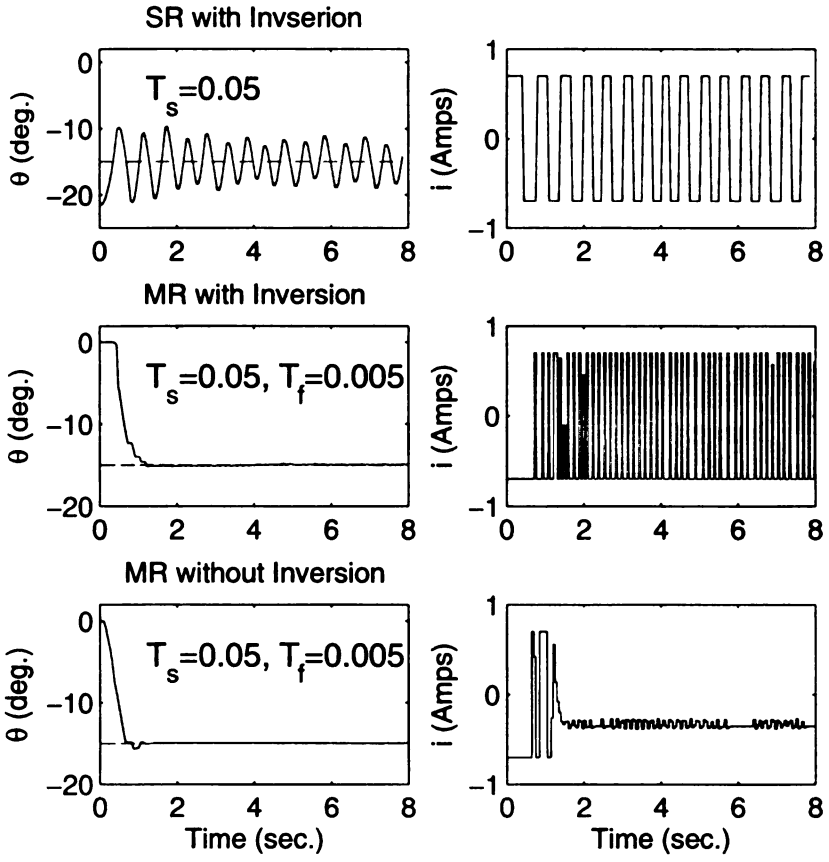

Figure 5.18. Plot of an angle regulation experiment for SR (top) and MR (middle) output *feedback* controllers with inversion and MR without inversion (bottom). Shown are the angle θ (solid) versus the setpoint r (dashed) (left) and the current i (right).

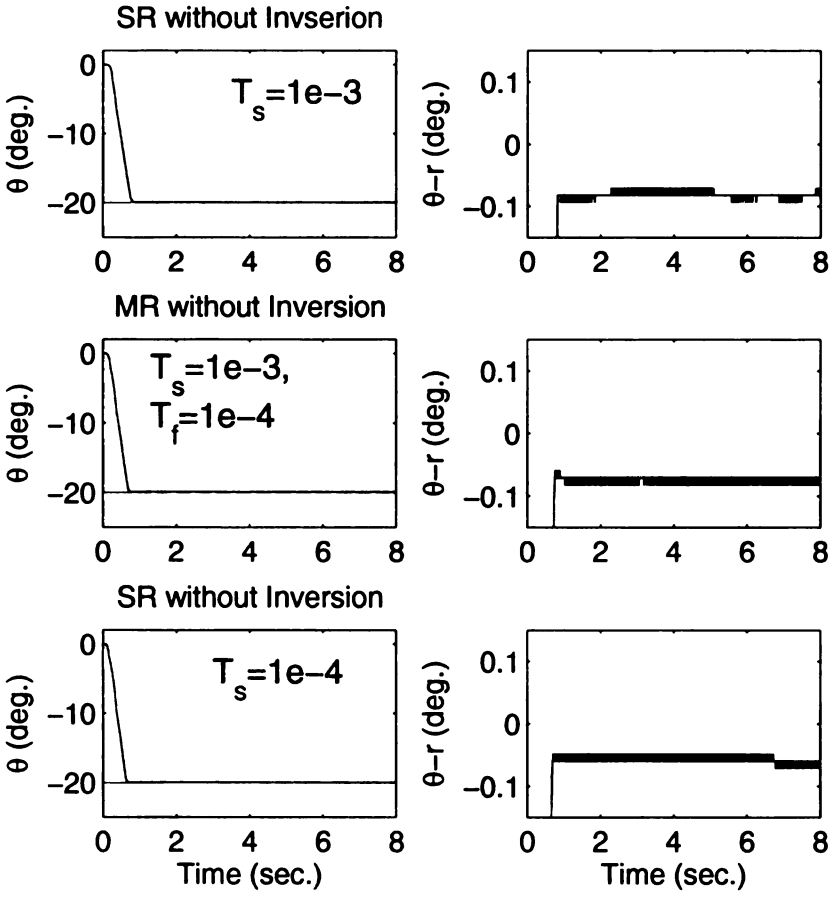

Figure 5.19. Plot of an angle regulation experiment for slow SR (top), MR (middle), and fast SR (bottom) output feedback controllers without inversion. Shown are the angle θ (solid) versus the setpoint r (dashed) (left) and the regulation error $\theta - r$ (right).

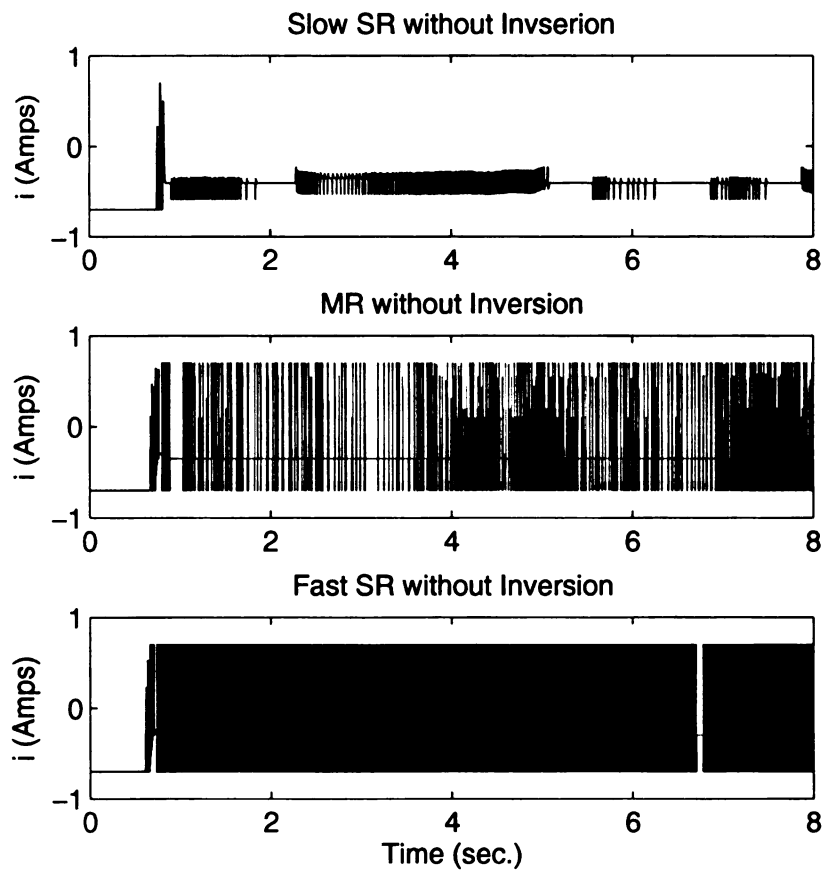

Figure 5.20. Plot of the current i for an angle regulation experiment for slow SR (top), MR (middle), and fast SR (bottom) output feedback controllers without inversion.

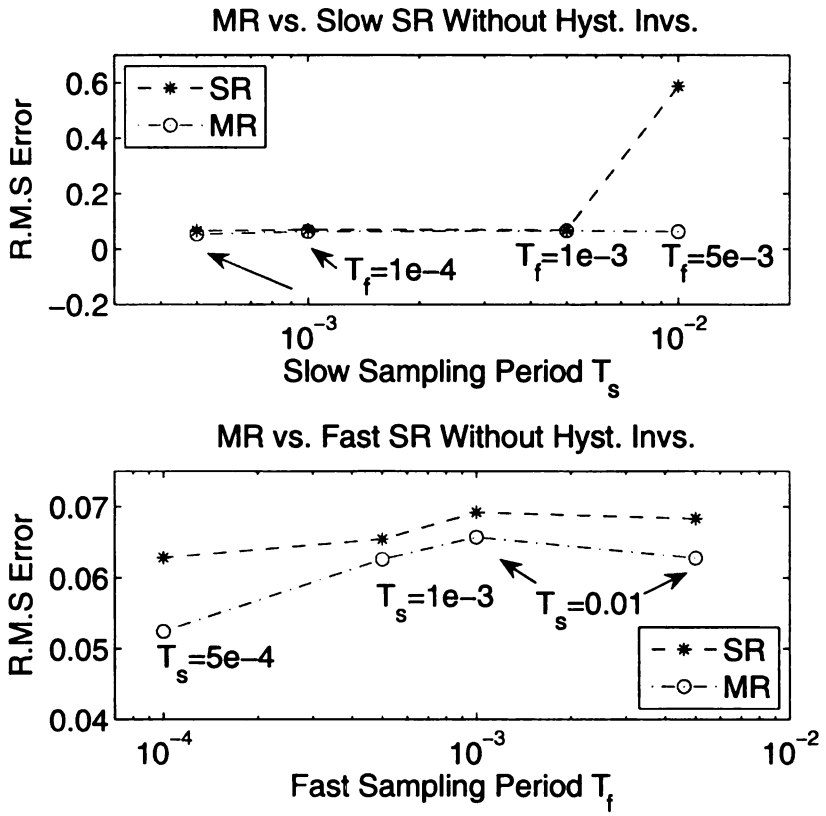

Figure 5.21. Comparison of MR versus slow SR (top) and MR versus fast SR (bottom) for a regulation experiment.

5.4.3 Experimental Results on Tracking

We now turn our attention to the tracking problem. We would like the shaft angle to track a reference trajectory r. To do this we use the control (5.42)-(5.45), where r and $r_d = \dot{r}$ are implemented in discrete-time. First, consider

$$r = 15\left[\frac{1}{2}sin\left(0.4t - \frac{\pi}{2}\right) + \frac{1}{2}sin\left(\frac{0.4}{\sqrt{2}}t - \frac{3\pi}{2}\right)\right] \tag{5.46}$$

We use $k_i = 2$, $k_p = 8$, $k_d = 0.1$, and $k_g = 0.0028$ as the controller gains. Figure 5.22 shows the response of the slow SR with $T_s = 0.01$, MR with $T_s = 0.01$ and $T_f = 0.001$, and fast SR with $T_s = 0.001$ under hysteresis inversion control. The plot shows good tracking for each scheme. Figure 5.23 shows that the error and control signals are comparable. Now, consider the same experiment this time without hysteresis inversion. The response is shown in Figure 5.24 and the tracking error and control signals appear in Figure 5.25. In this case, the MR and fast SR have similar performance, but the slow SR scheme exhibits an undesirable oscillation in the response.

As with the regulation case, a series of experiments were conducted for the tracking case for decreasing values of the sampling periods T_s and T_f. Comparisons between the MR scheme and the fast and slow SR schemes were made for the tracking problem with reference trajectory (5.46) and the R.M.S tracking error results are plotted in Figures 5.26 and 5.27. Figure 5.26 compares the MR with fast SR (top) and slow SR (bottom) for the controller without hysteresis inversion. It can be seen that the MR scheme is comparable to the fast SR scheme. The slow single-rate scheme is unstable at $T_s = 0.01$ and in general the MR outperforms the slow SR. Figure 5.27 compares the MR with fast SR (top) and slow SR (bottom) for the controller with hysteresis inversion. Here, the MR scheme appears to do a little better than the fast SR. This is most likely due to the sensitivity of the inversion scheme to measurement noise. The slow SR scheme appears to do better than the MR for $T_s = 0.01, 0.005, 0.001$, again due to measurement noise.

From both plots with the hysteresis inversion control, there is a range of sampling periods where the error increases with decreasing sampling period. This appears to be the result of sensitivity of the inversion to sensor noise. Thus, there is a range of sampling periods where faster output sampling does not improve performance.

To examine the effect of increasing the ratio T_S/T_f on the tracking performance for the multirate scheme, we plot the R.M.S tracking error for a fixed T_S and decreasing T_f. Figure 5.28 shows the results of such experiments for the controller with hysteresis inversion (top) and without hysteresis inversion (bottom). The data plotted corresponds to the tracking experiments with reference (5.46). Both the top and bottom plots show two data sets each; one for $T_S = 0.01$ and another for $T_S = 0.005$. In the top plot we see that with hysteresis inversion, the error tends to increase in both data sets as the measurement sampling period is decreased. Conversely, in the bottom plot, for the case without hysteresis inversion, the R.M.S error tends to decrease in both data sets as the sampling period is decreased. This seems to support the notion that the inversion algorithm is sensitive to measurement noise. Again, there is a practical limit on how small the sampling period can be decreased before the effect of measurement noise begins to degrade the performance. This was studied in [19] for discrete-time single-rate high-gain observers. Likewise, there will be a practical limit on how large the ratio T_S/T_f can be chosen before the effect of noise degrades the performance. We note that in any discrete-time control system, one must be aware of the effect of aliasing when choosing the measurement sampling rate. For the multirate scheme this is true when choosing the control sampling rate in addition to the measurement rate since there is downsampling involved in the scheme.

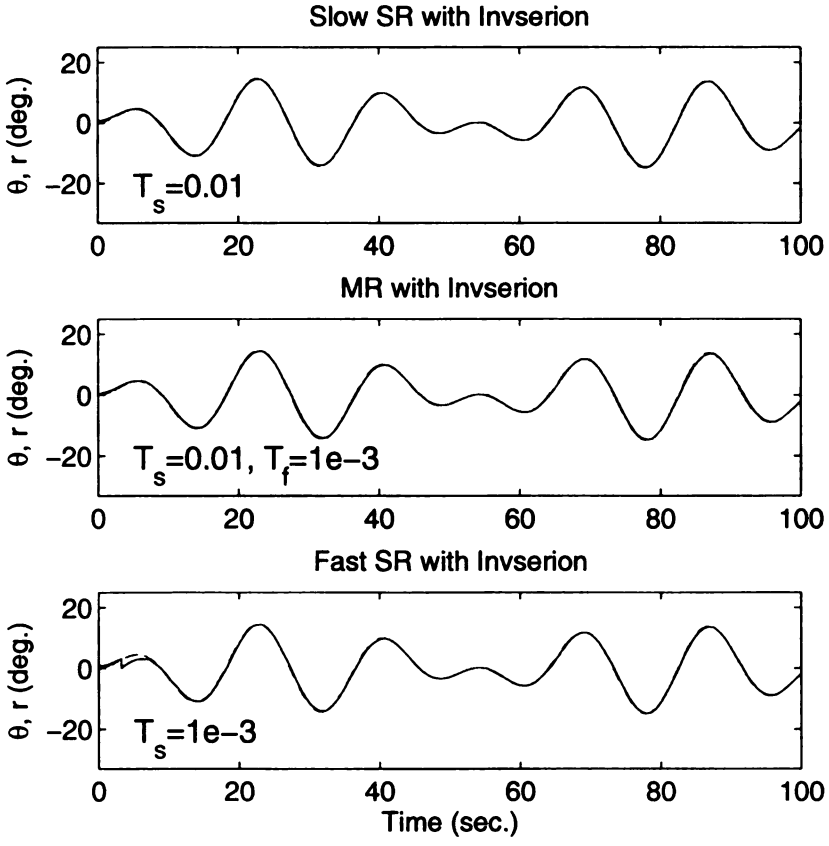

Figure 5.22. Plot of a sinusoidal tracking experiment for slow SR (top), MR (middle), and fast SR (bottom) output feedback controllers with inversion. Shown are the rotation angle θ (solid) versus the reference r (dashed).

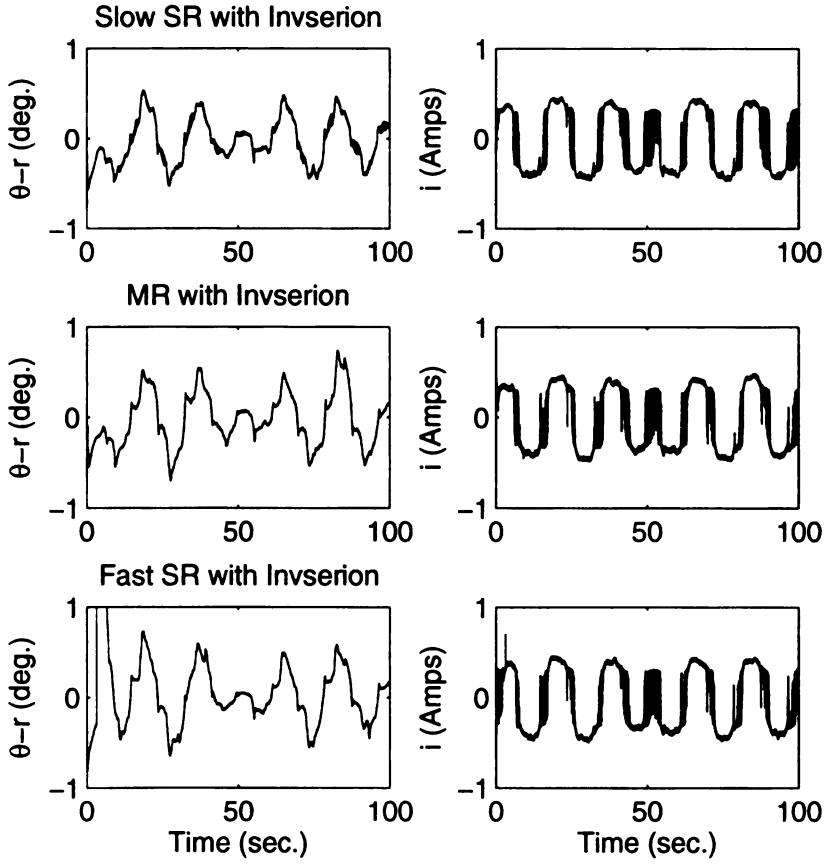

Figure 5.23. Plot of a sinusoidal tracking experiment for slow SR (top), MR (middle), and fast SR (bottom) output feedback controllers with hysteresis inversion. Shown are the tracking error $\theta - r$ (left) and current i (right).

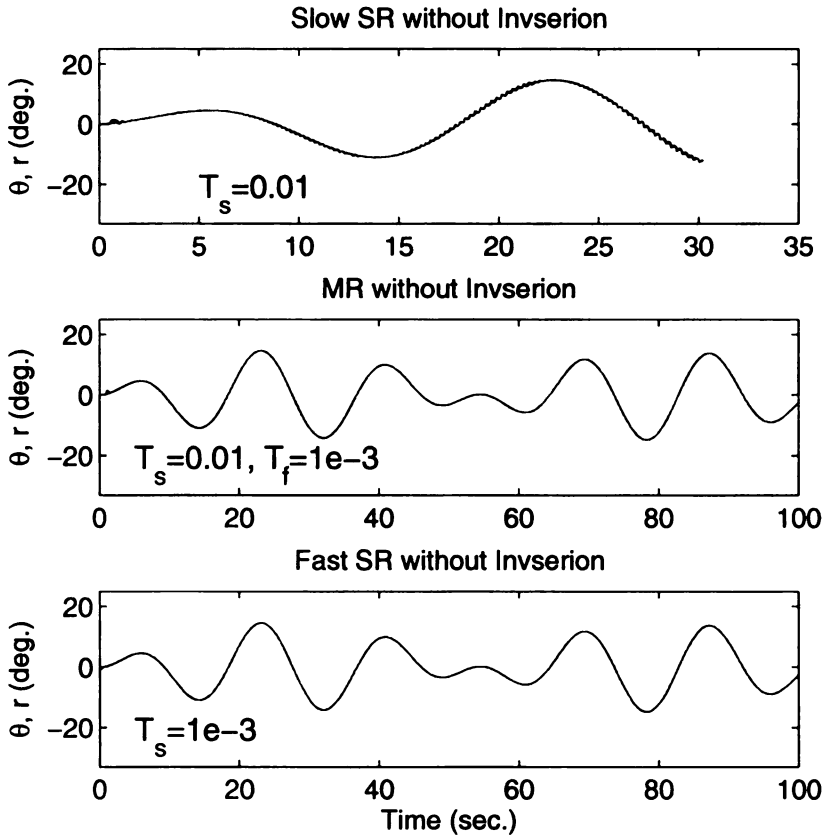

Figure 5.24. Plot of a sinusoidal tracking experiment for slow SR (top), MR (middle), and fast SR (bottom) output feedback controllers without hysteresis inversion. Shown are the rotation angle θ (solid) versus the reference r (dashed).

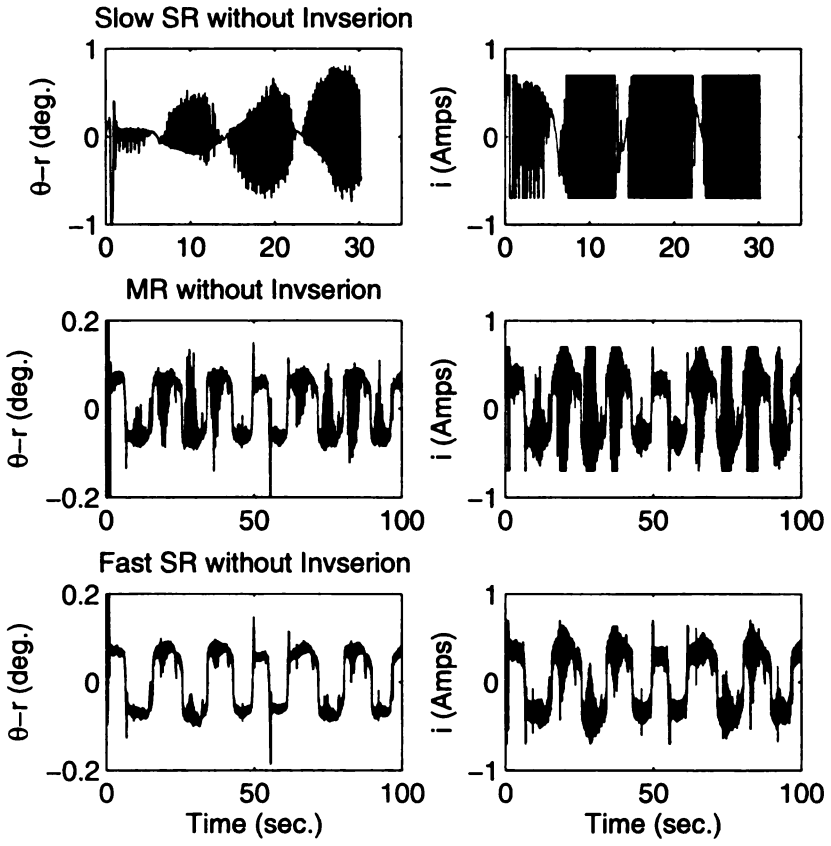

Figure 5.25. Plot of a sinusoidal tracking experiment for slow SR (top), MR (middle), and fast SR (bottom) output feedback controllers without inversion. Shown are the tracking error $\theta - r$ (left) and the current i (right).

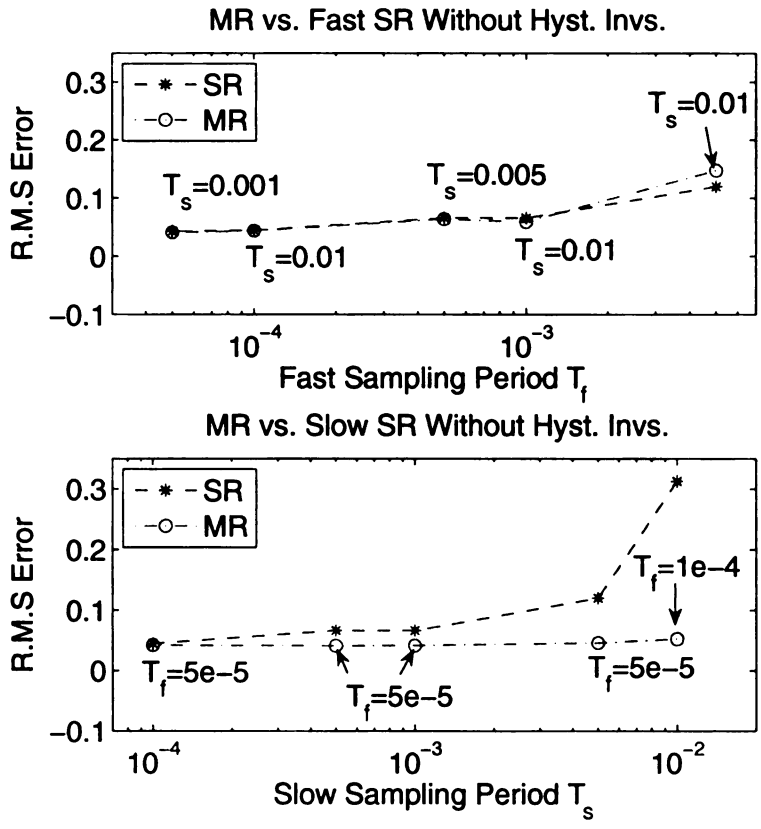

Figure 5.26. Comparison of MR versus fast SR (top) and MR versus slow SR (bottom) for the tacking experiment with reference given by (5.46) and controller without hysteresis inversion.

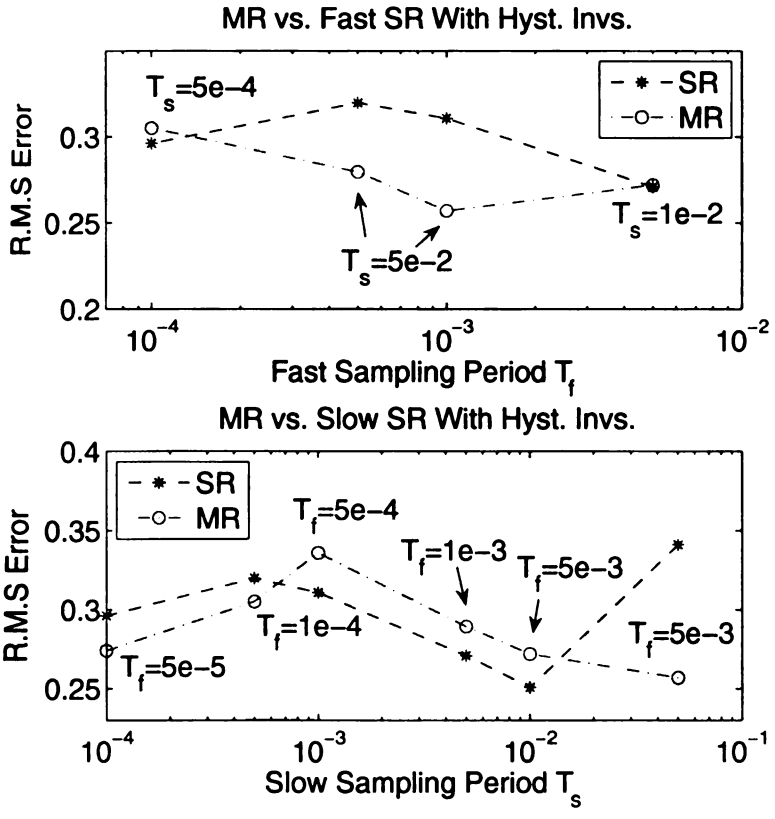

Figure 5.27. Comparison of MR versus fast SR (top) and MR versus slow SR (bottom) *for the tacking* experiment with reference given by (5.46) and controller with hysteresis *inversion.*

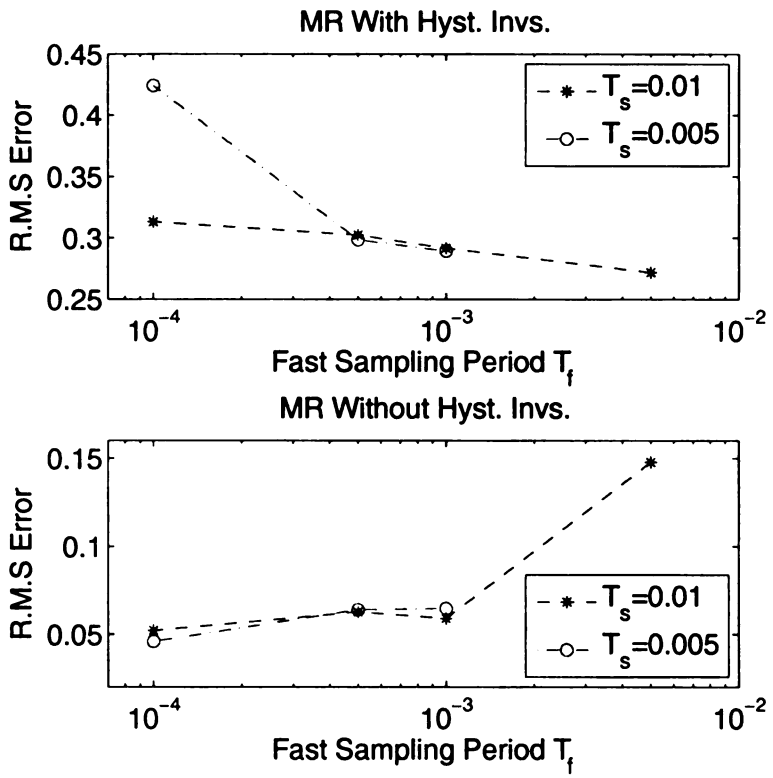

Figure 5.28. Plot illustrating the effect of increasing the ratio T_S/T_f for multirate output feedback with hysteresis inversion (top) and without hysteresis inversion (bottom). Both plots show two data sets each; one for $T_S = 0.01$ and another for $T_S = 0.005$.

5.4.4 PID versus PID with Hysteresis Inversion

Finally, we compare the PID with hysteresis inversion controller to PID without inversion. First, consider a tracking problem with

$$r = 20sin(0.1t)$$

In both cases we use a single-rate controller with sampling period of $0.01s$. We used gains of $k_i = 0$, $kp = 5$, and $k_d = 0.1$ for the PID case and $k_i = 2$, $kp = 8$, $k_d = 0.1$, and $k_g = 0.0028$ for the case of PID with hysteresis inversion. Figure 5.29 shows that the controller with hysteresis inversion achieves stable tracking. For the PID case without hysteresis inversion, the response is oscillatory and the control signal continuously saturates. Although stabilization for the PID case can be achieved with faster sampling, the hysteresis inversion provided added stability at this low sampling rate.

Next, we select a sampling period of $0.001s$ and use a single-rate controller to track the following angular reference

$$r = 15sin(0.4t)$$

We tuned the PID gains to give a similar tracking performance for the two controllers. The gains chosen were $k_i = 4$, $kp = 6$, and $k_d = 2$ for the PID case and $k_i = 2$, $kp = 5$, $k_d = 0.1$, and $k_g = 0.014$ for the case of PID with hysteresis inversion. The plots on the left of Figure 5.30 show the results of the case with hysteresis inversion and the plots on the right show those of the case with PID only. From the error plot we can see that both controllers were able to reduce the steady-state tracking error close the resolution of the encoder. Again the resolution is 0.0439 degrees. The plot of the current signal shows that the PID control saturated throughout the experiment. Under the PID with hysteresis inversion scheme, the control was noisy, but did not saturate. The R.M.S tracking error for the PID scheme was 0.00914 and the error for the PID with inversion was 0.0319. The R.M.S of the current was 0.05097 for the PID case and 0.03739 for the PID with inversion.

Thus, both controllers achieved good tracking results, but the inversion scheme used less control effort.

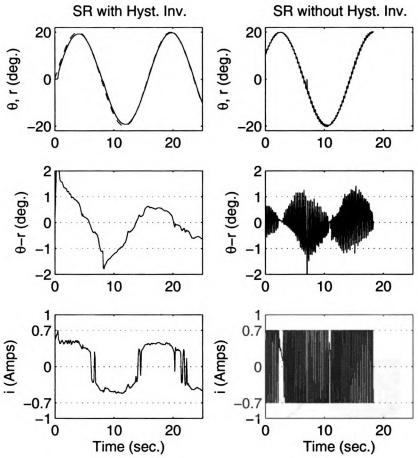

Figure 5.29. Plot of experimental results comparing PID with hysteresis inversion (left) with PID (right). Shown are the angle θ (solid) versus the reference r (dashed) (top), the tracking error $\theta - r$ (middle), and current i (bottom).

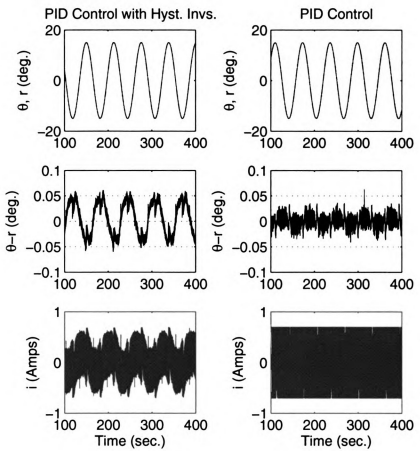

Figure 5.30. Plot of experimental results comparing PID with hysteresis inversion (left) with PID (right). Shown are the angle θ (solid) versus the reference r (dashed) (top), the tracking error $\theta - r$ (middle), and current i (bottom).

5.5 Conclusions

In this chapter we considered applications of multirate output feedback control to smart material actuated systems. We have argued that for smart materials modeled as in Figure 5.1 the closed-loop fits the class of systems developed in Chapter 4 and thus we can apply the stabilization results of that chapter. Furthermore, we presented experimental results of a shape memory alloy actuated rotary joint under multirate sampled-data output feedback control. We compared multirate and single-rate output feedback and studied the effectiveness of the multirate scheme in an experimental application.

CHAPTER 6

Conclusions

This dissertation has been concerned with the design and performance tradeoffs that are associated with the choice of gain in a high-gain observer. We have considered tradeoffs between fast reconstruction of the system states, better rejection of modeling uncertainty, and closed-loop stability versus amplification of measurement noise, large peaking amplitude, and computational cost in the discrete-time case. We have proposed several high-gain observer designs and examined their effectiveness at relaxing these tradeoffs.

We have examined the extended Kalman filter as a time-varying high-gain observer. Closed-loop stability results for nonlinear systems under EKF feedback have been limited and we have been able to show that for the special normal form class of systems the origin of the closed-loop system is asymptotically stable and the origin of the estimation error is exponentially stable. Many previous theoretical results on extended Kalman filters assumed the boundedness of the solution to the Riccati equation. From the two-time scale nature of our problem, we were able to argue boundedness and positive definiteness of the solution to the Riccati equation. We have shown that an important feature in the use of the extended Kalman filters is the need for globally bounded time-varying terms in the Riccati equation in order to guarantee stability. As the EKF has seen wide use in a variety of applications, we expect that closed-loop stability results will be useful to practicing engineers.

Through simulation we have compared the closed-loop performance of the time-varying EKF versus the time-invariant HGO. We have seen that the EKF with time-varying gain may provide closed-loop stability advantages over the fixed-gain observer. Furthermore, the Riccati equation can be initialized to eliminate peaking during the initial transients. Thus, for a particular system, a time-varying HGO may be able to achieve a better balance between closed-loop stability and suppression of peaking than a fixed-gain observer. This comes at the expense of added complexity of the extended Kalman filter when compared to a fixed-gain high-gain observer.

In response to a common criticism of high-gain observers we have considered a gain switching scheme to balance the tradeoff between state reconstruction speed and amplification of measurement noise. Furthermore, we have proved that when the switched-gain observer scheme is employed in output feedback, the closed-loop system remains bounded. We have derived relationships that exhibit the tradeoff between fast reconstruction of the states and rejection of modeling error versus the immunity to measurement noise for a high-gain observer. Based on this we have designed a switched-gain version of the high-gain observer in an attempt to relax the tradeoff between fast state reconstruction and rejection of measurement noise. To handle the peaking in the estimates we have included a switching delay in our scheme. We've also considered a nonlinear high-gain differentiator with smooth switching based on dead zone nonlinearity. Numerical examples illustrate the effectiveness of each design.

We have seen that using high-gain observers in sampled-data feedback control may require higher sampling rates than the sampling rate that was chosen under a state feedback design. Thus, fast sampling guarantees closed-loop stability under the discrete-time high-gain observer. On the other hand, operating at elevated processing rates is more computationally demanding and may not be cost effective. This has motivated the study of multirate sampled-data output feedback control using high-gain observers. This scheme uses a control update rate fixed by the state feedback design and a faster measurement

sampling rate. With our multirate scheme we were able to show that it practically stabilizes the origin of the closed-loop system. Further, with a sampled-data state feedback design that exponentially stabilizes the origin we have shown that the closed-loop system under multirate output feedback exponentially stabilizes the origin of the closed-loop system. We also examined stabilization with respect to a compact positively invariant set. This provided a theoretical framework for the application to smart material actuators where hysteresis inversion compensation is used.

We have designed the control to allow for initialization strategies to handle peaking in the initial transient. We have seen that the multirate scheme can be designed such that controller initialization need only be preformed for one slow sample. In addition, simulation examples show that the multirate scheme appears to be less sensitive than the single-rate scheme to impulsive-like disturbances that may occur at an unknown time.

Using a shape memory alloy actuated rotary joint we have experimentally tested our multirate output feedback control scheme. Using a controller based on hysteresis inversion we have shown that our multirate scheme indeed enjoys closed-loop stability at lower control update rates than the single-rate scheme. Further, at higher sampling rates we have seen that the multirate scheme performs well in comparison to both "fast" and "slow" single rate schemes in the presence of the encoder measurement noise.

The work described in this thesis provides a number of avenues for future research. The switching schemes introduced here lead to alternate variable gain designs. For example, an interesting design would explore the use of a nonlinear gain function that is smooth and results in a continuum of gain values rather than switch between two gain values. This would allow one to alter the noise and state reconstruction tradeoff depending on the size of the output estimation error.

For time-varying gains and the extended Kalman filter, expanding the results beyond the special normal form is complicated by a difficulty in rescaling the partitioned Riccati equation such that it will be in the standard singularly perturbed form. In addition, con-

sidering a general nonlinear function for the internal dynamics also presents a challenge. Clearly in that case, a first order approximation of the nonlinear function will only be valid locally. However, it may be of interest to formulate a stability result that, while it may be local in the direction of the estimation error of the internal dynamics, would be regional in the direction of the estimation error of the external dynamics.

For applications to smart materials, an interesting experimental direction may be to compute the hysteresis inversion and controller operations on an embedded controller while a high-gain observation can be performed on a separate processor. This additional computing power will allow more accurate models of the hysteresis and fast sampling rates for the high-gain observer. Furthermore, processing and communication delays may present interesting theoretical challenges. Embedded processing of hysteresis inversion is already an area of active research in the smart microsystems laboratory.

Finally, throughout this thesis we have considered single-input single-output systems (SISO). The extension to multi-input multi-output systems is fairly straightforward for systems that have a well-defined vector relative degree. But, for simplicity of presentation we have only shown the SISO case.

APPENDICES

APPENDIX A

Kronecker Matrices

Using the identity (2.38), the matrices in equations (2.39)-(2.40) are given by

$$M_1 = I \otimes A_{11} + A_{11} \otimes I, \quad M_2 = (A_{12} - \tilde{P}_2 C^T C) \otimes I, \quad M_3 = \bar{P}_2 C^T C \otimes I$$
$$M_4 = I \otimes (A_{12} - \bar{P}_2 C^T C)$$

and

$$N_1 = \begin{bmatrix} N_{11} & 0 & 0 \\ 0 & N_{21} & 0 \\ 0 & 0 & N_{31} \end{bmatrix}, N_2(t) = \begin{bmatrix} -N_{12}(t) & 0 & N_{14}(t) \\ 0 & -N_{22}(t) & N_{24}(t) \\ 0 & 0 & N_{32}(t) \end{bmatrix}$$

$$N_3(\pi_3) = \begin{bmatrix} -N_{13}(\pi_3) & 0 & 0 \\ 0 & -N_{23}(\pi_3) & 0 \\ 0 & 0 & N_{33}(\pi_3) \end{bmatrix}, N_q = \begin{bmatrix} N_{18} q_2 \\ N_{28} q_{2T} \\ 0 \end{bmatrix}$$

$$N_4 = \begin{bmatrix} N_{15} + N_{16} & 0 & 0 \\ 0 & N_{25} + N_{26} & 0 \\ \varepsilon N_{36} & \varepsilon N_{35} & N_{34} \end{bmatrix}, N_5 = \begin{bmatrix} N_{17} \\ N_{27} \\ 0 \end{bmatrix}$$

where

$$N_{11} = A^+ \otimes I, \quad N_{12} = (\bar{P}_3 - P_3^+) C^T C \otimes I, \quad N_{13} = \tilde{P}_3 C^T C \otimes I,$$

$$N_{14} = I \otimes (A_{12} - \bar{P}_2 C^T C), \quad N_{15} = I \otimes A_{11}, \quad N_{16} = A_{0\varepsilon} \otimes I,$$

$$N_{17} = DA_{21} \otimes I, \quad N_{18} = D \otimes I,$$

$$N_{21} = I \otimes A^+, \quad N_{22} = I \otimes (\bar{P}_3 - P_3^+) C^T C, \quad N_{23} = I \otimes \tilde{P}_3 C^T C$$

$$N_{24} = (A_{12} - \bar{P}_2 C^T C) \otimes I, \quad N_{25} = A_{11} \otimes I, \quad N_{26} = I \otimes A_{0\varepsilon}$$

$$N_{27} = I \otimes DA_{21}, \quad N_{28} = I \otimes D,$$

$$N_{31} = I \otimes A^+ + A^+ \otimes I, \quad N_{32} = I \otimes (\bar{P}_3 - P_3^+) C^T C + (\bar{P}_3 - P_3^+) C^T C \otimes I$$

$$N_{33} = I \otimes \tilde{P}_3 C^T C, \quad N_{34} = I \otimes A_{0\varepsilon} + A_{0\varepsilon} \otimes I, \quad N_{35} = DA_{21} \otimes I, \qquad \text{(A.1)}$$

$$N_{36} = I \otimes DA_{21}$$

To arrive at (2.42), consider the submatrices of N_2. Using (2.29) and (2.32) and the equalities $A_{12} = GC$ and $C = CC^T C$ it can be shown that these matrices satisfy

$$\|N_{12}\| \leq k_1 e^{-\lambda_1 t/\varepsilon}, \quad \|N_{14}\| \leq k_2 e^{-\lambda_2 t/\varepsilon}, \quad \|N_{22}\| \leq k_3 e^{-\lambda_3 t/\varepsilon}$$

$$\|N_{24}\| \leq k_4 e^{-\lambda_4 t/\varepsilon}, \quad \|N_{32}\| \leq k_5 e^{-\lambda_5 t/\varepsilon}$$

for some positive constants k_i and λ_i where, $i = 1 \cdots 5$. Using this we can arrive at the inequality (2.42).

APPENDIX B

Technical Lemma

The following result is a discrete-time analog to ([39],Ch. 5, Lemma 2.2)

Lemma B.1 *Consider equations (4.59), (4.63), and let (4.60)-(4.62) hold. Then, there exist* ε^*, κ_2, *and* $0 < \lambda_3 < 1$ *such that for all* $0 < \varepsilon \leq \varepsilon^*$

$$\|\Upsilon(n, n_0)\| \leq \varepsilon \kappa_2 \lambda_3^{n-n_0} \tag{B.1}$$

Proof: From the definition of $\Upsilon(n, n_0)$ (4.63) we have

$$\Upsilon(n, n) = 0$$

$$\Upsilon(n+1, n_0) = \tilde{A}(n)\Upsilon(n, n_0) + \left(\tilde{A}(n) + A_f\right) A_f^{n-n_0}$$

The solution to this equation can be written as

$$\Upsilon(n, n_0) = \sum_{i=n_0}^{n-1} \Upsilon(n, i+1)\left(\tilde{A}(i) - A_f\right) A_f^{i-n_0} + \sum_{i=n_0}^{n-1} A_f^{n-i}\left(\tilde{A}(i) - A_f\right) A_f^{i-n_0}$$

Multiply through by $\lambda_3^{-(n-n_0)}$, where $0 < \lambda_1 < \lambda_3 < 1$, and let $z(n,n_0) = \lambda_3^{-(n-n_0)}\Upsilon(n,n_0)$, we have

$$\begin{aligned} z(n,n_0) &= \sum_{i=n_0}^{n-1} \lambda_3^{-(n+1-n_0)} z(n,i+1)\left(\tilde{A}(i) - A_f\right) A_f^{i-n_0} \\ &\quad + \sum_{i=n_0}^{n-1} \lambda_3^{-(n-n_0)} A_f^{n-i-1}\left(\tilde{A}(i) - A_f\right) A_f^{i-n_0} \end{aligned} \tag{B.2}$$

Treating $z(n,n_0)$ as a functional on $[n_0,n]$ with norm

$$\sup_{n_0 \le \tau \le n} \|z(n,\tau)\|$$

we have

$$z = F(z) + B = T(z)$$

We show that T is a contraction mapping over the set $\{z : \|z\| \le \varepsilon\rho\}$, for some ρ chosen later on. We have

$$\|B\| \le \varepsilon c_3 \sum_{i=n_0}^{n-1} \lambda_3^{-(n-n_0)} \lambda_1^{n-n_0-1} \le \frac{\varepsilon c_3 (n-n_0)}{\lambda_1}\left(\frac{\lambda_1}{\lambda_3}\right)^{n-n_0} \le \varepsilon c_3 k_1$$

$$\|F\| \le \frac{\varepsilon^2 c_3 \rho}{\lambda_3} \sum_{i=n_0}^{n-1} \left(\frac{\lambda_1}{\lambda_3}\right)^{i-n_0} \le \varepsilon^2 c_3 \rho k_2$$

for some positive constants k_1 and k_2. Choosing

$$\rho = \frac{c_3 k_1}{(1-\nu)} \quad , \quad \varepsilon^* = \frac{\nu}{c_3 k_2}$$

where $0 < \nu < 1$ we have, for all $\varepsilon < \varepsilon^*$, $\|T(z)\| \leq \varepsilon\rho$. Moreover,

$$\begin{aligned}\|T(z_2) - T(z_1)\| &\leq \frac{\varepsilon c_3}{\lambda_3} \sum_{i=n_0}^{n-1} \left(\frac{\lambda_1}{\lambda_3}\right)^{i-n_0} \|z_2 - z_1\| \\ &\leq \varepsilon c_3 k_2 \|z_2 - z_1\| < \nu \|z_2 - z_1\| \quad \forall \varepsilon < \varepsilon^*\end{aligned}$$

Hence, T is a contraction mapping, and the unique solution to (B.2) satisfies

$$\|z(n, n_0)\| \leq \varepsilon\rho$$

Therefore,

$$\|\Upsilon(n, n_0)\| \leq \varepsilon\rho\lambda_3^{n-n_0}$$

◁

APPENDIX C

Inverse Preisach Operator

C.1 Preisach Operator Inversion Algorithm [63]

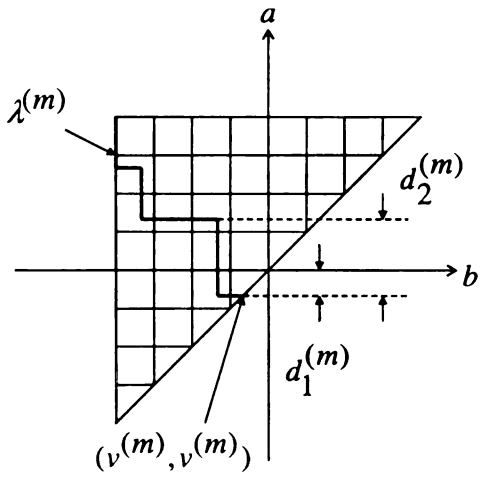

Figure C.1. Preisach plane with $L = 8$.

The task of the inversion algorithm is to find $\bar{v}$, given λ_0 and $\bar{u}_d$, such that

$$\bar{u}_d = \Gamma[\bar{v}, \lambda_0]$$

where Γ is a Preisach operator with a piecewise uniform density function. Let the input and output of Γ, corresponding to the memory curve λ_0, be v_0 and u_{d0}, respectively.

Algorithm ($\bar{u}_d > u_{d0}$)

Step 1. $v^{(0)} := v_0$, $u_d^{(0)} := u_{d0}$, $\lambda^{(0)} := \lambda_0$, $m := 0$;

Step 2.

$$\begin{cases} d^{(m)} & := & min\{d_0^{(m)}, d_1^{(m)}, d_2^{(m)}\} \\ v^{(m+1)} & := & v^{(m)} + d^{(m)} \\ u_d^{(m+1)} & := & \Gamma\left[v^{(m+1)}, \lambda^{(m)}\right] \end{cases}$$

where λ^m is the memory curve after $\left\{v^{(k)}\right\}_{k=1}^{m}$ is applied, and $d_0^{(m)}, d_1^{(m)}, d_2^{(m)}$ are determined in the following way:

-Let $d_1^{(m)} > 0$ be such that $v^{(m)} + d_1^{(m)}$ equals the next discrete input level;

-Let $d_2^{(m)} > 0$ be the minimum amount such that applying $v^{(m)} + d_2^{(m)}$ would eliminate the next corner of the memory curve (See Figure C.1);

-Since the Preisach density is constant within each discretization cell, for $d < min\left\{d_1^{(m)}, d_2^{(m)}\right\}$, we have

$$\Gamma\left[v^{(m)} + d, \lambda^{(m)}\right] - \Gamma\left[v^{(m)}, \lambda^{(m)}\right] = a_2^{(m)} d^2 + a_1^{(m)} d$$

where $a_1^{(m)}, a_2^{(m)} \geq 0$ can be computed from the density function, and the square term is due to the contribution from the triangular region inside the diagonal cell. Let $d_0^{(m)} > 0$

be the solution to

$$\bar{u}_d - \Gamma\left[v^{(m)}, \lambda^{(m)}\right] = a_2^{(m)}\left(d_0^{(m)}\right)^2 + a_1^{(m)} d_0^{(m)}$$

If $d^{(m)} = d_0^{(m)}$, go to Step 3; otherwise let $m := m + 1$ and go to Step 2;

Step 3. $\bar{v} := v^{(m+1)}$ and stop.

The algorithm for $\bar{u}_d < u_{d0}$ is analogous to the above.

C.2 Inversion Error [63]

Let ν be a nonsingular, nonnegative measure with density μ. For a discretization scheme of level L, let ν_p be a piecewise uniform approximation to ν obtained as described in Section 5.2.2. Denote Γ_ν as the Preisach operator that corresponds to the measure μ. Let

$$v = \Gamma_{\nu_p}^{-1}[u_d, \lambda_0]$$

where $\Gamma_{\nu_p}^{-1}$ is the exact inverse of Γ_{ν_p}. Consider

$$\tilde{u}_d = \Gamma_\nu[v, \lambda_0]$$

and define the inversion error as $e_i = \tilde{u}_d - u_d$. We have the following result the proof of which can be found in [63].

Theorem C.1 *Let $\mu \leq \bar{\mu}$ for some constant $\bar{\mu}$. Denote the integral of μ over discretization cell i as , $1 \leq i \leq N_c$, where Nc is the number of cells. Denote by ν_i the identified Preisach weighting mass for cell i. Assume that the relative error in identification is δ_I, i.e., $\frac{|\nu_i - \nu_i^0|}{\nu_i^0} \leq \delta_I$, $1 \leq i \leq N_c$. Then $\|e_m\|_\infty \leq \delta_I C_s + \frac{8\bar{\mu}s_0^2}{L}$, where C_s is the saturation output of Γ_ν, and s_0 is as defined in Section 5.2.2.*

BIBLIOGRAPHY

BIBLIOGRAPHY

[1] J. H. Ahrens and H. K. Khalil. Output feedback control using high-gain observers in the presence of measurement noise. In *Proc. American Control Conf.*, pages 4114–4119, Boston, MA, 2004.

[2] M. Arcak and D. Nešić. A framework for nonlinear sampled-data observer design via approximate discrete-time models and emulation. *Automatica*, 40:1931–1938, 2004.

[3] H. Ashrafiuon, M. Eshraghi, and M. H. Elahinia. Position control of a three-link shape memory alloy actuated robot. *Journal of Intelligent Material Systems and Structures*, 17:381–392, 2006.

[4] K. J. Åström and B. Wittenmark. *Computer Controlled-Systems: Theory and Design.* Prentice Hall, Upper Saddle river, New Jersey, third edition, 1998.

[5] P. Astuti, M. Corless, and D. Williamson. On the convergence of sampled data nonlinear systems. In E. Van Groesen and E. Soewono, editors, *Differential Equations: Theory, Numerics and Applications*, pages 201–210. Kluwer Academic, Dordrecht, 1998.

[6] A. N. Atassi. *A separation principle for the control of a class of nonlinear systems.* PhD thesis, Michigan State University, East Lansing, 1999.

[7] A. N. Atassi and H. K. Khalil. A separation principle for the stabilization of a class of nonlinear systems. *IEEE Trans. Automat. Contr.*, 44:1672–1687, 1999.

[8] A. N. Atassi and H. K. Khalil. Separation results for the stabilization of nonlinear systems using different high-gain observer designs. *Syst. Contr. Lett.*, 39:183–191, 2000.

[9] J. S. Baras, A. Bensoussan, and M. R. James. Dynamic observers as asymptotic limits of recursive filters: Special cases. *SIAM J. Appl. Math.*, 48(5):1147–1158, 1988.

[10] D. S. Bernstein. *Matrix Mathematics.* Princeton University Press, Princeton, New Jersey, 2005.

[11] M. Boutayeb and D. Aubry. A strong tracking extended Kalman observer for nonlinear discrete-time systems. *IEEE Trans. Automat. Contr.*, 44:1550–1556, 1999.

[12] M. Boutayeb, H. Rafaralahy, and M. Darouach. Convergence analysis of the extended Kalman filter used as an observer for nonlinear deterministic discrete-time systems. *IEEE Trans. Automat. Contr.*, 42:581–586, 1997.

[13] M. Brokate and J. Sprekels. *Hysteresis and Phase Transitions.* Springer-Verlag, New York, 1996.

[14] F. M. Callier, J. Winkin, and J. L. Willems. Convergence of the time-invariant Riccati differential equation and LQ-problem: Mechanisms of attraction. *Int. J. Control*, 59:983–1000, 1994.

[15] B. Castillo, S. Di Gennaro, S. Monaco, and D. Norman-Cyrot. On regulation under sampling. *IEEE Trans. Automat. Contr.*, 42:864–868, 1997.

[16] Z. Chen, X. Tan, and M. Shahinpoor. Quasi-static positioning of ionic polymer-metal composite (IPMC) actuators. In *Proc. of the IEEE/ASME Int. Conf. on Advanced Intelligent Mechatronics*, pages 60–65, Monterey, CA, 2005.

[17] Y. Chitour. Time-varying high-gain observers for numerical differentiation. *IEEE Trans. Automat. Contr.*, 47:1565–1569, 2002.

[18] F. H. Clarke, Y. S. Ledyaev, E. D. Sontag, and A. I. Subbotin. Asymptotic controllability implies feedback stabilization. *IEEE Trans. Automat. Contr.*, 42:1394–1407, 1997.

[19] A. Dabroom and H. K. Khalil. Discrete-time implementation of high-gain observers for numerical differentiation. *Int. J. Contr.*, 72:1523–1537, 1999.

[20] A. M. Dabroom and H. K. Khalil. Output feedback sampled-data control of nonlinear systems using high-gain observers. *IEEE Trans. Automat. Contr.*, 46:1712–1725, 2001.

[21] F. Deza, E. Busvelle, J. P. Gauthier, and D. Rakotopara. High gain estimation for nonlinear systems. *Syst. Contr. Lett.*, 18:295–299, 1992.

[22] C. A. Dickinson and J. T. Wen. Feedback control using shape memory alloy actuators. *Journal of Intelligent Material Systems and Structures*, 9:242–250, 1998.

[23] T. W. Duering, K. N. Melton, D. Stöckel, and C. M. Wayman. *Engineering Aspects of Shape Memory Alloys.* Butterworth-Heinemann, London, 1990.

[24] M. H. Elahinia, M. Ahmadian, and H. Ashrafiuon. Design of a Kalman filter for rotary shape memory alloy actuators. *Smart Mater. Struct.*, 13:691–697, 2004.

[25] E. M. Elbeheiry and H. A. Elmaraghy. Robotic manipulators state observation via one-time gain switching. *Journal of Intelligent and Robotic Systems*, 38:313–344, 2003.

[26] F. Esfandiari and H. K. Khalil. Output feedback stabilization of fully linearizable systems. *Int. J. Contr.*, 56:1007–1037, 1992.

[27] A. Gelb. *Applied Optimal Estimation.* MIT Press, Cambridge, 1974.

[28] R. B. Gorbet, K. A. Morris, and D. W. L. Wang. Passivity-based stability and control of hysteresis in smart actuators. *IEEE Trans. Contr. Syst. Tech.*, 9:5–16, 2001.

[29] R. B. Gorbet, D. W. L. Wang, and K. A. Morris. Preisach model identification of a two-wire SMA actuator. In *IEEE ICRA*, pages 2161–2167, Leuven, Belgium, May 1998.

[30] A. M. Guillaume, G. Bastin, and G. Campion. Sampled-data adaptive control of a class of continuous nonlinear systems. *Int. J. Contr.*, 60:569–594, 1994.

[31] M. Hashimoto, M. Takeda, H. Sagawa, I. Chiba, and K. Sato. Application of shape memory alloy to robotic actuators. *Journal of Robotic Systems*, 2:3–25, 1985.

[32] L. Hou, A. N. Michel, and H. Ye. Some qualitative properties of sampled-data control systems. *IEEE Trans. Automat. Contr.*, 42:1721–1725, 1997.

[33] S. Ibrir. Linear time-derivative trackers. *Automatica*, 40:397–405, 2004.

[34] A. Isidori. *Nonlinear control systems II.* Springer-Verlag, New York, 1999.

[35] Z. P. Jiang and Y. Wang. A converse lyapunov theorem for discrete-time systems with disturbances. *Syst. Contr. Lett.*, 45:49–58, 2002.

[36] H. K. Khalil. *Nonlinear Systems.* Prentice Hall, Upper Saddle River, New Jersey, 3nd edition, 2002.

[37] H. K. Khalil. Performance recovery under output feedback sampled-data stabilization of a class of nonlinear systems. *IEEE Trans. Automat. Contr.*, 49:2173–2184, 2004.

[38] P. V. Kokotović, H. K. Khalil, and J. O'Reilly. *Singular Perturbations Methods in Control: Analysis and Design.* Academic Press, New York, 1986. Republished by SIAM, 1999.

[39] K. Kuhnen and H. Janocha. Adaptive inverse control of piezoceramic actuators with hysteresis operators. *Proc. European Control Conf., Karsruhe, Germany*, page F0291, 1999.

[40] H. Kwakernaak and R. Sivan. *Linear Optimal Control Systems.* Wiley-Interscience, New York, 1972.

[41] D. S. Laila, D. Nešić, and A. R. Teel. Open and closed loop dissipation inequalities under sampling and controller emulation. *European Journal of Control*, 8:109–125, 2002.

[42] Y. Lin, E. Sontag, and Y. Wang. A smooth converse lyapunov theorem for robust stability. *SIAM J. Contr. Optim.*, 34:124–160, 1996.

[43] S. Majima, K. Kodama, and T. Hasegawa. Modeling of shape memory alloy actuator and tracking control system with the model. *IEEE Trans. Contr. Syst. Tech.*, 9:54–59, 2001.

[44] I. M. Y. Mareels, H. B. Penfold, and R. J. Evans. Controlling nonlinear time-varying systems via Euler approximations. *Automatica*, 28:681–696, 1992.

[45] I. D. Mayergoyz. *Mathematical Models of Hysteresis.* Springer-Verlag, Berlin, 1991.

[46] D. Q. Mayne, R. W. Grainger, and G. C. Goodwin. Nonlinear filters for linear signal models. *IEE Proc. Control Theory Appl.*, 144:281–286, 1997.

[47] S. O. R Moheimani and G. C. Goodwin. Guest editorial introduction to the special issue on dynamics and control of smart structures. *IEEE Trans. Contr. Syst. Tech.*, 9:3–4, 2001.

[48] S. Monaco and D. Normand-Cyrot. On nonlinear digital control. In A.J. Fossard and D. Normand-Cyrot, editors, *Nonlinear Systems, Vol. 3, Control*, pages 127–155. Chapman & Hall, London, 1995.

[49] P. E. Moraal and J. W. Grizzle. Observer design for nonlinear systems with discrete-time measurements. *IEEE Trans. Automat. Contr.*, 40:395–404, 1995.

[50] D. Nešić and D. S. Laila. A note on input-to-state stabilization for nonlinear sampled-data systems. *IEEE Trans. Automat. Contr.*, 47:1153–1158, 2002.

[51] D. Nešić and A. R. Teel. A framework for stabilization of nonlinear sampled-data systems based on their approximate discrete-time model. *IEEE Trans. Automat. Contr.*, 49:1103–1122, 2004.

[52] D. Nešić, A. R. Teel, and P. V. Kokotović. Sufficient conditions for stabilization of sampled-data nonlinear systems via discrete-time approximations. *Syst. Contr. Lett.*, 38:259–270, 1999.

[53] D. H. Owen, Y. Zheng, and S. A. Billings. Fast sampling and stability of nonlinear sampled-data systems: Part 1. existence theorems. *IMA Journal of Mathematics & Information*, 7:1–11, 1990.

[54] I. G. Polushin and H. J. Marquez. Multirate versions of sampled-data stabilization of nonlinear systems. *Automatica*, 40:1035–1041, 2004.

[55] Z. Qu. *Robust Control of Nonlinear Uncertain Systems.* Wiley-Interscience, New York, 1998.

[56] K. Reif, F. Sonnemann, and R. Unbehauen. An EKF-based nonlinear observer with a prescribed degree of stability. *Automatica*, 34:1119–1123, 1998.

[57] K. Reif and R. Unbehauen. The extended Kalman filter as an exponential observer for nonlinear systems. *IEEE Trans. Signal Processing*, 47:2324–2328, 1999.

[58] W. J. Rugh. *Linear Systems Theory.* Prentice Hall, Upper Saddle River, New Jersey, 1996. second edition.

[59] I. A. Shkolnikov, Y. B. Shtessel, and S. V. Plekhanov. Multi-rate digital design for sliding-mode-observer-based feedback control. In *Proc. American Control Conf.*, pages 2427–2432, Portland, OR, 2005.

[60] E. Skafides, A. Fradkov, R. J. Evans, and I. M. Y. Mareels. Trajectory based adaptive control for nonlinear systems under matching conditions. *Automatica*, 34:287–299, 1998.

[61] Y. K. Song and J. W. Grizzle. The extended Kalman filter as a local asymptotic observer for nonlinear discrete-time systems. *Journal of Mathematical Systems, Estimation and Control*, 5:59–78, 1995.

[62] H. Sorenson. Special issue on application of Kalman filtering. *IEEE Trans. Automat. Contr.*, AC-28, 1983.

[63] X. Tan and J. S. Baras. Modeling and control of hysteresis in magnetostrictive actuators. *Automatica*, 40:1469–1480, 2004.

[64] X. Tan, R. Venkataraman, and P. S. Krishnaprasad. Control of hysteresis: Theory and experimental results. In V. S. Rao, editor, *Modeling, signal processing, and control in smart structures*, volume 4326, pages 101–112. SPIE, 2001.

[65] G. Tao and P. V. Kokotović. Adaptive control of plants with unknown hystereses. *IEEE Trans. Automat. Contr.*, 40:200–212, 1995.

[66] A. R. Teel and J. Hespanha. Examples of GES systems that can be driven to infinity by arbitrarily small additive decaying exponentials. *IEEE Trans. Automat. Contr.*, 49:1407–1410, 2004.

[67] A. Tilli and M. Montanari. A low-noise estimator of angular speed and acceleration from shaft encoder measurements. *Journal Automatika*, 42:169–176, 2001.

[68] L. K. Vasiljevic and H. K. Khalil. Differentiation with high-gain observers in the presence of measurement noise. In *Proc. IEEE Conf. on Decision and Control*, San Diego, CA, December 2006 (To Appear).

[69] R. Venkataraman and P. S. Krishnaprasad. Approximate inversion of hysteresis: theory and numerical results. In *Proc. IEEE Conf. on Decision and Control*, pages 4448–4454, Sydney, Australia, December 2000.

[70] F. Viel, E. Busvelle, and J. P. Gauthier. Stability of polymerization reactors using I/O linearization and a high-gain observer. *Automatica*, 31:971–984, 1995.

[71] A. Visintin. *Differential Models of Hysteresis.* Springer, Berlin, 1994.

[72] W. R. Wade. *An Introduction to Analysis.* Prentice Hall, Upper Saddle River, New Jersey, 2000. second edition.

[73] G. V. Webb, D. C. Lagoudas, and A. J. Kurdila. Hysteresis modeling of SMA actuators for control applications. *Journal of Intelligent Materials Systems and Structures*, 9:432–448, 1998.

[74] Y. Zheng, D. H. Owen, and S. A. Billings. Fast sampling and stability of nonlinear sampled-data systems: Part 2. sampling rate estimation. *IMA Journal of Mathematics & Information*, 7:13–33, 1990.